Synthesis and Structural Features of α-Fluorocarbonyl Systems

FISHER, CRAIG,AARON

Durham University

A thesis entitled

Synthesis and Structural Features of α-Fluorocarbonyl Systems

By

Craig A. Fisher

(Grey College)

A candidate for the degree of Doctor of Philosophy

Department of Chemistry

Abstract

Molecules that bear carbon-fluorine bonds, especially on chiral centres, are becoming of interest to the pharmaceutical industry due to the effects on the bioactivity of a drug molecule. This thesis adds to the pool of chiral α-fluorocarbonyl systems and the discussion of the grey area surrounding their conformational preference. First, dimethyl 2-fluoromalonate was investigated as a nucleophile and as an electrophile. The fluorodiester was successfully reacted with a short series of electrophilic alkylating agents and, separately, a nucleophilic amine. Consequently, in collaboration with GlaxoSmithKline, these two strategies were combined to use dimethyl 2-fluoromalonate as a fluorinated 'building block' in the synthesis of a 6-membered fluorolactam.

This fluorolactam subsequently underwent an enzymatic chiral resolution to yield an enantiomerically enriched analogue as an intermediate in the synthesis of a pre-clinical candidate spleen tyrosine kinase (Syk) inhibitor being developed by GSK. The process was optimised and quantitatively analysed by a 'green metrics' package developed by the EU IMI Chem21 consortium and found to be significantly less wasteful than the literature alternative synthetic route. Work on analogous 5- and 7-membered fluorolactams was carried out following the success of the 6-membered system.

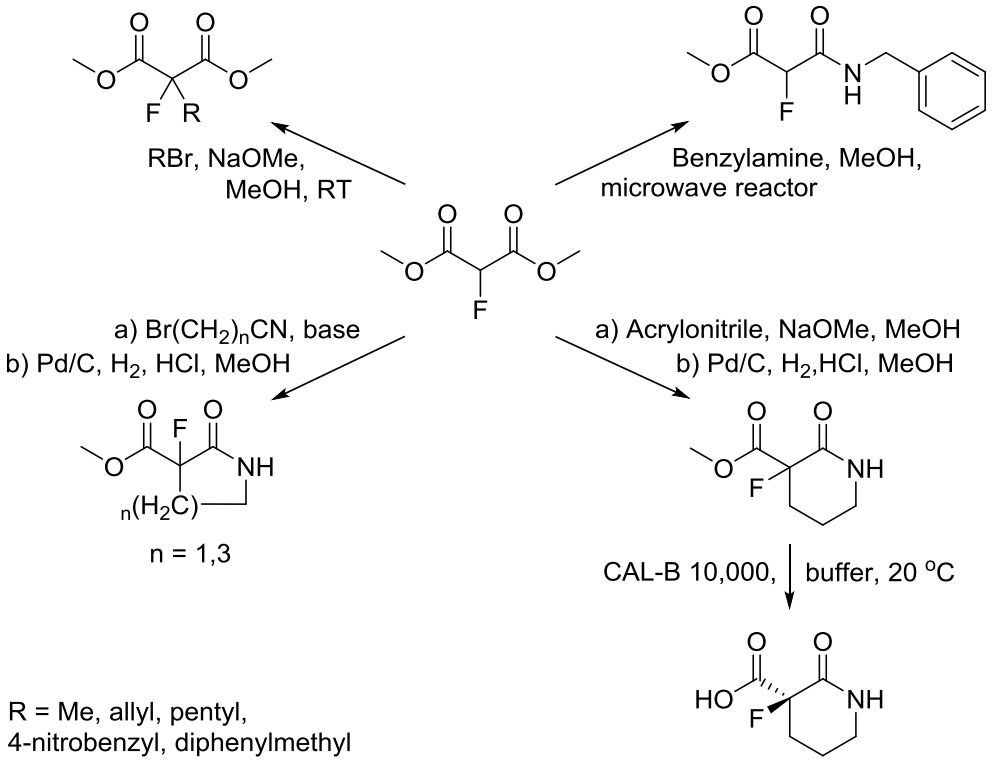

In collaboration with Almac Group, another α-fluorodicarbonyl species, ethyl 2-fluoroacetoacetate, was chosen as a substrate for carbonyl reductase (CRED) screening. Enzymatic routes to all four possible diastereomeric fluoroalcohol derivatives were found and work to determine the absolute stereochemistries of the products is ongoing.

Following analysis of the structural preferences of the X-ray crystal structures of products developed in this thesis, the final chapter investigates the conformational preference of α-fluorocarbonyl moieties in the Cambridge Structural Database. This research was coupled with NMR experiments and computational calculations, from the literature and our own work, of these species in the solution state to determine that there is a greater *syn* F-C-C=O preference in more polar environments and that any inherent preference may potentially be overridden by a number of competing factors. The assumption that *anti* is the preferred conformation of α-fluorocarbonyl species must, therefore, be treated with caution.

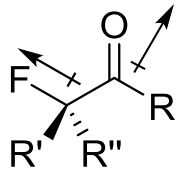

R = OC, OH, C, Ph, H, N

Acknowledgements

First, I'd like to thank Professor Graham Sandford for his high quality supervision, support, patience and encouragement throughout my time in his research group. I really couldn't have asked for a better supervisor.

During my PhD I was fortunate enough to work alongside two networks and gain invaluable experience with industrial collaborators. From GSK (Chem21 consortium) I'd like to thank Nicky Willis, Catherine Alder and Joe Adams, and from Almac Group (FLUORINE21 ITN) I'd like to thank Gareth Brown, Stefan Mix and Bart Tomaszewski for their work, support, and hospitality during my secondment to Almac.

I'd like to thank the many members of support staff here in the department, without whom my research simply would not have been possible. Thanks go to Alan, Catherine and Juan in NMR, Dave and Pete in MS and Paul, Neil and Omer in the mechanical and electrical workshops. Special thanks to Mark Fox for his computational contributions and for all the fun these past years (and I forgive him for the infamous chip shot in the John Duck…), to Dima Yufit in crystallography for his expertise, willingness to help me with any questions I had and his contagious enthusiasm, and to Annette Passmoor for all the laughs and for working absolute wonders with the departmental stores.

I've had a fantastic time working in CG115 and would like to thank all its members (present and past), especially Adam, Ffion, Rob, Vicky, Max, Dan, Jon, Etienne, Darren, Hédi, Josh, Alex, Alex 2.0, Ben and Anne, plus Oliver, David and Peter from the AMOD group. I'd like to thank Marcus Lancashire separately for having to bear with me in the lab, at Grey and on the pool team. I can't express my gratitude enough for Tony Harsanyi for his friendship, for all the good times, for his help and ideas and for taking me under his wing and always encouraging me to be the best I could be.

I'd like to thank Grey MCR for the fun, the friendship, and for keeping me off the streets, and to Grey College staff for the past 8 years. Thanks to Grey C pool team for all the laughs, alcohol and occasional pool games. Finally, and importantly, I'd like to thank my family and friends for their continued support throughout my time at Durham.

Memorandum

The work described in this thesis was carried out at Durham University between October 2013 and December 2016. This thesis is the work of the author, except where acknowledged by reference, and has not been submitted for any other degree. The copyright of this thesis rests with the author. No quotation from it should be published without prior written consent and information derived from it should be acknowledged.

Parts of this work have been the subject of the following publication:

1) Willis, N. J.; Fisher, C. A.; Alder, C. M.; Harsanyi, A.; Shukla, L.; Adams, J. P.; Sandford, G. *Green Chem.* **2016**, *18*, 1313-1318, *Sustainable synthesis of enantiopure fluorolactam derivatives by a selective direct fluorination - amidase strategy*.

This work has been present, in part, at:

1) 16th Annual RSC Fluorine Subject Group Postgraduate Meeting, 22-23 September 2016, Oxford, United Kingdom, *oral presentation*.
2) Sustainability in Industrial Chemistry, Symposium and Workshop, 4-5 November 2015, Durham, United Kingdom, *poster presentation*.
3) 21st International Symposium on Fluorine Chemistry & 6th International Symposium on Fluorous Technologies, 23-28 August 2015, Como, Italy, *poster presentation*.
4) IMI Chem21 Annual General Meeting, 22-23 September 2014, Graz, Austria, *poster presentation*.

Nomenclature and Abbreviations

Ac	Acyl
AE	Atom economy
Ar	Aryl
ASAP	Atmospheric solid analysis probe
BINAP	(2,2'-bis(Diphenylphosphino)-1,1'-binaphthyl)
Bn	Benzyl
Boc	*Tert*-Butyloxycarbonyl
CAL	*Candida antarctica* lipase
Cat.	Catalyst
CCDC	Cambridge crystallographic data centre
Conc.	Concentrated
Cpd	Compound
CRED	Carbonyl reductase
CSD	Cambridge structural database
DAST	Diethylaminosulfur trifluoride
DBU	1,8-Diazabicyclo[5.4.0]undec-7-ene
DCC	*N*,*N'*-Dicyclohexylcarbodiimide
DCM	Dichloromethane
de	Diastereomeric excess
DFT	Density functional theory
DKR	Dynamic kinetic resolution
DMAP	4-Dimethylaminopyridine
DMF	Dimethylformamide
DMSO	Dimethyl sulfoxide
dr	Diastereomeric ratio
EDCl·HCl	1-Ethyl-3-(3-dimethylaminopropyl)carbodiimide hydrochloride
EI	Electron impact (ionisation)
ee	Enantiomeric excess
Eq.	Equivalents
Et	Ethyl
Fmoc	Fluorenylmethyloxycarbonyl protecting group
FTIR	Fourier transform infrared spectroscopy
GC	Gas chromatography

GC-MS	Gas chromatography-mass spectrometry
GDH	Glucose dehydrogenase
GSK	GlaxoSmithKline
HIV	Human immunodeficiency virus
HPLC	High performance liquid chromatography
HOBt	Hydroxybenzotriazole
Hz	Hertz
Isomer Excess	The excess of one diastereomer over the other three. Calculated in a similar manner to enantiomeric excess
IR	Infrared
LDA	Lithium diisopropylamide
Me	Methyl
MI	Mass intensity
Mp	Melting point
MTBE	Methyl tertiary butyl ether
MW	Molecular weight
NAD	Nicotinamide adenine dinucleotide
NADP	Nicotinamide adenine dinucleotide phosphate
NFSI	*N*-Fluorobenzenesulfonimide
NMR	Nuclear magnetic resonance
Ph	Phenyl
PLE	Pig liver esterase
PMI	Process mass intensity
ppm	Parts per million
^{i}Pr	*iso*-Propyl
psi	Pounds per square inch
RME	Reaction mass efficiency
rpm	Revolutions per minute
RT	Room temperature
T, Temp.	Temperature
Tf	Trifluoromethylsulfonyl
THF	Tetrahydrofuran
TLC	Thin layer chromatography
TMS	Trimethylsilyl
Ts	Tosyl, 4-toluenesulfonyl
UPLC-MS	Ultra performance liquid chromatography-mass spectrometry

Table of Contents

Chapter 1. Literature Review of General Organofluorine Chemistry and the Synthesis of α-Fluoroamidoesters

1.1. Organofluorine Chemistry and Fluorinated Heterocycles

1.1.1. Introduction

Heterocycles are a common feature in the structures of many pharmaceutically or agriculturally active molecules.[1,2,3] Despite the extreme scarcity of naturally occurring fluorine containing molecules[4] many new drugs and agrochemicals contain fluorinated heterocycles or fluorine in their molecular structures (up to 20% of pharmaceuticals in 2010) (***Figure 1***).[5,6] This trend is due to the unique properties of the fluorine atom that allow increased control over how the fluorinated molecule interacts with a biological system, be it for medicinal or agricultural purposes. The pharmaceutical industry is turning away from the "flatland" of aromatic fluorinated drugs towards more three-dimensional systems with sp^3 centres[7] and, since chirality often plays an important role in bioactive molecules, synthetic strategies to systems with chiral C-F bonds are becoming of interest.[8,9,10]

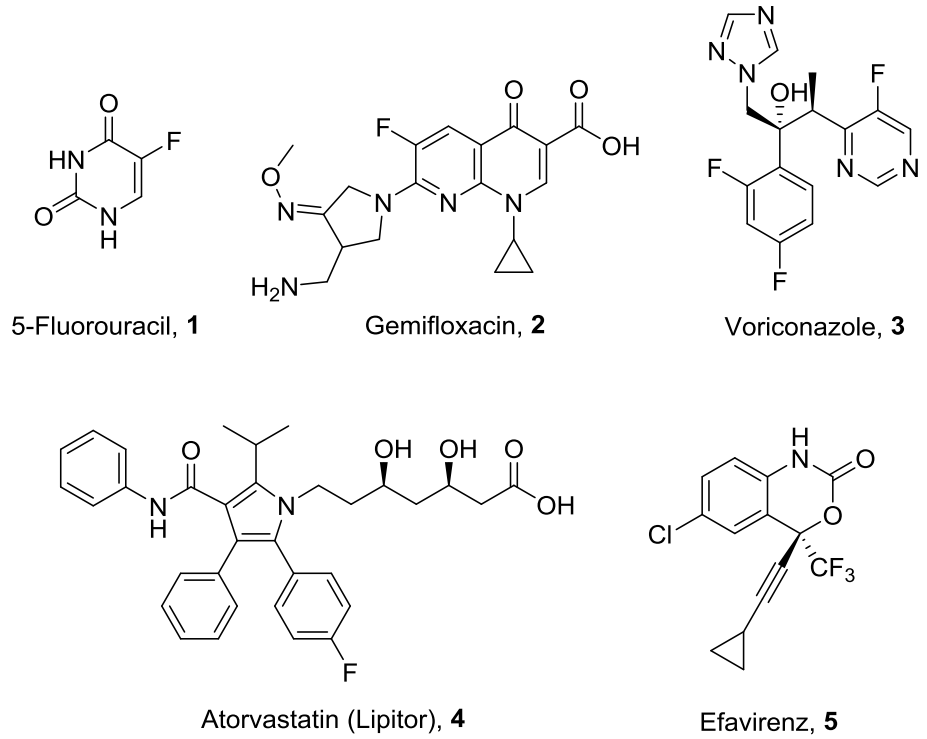

Figure 1 *- Structures of some fluorine containing drugs; 5-fluorouracil (anti-cancer),*[11] *Gemifloxacin (antibacterial),*[12] *Voriconazole (antifungal),*[13] *Atorvastatin (cholesterol lowering)*[14] *and Efavirenz (HIV treatment).*[15]

Many facets of drug activity of an organic molecule, including binding site interactions, reactivity, metabolism, lipophilicity and bioavailability, are the result of the electron donors and acceptors present in the molecular structure. Polarisable functional groups are influenced by the presence of adjacent electron withdrawing or donating groups and, given that fluorine is the most electronegative element, fluorine incorporation into a drug molecule will have a larger effect on these properties than would the other halogens or electronegative elements.

Additionally, fluorine atoms are only marginally larger than hydrogen atoms (with Van der Waals radii of 1.47 Å and 1.20 Å respectively)[16] so there should be minimal disruption to steric requirements between a fluorinated molecule and an enzyme binding site, something that may not be the case with other electronegative elements or functional groups. The C-F bond is also similar in length to that of the C-H bond though is considerably stronger, another property that can be exploited without disrupting steric requirements.

1.1.2. Effects of Fluorine Substitution on Drug Activity

The introduction of one or more fluorine atoms to a molecule can alter bioactivity of an organic molecule through a number of effects which are briefly outlined below.

1.1.2.1. Lipophilicity

Polar moieties of a drug molecule are responsible for hydrogen bonding with water molecules and determine the hydrophilicity of the system. The electron withdrawing effect of fluorine atoms can reduce the polarity of electron rich moieties involved in hydrogen bonding thus reducing their ability to form hydrogen bonds leading to increased lipophilicity of the drug molecule. Hydrophilic drugs are unable to pass through the lipid based blood brain barrier and will, therefore, be less potent. Conversely, if a drug molecule is too lipophilic then there will be issues involved with transporting the drug in the blood since it will not be soluble and this too will have a detrimental effect on bioavailability.[4]

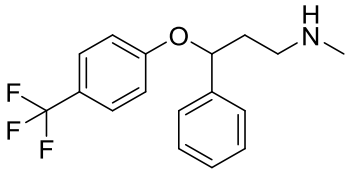

6

***Figure 2** – The structure of Prozac (fluoxetine).*

The $-CF_3$ moiety is one of the most lipophilic groups and, as such, is found in a number of drugs including the antidepressant Prozac (fluoxetine) which features a *para*-CF_3 aryl group (***Figure 2***).[17] Other examples include antidepressant and OCD treatment Luvox (fluvoxamine), nonsteroidal anti-inflammatory drug (NSAID) Celebrex (celecoxib), antimalarial drug Lariam (mefloquine) and inhalational anaesthetic Fluoromar (fluoroxene).[18]

1.1.2.2. Electronic Effects and Interactions

Due to the electronegative nature of the fluorine atom its introduction into a molecule will affect adjacent polarisable functional groups, which can be exploited to tune pK_a values and reactivities of the drug molecule's functional groups to increase the efficacy of the drug. For example, a fluorine atom next to a carbonyl moiety may activate it towards nucleophilic attack. A fluorine atom will increase the acidity of an adjacent hydroxyl proton, as is the case of fluticasone propionate (anti-inflammatory steroid) in which fluorination resulted in an increased affinity of the drug to the enzyme active site preventing oxidation.[4]

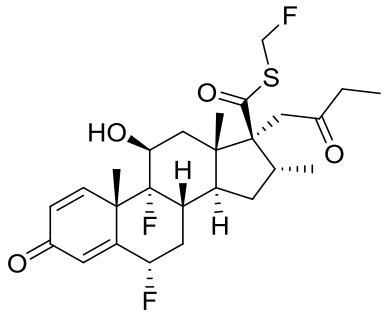

7

Figure 3 *- The structure of fluticasone propionate.*

1.1.2.3. Inhibition of Metabolic Degradation of Drugs

A key stage in the metabolism of drugs and other substances by the liver is oxidation of the molecule, for example, C-H to C-OH. If the key metabolic sites of a drug molecule are determined then the addition of fluorine may be investigated in a bid to resist or decrease the rate of drug metabolism. The strong C-F bond cannot be oxidised, unlike the analogous C-H bond, and so oxidation at that site is prevented. This methodology has been used in the development of a vitamin D_3 derivative that has resulted in a more potent drug due to this decreased rate of metabolism.[19] Hydroxylation of the $–CH_2-$ group at the 24-position deactivates the active form of the molecule ($1,25-(OH)_2-D_3$) and leads to excretion. Substituting the $–CH_2-$ group with a $–CF_2-$ group inhibits this key metabolic step thus increasing drug bioavailability (***Figure 4***).

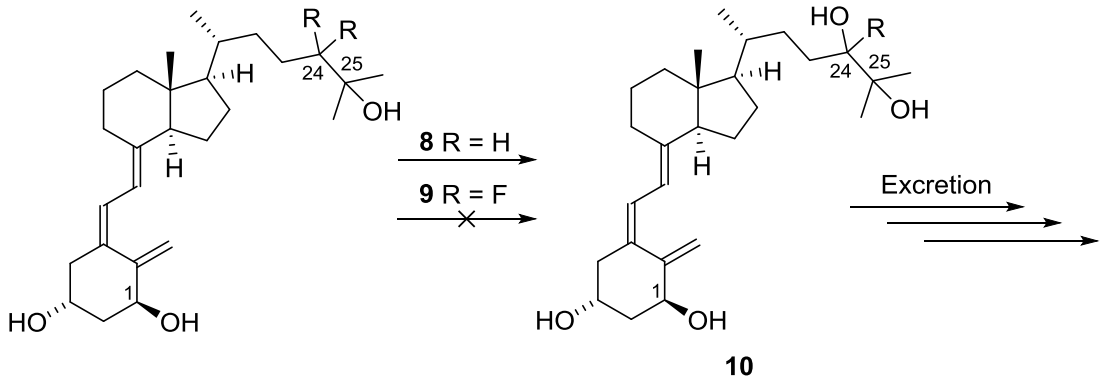

Figure 4 – *Substitution of the 24-position by fluorine prevents metabolism at this site.*

1.1.2.4. The Mimic Effect

Fluorine and hydrogen atoms are not too dissimilar in size (Van der Waals radii 1.47 Å (fluorine), 1.20 Å (hydrogen)) [16] and often go undetected by enzymes. The mammalian citric acid cycle is interrupted in this way.[20,21] Fluoroacetic acid is not distinguished from acetic acid by the first enzyme involved (coenzyme A) and, after some steps, is converted into fluorocitrate which cannot be processed by aconitase and so the catalytic cycle is interrupted.

1.2. Synthesis and Reactions of Organofluorine Derivatives

Since C-F bonds are so rare in nature, the development of methodologies for the formation of new C-F bonds constitutes an important topic in organofluorine chemistry. Numerous fluorinating agents used for the creation of C-F bonds have been developed over the years and some of the key reagents will be discussed in the following sections of this review with a focus on reagents used for the fluorination of heterocycles.

1.2.1. Fluorinating Agents

There are two main types of fluorinating agent available: nucleophilic and electrophilic. Nucleophilic fluorinating reagents generally consist of fluoride ion sources as nucleophiles whereas electrophilic fluorinating agents utilise "F^+" equivalents that are attacked by the nucleophilic moiety of a non-fluorinated starting material.

1.2.1.1. Nucleophilic Fluorinating Agents

1.2.1.1.1. Halogen Exchange (Halex)

One common synthetic route to fluorinated molecules involves the reaction of a nucleophilic fluorinating agent with the analogous halogenated (usually chlorinated) molecule. One such nucleophilic fluorinating agent is spray dried potassium fluoride which is often used in conjunction with 18-crown-6 such as for the halogen exchange reaction of a chlorinated quinolinedione (***Figure 5***).[22]

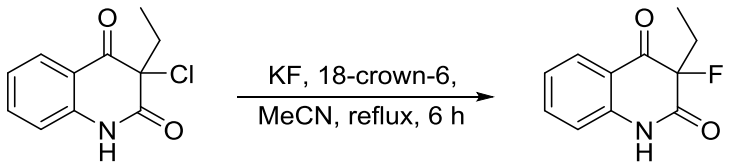

11 76% **12**

Figure 5 *- Halogen exchange reaction of a chlorinated quinolinedione derivative to yield the fluorinated heterocycle.*

1.2.1.1.2. Hydrogen Fluoride Complexes

In terms of practicality of use in a laboratory, HF has an unfavourably low boiling point and so it is frequently used in conjunction with, for example, pyridine or triethylamine to decrease the volatility of the reagent. Additionally, anhydrous HF forms short polymeric chains held together by hydrogen bonds.[23] Solvation disrupts this polymeric interaction making the HF molecules more available for reaction. HF-pyridine is used for the nucleophilic fluorination of a piperidine derivative (***Figure 6***).[24]

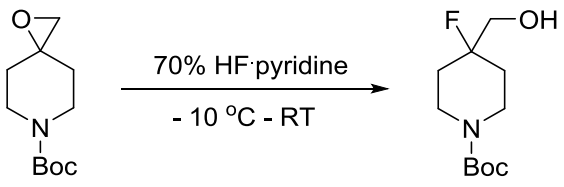

13 **14**

Figure 6 *- Synthesis of fluorinated piperidine using HF-pyridine as the fluorinating agent.*

Hammond and coworkers noted that these HF complexes reduce the acidity of the HF and may interfere with metal catalysts and so developed an HF complex with the cyclic urea 1,3-dimethyl-3,4,5,6-tetrahydro-2(1H)-pyrimidinone (DMPU). DMPU is less basic and is a better hydrogen acceptor than pyridine and is only weakly coordinating to metal catalysts. The resulting DMPU/HF complex is, therefore, more acidic.[25]

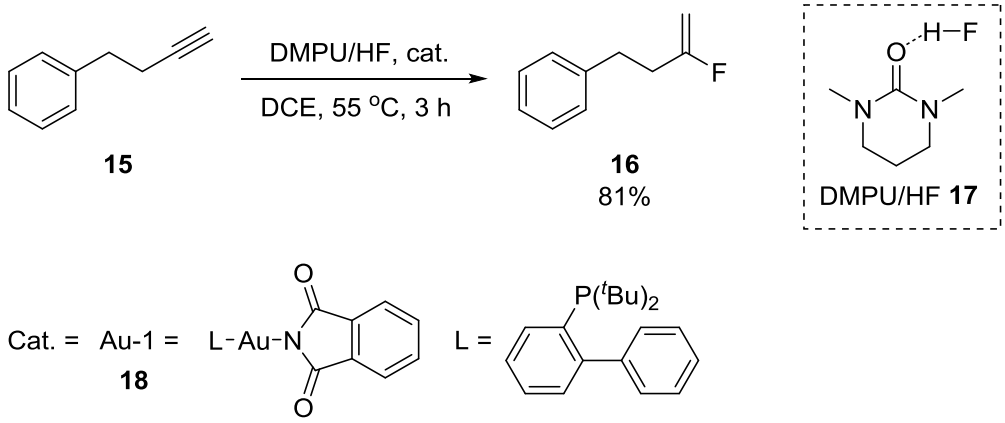

Figure 7 *– Fluorination reaction of a terminal alkyne with DMPU/HF and a gold based catalyst.*

Complexes of HF with BF_3 have also been reported. The $HBF_4{\cdot}OEt_2$ complex has been used in the diazotisation/fluorination reaction of a 1,3-dicarbonyl system (***Figure 8***).[26]

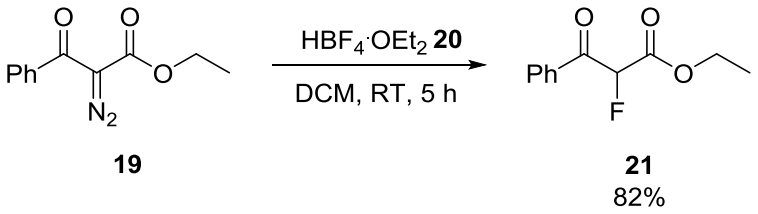

Figure 8 *– Diazotisation/fluorination reaction utilising the HF/BF_3 complex in diethyl ether.*

1.2.1.2. Electrophilic Fluorinating Agents

1.2.1.2.1. N-F Class

One commonly used electrophilic fluorinating agent is Selectfluor™ [27,28] which is convenient to use in any synthetic laboratory and is safer and easier to handle than some alternatives. Selectfluor™ has been used in the synthesis of 3-fluorooxindoles (***Figure 9***).[29]

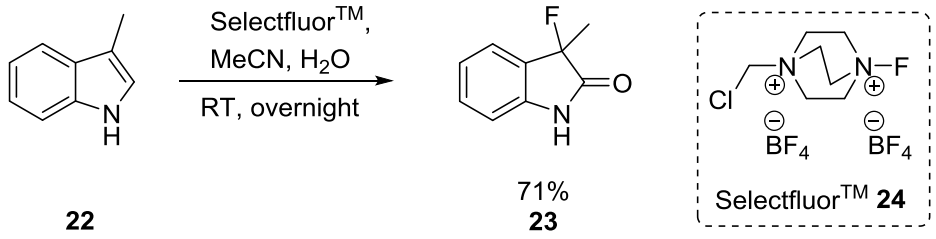

Figure 9 *- Synthesis of fluorinated oxindole derivative by use of Selectfluor™.*

N-Fluorobenzenesulfonimide (NFSI) is another commonly used electrophilic fluorinating agent. ***Figure 10*** shows the use of NFSI in the synthesis of a fluorinated dihydroquinoline derivative in which the cyclic system undergoes a 'late stage' fluorination step to reach the fluorinated heterocyclic product.[30]

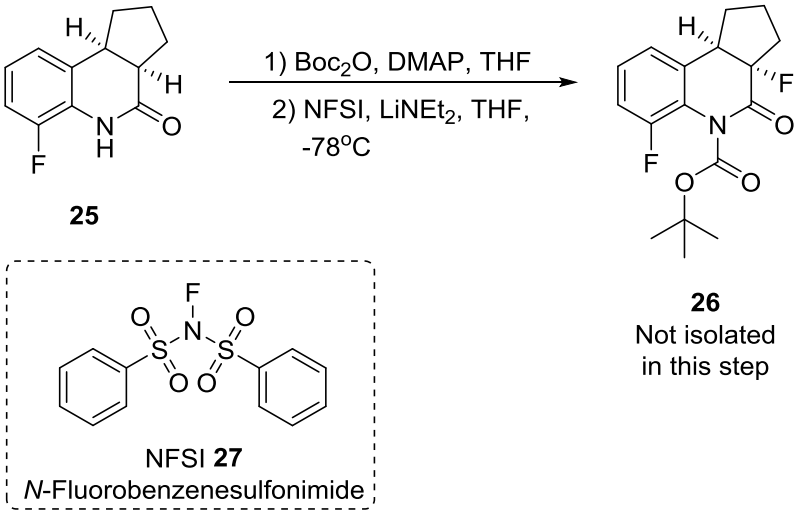

Figure 10 *- An example of the use of NFSI in the synthesis of a fluorinated dihydroquinoline derivative.*

N-Fluoropyridinium salts have also been reported as fluorinating agents. For example, *N*-fluoropyridinium triflate reacts with a silyl enol ether to give the fluorinated product in good yield (***Figure 11***).[31]

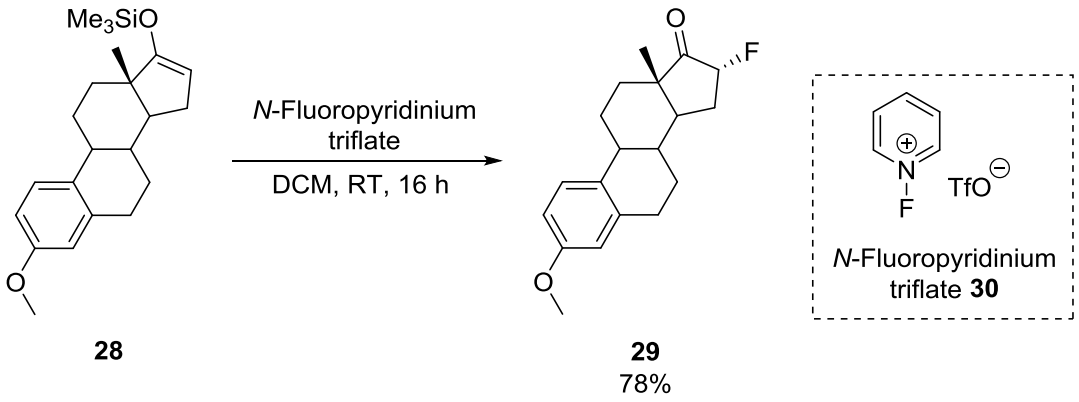

Figure 11 *– A fluoropyridinium salt fluorinates the silyl enol ether of a steroid derivative in good yield.*

1.2.1.2.2. Deoxyfluorinating Agents

This class of fluorinating agents typically substitute a hydroxyl moiety with a fluorine atom. One of the most notable of these reagents is diethylaminosulfur trifluoride (DAST).[32] Deoxo-Fluor® [33] and Fluolead™ [34] were later developed to overcome the thermal instability of DAST. ***Figure 12*** shows the closely related structures of these three deoxyfluorinating reagents and an example reaction for each.

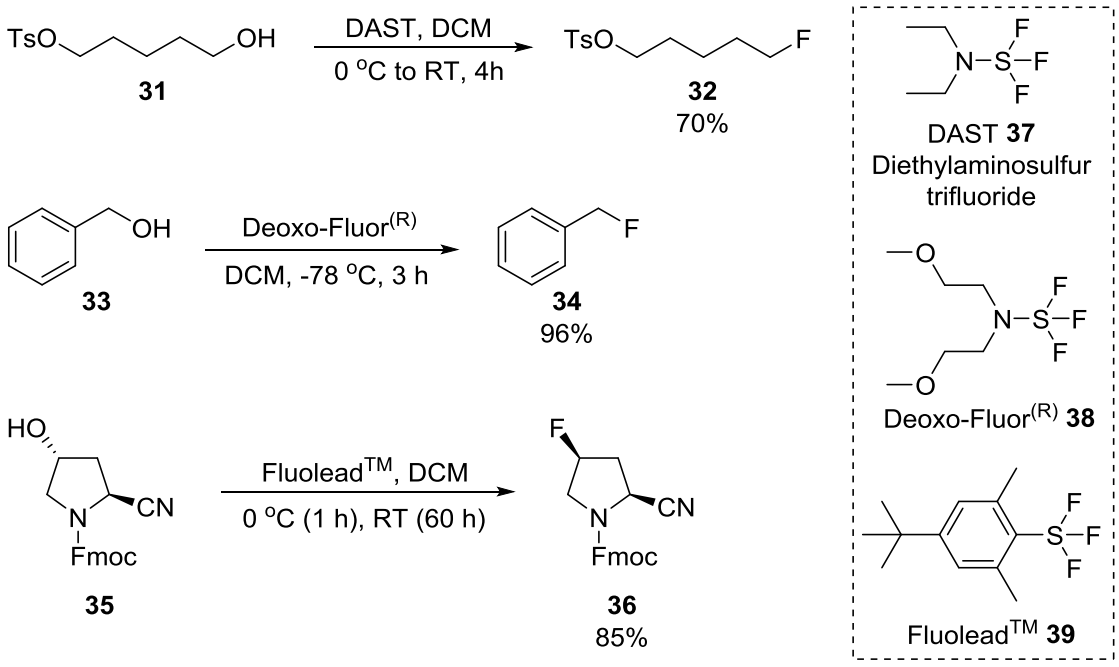

Figure 12 *– The structures and example reactions of DAST, Deoxo-Fluor® and Fluolead™ showing deoxyfluorination of the substrates in very good yield.*

A further development led to two XtalFluor reagents with ethyl (XtalFluor-E®) and morpholine (XtalFluor-M®) based structures similar to DAST. These crystalline tetrafluoroborate salts, however, do not produce corrosive free-HF, are more stable and do not require a hazardous distillation unlike their predecessors. ***Figure 13*** shows the structures of these reagents and example reactions involving the deoxyfluorination of an alcohol and the deoxyfluorination reaction of an aldehyde to a geminal-difluoride.[35]

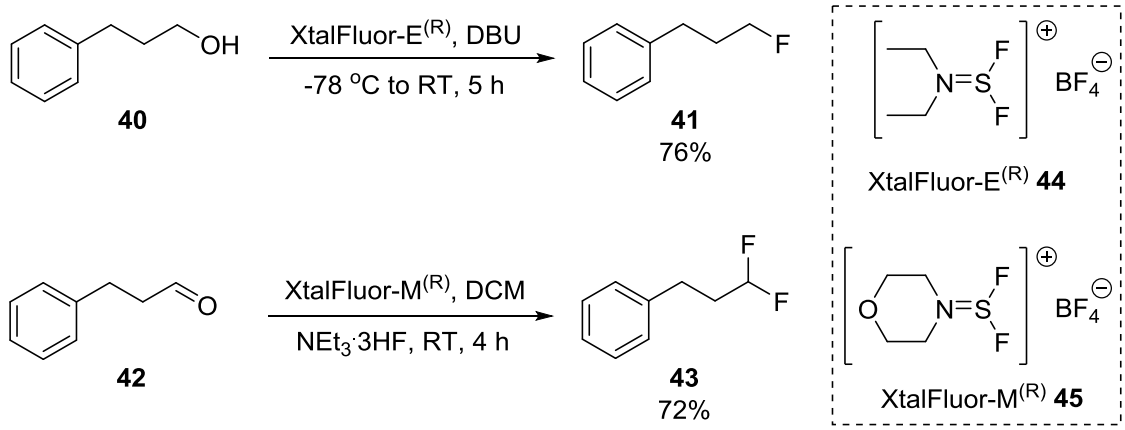

Figure 13 *– The structures of the two XtalFluor® reagents with example deoxyfluorination reactions.*

Another example of a deoxyfluorinating agent is PhenoFluor™.[36] Unlike the previous reagents PhenoFluor™ is not S-F based but instead contains two geminal C-F groups on a nitrogen heterocycle with bulky substituents. This reagent typically works with CsF to deoxyfluorinate alcohols, as in the example in ***Figure 14*** which gives the fluoride in excellent yield.

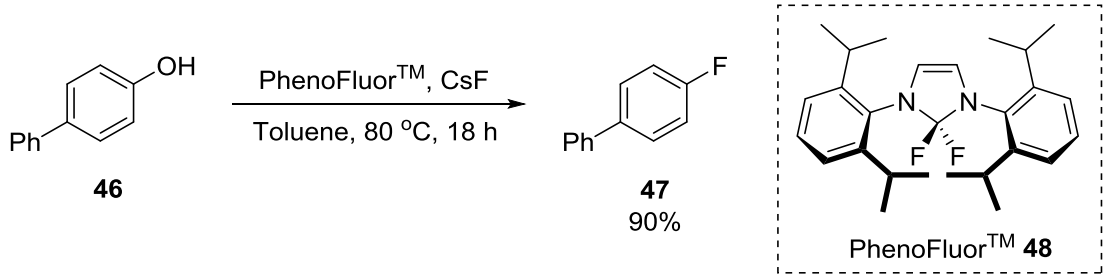

Figure 14 *– The structure and an example deoxyfluorination reaction of PhenoFluor™.*

1.2.1.2.3. Direct Fluorination

One interesting electrophilic fluorinating agent is fluorine gas itself. Research into the use of F_2 as a reagent has increased and it is now generally used as a diluted mixture in nitrogen gas for practical purposes. ***Figure 15*** shows the synthesis of a fluorinated 5-membered oxygen heterocycle giving the product in reasonably high yield.[37]

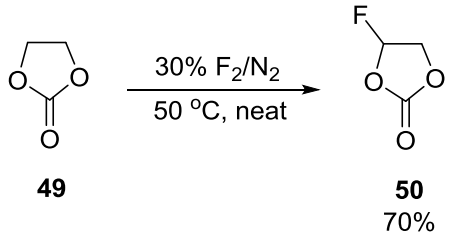

49 **50**
70%

Figure 15 - *Synthesis of a fluorinated 1,3-dioxolan-2-one derivative using direct fluorination methodology.*

One notable benefit to the use direct fluorination methodology over the use of other electrophilic fluorinating reagents is low expense because many electrophilic fluorinating agents are themselves synthesised from F_2. Additional reaction steps are required, therefore, in the synthesis of the fluorinating agents.

Selective fluorination reactions using direct fluorination methodology have been reported. ***Figure 16*** shows the fluorination of a quinolone derivative by a 10% fluorine in nitrogen mixture where a perfluorocarbon fluid (PP11) is used as an inert heat transfer fluid.[38]

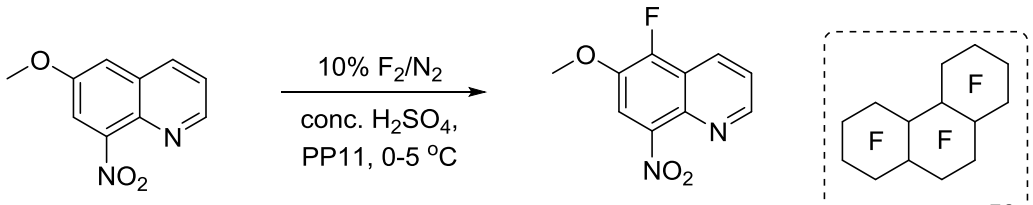

51 **52**
59% conversion 99%

Figure 16 - *The use of direct fluorination methodology in the synthesis of a fluorinated quinolone derivative.*

1.2.1.3. Trifluoromethylating Agents

Though these reagents form C-C bonds rather than C-F bonds, one notable class of reagents include the trifluoromethylating reagents that can be used to deliver a $–CF_3$ group to a molecule. ***Figure 17*** shows an example reaction between one of Umemoto's reagents and a 1,3-dicarbonyl system to give the 2-trifluoromethylated product.[39]

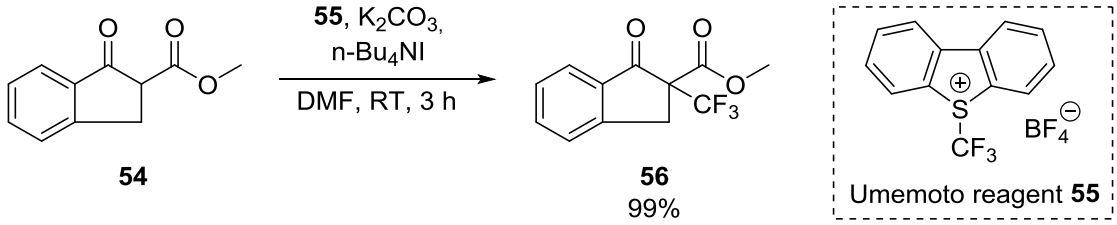

Figure 17 *– The addition of a trifluoromethyl group to a 1,3-dicarbonyl species in excellent yield.*

1.2.2. 'Building Block' Approach for the Synthesis of Fluoroheterocycles

Fluorinated 'building block' processes involve the synthesis of a heterocycle from fluorinated precursor or 'building block' molecules that contain one or more fluorine atom. A potentially important example of a fluorinated 'building block' is the fluoromalonate derivative class of molecules which, in principle, can be used as substrates for the synthesis of a range of fluorinated heterocycles.

These mainly consist of fluoromalonic esters and acids, though can be extended to the use of, for example, amides, α,β-ketoesters or, indeed, other 1,3-dicarbonyl systems.

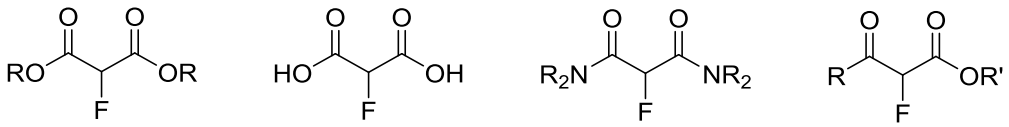

Figure 18 *- Structures of some fluoromalonate analogues.*

In this thesis we develop the chemistry of fluoromalonate esters in the synthesis of fluorinated heterocycles and acyclic analogues, and a brief summary of the current literature is included here.

1.2.3. 2-Fluoromalonate Esters for Heterocyclic Synthesis

The chemistry of 2-fluoromalonate esters has recently been reviewed in the literature[40] and so the following section outlines examples of key syntheses and reactions of these systems.

1.2.3.1. Synthesis of 2-Fluoromalonate Esters

1.2.3.1.1. Halogen exchange

The use of triethylamine trihydrofluoride as the fluorinating agent in this process has been reported for the synthesis of dialkyl fluoromalonic esters from respective chloromalonates.[41] Similarly, this has been achieved by use of potassium fluoride.[42]

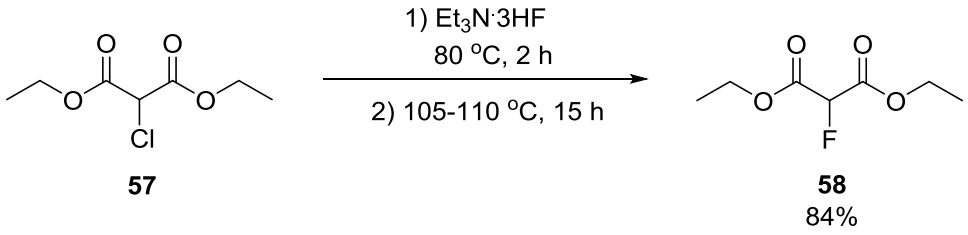

57 **58** 84%

Figure 19 *- Synthesis of diethyl fluoromalonate by halogen exchange methodology.*

1.2.3.1.2. Hexafluoropropene

Another synthetic route to fluoromalonic esters is the alkoxylation of hexafluoropropene. ***Figure 20*** shows the synthetic route to diethyl fluoromalonate by reaction of hexafluoropropene with sodium ethoxide.[43]

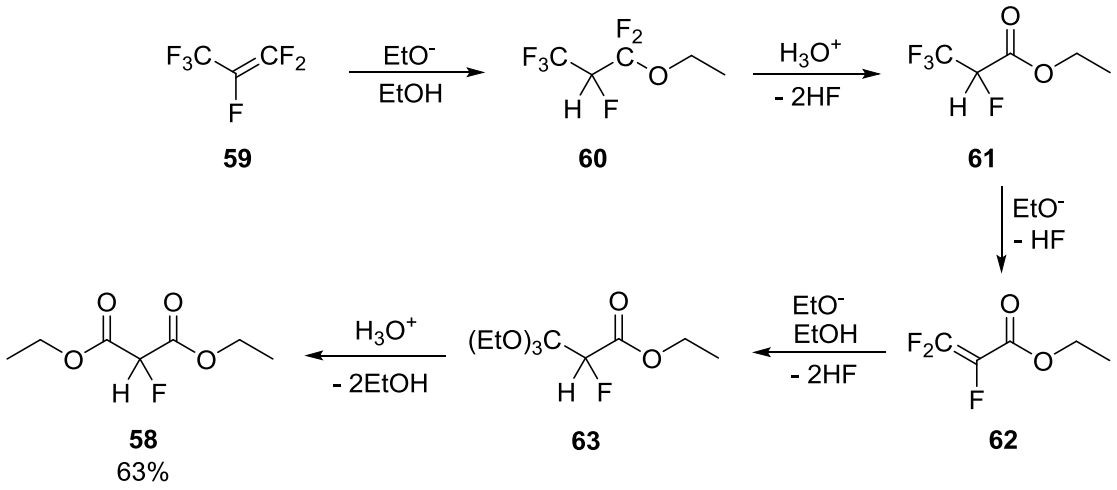

Figure 20 *- Synthesis of diethyl fluoromalonate by alkoxylation of hexafluoropropene.*

1.2.3.1.4. Direct Fluorination

Early attempts to synthesise diethyl fluoromalonate from diethyl malonate using a 10% fluorine in nitrogen gas mixture were generally unsuccessful with the desired product being only one of several products formed. ***Figure 21*** shows the ratio of the isolated products in one such reaction in a microreactor.[44]

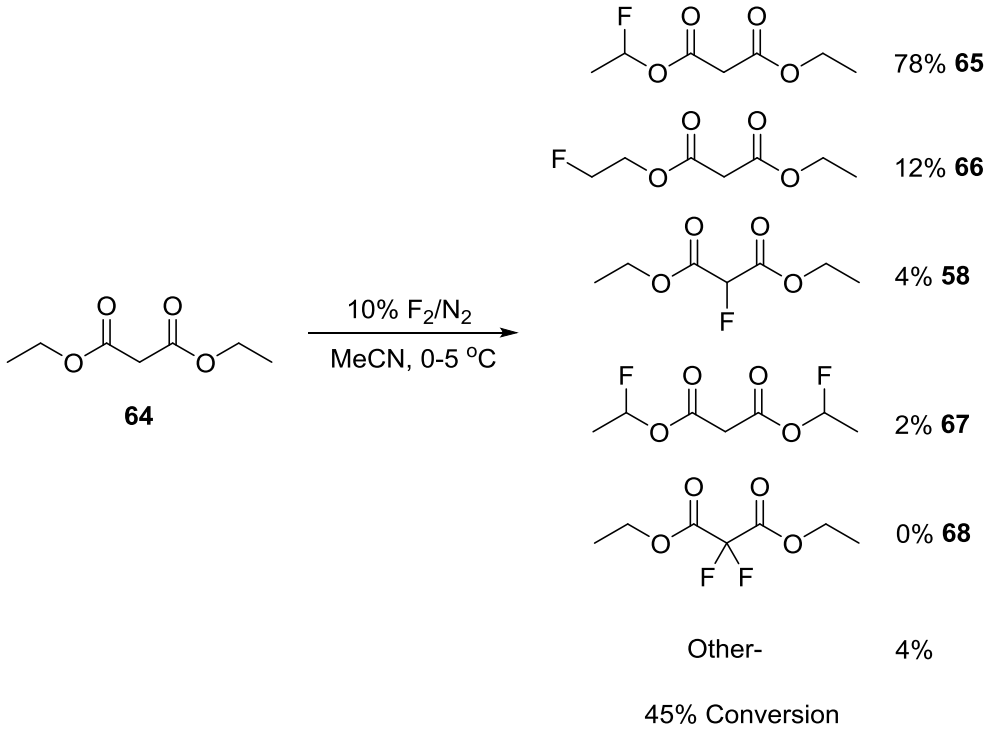

Figure 21 *- Products formed from the direct fluorination reaction of diethyl malonate.*

The use of Meldrum's acid was investigated in a bid to increase selectivity of the fluorination reaction. By removing some of the sites available to fluorination a greater level of control over the products formed was achieved. With a conversion of 83% to the desired fluoromalonate and 17% to the difluorinated by-product this process is a significant improvement to the analogous fluorination reactions of diethyl malonate.[44]

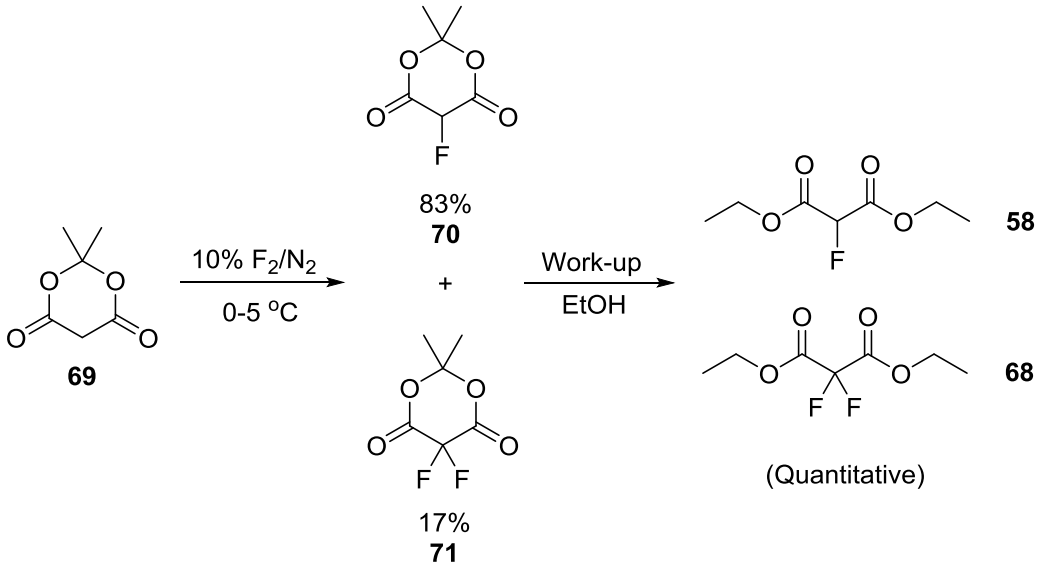

Figure 22 *- Fluorination of Meldrum's acid.*

The direct fluorination of malonic esters has also been reported with the use of transition metal salt catalysts.[45] Copper (II) nitrate salts were shown to catalyse the synthesis of diethyl fluoromalonate from diethyl malonate in good yield and good selectivity, with the difluorinated by-product being formed in only small amounts. ***Figure 23*** shows the synthetic route to the fluorinated product catalysed by copper nitrate.[46] More recently, this reaction has been optimised by the Durham group.[40]

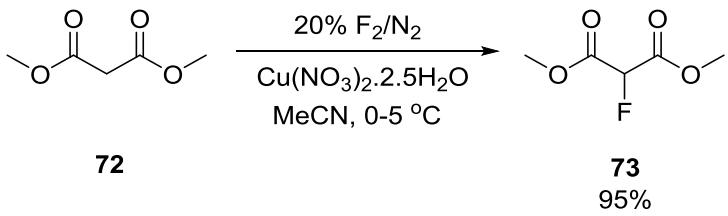

Figure 23 *- Synthesis of fluoromalonate by direct fluorination methodology with a copper nitrate catalyst.*

The malonate precursors coordinate to the copper and enolise. The enolate form is the reactive form that undergoes the fluorination reaction.

1.2.3.2. Reactions of Fluoromalonate

Given that the syntheses and reactions of fluoromalonate have recently been extensively reviewed[40] the following section offers an overview, therefore, of some of the key reactions that demonstrate the versatility of the fluorodiester building block as it reacts as a nucleophile and an electrophile.

1.2.3.2.1. Alkylation Reactions

An important factor concerning the reactivity of fluoromalonates or other analogous 1,3-dicarbonyl systems is the stability of the corresponding carbanion. Interestingly, alkylation reactions of fluoromalonates proceed slower than those of the analogous malonates because the electron withdrawing fluorine atom removes electron density from the carbanion making it a poorer nucleophile.[43]

Alkylation reactions of malonates have been reported. ***Table 1*** shows the results of reactions between diethyl fluoromalonate with several different alkyl bromides and the subsequent ester hydrolysis reactions to form the corresponding substituted fluorinated diacids.[42]

Table 1 *- Alkylation reactions of diethyl fluoromalonate with various alkyl bromides.*

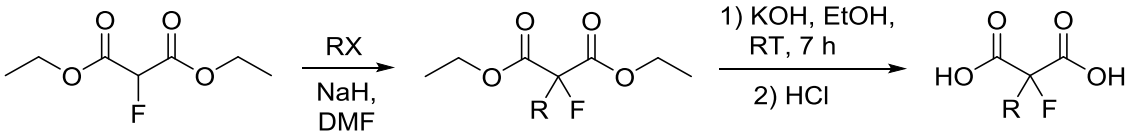

58

Alkyl halide (RX)	Yield of diacid / %
CH_3CH_2Br	78
$CH_3(CH_2)_2Br$	74
$(CH_3)_2CHBr$	57
$CH_3(CH_2)_3Br$	51
$F(CH_2)_4Br$	78
$EtO_2C(CH_2)_4Br$	58
$CH_3(CH_2)_{15}Br$	81
$C_6H_5CH_2Cl$	75

1.2.3.2.2. Michael Addition Reactions

Michael addition reactions of fluoromalonic esters with a variety of Michael acceptors have been reported. Of particular interest are those reactions that yield an enantiomerically enriched product via an asymmetric synthesis route, often involving an enantiomerically pure catalyst. For example, reactions of diethyl fluoromalonate with chalcone derivatives make use of chiral phase transfer catalysts and have been reported to yield asymmetric Michael addition products in up to 47% *ee* (***Figure 24***).[47] Michael reactions of dibenzyl malonate with chalcones have also been investigated.[48]

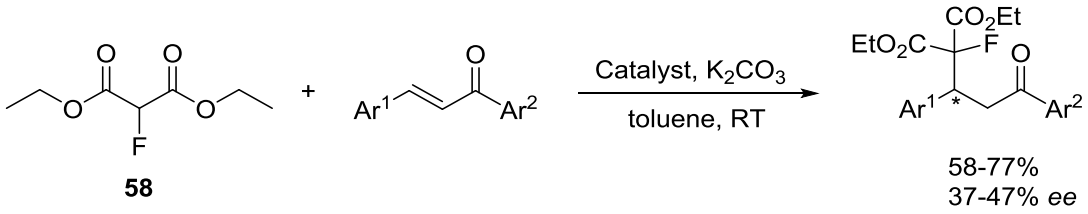

Figure 24 - *Synthesis of chiral Michael addition products from diethyl fluoromalonate and Michael acceptors with an asymmetric catalyst.*

The asymmetric Michael addition reactions of fluoromalonate with α,β-unsaturated aldehydes have been catalysed by enantiomerically pure pyrrolidine derived catalysts with good *ee* (***Figure 25***).[49]

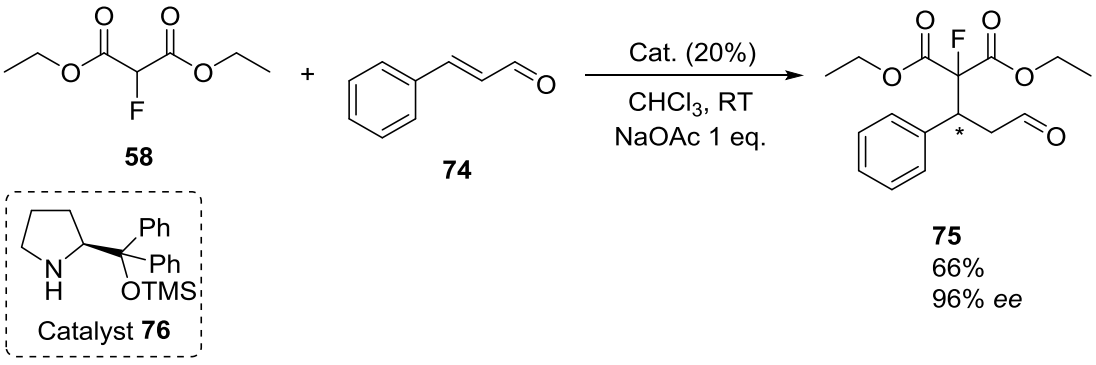

Figure 25 - *Synthesis of an enantiomerically enriched Michael addition product from fluoromalonate and an α,β-unsaturated aldehyde with an asymmetric pyrrolidine base catalyst.*

The reactions of diethyl fluoromalonate with nitroalkenes have been investigated using a large enantiomerically pure nickel complex catalyst (***Figure 26***) giving product **78a** in 97% yield and 97% *ee* in 20 h. Substituted phenyl derivatives were also obtained in good yields and enantioselectivities (≥ 91% yield, ≥ 91% *ee*).[50]

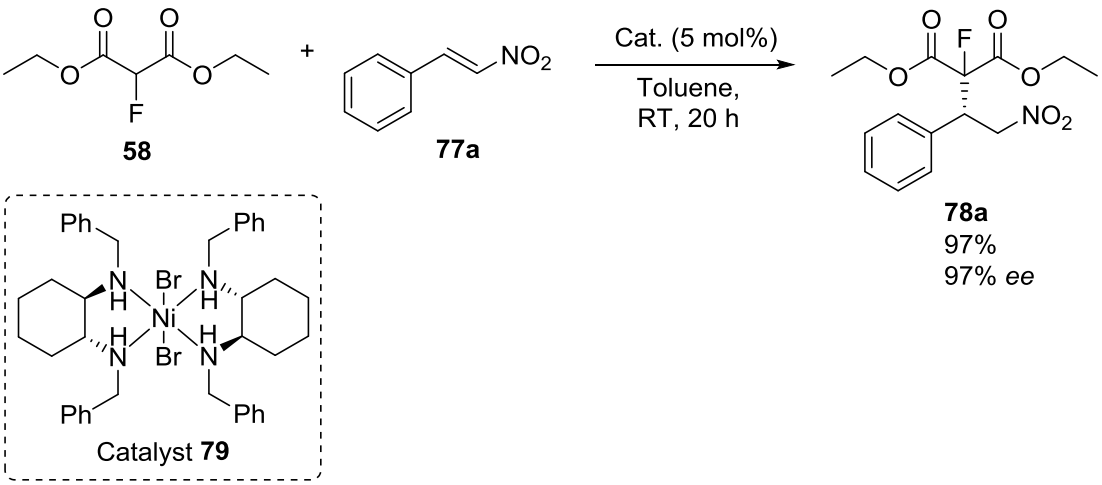

Figure 26 *- Synthesis of enantiomerically enriched Michael addition product using enantiomerically pure nickel complex catalyst.*

Michael addition reactions of fluorinated 1,3-dicarbonyl systems other than fluoromalonates have also been reported. The reactions of α-fluoro-β-ketoesters with Michael acceptors have been reported and the resulting fluorinated 1,5-dicarbonyl compound has been used in the synthesis of fluorinated carbocycles (***Figure 27***).[51]

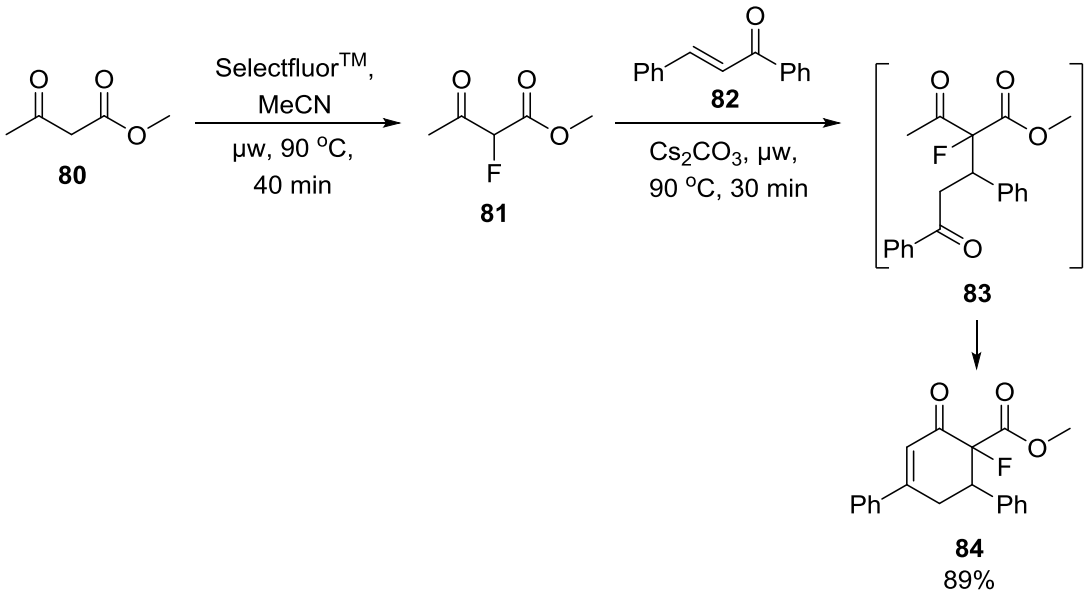

Figure 27 *- Microwave assisted synthesis of a fluorinated 1,5-dicarbonyl system via Michael addition reaction of a fluorinated β-ketoester with a phenyl substituted Michael acceptor, and subsequent transformation to a fluorinated carbocycle.*

1.2.3.2.3. Reaction of 2-Fluoromalonate Esters with Dinucleophiles

Other than the nucleophilic 2-position of the 1,3-dicarbonyl system, the other reactive sites of fluoromalonate systems are the carbonyl carbons that are susceptible to nucleophilic attack. Cyclic systems can be formed through reaction at the carbonyl groups with two complementary reactive sites. ***Figure 28*** shows the formation of a fluorinated 7-membered heterocycle by reaction of fluoromalonate with a diamine.[43]

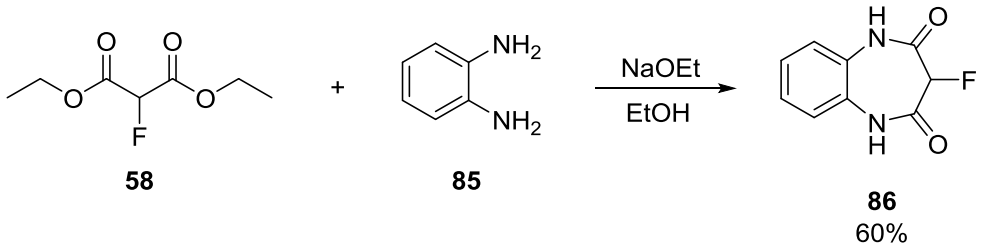

Figure 28 - *Synthesis of a 7-membered fluorinated heterocycle by reaction of diethyl fluoromalonate with a dinucleophile.*

Similarly, fluoromalonate has been used as a fluorinated 'building block' in the synthesis of large macrocyclic ring systems. Reaction with the dinucleophile tetraethylenepentamine yielded the fluoromacrocycle shown in ***Figure 29***.[52] The macrocycle has been used as a chelating ligand for heavy metals and some have been shown to exhibit biological activity.[53]

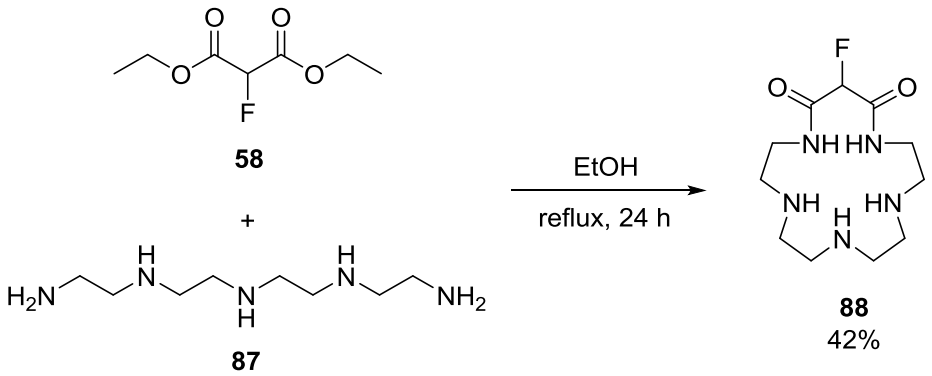

Figure 29 - *Synthesis of fluorinated macrocycle from diethyl fluoromalonate.*

The Durham group have reported the synthesis of heterocycles by reaction at one carbonyl site and the nucleophilic 2-position of diethyl fluoromalonate (***Figure 30***).[54] The first step involves alkylation of fluoromalonate by a 2-nitrobenzyl bromide derivative which is, after reduction, followed by nucleophilic attack of the carbonyl carbon by the amine group.

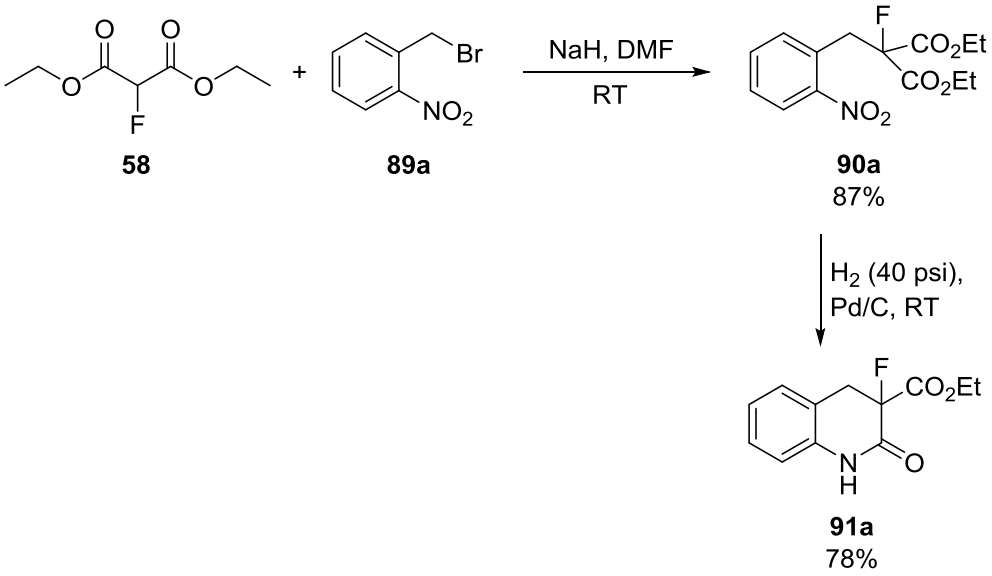

58 **89a** **90a** 87% **91a** 78%

Figure 30 *- Synthesis of a fluorinated tetrahydroquinoline derivative from diethyl fluoromalonate.*

Similarly, 1-fluoro-2-nitrobenzene was reacted with fluoromalonate and, upon reduction, yielded a 5-membered fluorinated indole derivative.[55]

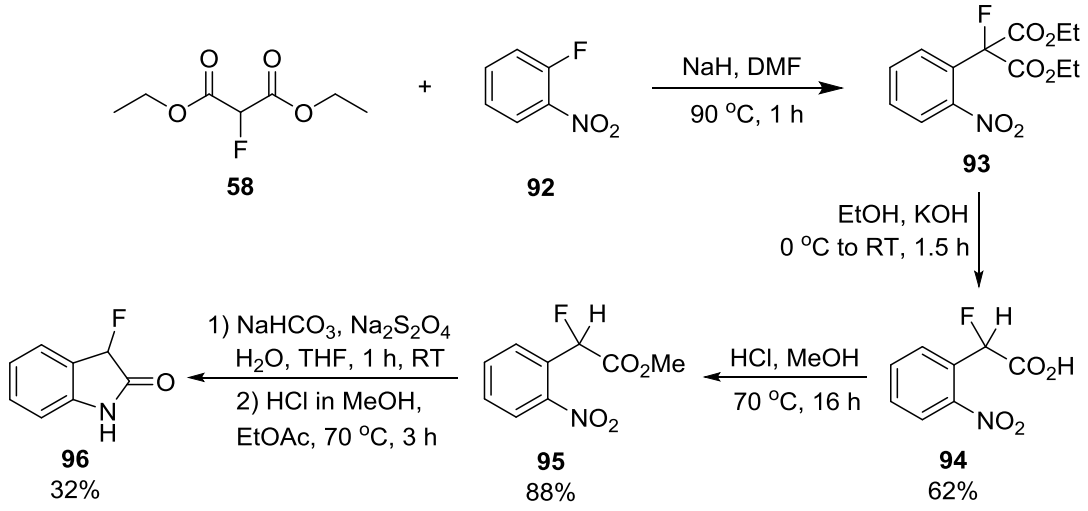

58 **92** **93** **94** 62% **95** 88% **96** 32%

Figure 31 *- Reactions of diethyl fluoromalonate first with the electrophilic fluorine and then with the nucleophilic amide group of the substituted benzene compound.*

Fluoromalonate has also been used in the synthesis of fluorinated carbocycles in a similar manner (***Figure 32***).[56]

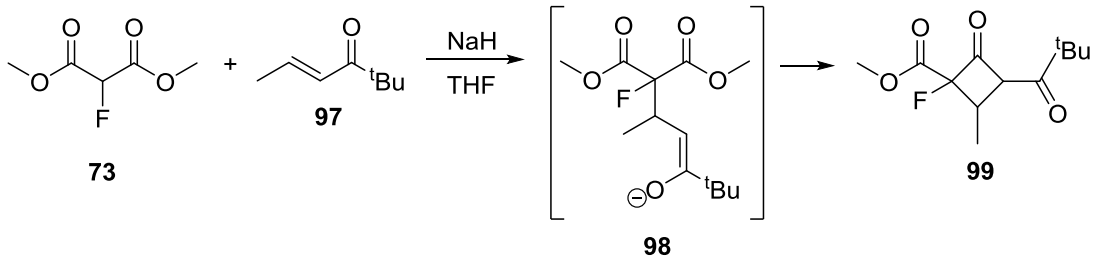

Figure 32 - *Synthesis of a 4-membered carbocycle from dimethyl fluoromalonate.*

Thus, fluoromalonates are potentially useful 'building blocks' for a wide range of systems and their chemistry is developed further in this thesis. A related form of the research described in this thesis is the synthesis of fluoroamidoesters and so their literature syntheses are discussed below.

1.3. Synthetic Routes to Fluoroamidoesters

This literature review outlines the synthetic routes to 2-fluoro-1,3-amidoesters present in the literature as of February 2017 and, since these examples are numerous, only entries describing the initial formation of a fluoroamidoester from a non-fluoroamidoester starting material are included in this review rather than subsequent reactions of fluoroamidoester substrates.

1.3.1. Fluorination of Amidoesters

There are four main classes of starting material that can be fluorinated to form fluoroamidoesters (***Figure 33***). Though examples are found from each category, by far the most populous route in the literature is the fluorination of lactams with adjacent ester moieties. Considerably fewer examples exist of fluorination reactions of lactones (with adjacent amide moieties), diheterocyclic derivatives or acyclic amidoesters.

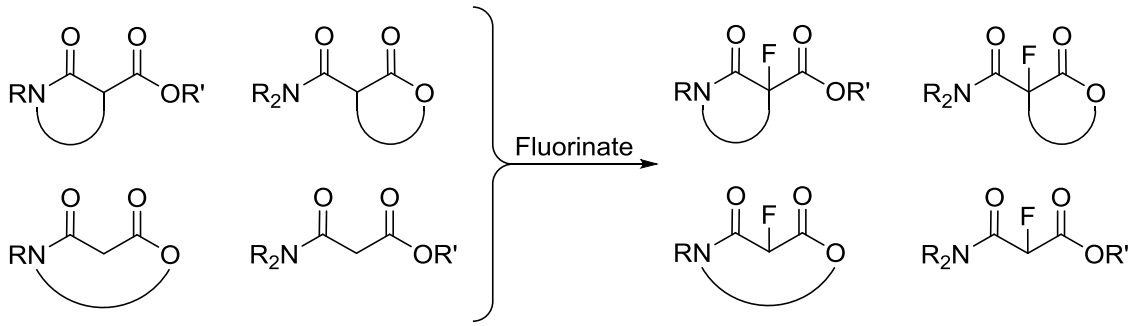

Figure 33 – *Amidoester substrates for fluorination.*

1.3.1.1. Fluorination Reactions of Lactams

Fluorination reactions of lactams, either 5- or 6-membered ring systems, using a variety of fluorinating agents have been reported in symmetric and asymmetric syntheses.

Behenna *et al*. claim to have fluorinated 5- and 6-membered lactams to give the corresponding fluoroamidoesters (***Figure 34***).[57] Subsequent enantioselective palladium-catalysed decarboxylative allylic alkylation of these, and related, systems afforded a series of enantiomerically enriched fluorolactams.[58]

Similarly, Norman *et al*. investigated and developed a series of new class II c-Met inhibitors. The authors used NFSI to fluorinate a 5-membered lactam to give the desired fluoroamidoester in 64% yield (***Figure 34***).[59]

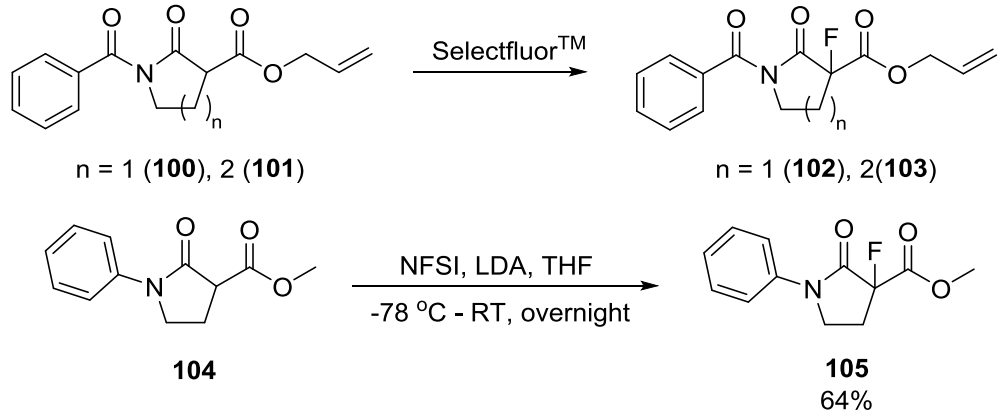

Figure 34 *– Fluorination of lactam derivatives by Selectfluor™ and NFSI.*

Wang *et al*. reported the fluorination of a pyridazinone derivative in 100% yield after purification by silica column chromatography (***Figure 35***).[60] The product was investigated as an intermediate in the development of potential mitogen-activated protein/extracellular signal-regulated kinase kinase (MEK) inhibitor for the treatment of hyper-proliferative diseases such as cancer and inflammation.

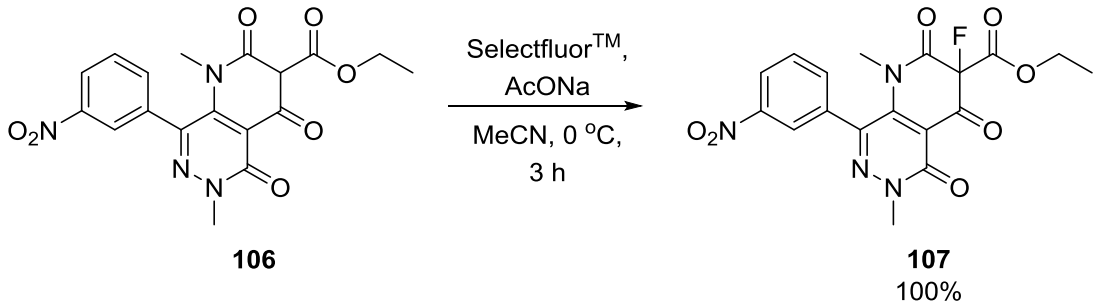

Figure 35 *– Fluorination of a more complex pyridazinone lactam derivative by Selectfluor™.*

Miyashita and co-workers investigated a series of 5-fluorouracil derivatives to improve the efficacy of this important anticancer drug. A portion of this work involved the synthesis of fluoroamidoester derivatives. ***Table 2*** displays selected results of the direct fluorination of uracil derivatives using fluorine gas.[61] ***Figure 36*** is an example of related work using trifluoromethyl hypofluorite as the fluorinating agent.[62]

Table 2 – *Yields and conditions of a series of fluorination reactions of uracil derivatives.*

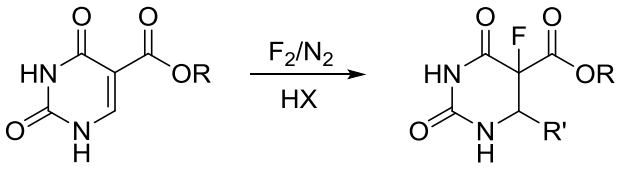

108a-g **109a-g**

Entry	Product	R	R'	F_2/N_2 /%	Yield /%
1	**109a**	Me	OH	25	79
2	**109b**	Et	OH	25	51
3	**109c**	^{i}Pr	OH	25	58
4	**109d**	Bu	OH	25	50
5	**109e**	^{sec}*Bu*	OH	23	29
6	**109f**	Me	OAc	10	81
7	**109g**	Et	OAc	15	72[a]

[a] Used without further purification

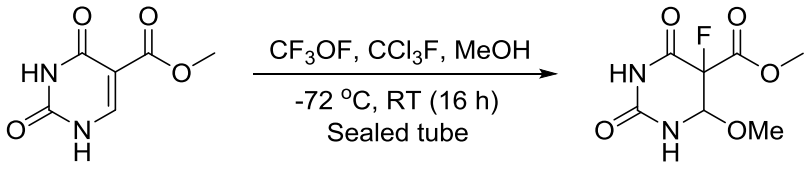

108a **109h** 93%

Figure 36 – *Fluorination of a uracil derivative by trifluoromethyl hypofluorite.*

Trzupek *et al*. reported the fluorination reaction of a bicyclic fused amidoester in good yield in their investigations for the treatment of autoimmune and inflammatory diseases associated with Interleukin-1 Receptor Associated Kinase (IRAK) (***Figure 37***).[63]

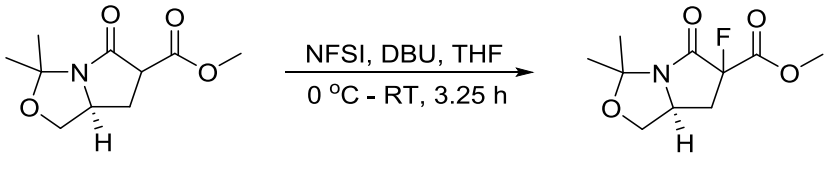

110 **111** 68%

Figure 37 – *Fluorination reaction of a lactam using NFSI.*

Liu *et al*. reported the cyclisation/fluorination reaction of an acyclic amidoester where mechanistic studies suggest that the fluorination reaction occurs after formation of the lactam (***Figure 38***).[64]

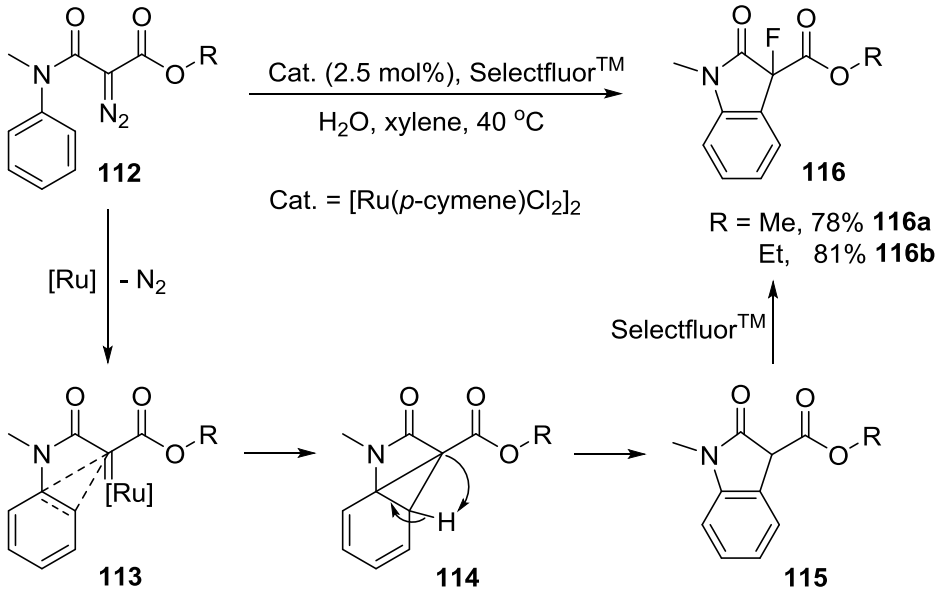

Figure 38 – *Proposed mechanism of the cyclisation/fluorination reaction of an acyclic amidoester.*

Bloxham *et al*. reported the NFSI fluorination of a lactam derivative to give the fluoroamidoester in 86% yield (***Figure 39***).[65]

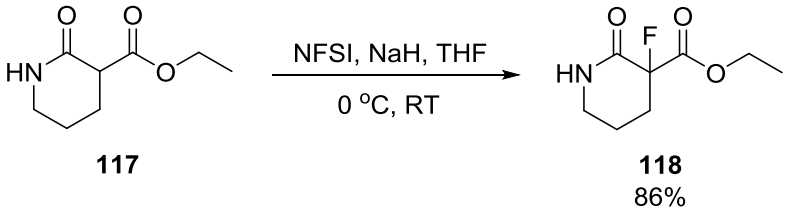

Figure 39 *- Fluorination of a 6-membered lactam derivative by NFSI.*

The analogous enantioselective late stage fluorination of this lactam has been reported using a bulky chiral palladium based catalyst on >100 g scale (***Figure 40***).[66] The *ee* of the product was 44% which improved to >99% by chiral HPLC. These systems were being investigated in the development of spleen tyrosine kinase (Syk) inhibitors by GSK.

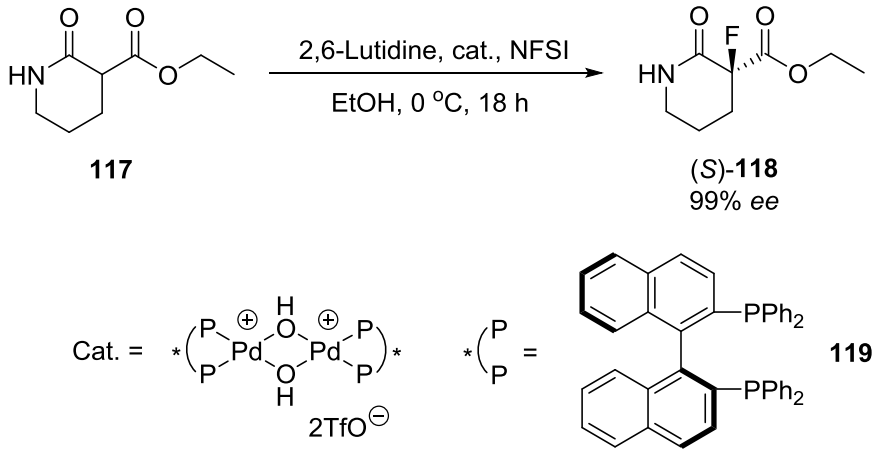

Figure 40 *- Enantioselective late stage fluorination of a 6-membered lactam by NFSI using chiral Pd based catalyst.*

This reaction was later modified and scaled up to 37.0 kg of amidoester starting material. Reaction with (+)-menthol followed by a palladium complex catalysed enantioselective fluorination step gave the diastereomeric fluoroamidoester in 68% yield and 100% *de* (***Figure 41***).[67]

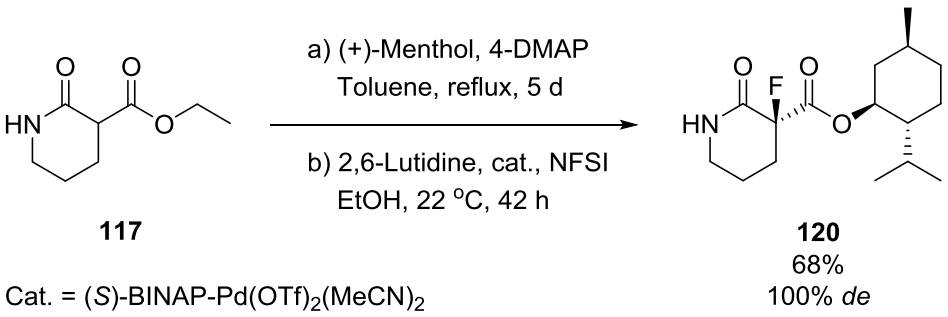

Figure 41 *- Transesterification and subsequent enantioselective late stage fluorination of a 6-membered lactam by NFSI using chiral Pd based catalyst on multikilo scale.*

Suzuki *et al*. reported the enantioselective fluorination reactions of 6- and 5-membered lactams in good yields and excellent *ee*s (***Figure 42***).[68] ***Figure 43*** shows the synthesis of a related enantiomerically enriched 5-membered fluorolactam with considerably bulkier ester and amide moieties in 45% yield and 99% *ee*.

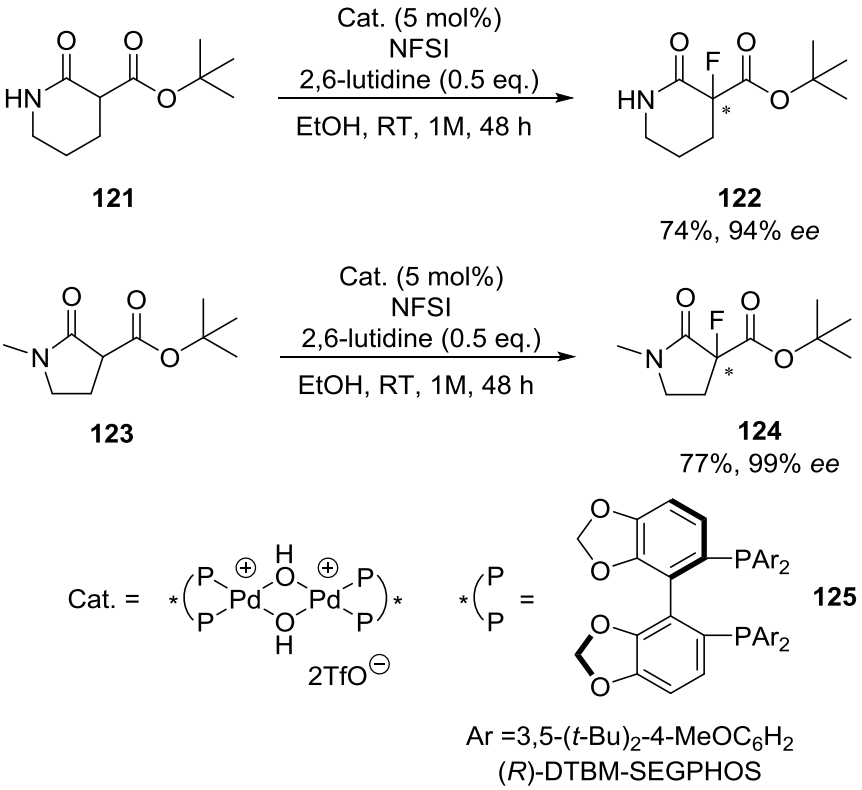

***Figure 42** – Enantioselective fluorination reactions of a 6-membered lactam catalysed by a palladium based SEGPHOS derived catalysts.*

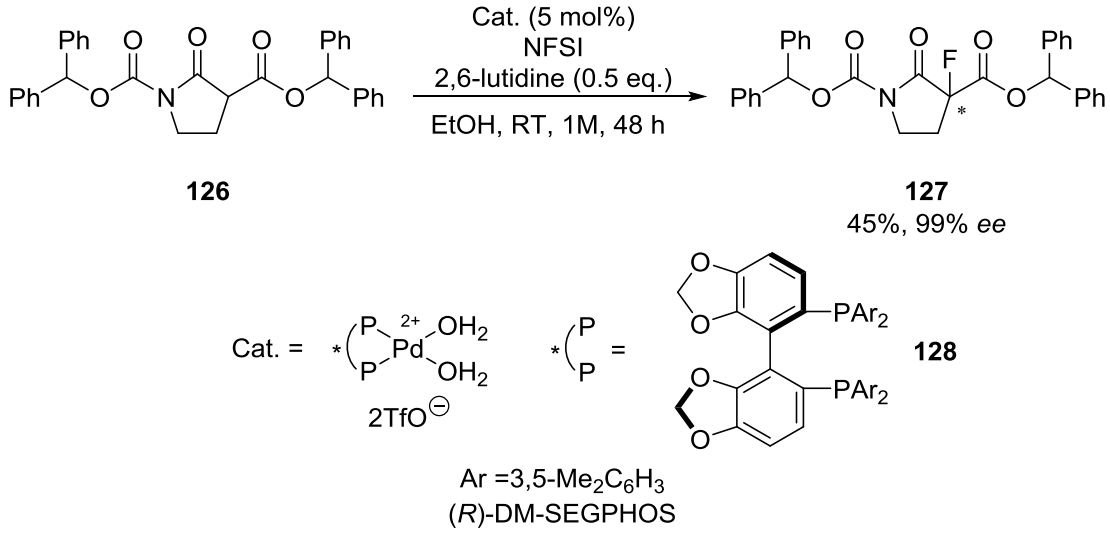

***Figure 43** – A related synthesis of a more sterically bulky fluoroamidoester using NFSI and a palladium based SEGPHOS derived catalysts.*

Shibata *et al*. used a cinchona alkaloid/Selectfluor™ combination to fluorinate an amidoester with some stereoselectivity (37% *ee*, absolute configuration not determined) (***Figure 44***).[69] The alkaloid/Selectfluor™ combination consisted of 1.5 equivalents of each and the alkaloid used was a *bis*-dihydroquinidine (DHQD) derivative.

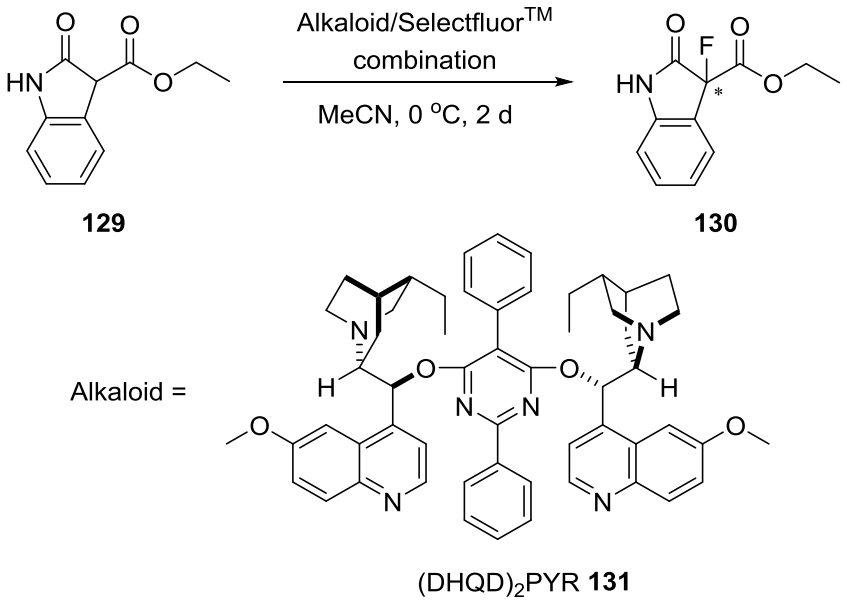

Figure 44 – *Selectfluor™ mediated fluorination reaction of a lactam using an alkaloid derivative to induce asymmetry.*

Heinrich *et al*. claim to have synthesised an enantiomerically enriched fluoroamidoester by reaction of diethylamino-sulfur trifluoride (DAST) with the analogous hydroxyamidoester of inverse stereogenicity. The hydroxyl precursor was prepared by resolution of the racemate by chiral HPLC (***Figure 45***).[70] These systems are being investigated in the development of methionine aminopeptidase (MetAP-2) inhibitors.

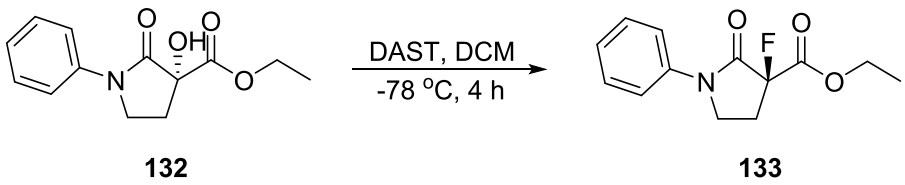

Figure 45 – *Fluorination reaction of a 5-membered hydroxyl-lactam derivative with inversion of configuration.*

1.3.1.2. Fluorination Reactions of Lactones

Hayamizu *et al*. reported the stereoselective late stage fluorination of a lactone derivative giving the (-) enantiomer in 96% yield and 79% *ee* (***Figure 46***).[71]

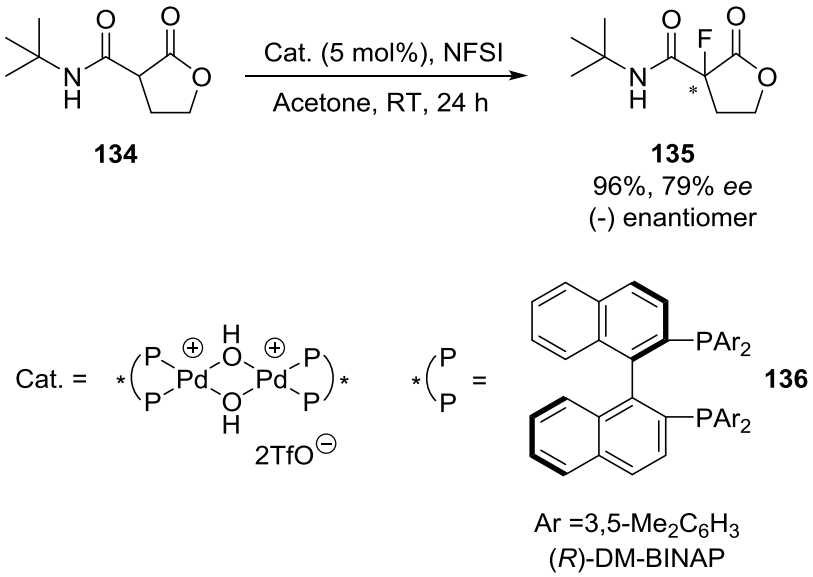

Figure 46 *– Palladium based catalysed enantioselective fluorination of a lactam.*

1.3.1.3. Fluorination Reactions of Diheterocycles

Sato *et al*. reported the fluorination reaction of an oxazine derivative by treating it with 1-fluoro-2,4,6-trimethylpyridinium triflate (FTT) to give the cyclic fluoroamidoester in quantitative yield (***Figure 47***).[72]

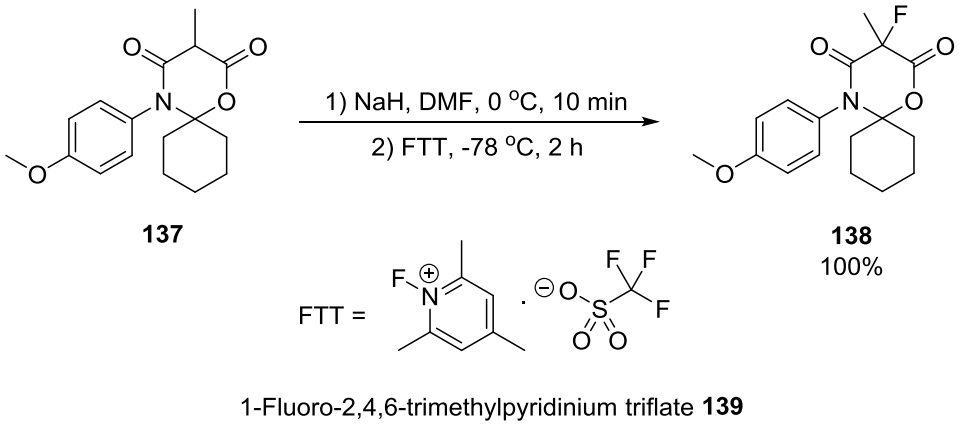

Figure 47 *– Fluorination reaction of an oxazine derivative by FTT.*

The authors also reported an analogous diastereoselective fluorination of a related oxazine derivative containing a chiral menthyl group (***Figure 48***). The preferred conformation of this oxazine strongly influences the angle of electrophilic attack of the enolate such that attack of the α face is favoured with a diastereomeric ratio of around 20:1 versus attack of the β face. Facile recrystallisation of the diastereomeric mixture gives the desired fluoroamidoester diastereomer in high yield.

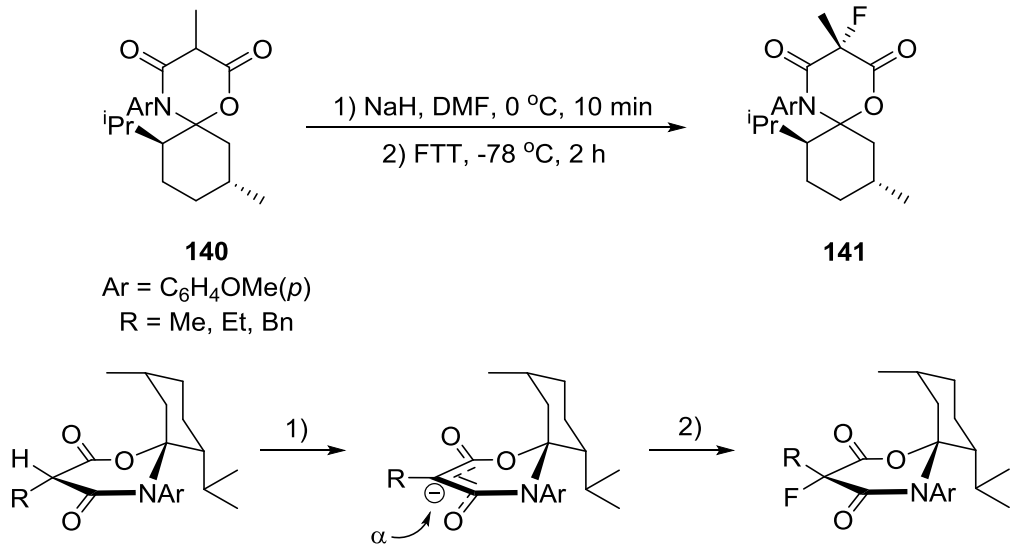

Figure 48 *– Diastereoselective fluorination reaction of an oxazine derivative by FTT.*

1.3.2. Esterification and Amidation Reactions of Acyclic Fluorodicarbonyl Derivatives

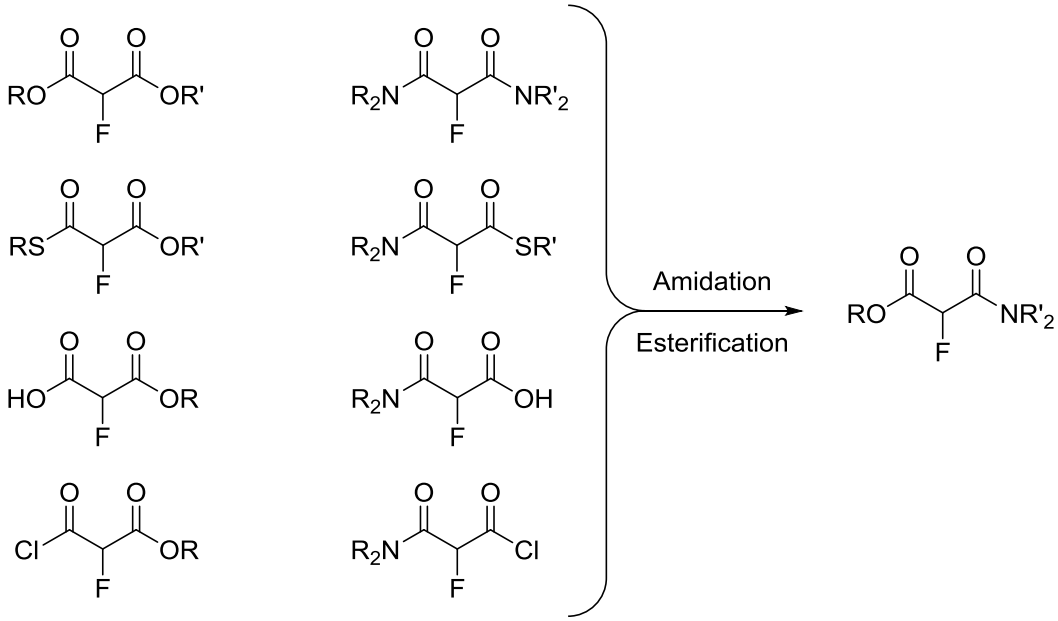

Figure 49 – *Eight possible classes of substrates for amidation or esterification reactions to yield fluoroamidoesters.*

Figure 49 shows eight examples of starting material structures in this category, five of which are realised in the literature. All four examples with ester moieties have literature precedence as does the fluoroamido acid derivative. The most populous synthetic routes are the amidation reactions of fluorodiester derivatives, followed by amidation reactions of fluoroester acids.

This discrepancy between the prevalence of fluoroester starting materials and the lack of fluoroamide starting materials in this section possibly reflects the commercial availability of fluoromalonate esters or is possibly due to the relative difficulties involved with esterification reactions in the presence of unprotected amide moieties. The few literature examples of esterification in the presence of an amide proceed not by the nucleophilic attack of an alcohol but rather by alkylation of the carboxylate moiety by an electrophilic methylating agent or by use of a coupling reagent.

1.3.2.1. Amidation Reactions of Fluorodiesters

1.3.2.1.1. Intermolecular Amidation Reactions Yielding Acyclic Products

Wang *et al.* reported a series of amidation reactions of diethyl fluoromalonate with small to relatively large amines in good yields (***Table 3***).[73] These reactions are generally solventless unless an HCl/HBr salt of the amine is used.

Table 3 – *Conditions and yields of amidation reactions of diethyl fluoromalonate.*

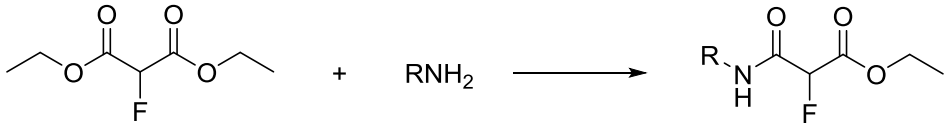

58 **142a-h**

Entry	Cpd	Amine		Time /h	Temp. /°C	Solvent	Base	Yield /%
1	**142a**	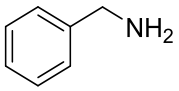	**143**	16	25	-	-	65
2	**142b**	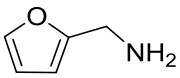	**144**	16	25	-	-	85
3	**142c**	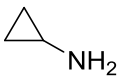	**145**	16	25	-	-	95
4	**142d**	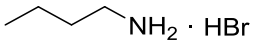	**146**	12	25	Dioxane	NEt_3	99
5	**142e**	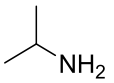	**147**	8	25	-	-	41
6	**142f**	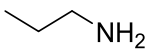	**148**	16	25	-	-	99
7	**142g**	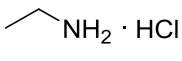	**149**	10	50	EtOH	Na_2CO_3	95
8	**142h**	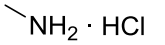	**150**	10	50	MeOH	NEt_3	90

Similarly, Pritchard and Chhabra reported the reaction of diethyl fluoromalonate with n-octylamine to give the resulting fluoroamidoester in 47% yield which was being investigated for its immunosuppressive activity (***Figure 50***).[74]

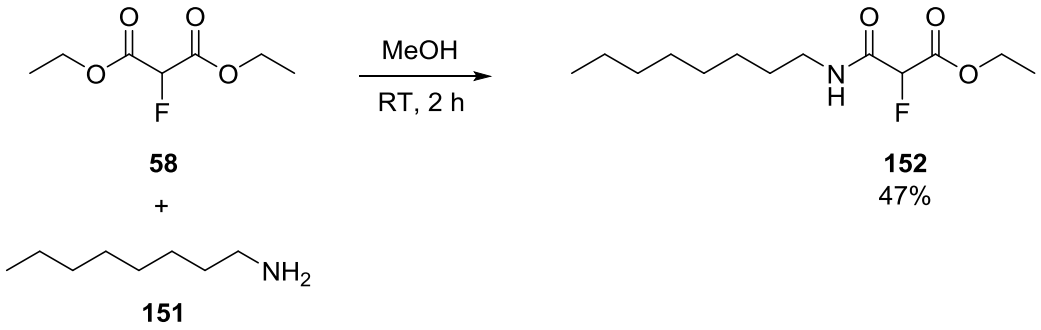

Figure 50 – *The reaction of diethyl fluoromalonate with octylamine to form the corresponding fluoroamidoester.*

Boyd *et al*. claim to have reacted diethyl fluoromalonate with 4-amino-1-benzyl-piperidine in a solventless reaction to produce the desired fluoroamidoester as VLA-1 integrin antagonists (***Figure 51***).[75]

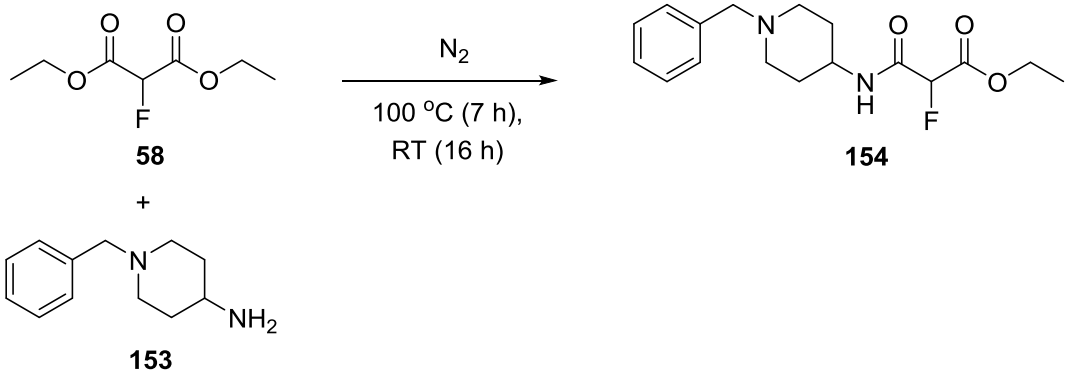

Figure 51 – *An amidation reaction of diethyl fluoromalonate with heat under an inert atmosphere.*

Asano *et al*. claim to have reacted diethyl fluoromalonate with a benzyl indol-amine derivative using the fluoromalonate as solvent (***Figure 52***).[76] These systems show activity as thyroid hormone receptor ligands.

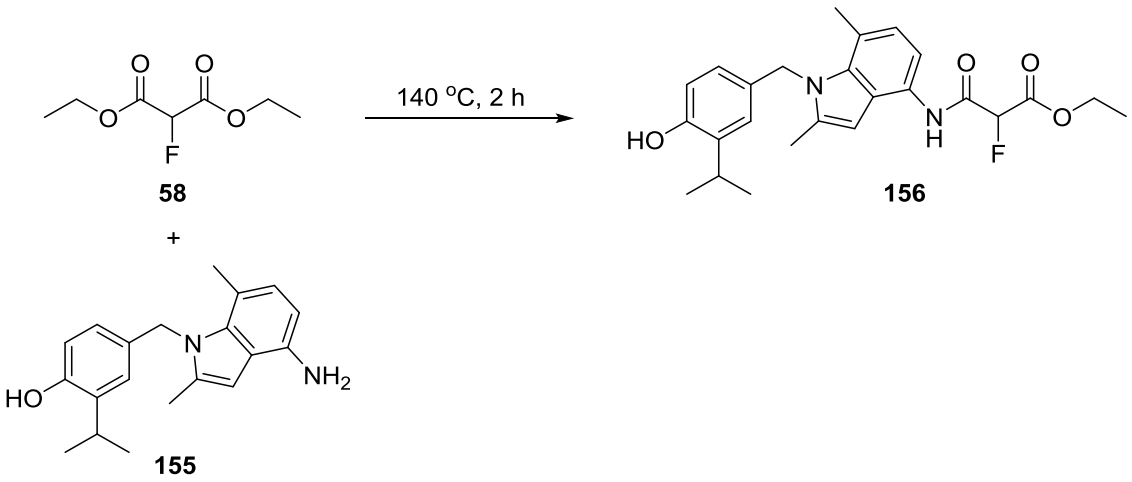

Figure 52 – *A thermal mediated amidation reaction of diethyl fluoromalonate with a more complex amine.*

Syntheses of related enantiomerically enriched derivatives have also been reported in the literature. Reddy *et al*. described the zirconium tetra-*t*-butoxide/HOAt catalysed reaction of an enantiomerically pure fluoromalonate derivative with benzylamine to give the desired asymmetric fluoroamidoester in 55% yield (***Figure 53***).[77]

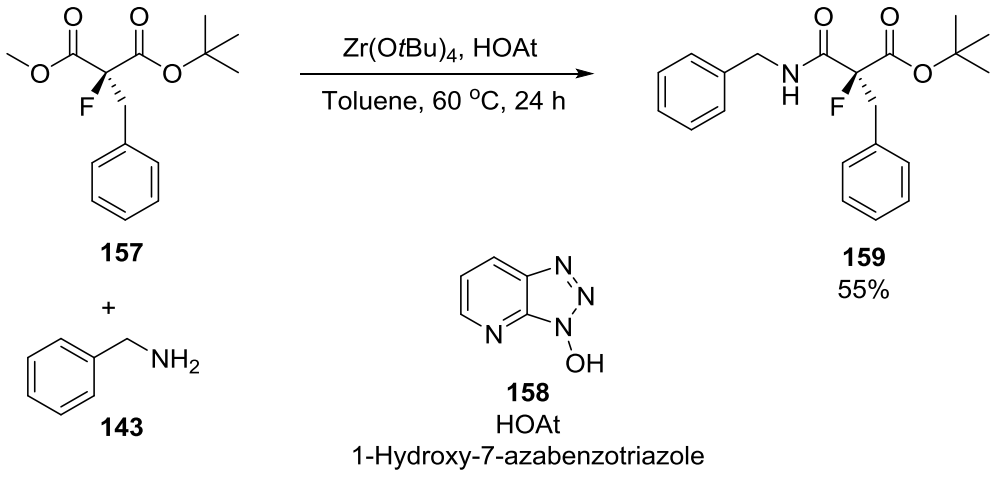

Figure 53 – *Amidation reaction of an asymmetric alkylated fluoromalonate derivative.*

1.3.2.1.2. Intramolecular Amidation Reactions Yielding Cyclic Products

Amidation reactions of fluorodiesters can also be intramolecular reactions that result in the formation of lactam moieties. The Durham group reported the ring forming amidation reactions of a small series of nitrobenzyl substituted fluoromalonate derivatives (***Table 4***).[54] Upon reduction of the nitro moieties the amines react with ester moieties to give the tetrahydroquinoline derived fluoroamidoesters.

Table 4 *- The reduction and subsequent ring-forming amidation reaction of a nitrobenzyl substituted fluoromalonate derivative.*

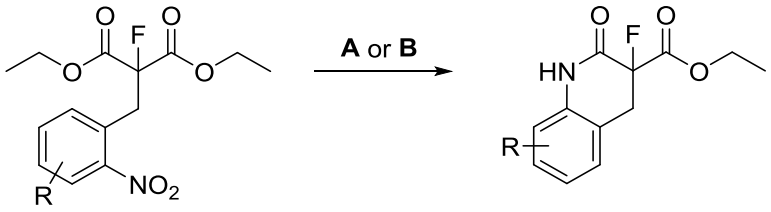

90a-e **91a-e**

A = H_2, (40 psi), Pd/C, AcOH, RT, 1 h
B = $Na_2S_2O_3$, $NaHCO_3$, THF, RT, 0.5 h

Entry	Product	R	Reduction Method	Yield /%
1	**91a**	H	A	78
2	**91b**	H	B	57
3	**91c**	4-CN	B	76
4	**91d**	4-OMe	A	67
5	**91e**	6-F	A	87

Huang *et al*. reported a one-pot synthesis from diethyl fluoromalonate to a related fluorolactam with four chiral centres (***Figure 54***).[78] Yields, *dr* and *ee* values are very good for a number of systems and selected results are shown in ***Table 5***.

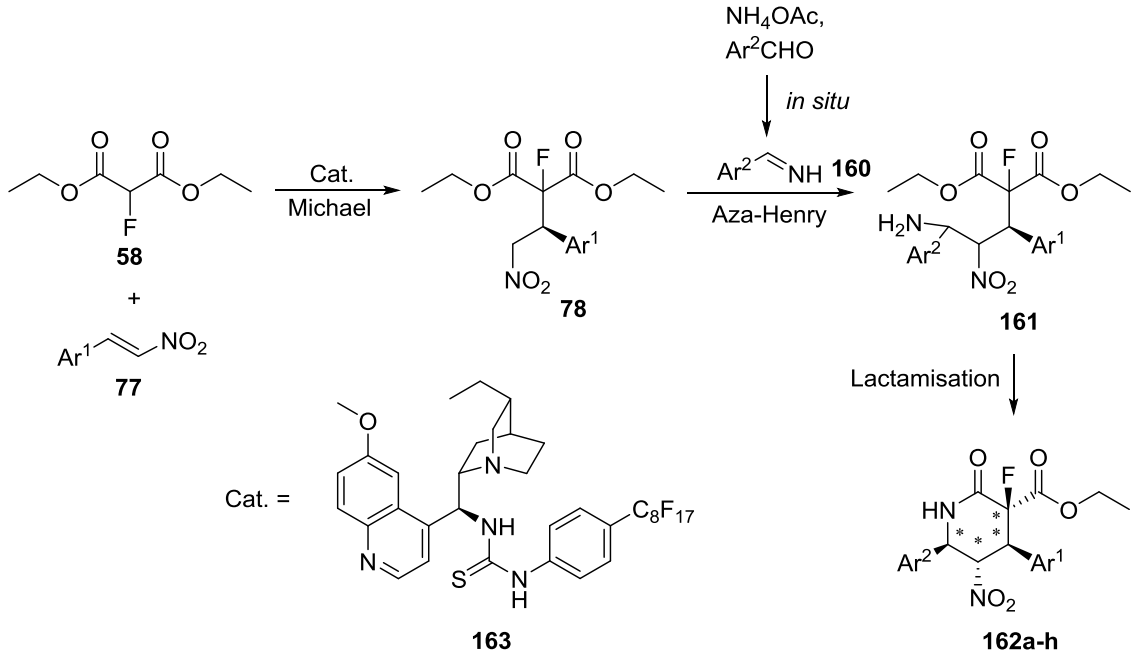

Figure 54 – *Mechanism of the synthesis of a chiral fluorolactam from diethyl malonate.*

Table 5 *- Yields and enantiopurities of some fluorolactam forming reactions of diethyl fluoromalonate.*

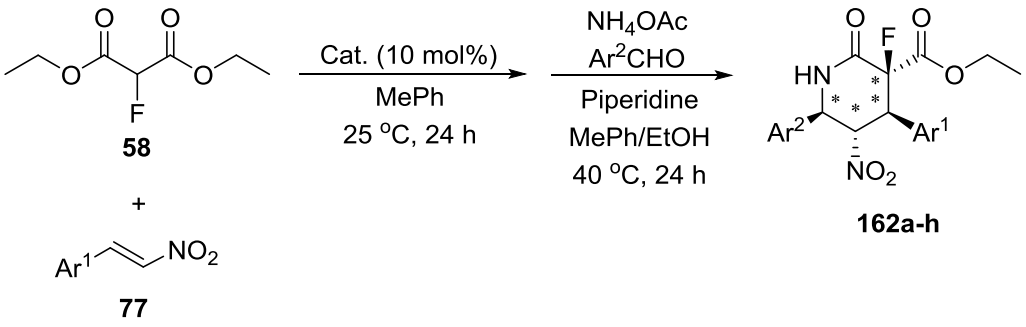

Entry	Product	Ar^1	Ar^2	Yield /%	*dr*	*ee*
1	**162a**	C_6H_5	4-FC_6H_4	85	8 : 1	98
2	**162b**	C_6H_5	4-BrC_6H_4	87	10 : 1	96
3	**162c**	C_6H_5	4-$NO_2C_6H_4$	83	10 : 1	96
4	**162d**	C_6H_5	4-$CF_3C_6H_4$	85	15 : 1	97
5	**162e**	4-BrC_6H_4	C_6H_5	68	3.5 : 1	93
6	**162f**	4-MeC_6H_4	C_6H_5	55	5 : 1	95
7	**162g**	2-Furyl	C_6H_5	62	3.5 : 1	96
8	**162h**	4-BrC_6H_4	4-BrC_6H_4	67	4 : 1	99

1.3.2.1.3. Amidation Reactions of Fluoroesterthioesters

It is also possible for a fluorinated thioester derivative to undergo amidation reactions to form fluoroamidoester products. Cosimi *et al*. reported the amidation of a diastereomeric fluorinated thioester/ester derivative to give the diastereomeric 5-membered fluorolactam (***Figure 55***).[79]

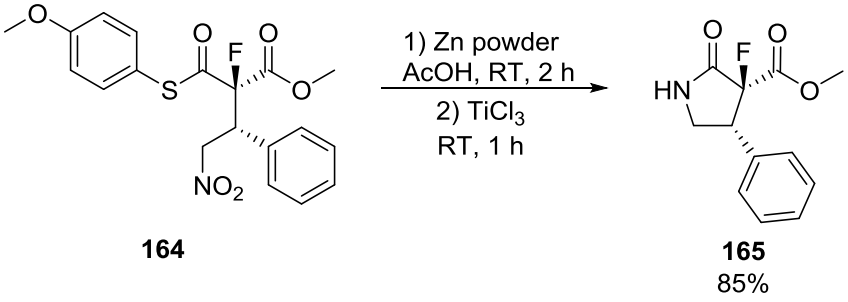

Figure 55 – *Reduction and subsequent amidation reactions of a diastereomeric fluoroesterthioester.*

1.3.2.2. Amidation Reactions of Fluoroester Acids

This section of amidation reactions often includes the use of carbodiimide derivatives and HOBt which are commonly used reagents in peptide chemistry for amide bond formation (***Figure 56***).

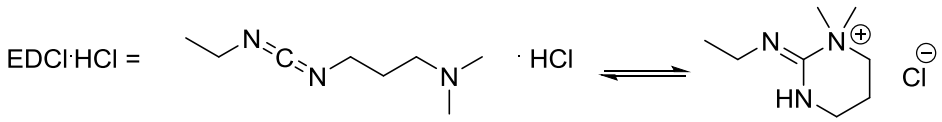

1-Ethyl-3-(3-dimethylaminopropyl)carbodiimide hydrochloride **166**

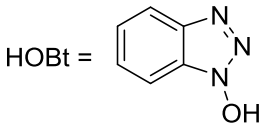

Hydroxybenzotriazole **167**

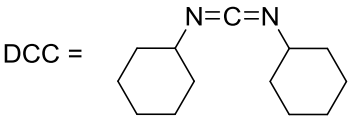

N,N'-Dicyclohexylcarbodiimide **168**

Figure 56 *- The structures of some common reagents used in peptide coupling reactions.*

2-Fluoromalonic acid methyl ester and biphenyl-4-ylamine gave the analogous fluoroamidoester in good yield using EDCl·HCl (***Figure 57***).[80] These systems have been investigated for their use as inhibitors of stearoyl-CoA desaturase.

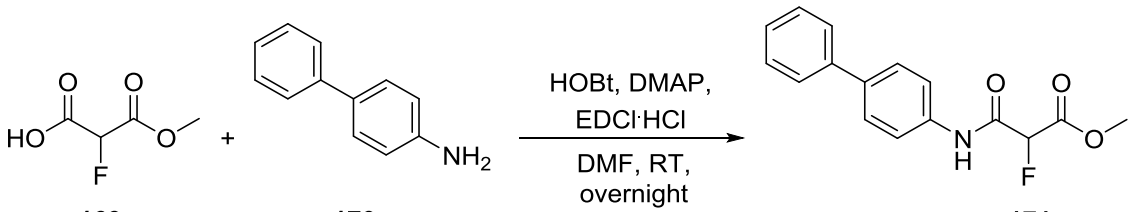

169 **170** **171**
80%

Figure 57 *- Amidation reaction of 2-fluoromalonic acid methyl ester.*

Flohr *et al*. reported a related amidation reaction between a 2-propyl substituted derivative with 3,5-difluorobenzylamine (***Figure 58***).[81]

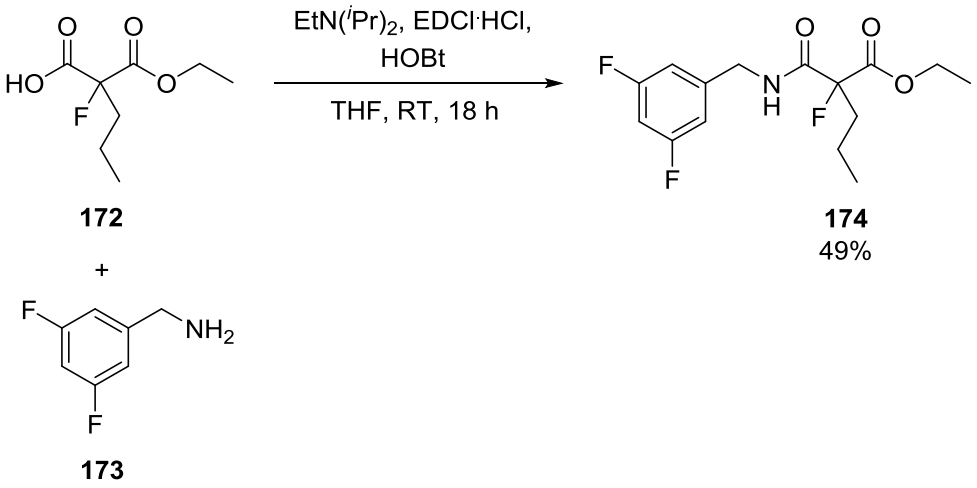

Figure 58 *- Amidation reaction of a 2-*^{i}*propyl substituted 2-fluoromalonic acid methyl ester.*

The authors reported the synthesis of enantiomerically enriched analogues such as the example shown in ***Figure 59*** where an enantiomerically pure fluoromalonic acid derivative reacts with an enantiomerically pure amine.[82,83] These systems are being investigated as γ-secretase inhibitors for the treatment of Alzheimer's disease.

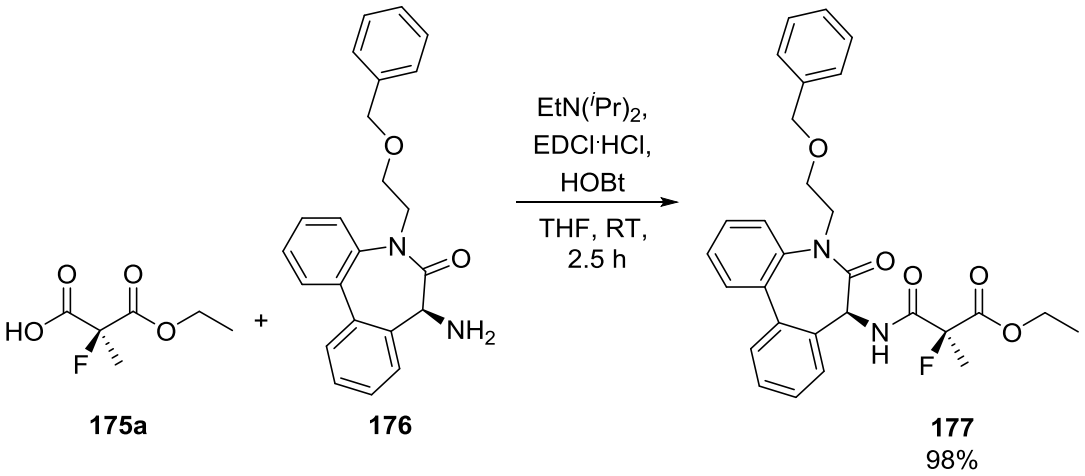

Figure 59 *- Reaction of an enantiomerically pure 2-methyl substituted 2-fluoromalonic acid methyl ester with a large, enantiomerically pure amine derivative.*

Similarly, Sato *et al.* coupled the enantiomerically enriched 2-methyl substituted derivative with *p*-anisidine using a peptide coupling catalyst (DCC) (***Figure 60***).[72]

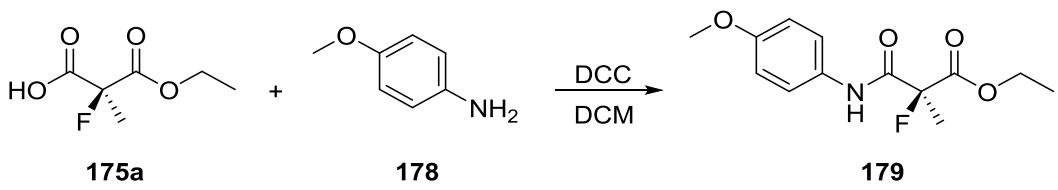

175a **178** **179**

Figure 60 *- Amidation reaction of a 2-methyl substituted 2-fluoromalonic acid methyl ester.*

Hong *et al*. reported a related reaction in the synthesis of a precursor to Welch's (*R*,*R*)-HIV-1 protease inhibitor (***Figure 61***).[84]

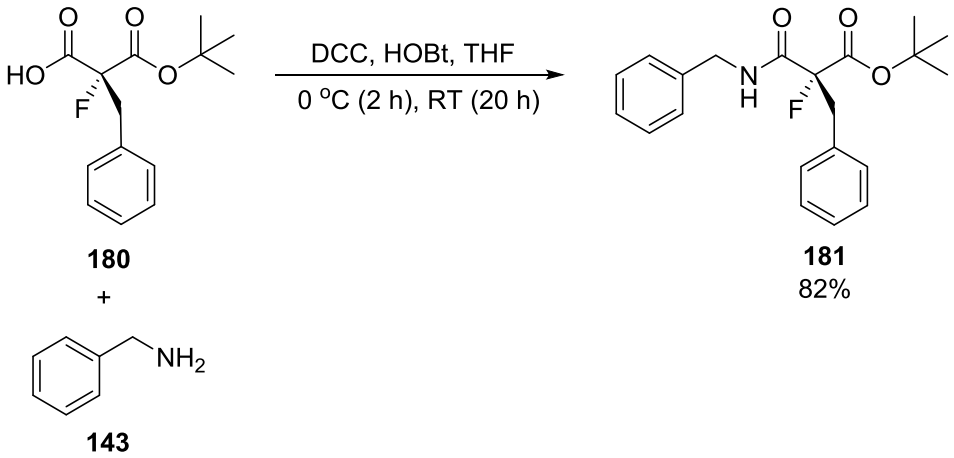

180 **181**
82%

143

Figure 61 *- Reaction of chiral 2-fluoromalonic acid methyl ester derivative with benzylamine.*

Kitazume *et al*. used the Mukaiyama reagent (2-chloro-1-methylpyridinium iodide, CMPI) as a condensing agent in reactions of both (*S*)- and (*R*)- 2-fluoro-2-methylmalonic acid ethyl ester with a short series of amines. The resulting fluoroamidoesters were prepared in high yields (***Table 6***).[85]

Table 6 *- Some amidation reactions of both enantiomers of an enantiomerically enriched 2-methyl substituted 2-fluoromalonic acid methyl ester derivative.*

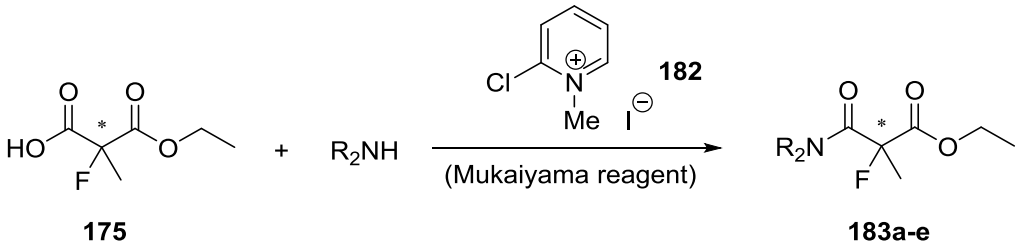

175 **183a-e**

Entry	Product	Acid	Amine		Yield /%
1	**183a**	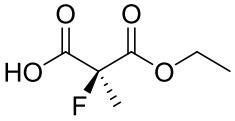	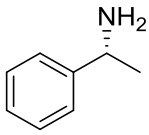	**184**	98
2	**183b**	91% *ee*	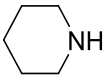	**185**	60
3	**183c**	**(*S*)-175**	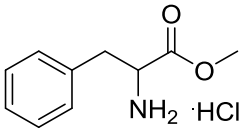	**186**	69
4	**183d**	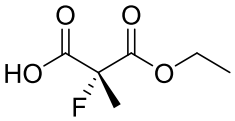	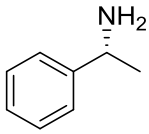	**184**	98
5	**183e**	56% *ee* **(*R*)-175**	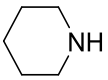	**185**	76

1.3.2.3. Amidation Reactions of Fluoroester Acid Chlorides

Acid chlorides are commonly used to activate a carboxylic acid moiety towards nucleophilic attack by, in this case, amines.

Kitazume *et al*. reported reactions of acid chloride derivatives of both (*S*) and (*R*) enantiomers of 2-fluoro-2-methylmalonic acid chloride ethyl ester with a short series of amines (***Table 7***).[85]

Table 7 *- Some amidation reactions of both enantiomers of a chiral 2-methyl substituted 2-fluoromalonic acid chloride methyl ester derivative.*

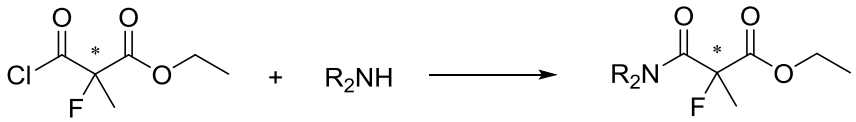

187 **188a-e**

Entry	Product	Acid Chloride	Amine		Yield /%
1	**188a**	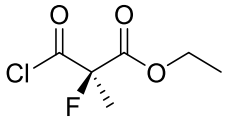 91% *ee* **(*S*)-187**	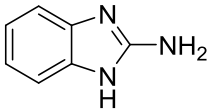	**189**	67
2	**188b**		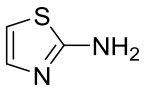	**190**	74
3	**188c**		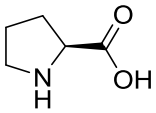	**191**	99
4	**188d**	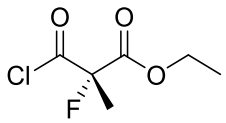 56% *ee* **(*R*)-187**	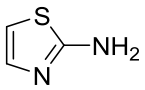	**190**	72
5	**188e**		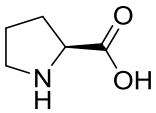	**191**	99

Jadhav *et al*. reported the synthesis of a fluoroamidoester by reaction of 2-fluoromalonic acid chloride ethyl ester with a long chain amine (***Figure 62***).[86] The fluoroamidoester was not isolated but was instead used *in situ* as a substrate for ester hydrolysis by the addition of sodium hydroxide. These systems were being investigated to find more effective immunosuppressive reagents. Metabolism of the fluoroamidoester derivative was predicted to occur at the 2-position of the malonate moiety and so the addition of a fluorine atom to this position was predicted to retard metabolism.

Immunosuppressive activity was maintained with the addition of one fluorine atom but disrupted with the addition of two fluorine atoms in the corresponding geminal difluoride.

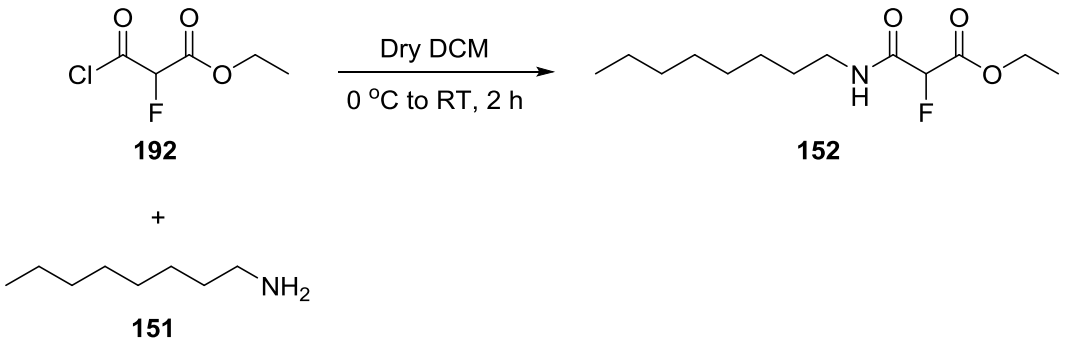

Figure 62 *- Reaction of octylamine with 2-fluoromalonic acid chloride methyl ester.*

Tsai *et al*. reported the reaction of a 2-diethyl phosphoryl substituted analogue with benzylamine but the major fluoroamidoester products were not separated from each other (***Figure 63***).[87]

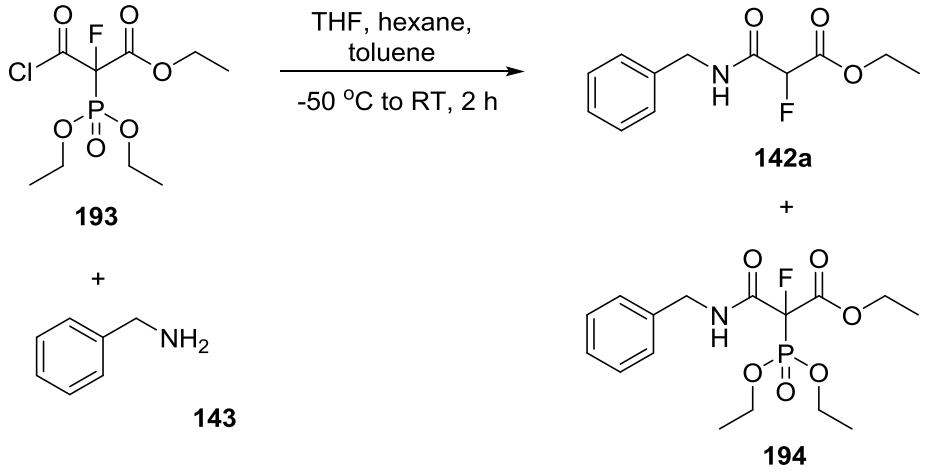

Figure 63 *- Reaction of benzylamine with a 2-fluoromalonic acid chloride methyl ester derivative.*

1.3.2.4. Esterification Reactions of Fluoroamido Acids

Reactions involving ester formation of a fluoroamide derivative are considerably rarer. Sliskovic *et al*. reported the esterification of a fluoroamido acid mediated by DCC to give the corresponding fluoroamidoester in 39% yield (***Figure 64***).[88] These systems were investigated for their abilities to inhibit acyl-CoA:cholesterol *O*-acyl transferase activity and to examine the relationship between adrenal activity and ACAT inhibition.

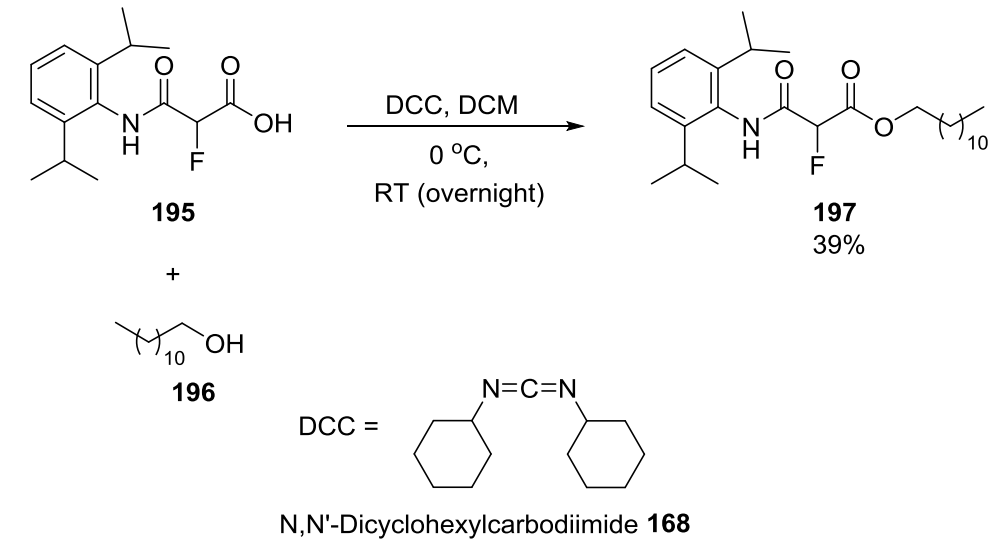

Figure 64 *- Esterification of a fluoroamido acid by a long-chain alcohol.*

Sato *et al*. used a similar technique to synthesis the ethyl esters of a short series of enantiopure 2-substituted fluoroamidoacids (***Figure 65***). The authors also used diazomethane to form the methyl esters of racemic and enantiomerically enriched fluorinated amidoacids (***Figure 66***).[72]

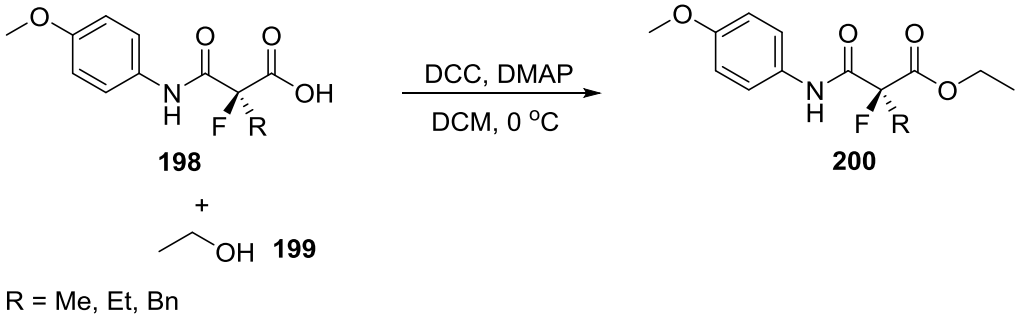

Figure 65 *- Esterification of a fluoroamido acid by ethanol using a coupling reagent.*

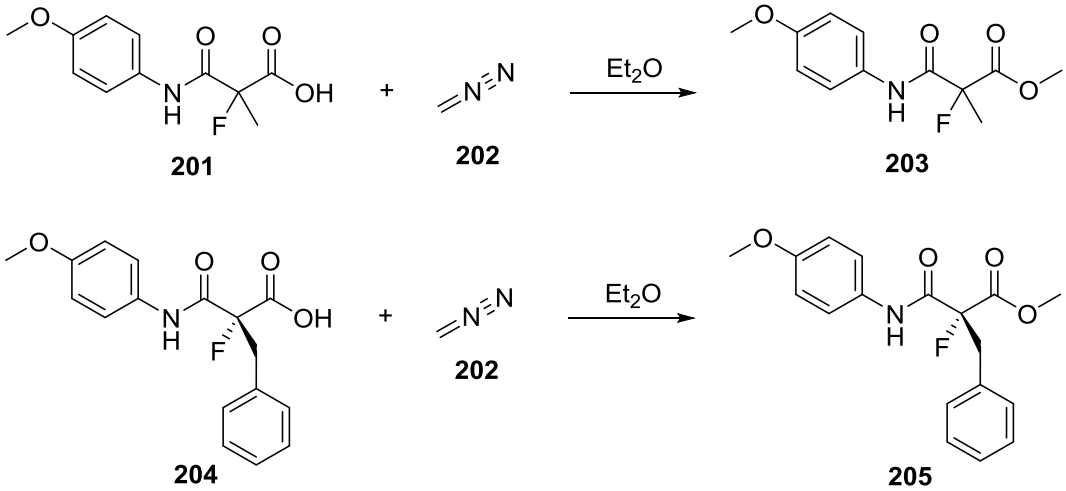

Figure 66 *- Esterification of a fluoroamido acid by a methylating agent.*

1.3.3. Ring-Opening Esterification and Amidation Reactions of Cyclic Fluorodicarbonyl Derivatives

Four of the possible starting material categories for the synthesis of acyclic fluoroamidoesters are shown in ***Figure 67*** and only the ring-opening reaction of a fluorolactone derivative has been reported in the literature.

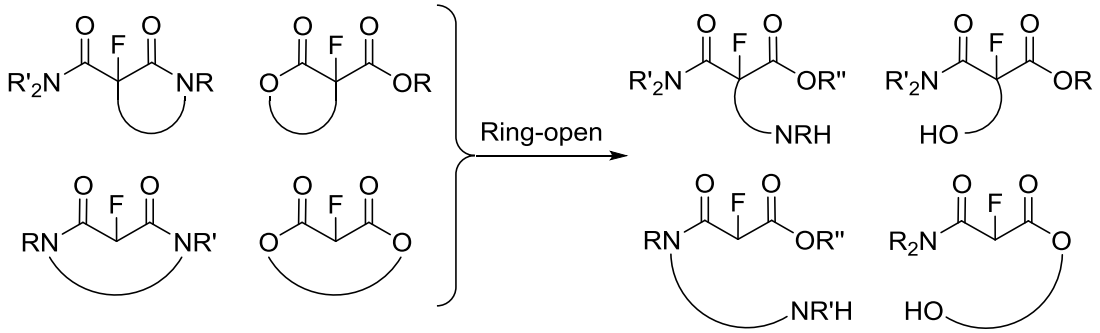

Figure 67 *- The structures of four possible classes of compounds that could undergo ring-opening reactions to form fluoroamidoesters.*

1.3.3.1. Ring-Opening Reactions of Fluorolactones

Suzuki *et al*. reported the ring-opening amidation reactions of fluorolactone derivatives to give the acyclic fluoroamidoesters (***Figure 68***).[68] The derivatives are enantiomerically enriched following a stereoselective fluorination step.

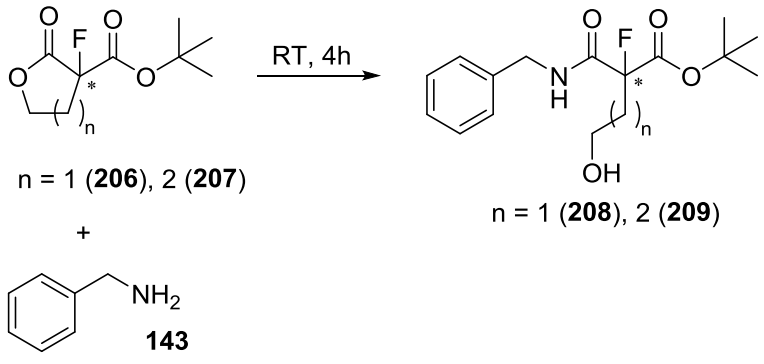

Figure 68 *- Ring-opening amidation of a fluorolactone derivative by benzylamine.*

1.3.4. Miscellaneous Synthetic Routes to Fluoroamidoesters

A number of synthetic routes to fluoroamidoesters present in the literature do not fit so well into the previously outlined categories. The reactions described in this section involve reactions of fluorinated monocarbonylic species and the reaction steps involve synthesis of the second carbonyl moiety.

Adolph *et al*. described the reaction of ethyl fluoronitrocyanoacetate with concentrated sulfuric acid where the nitrile moiety was hydrogenated to a carbamoyl group yielding the fluoroamidoester (***Figure 69***).[89]

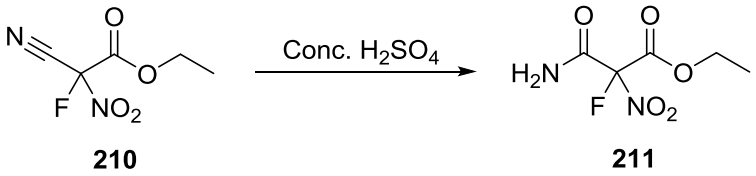

210 **211**

Figure 69 *- Formation of a carbamoyl moiety from a nitrile moiety to yield the corresponding fluoroamidoester.*

Bogolyubskii *et al*. reported the acid catalysed formation of a fluoroamidoester from a trimethoxy derivative of a fluoroamide (***Figure 70***).[90]

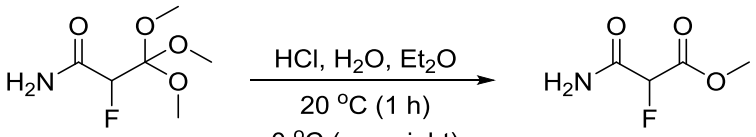

212 **213**
83%

Figure 70 *- Reaction of a trimethoxy group to form a methyl ester and give the fluoroamidoester.*

Bogolyubskii *et al*. also reported the tautomerism of an iminol hydrochloride salt to the amide, yielding the fluoroamidoester (***Figure 71***).[91]

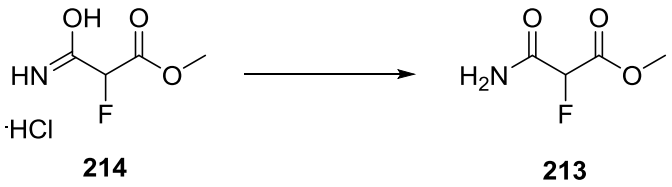

214 **213**

Figure 71 *- Tautomerism of an iminol derivative to the corresponding fluoroamidoester.*

Portella and Iznaden reported the base catalysed sequential dehydrofluorination reaction of a trifluoromethyl derivative to form the amide moiety of a cholestanol derived fluoroamidoester (***Figure 72***).[92]

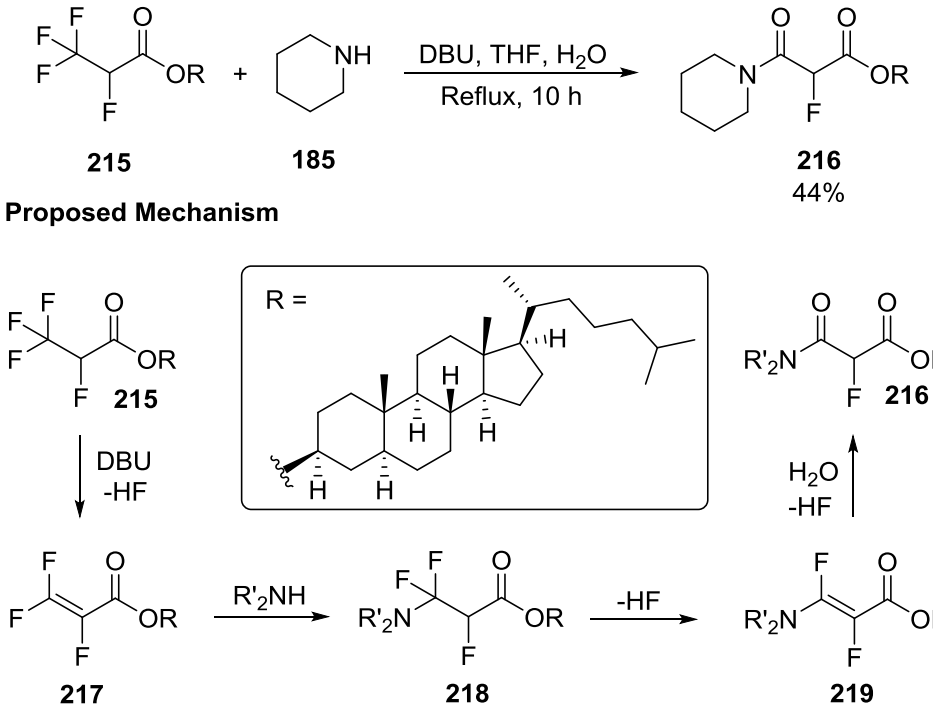

Figure 72 *- Dehydrofluorination, amination and hydration reactions of a trifluoromethyl derivative to form the fluoroamidoester.*

Similarly, Svoboda *et al*. reported the synthesis of a fluoroamidoester from a 3-fluoro derivative of a difluoroaminoester (***Figure 73***).[93]

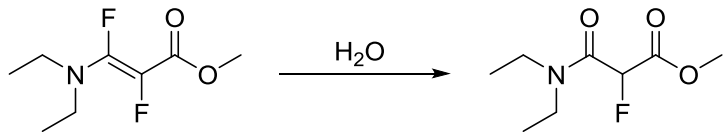

220 **221**
72%

Figure 73 *- Dehydrofluorination and hydration reactions of a trifluoromethyl derivative to form the fluoroamidoester.*

Brooke and Ferguson investigated new synthetic routes to 5-fluorouracil and barbituric acid derivatives. They reported the ring-opening reaction of a methoxy-substituted fluorouracil derivative to give an acyclic fluoroamidoester in excellent yield (***Figure 74***).[94]

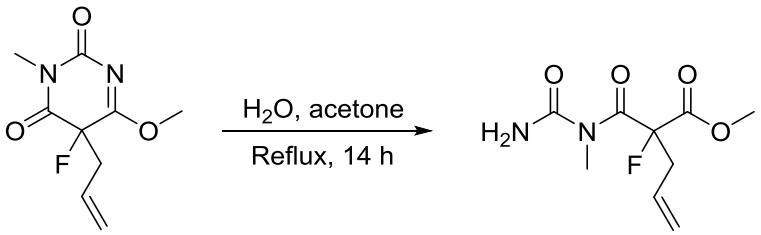

222 **223**
96%

Figure 74 *- Ring-opening reaction of a fluorouracil derivative to an acyclic fluoroamidoester.*

1.4. Amidation Reactions of Malonates

Whilst the literature describing the synthesis of fluoroamidoesters has been covered above, the following short review will outline more specific approaches to the reactions of, primarily, fluoromalonate and benzylamine as an introduction to the chemistry described in Chapter 2.

One of the main challenges facing the synthesis of an amidoester from a diester is the formation of a diamide by further reaction of the product with another equivalent of the amine. Reaction of the amine with an asymmetric derivative of the diester is, therefore, a key approach to the synthesis of these amidoesters in the literature.

Hydrolysis of dimethyl malonate by slow addition of one equivalent of potassium hydroxide solution yields the monoester monopotassium salt in 80% yield.[95] Subsequent reaction with thionyl chloride yields the monoacid chloride derivative.[96] This acid chloride is reported to react with benzylamine to give the corresponding amidoester in 82% yield (***Figure 75***).[97]

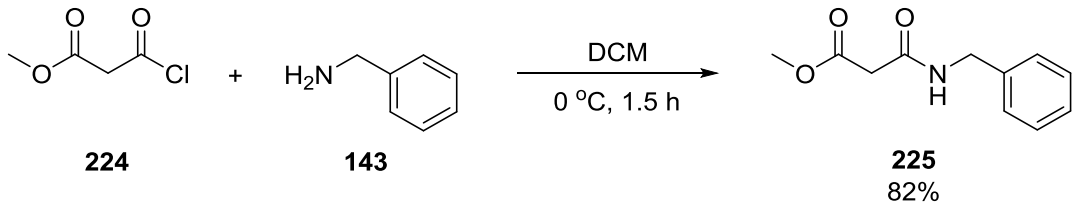

224 **143** **225** 82%

Figure 75 *– Reaction of methyl malonyl chloride with benzylamine to yield the corresponding amidoester.*

Methyl malonyl chloride has also been reacted with methylamine to give the amidoester (***Figure 76***).[98]

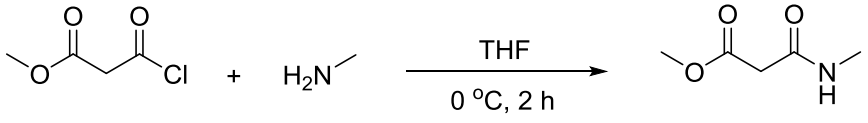

224 **226** **227** 92%

Figure 76 *– Reaction of methyl malonyl chloride with methylamine to yield the corresponding amidoester.*

Reactions with the diester have also been reported. The lipase CAL catalyses the enantioselective aminolysis of dimethyl malonate by (±)-*trans*-2-aminocyclohexanol giving the chiral amidoester in high *ee* at low yield. It was found that increasing the reaction time, and conversion, decreased stereoselectivity (***Figure 77***).[99]

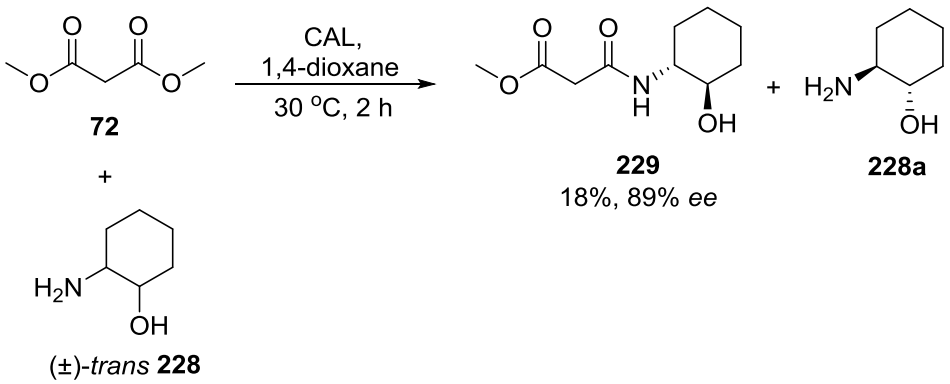

Figure 77 *– Enantioselective reaction of dimethyl malonate with a trans hydroxyl amine catalysed by CAL.*

Reactions of diethyl malonate with two equivalents of benzylamine have been reported to yield the diamide (***Figure 78***).[100]

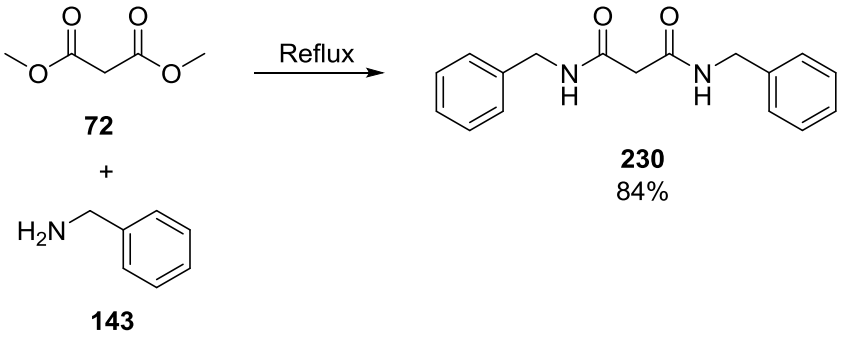

Figure 78 *– Reaction of diethyl malonate with benzylamine to yield the corresponding diamide.*

Reaction of the fluorinated analogue with the dinucleophile tetraethylenepentamine yielded the macrocyclic fluorodiamide in 42% yield (***Figure 79***).[52]

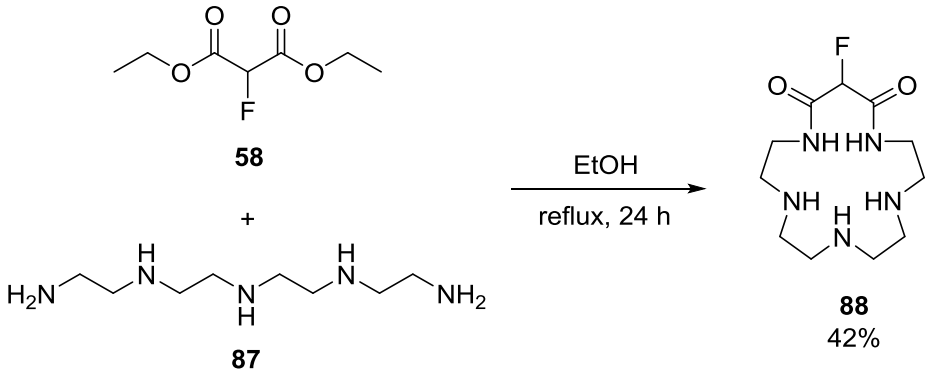

Figure 79 - *Synthesis of fluorinated diamide macrocycle from diethyl fluoromalonate.*

Since the completion of our amidation reactions in Chapter 2 a patent has been published by Wang *et al.* describing the reaction of diethyl fluoromalonate with benzylamine and several other amines in good yields. Selected results are shown in ***Table 8***.[73]

Table 8 – *Conditions and yields of amidation reactions of diethyl fluoromalonate.*

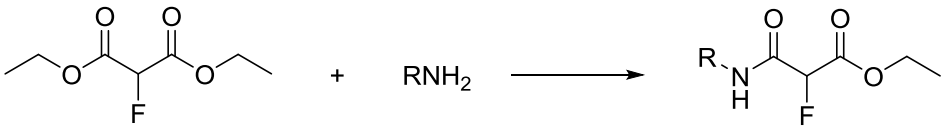

58 **142a-c**

Entry	Product	Amine		Time /h	Temp. /°C	Solvent	Base	Yield /%
1	**142a**	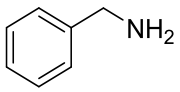	**143**	16	25	-	-	65
2	**142b**	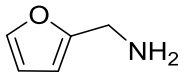	**144**	16	25	-	-	85
3	**142c**	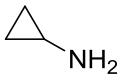	**145**	16	25	-	-	95

1.5. Conclusions

Heterocycles are a common feature in pharmaceutically active molecules and, in recent years, there has been a growing interest in the incorporation of fluorine atoms due to the unique contribution to the physiological properties of a drug offered by this methodology. A number of fluorinating agents are available, of particular note are the electrophilic fluorinating agents including the 'N-F' agents, F_2 gas and the deoxyfluorinating agents. Fluorinated heterocycles are generally synthesised by either late stage fluorination of a heterocycle or early stage synthesis using fluorinated 'building blocks'. One versatile class of building blocks are the 1,3-dicarbonyl systems, notably fluoromalonates and fluorinated β-ketoesters and various methods for the synthesis of fluoroheterocycles using these 'building blocks' have been discussed.

The main literature synthetic routes to fluoroamidoesters include fluorination of fluorolactam derivatives and amidation of fluorodiesters. Several other synthetic routes have more limited literature precedent and some theoretical synthetic routes have not been realised in the literature. While most routes involve fluorination of amidoesters or transformations of fluorodicarbonyl species, a small number of reactions involving fluoromonocarbonyl derivatives exist. Both ring formation and ring-opening reactions are observed and the literature covers a good selection of both racemic and, often analogous, enantiomerically enriched fluoroamidoesters.

A brief overview of amidation reactions of malonate derivatives was discussed, though few amidation reactions of fluorinated malonate derivatives exist in the literature.

Chapter 2. Reactions of Dimethyl 2-fluoromalonate

2.1. Aims and Approach

The synthesis of dimethyl 2-fluoromalonate from F_2 has been previously optimised by the Durham group. As outlined in Chapter 1, whilst there is some literature precedent for the use of fluoromalonate esters as synthetic 'building blocks',[40] there remains plenty of scope for further exploration. The aims of this thesis, therefore, are to develop the chemistry of dimethyl 2-fluoromalonate by:

- reaction of the carbanion with alkyl electrophiles
- reaction of the carbonyl carbons with nucleophiles
- combining these two strategies towards synthesis of fluoroheterocycles

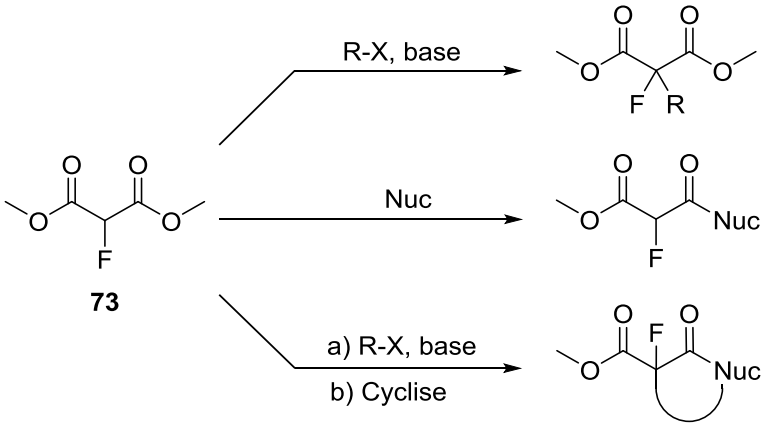

The conformational preferences of each class of synthons will be assessed.

2.2. Alkylation Reactions

Synthesis of the methyl substituted fluoromalonate by reaction of dimethyl fluoromalonate with methyl iodide following a literature procedure of a non-fluorinated analogue[101] was successful, giving the desired product **232** in 76% crude yield. No impurities were observed by ^{1}H and ^{19}F NMR spectroscopy following dissolution of the crude product in ethyl acetate and washing with an aqueous solution of sodium thiosulfate to remove iodine. The resulting methylmalonate derivative was obtained as a yellow oil in 58% yield.

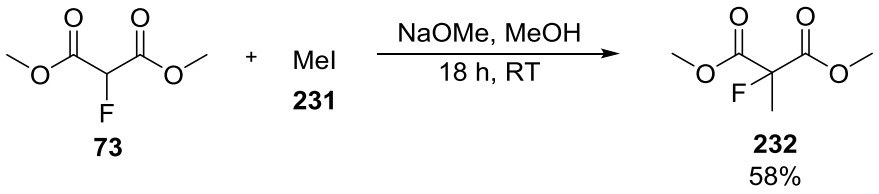

***Figure 80** – Synthesis of dimethyl 2-fluoro2-methylmalonate.*

A sample of the oil was submitted for X-ray crystallographic studies and, upon cooling on the diffractometer probe, the oil crystallised and the structure was confirmed (***Figure 81***).

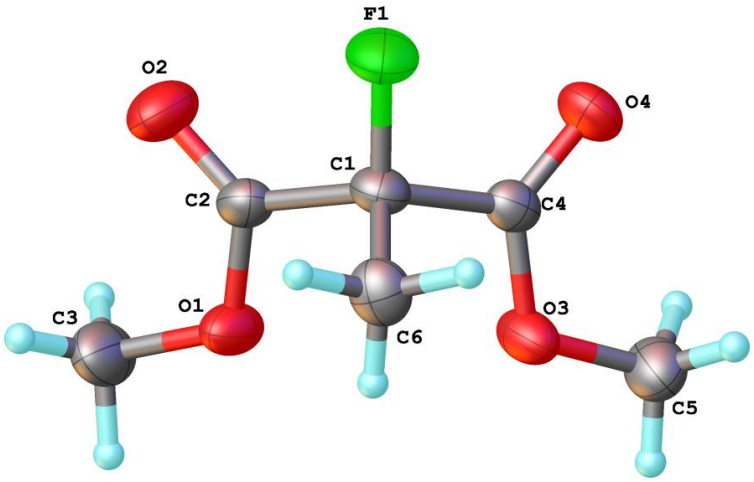

***Figure 81** – Molecular structure of methyl substituted dimethyl fluoromalonate **232**.*

The allyl derivative **234** was also successfully synthesised from allyl bromide in 85% yield using similar reaction conditions.

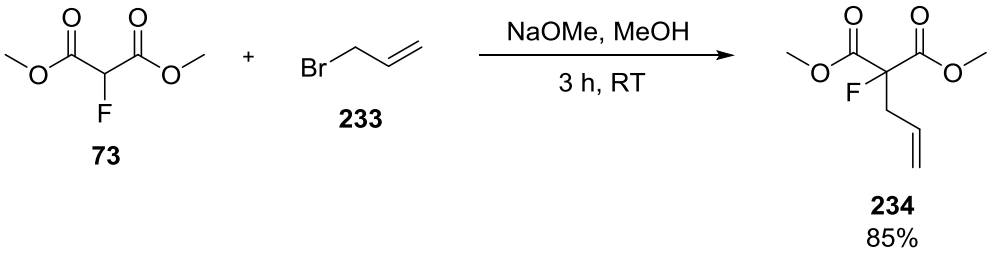

Figure 82 – *Synthesis of dimethyl 2-allyl-2-fluoromalonate.*

Since previous experiments involving a 2-nitrobenzyl bromide analogue had been successfully carried out using sodium hydride as base, [54] a similar reaction of analogous 4-nitrobenzyl bromide and fluoromalonate was carried out. ^{19}F NMR analysis of the crude reaction mixture after 1.5 h showed the reaction was selective and had gone to completion. The crude solid was recrystallized from ethyl acetate and hexane to yield the desired product **236** in 84% yield and the structure was confirmed by X-ray crystallography.

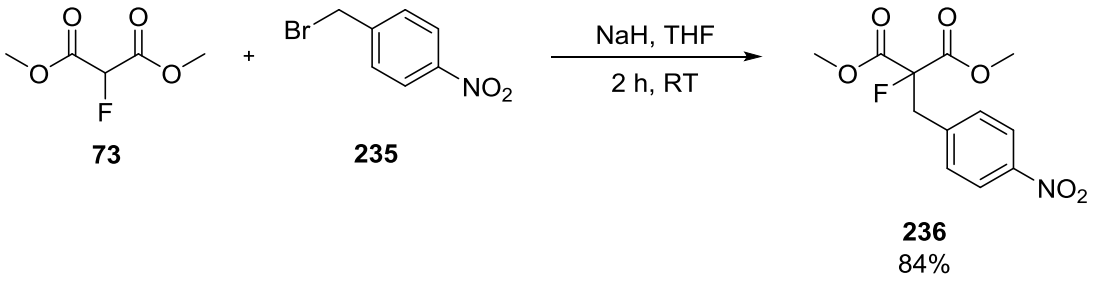

Figure 83 – *Synthetic route to 4-nitrobenzyl substituted dimethyl fluoromalonate.*

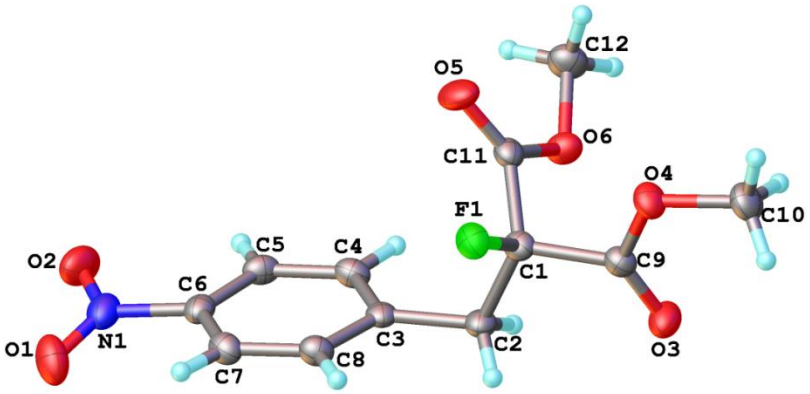

***Figure 84** – Molecular structure of 4-nitrobenzyl substituted dimethyl fluoromalonate **236**.*

The reaction between dimethyl fluoromalonate and bromo diphenylmethane using sodium hydride as base showed 50% conversion by ^{19}F NMR spectroscopy after 24 h. No change in conversion was observed after the reaction solution was heated at 50 ^{o}C for 3 h and so a further 1.2 equivalents of base were added and the solution stirred overnight. Upon aqueous work-up, ^{19}F NMR spectroscopy showed conversion to two products in a 2:3 ratio, one consistent with the desired product **238** (major) and one consistent with mono-decarboxylation product **239** (minor).

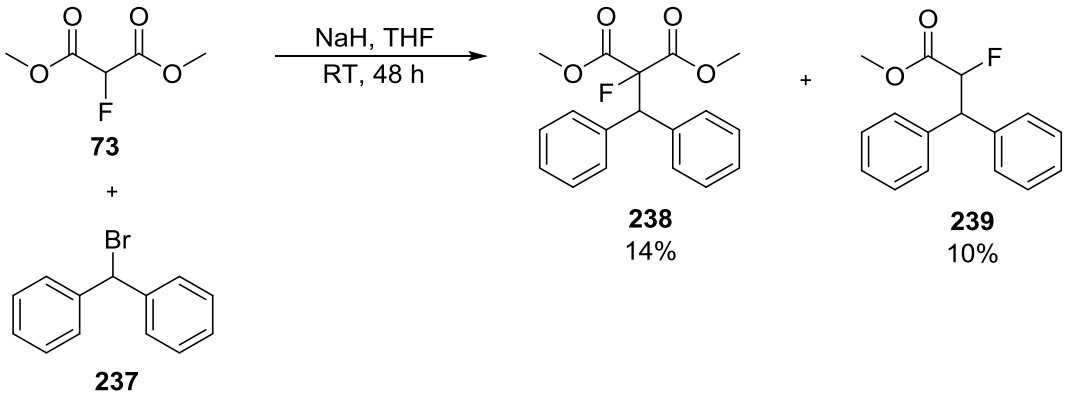

***Figure 85** – Synthetic route to diphenylmethyl substituted dimethyl fluoromalonate **238** and by-product **239**.*

Several products were observed by TLC analysis suggesting decomposition of the products on silica gel. Indeed, subsequent TLC analysis of pure (confirmed by ^{1}H NMR spectroscopy) bromo diphenylmethane starting material gave 3 distinct spots. However, despite these limitations silica column chromatography allowed us to isolate analytical samples of both the product **238** and by-product **239** in low yield and the structure of **238** was confirmed by X-ray crystallography (***Figure 86***).

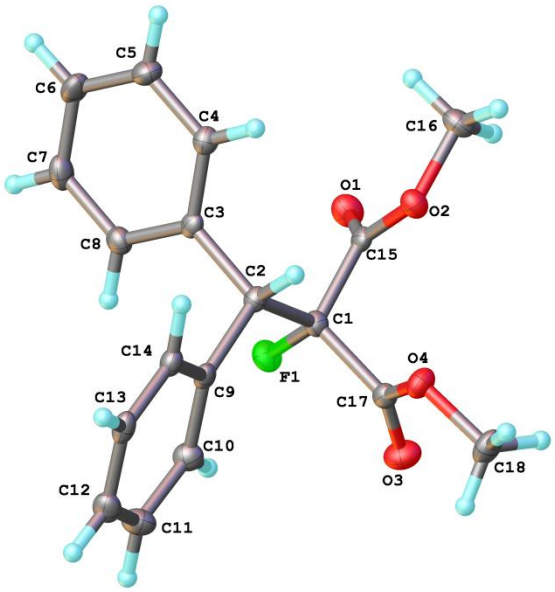

Figure 86 – *Molecular structure of diphenylmethyl substituted dimethyl fluoromalonate* ***238****.*

In summary, a series of alkylated dimethyl fluoromalonate derivatives have been successfully synthesised and products **232**, **236** and **238** were characterised by X-ray crystallography.

Table 9 *– Summary table of alkylation reactions of dimethyl 2-fluoromalonate.*

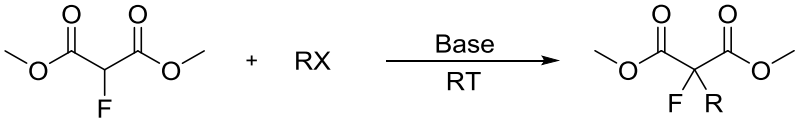

Entry	Product	R	X	Base	Solvent	Time /h	Yield /%
1	**232**	Methyl	I	NaOMe	MeOH	18	58
2	**234**	Allyl	Br	NaOMe	MeOH	3	85
3	**236**	4-Nitrobenzyl	Br	NaH	THF	2	84
4	**238**	Diphenylmethyl	Br	NaH	THF	48	14

2.3. Synthesis of Fluoroamidoesters and Fluoroamides

Benzylamine is visible under ultraviolet light and so was selected as the amine to aid with purification should column chromatography be required. A series of reactions were carried out on a 5 mmol dimethyl fluoromalonate (0.75 g) scale with one equivalent of benzylamine (0.54 g) in methanol (***Table 10***). In addition to the desired monoamide **240,** a by-product was formed in these reactions which was determined to be the diamide **241**.

Table 10*- Table displaying reaction conversions in the temperature screening reactions for the synthesis of monoamide* ***240****.*

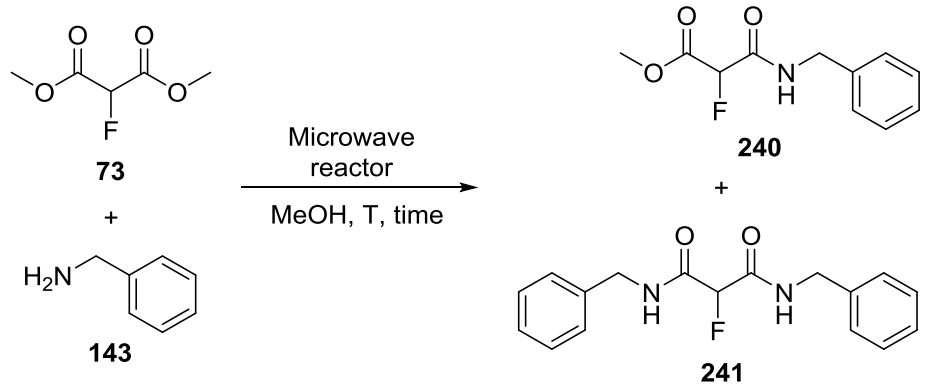

Temp. / °C	Time /min	Compounds present* /%			
		Amidoester 240	Diamide 241	Fluoromalonate 73	Other
150	20	41	17	27	14
150	10	46	16	25	11
100	20	51	20	27	4
100	10	51	19	27	4
60	20	52	17	29	2
60	10	51	14	33	2
25	10	46	6	48	<1
25	20	53	10	36	<1
25	30	57	12	31	<1
25	40	58	15	27	<1

*As determined by ^{19}F NMR spectroscopy

After 10 min at room temperature the relative ratio of fluoromalonate was significantly higher than in the heated reactions. After 40 min at room temperature the relative ratios of the three compounds were comparable with the previous heated reactions but achieved at room temperature. These conditions also almost completely prevented the formation of unwanted side-products, with only three peaks in the ^{19}F NMR spectrum (monoamide, diamide and fluoromalonate) (***Figure 87***). Consequently, these conditions (room temperature, 40 min) were used in subsequent syntheses.

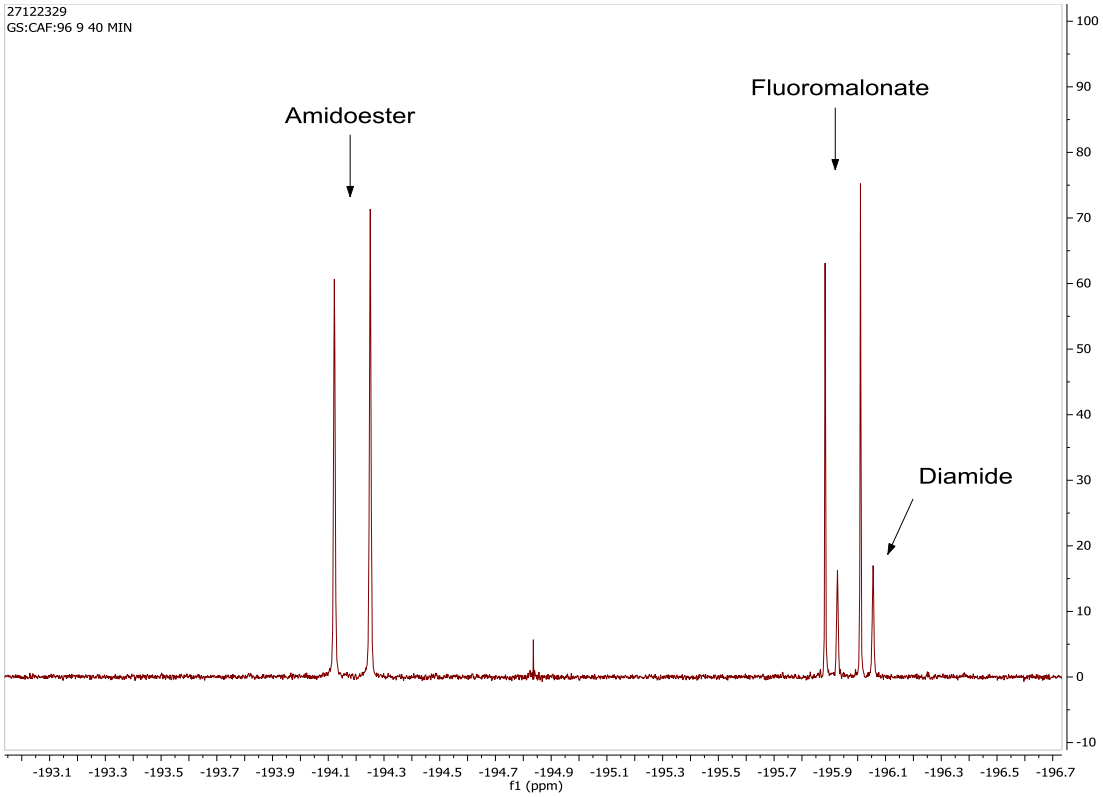

Figure 87 – *^{19}F NMR spectrum for the amidation reaction of dimethyl 2-fluoromalonate* ***73*** *and benzylamine* ***143*** *after 40 min at 25 ^{o}C.*

It is of note that the chemical shift of the diamide in the ^{19}F NMR spectrum apparently varied with the concentration of the fluoromalonate present. ^{19}F NMR spectroscopy of a pure sample of the diamide was obtained and confirmed the chemical shift to be – 197.36 ppm, relative to the dimethyl fluoromalonate shift of – 195.27 ppm and the monoamide shift of – 192.69 ppm.

Therefore, care must be used in determining reaction conversion and ^{19}F NMR spectroscopy must be used in conjunction with ^{1}H NMR spectroscopy and GC-MS measurements.

In summary, amidation occurs without heating, although at a slightly slower rate. The room temperature reactions are also more selective than when heated, yielding only three compounds (the monoamide **240**, the diamide **241** and residual fluoromalonate **73**) though concentration effects were observed to shift the corresponding signals in ^{19}F NMR spectra.

A series of screening reactions was carried out with various equivalents of fluoromalonate **73** (***Table 11***). The reactions were carried out on a 2 mmol benzylamine scale at room temperature for 40 min.

Table 11*- Synthesis of monoamide **240**.*

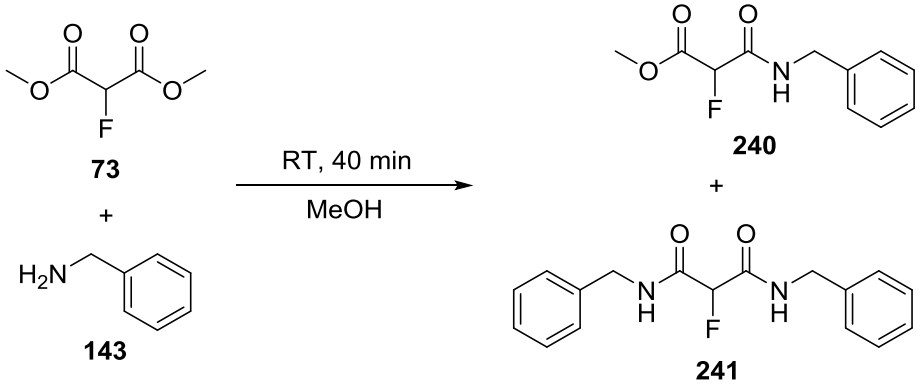

Equiv. Fluoromalonate 73	Product ratio* /% Amidoester 240	Diamide 241
1	79	21
2	89	11
3	90	10†

*As determined by ^{19}F NMR spectroscopy
†Ratio after one recrystallization

While the addition of two equivalents of fluoromalonate successfully increased fluoroamidoester conversion from 79% to 89% the use of three equivalents of fluoromalonate had little further effect in hindering by-product formation.

A scaled up reaction (benzylamine, 2 eq. fluoromalonate, MeOH, 40 min, 89% amidoester, 11% diamide by ^{19}F NMR spectrometry) provided sufficient material for purification. Sequential washings of the product with hexane and ethyl acetate yielded pure analytical samples of both products and the structure of the fluoroamidoester **240** was confirmed by X-ray crystallography (***Figure 88***).

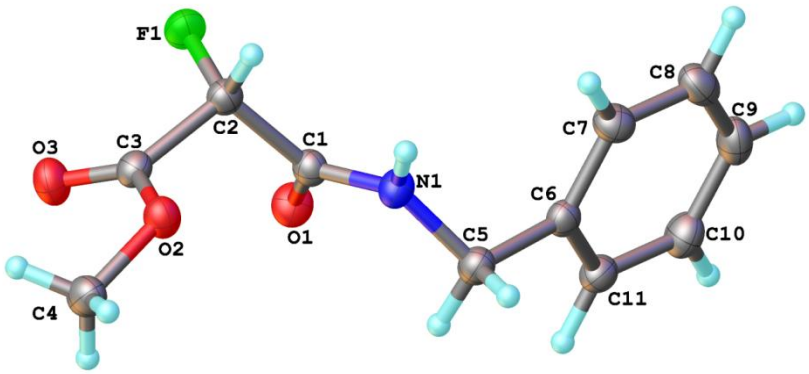

Figure 88 – *Molecular structure of amide* ***240****.*

In summary, although the ^{19}F NMR spectroscopic yields for the reaction between dimethyl fluoromalonate and benzylamine are good (>75% with respect to benzylamine consumption) there are significant difficulties in purification of the monoamide product from the diamide by-product and unreacted dimethyl fluoromalonate since the three compounds have very similar physical properties. However, pure samples of both the monoamide and the diamide were obtained following recrystallization and precipitation.

2.4. Conclusions

The alkylation reactions of dimethyl fluoromalonate were largely successful and, whilst there were difficulties with diamide formation, the amidation reactions of dimethyl fluoromalonate proceeded readily at room temperature. However, the presence of the diamide and, as a result, unreacted fluoromalonate in the crude product mixture proved difficult to separate by conventional separation methods. Despite this, analytical samples of the amidoester and the diamide were successfully obtained.

Chapter 3. Development and Process Optimisation for the Synthesis of Cyclic Fluorolactam (*S*)-Methyl 3-fluoro-2-oxopiperidine-3-carboxylate (*S*)-248

3.1. Introduction

The following chapter aims to combine the two strategies discussed in the previous chapter by alkylation of dimethyl fluoromalonate by an alkylnitrile group. Subsequent reduction to the amine would then, in theory, lead to intramolecular amidation reactions to yield fluorolactams. This intramolecular amidation strategy would also potentially eliminate the formation of diamides and resolve the difficulties encountered with the acyclic amidation reactions described in the previous chapter.

The following section describes the synthesis and process optimisation of an enantiopure fluorolactam system and, subsequently, the synthesis of two of its analogues in Chapter 4. This work was carried out in collaboration with GSK[102] as part of the Innovative Medicines Initiative's (IMI) CHEM21 project whose aim is to deliver more environmentally friendly drug manufacturing processes to the pharmaceutical industry.[103] There is an increasing effort among pharmaceutical companies to consider (and reduce) the environmental impacts of their processes. For example, in 2011 GSK announced a long-term goal of becoming carbon neutral by 2050.[104] Additionally, the optimisation of processes will also help companies to reduce costs which should lead to cheaper medicines for patients.

GSK have developed[66,67] a series of pre-clinical candidate spleen tyrosine kinase (Syk) inhibitors including **242** (***Figure 89***) but the synthetic process for multikilo quantities of material relied on an expensive electrophilic fluorinating agent and a structurally complex precious metal catalyst which required multiple steps in its synthesis in the key fluorination step (***Figure 90***).[65] Additionally, on the large scale, the *ee* of the target intermediate (*S*)-**118** was low (44%) and so time-consuming chiral HPLC was required for chiral resolution and a large proportion of the material was wasted as it was of the undesired stereochemistry.[66]

As such, intermediate (*S*)-**118** was identified by GSK as a suitable target for process optimisation as part of the CHEM21 collaboration with Durham University.

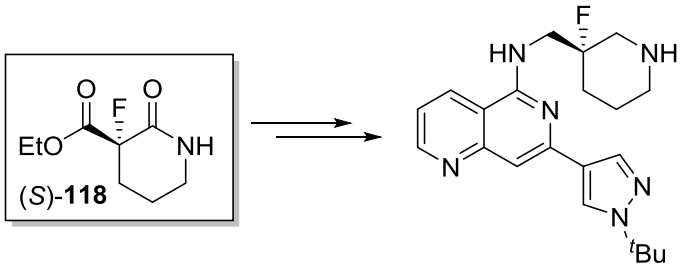

242

Figure 89 *– Target asymmetric fluorolactam (S)-**118**, intermediate for the pre-clinical candidate spleen tyrosine kinase (Syk) inhibitor **242**.*

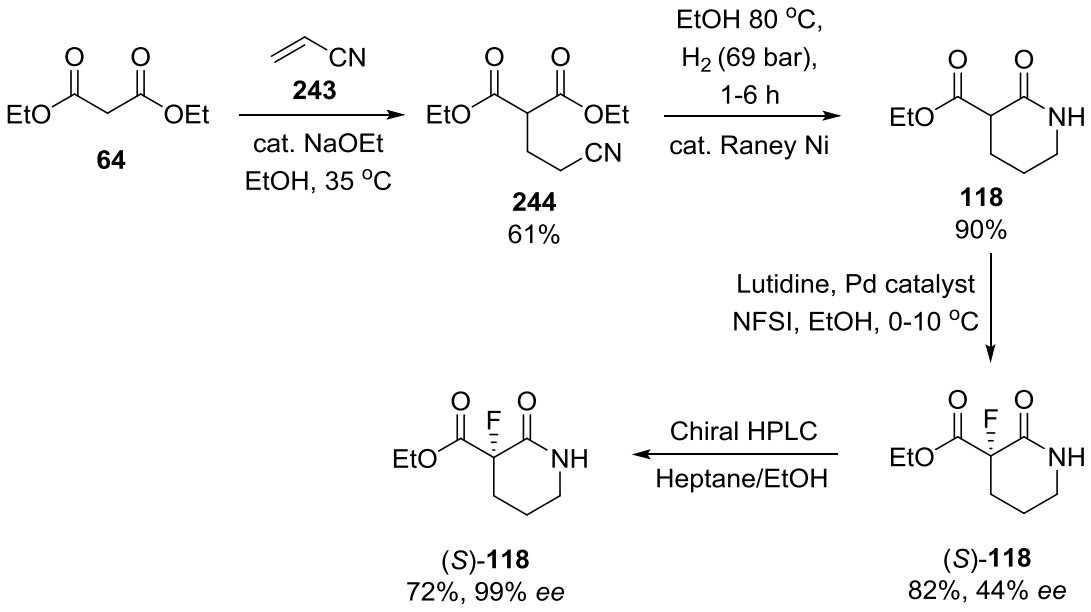

32% overall yield, 99% *ee*

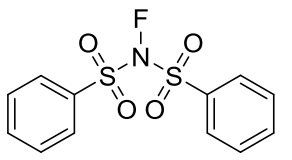

NFSI **27**
N-Fluorobenzenesulfonimide

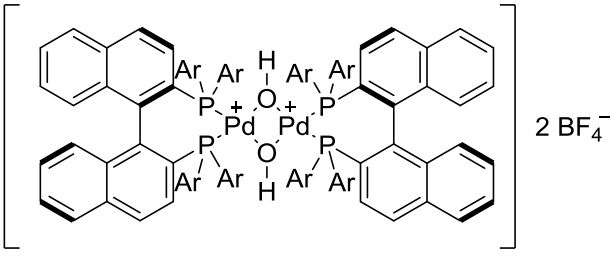

Pd catalyst =
[(*S*)-BINAP] palladium (II) dihydrate ditriflate
245

Figure 90 *– GSK route to enantiomerically enriched fluorolactam (S)-**118**.*

The collaboration consisted of two key areas. The synthesis of the racemic fluoroheterocycles, their intermediates and their derivatives were investigated in Durham and the second part of the collaboration, carried out by Dr. Nicky J. Willis and colleagues at GSK, involves the desymmetrisation of the system to form an enantiopure heterocycle using biotransformation techniques.

3.1.1. Literature Route to (*S*)-Ethyl 3-fluoro-2-oxopiperidine-3-carboxylate (*S*)-118

The literature supporting the proposed synthesis of the racemic fluorolactam and desymmetrisation of the intermediates is discussed in the appendix of this thesis (section A1.1.1.). Having considered several potential synthetic routes to reach the desired chiral fluorolactam (*S*)-**248** our chosen approach, based on adaption of literature routes, is shown in ***Figure 91***.

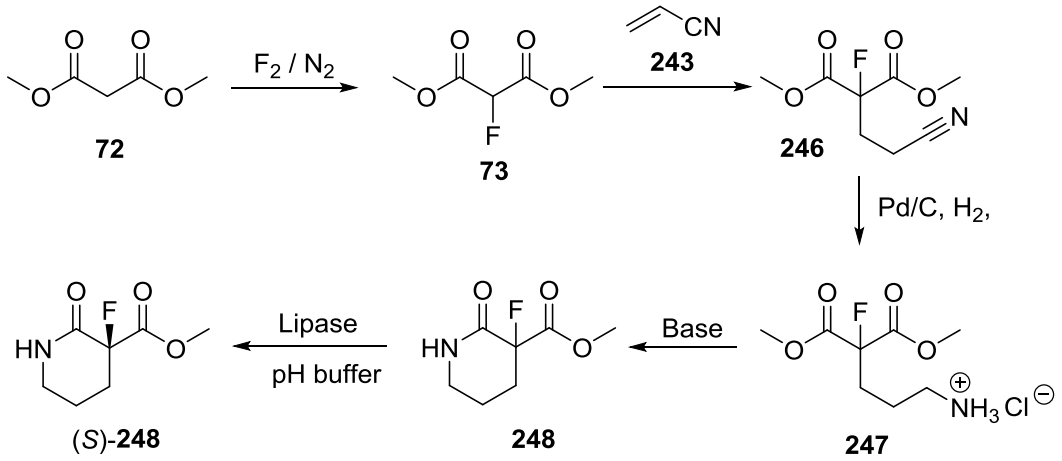

Figure 91 *– The proposed alternative scheme for the synthesis of enantiomerically enriched fluorolactam (S)-**248**.*

Having previously optimised the fluorination reaction of dimethyl malonate to dimethyl fluoromalonate **73** this step was included in the synthetic strategy. The Michael addition reaction of fluoromalonate **73** to acrylonitrile would then be optimised before a one-pot style fluorination/alkylation reaction is attempted to reach alkylated product **246** from dimethyl malonate without isolation or purification of intermediate fluoromalonate **73**. Next, the reduction of nitrile **246** to amine derivative **247** would be optimised, followed by basic workup of salt **247** to racemic fluorolactam **248**.

Lipase reactions of racemic salt **247** will be investigated. If unsuccessful, racemic fluorolactam **248** would then be investigated as a substrate for enzymatic resolution.

This chapter compares our alternative synthetic route to the current GSK literature route in terms of a green chemistry perspective. Consequently an introduction to green metrics and outlines of definitions of terms are given here, followed by analysis of the literature process as a benchmark for process development of our alternative synthetic process.

3.1.2. Green Metrics Analysis

The increase in environmental impact awareness in the chemical industries has led to the emergence of new systems to analyse existing and developing processes in terms of assessing quantities of waste generated. Among these are the green metrics calculation packages that provide a more quantitative approach to process developments and comparison to existing alternatives than simple qualitative approaches.

3.1.2.1. Definitions

Many green metrics systems have been developed and used in recent years[105,106,107] but for this research project a new metrics package developed by the CHEM21 network was utilised[108] because it combines qualitative and quantitative approaches to green chemistry. The four-stage system spans from screening level reactions (Zero Pass) all the way through to manufacturing scale reactions (Third Pass), via comparison of optimised processes with alternative literature processes (First Pass) and, subsequently, pilot scale reactions (Second Pass). This project focusses on the First Pass stage as it comprises of laboratory scale reactions in comparison with literature alternatives.

The quantitative section of the metrics package includes the use of a spreadsheet into which mass data is input and metric calculations are auto-completed. The metrics terms include Yield (%), Conversion (%), Selectivity (%), Reaction Mass Efficiency (RME), Atom Economy (AE) and Process Mass Intensity (PMI), the latter of which is also split into three sections: 'Reaction MI' 'Solvents MI' and 'Workup MI'. This subcategorisation helps to determine exactly which parts of the process contribute most to the overall PMI and aids process development. It has been established that the largest contributor of mass to a process is, by far, the use of solvents. A recent GSK paper discussed the use of solvents in industry and stated the median amount of materials used to produce 1 kg of an active pharmaceutical ingredient (API) was 46 kg. Of the 46 kg, solvents accounted for 56% of this mass and water accounted for a further 32%. The reactants only accounted for 7%.[109] Whilst all the above terms are defined below, metrics discussion throughout this report will focus primarily on the most useful metric indicators: Yield, AE and PMI.

Percentage yield is a simple and commonly used metric and a high percentage yield is desirable. Percentage conversion compares the initial amount of a yield limiting reactant with the amount that remains at the end of the reaction. Percentage selectivity is a ratio between yield and conversion and a high number is desired. A low yield but high conversion (low selectivity) may indicate that the yield limiting reactant is undergoing unwanted side-reactions. The definitions of Percentage yield, Percentage conversion and Percentage selectivity are shown in ***Figure 92***.

$$Percentage\ yield = \frac{moles\ of\ product}{moles\ of\ limiting\ reactant} \times 100$$

$$Percentage\ conversion = 100 - \left(\frac{final\ mass\ of\ limiting\ reactant}{initial\ mass\ of\ limiting\ reactant}\right) \times 100$$

$$Percentage\ selectivity = \frac{\%\ yield}{\%\ conversion} \times 100$$

Figure 92 *– The definitions of Percentage yield, Percentage conversion and Percentage selectivity.*

Atom economy (AE) is another well-known term and, although simple, provides a very useful first approach to the metrics of a process. No laboratory work is required to calculate AE as it uses only the molecular weights of the reactants and product and so is a rapid analysis of a potential process. Limitations to this metric include the assumption that 100% yield is achieved and that loading is stoichiometric. As such, the AE of a process will not change with the optimisation of the process (e.g. reduction of solvent volumes, increased selectivity).

Reaction mass efficiency (RME) incorporates AE with mass based data (such as yield and stoichiometry) and so offers a more detailed metric analysis of a process as it develops. Mass intensity/Process mass intensity (MI/PMI) improves upon RME as it includes all additional sources of mass, including the masses of other reagents, solvents, catalysts and masses pertaining to work-up steps. As such, this metric is generally regarded to be of more use than RME and so is used by process chemists in industry and throughout this report.

$$AE = \frac{molecular\ weight\ of\ product}{total\ molecular\ weight\ of\ reactants} \times 100$$

$$RME = \frac{mass\ of\ isolated\ product}{total\ mass\ of\ reactants} \times 100$$

$$MI = \frac{total\ mass\ in\ a\ process\ or\ process\ step}{mass\ of\ product}$$

Figure 93 *– The definitions of Atom economy (AE), Reaction mass efficiency (RME) and Mass intensity (MI).*

The metrics defined above relate to single steps in a process. In order to calculate the cumulative metrics of a multi-step process the equations in ***Figure 94*** were used.

For a process involving the steps $A + B \rightarrow C$ and $C + D \rightarrow E$

where *MW* = Molecular weight of compound and *m* = Weight of compound;

$$AE(E) = \frac{MW\ (E)}{MW(A) + MW(B) + MW(D)} \times 100 = \frac{MW(E)}{\frac{MW(C)}{\frac{AE(C)}{100}} + MW(D)} \times 100$$

$$RME(E) = \frac{m(E)}{m(D) + m(C)} \times 100 = \frac{m(E)}{\frac{m(C)}{\frac{RME(C)}{100}} + m(D)} \times 100$$

$$MI(E) = \frac{m(C)\ \times MI(C) + total\ mass\ of\ other\ chemicals\ in\ the\ step}{mass\ of\ product}$$

Figure 94 *– The cumulative definitions of Atom economy (AE), Reaction mass efficiency (RME) and Mass intensity (MI) for a two-step process.*

Qualitative aspects of the metrics package[108] include analysis of solvents, health and safety, catalysts used, catalysts recovered, type of reactor, elements used, energy and work-up methods. For each of these categories (and, additionally, the yield, conversion and selectivity criteria) the metrics package assigns a flag either green, yellow or red in colour.

Whilst green is generally considered good and red is generally considered poor, these flags are to be regarded as a way of drawing attention to certain aspects of a process that may be of interest or concern. A red flag does not necessarily imply that a process step is to be avoided, only that some aspects of it are to be considered further.

As previously alluded to, solvents are a key factor in mass based metrics analysis and because of the large scales on which they are used other factors are also worth considering. The 'greenness' of a solvent includes health and safety criteria in addition to environmental criteria since health and safety considerations are an important part of process development from an industrial perspective. The CHEM21 initiative published a solvent selection guide[110] and it is this guide that the associated metrics package incorporates into its analysis.

The health and safety impact of chemicals used is assessed according to the associated material safety data forms for each chemical. The catalyst used is noted and assessed and also whether the catalyst is recovered (preferable) or lost in the process. The reactor category compares the type of process used e.g. flow or batch. The elements category lists any disfavoured chemical elements used in a process step. The energy category highlights any outstanding factors such as heating the reaction mixture above the boiling point of the solvent whilst the work-up section flags up any unfavourable work-up or purification processes, such as chromatography.

3.1.2.2. Metrics Analysis of Literature Synthetic Route to (*S*)-Ethyl 3-fluoro-2-oxopiperidine-3-carboxylate (*S*)-118

This work was carried out in collaboration with GSK and Durham PhD student Antal Harsanyi. Whilst the metric analyses of the literature procedures are discussed here, the full calculations and further details are available in the appendix of this thesis (section A2.).

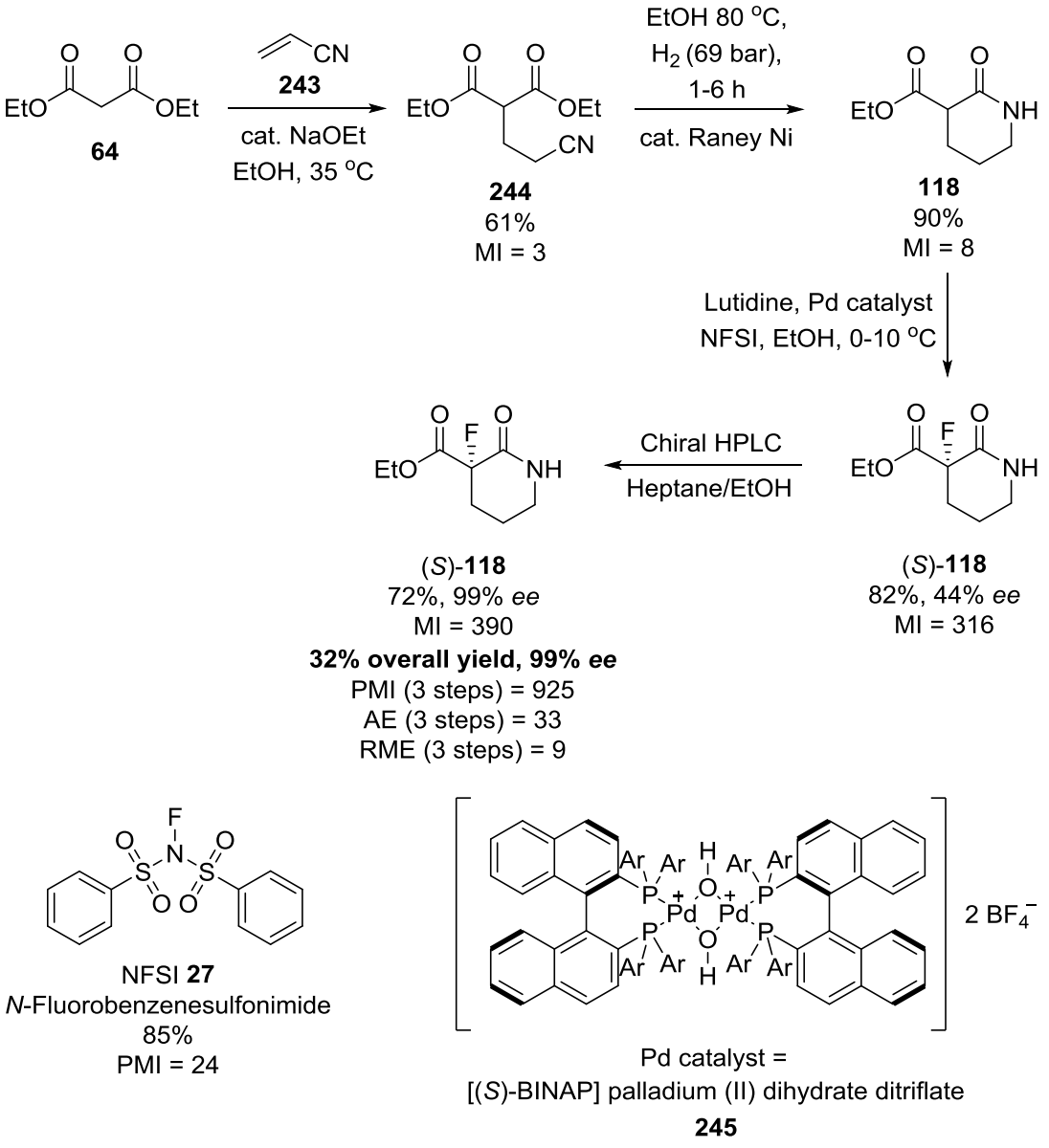

***Figure 95** – The overall scheme for the GSK route to chiral fluorolactam (S)-**118** (the ethyl ester of target (S)-**248**) with metric calculations.*

The first step of the synthesis (**64** to **244**) has a low MI value of 3.1. This is, in part, due to the scale of the reaction between the two liquid reagents relative to the low solvent volume. 992 g (6.2 mol) of malonate ester and 168.5 g (3.2 mol) of acrylonitrile were reacted in a 200 mL solution of sodium ethoxide (7.0 g (0.3 mol) sodium in 200 mL ethanol) making the solvent contribution to PMI very low due to the high concentration of reagents.

The second step involving the cyclisation of nitrile **244** to lactam **118** also has a low PMI value (7.5) and was carried out on large scale (380 g nitrile **244**) giving very good yield (90%) with minimal work-up (evaporation, dissolution in hexanes and filtration).

The key enantioselective fluorination step (step 3) has a much larger MI value. This can be explained by the use of the NFSI fluorinating agent which itself is synthesised from fluorine gas[111] which needs to be accounted for in MI calculations. With a molecular weight of 315 g/mol, only 19 g/mol of which is the fluorine atom, it is clear that the use of NFSI generates a very large mass of waste relative to the fluorine atom it transfers.

Additionally, the product (*S*)-**118** has a low *ee* (44%) and so the subsequent chiral resolution generates a large loss of material even though HPLC solvents were assumed to be recovered and recycled. The resolution step itself has a MI value of 390.2 due to large solvent usage.

Overall, the calculated PMI value for the GSK preparation of enantiopure fluorolactam (*S*)-**118** is 925, for a 32% overall yield. Although very high, this estimate is actually conservative as it assumes the HPLC solvents were recovered and it does not include the waste generated in the multi-step synthesis of the large, palladium catalyst. The AE is low at 33 and the RME is low at 9.

3.2. Synthesis of Racemic Methyl 3-fluoro-2-oxopiperidine-3-carboxylate 248 and (*S*)-Methyl 3-fluoro-2-oxopiperidine-3-carboxylate (*S*)-248

Having assessed the PMI and related metrics of the existing literature synthetic process an alternative synthetic route that avoided many of these issues was proposed (***Figure 96***). The main concerns were identified as follows; poor *ee* (44%), time consuming chiral HPLC, precious metal (Pd) based catalyst (cost, sustainability and toxicity concerns), multi-step synthesis of catalyst, low AE, high PMI and use of NFSI (cost and low AE).

The proposed synthesis (***Figure 96***) uses a lipase enzymatic step to induce asymmetry to the process. This eliminates the use of the palladium catalyst, is cheaper and is readily recyclable and, if successful, would also remove the need for chiral HPLC purification. The use of fluorine gas in this early stage fluorination reaction eliminates the costly and wasteful use of NFSI later in the synthesis. The use of the methyl ester in (*S*)-**248** (as opposed to the ethyl ester in (*S*)-**118**) aids in selectivity of the fluorination reaction and also reduces the relative mass loss (by one $–CH_2-$ unit per molecule) in the amidation step.

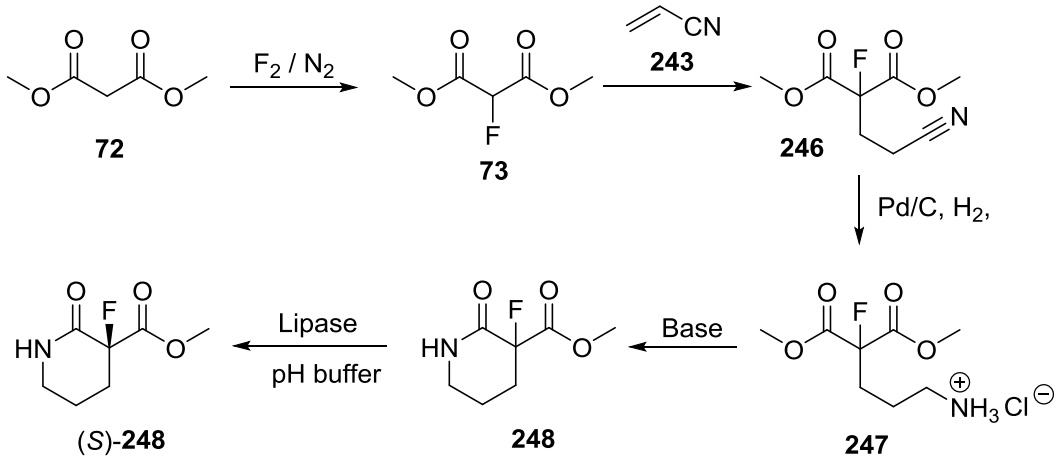

Figure 96 *– The proposed alternative scheme for synthesis of chiral fluorolactam (S)-**248**.*

The direct fluorination of dimethyl malonate to dimethyl 2-fluoromalonate **73** has been previously optimised in Durham (MI = 9.0 (11.6 after distillation), RME 88.6 (69.3 after distillation, AE 89.9).[112]

3.2.1. Michael Addition Reaction of Fluoromalonate

Following a review of the related literature (appendix section A1.1.2.) [40,113] our first attempt to synthesise **246** from acrylonitrile **243** and dimethyl fluoromalonate **73** used potassium carbonate and Aliquat 336 as a phase transfer catalyst, based on a literature procedure for Michael addition reactions of non-fluorinated malonates using chiral phase transfer catalysts.[48] The reaction gave good conversion (by ^{19}F NMR spectroscopy analysis) at room temperature in 1 h but this method proved to be problematic due to the difficulty in removing the phase transfer catalyst in the purification of product **246** using conventional separation methods.

The Michael reaction was then carried out using 10 mol% sodium methoxide in methanol to give 78% conversion by ^{19}F NMR spectroscopy after 3 h. The amount of sodium methoxide was then doubled to 0.2 eq. and the amount of acrylonitrile was increased to 2 eq. This alteration (***Figure 97***) increased conversion to 99% after 1 h and gave pure **246** in 90% yield after workup, with the excess acrylonitrile being evaporated with the solvent.

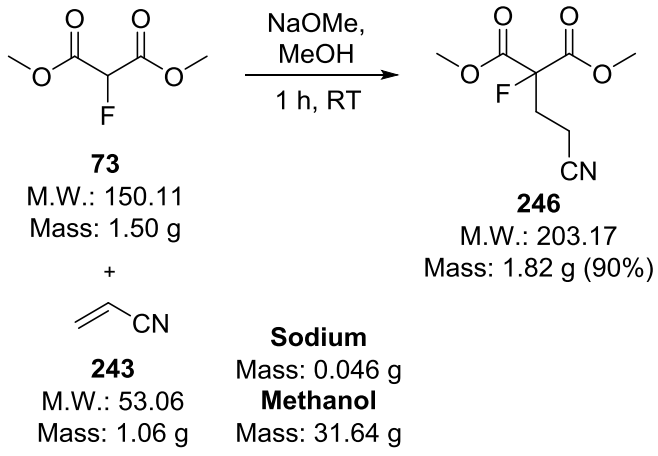

73
M.W.: 150.11
Mass: 1.50 g

+

243
M.W.: 53.06
Mass: 1.06 g

Sodium
Mass: 0.046 g
Methanol
Mass: 31.64 g

246
M.W.: 203.17
Mass: 1.82 g (90%)

Yield	89.6
Conversion	100.0
Selectivity	89.6
AE	100.0
RME	71.1
PMI total	181.1
PMI Reaction	18.8
PMI Solvents	179.6
PMI Workup	162.3

Materials used for workup and isolation: Water (100 g), ethyl acetate (135.3 g), brine (60 g).

$$AE = \frac{203.17}{150.11 + 53.06} \times 100 = \mathbf{100.0}$$

$$RME = \frac{1.82}{1.50 + 1.06} \times 100 = \mathbf{71.1}$$

$$MI = \frac{1.50 + 1.06 + 0.046 + 31.64 + 100 + 135.3 + 60}{1.82} = \mathbf{181.1}$$

Figure 97 - *Synthesis and selected metric calculations of Michael addition product* ***246****.*

The AE of the reaction was calculated to be 100.0, the RME was 71.1 and the total PMI was calculated to be 181.1, of which the MI of solvents was 179.6. Although the synthetic route to the addition product is significantly better than for the literature GSK method, the PMI value for this initial reaction was noticeably high due to the use of large volumes of solvent used in the workup stage.

Scale-up of this reaction was carried out on a 100 mmol (15 g) dimethyl fluoromalonate scale giving 94% crude yield using a similar work-up. Subsequent reactions determined that the purity of the product in this reaction was heavily dependent on reaction time. ^{19}F NMR spectroscopy showed that the reaction had gone to completion and was 99% pure after 1 h, which decreased to 88% purity after 1.5 h and to 64% purity after a total of 4 h.

Subsequently, a weaker base (DBU) was investigated as a replacement for sodium methoxide as it is less likely to promote elimination. Additionally, DBU is listed by GSK as a preferred base in their base selection guide[114] that rates bases on a number of factors including environmental, health and safety and ease of removal/recovery. A 2 h reaction using DBU in acetonitrile yielded the desired product in 95% purity and 85% yield. Since only the catalytic base was changed, the AE remained unchanged for this reaction. The RME was calculated to be 80.9 and the total PMI was 26.5 (***Figure 98***). The decrease in total PMI is a reflection of the use of significantly smaller volumes of solvent.

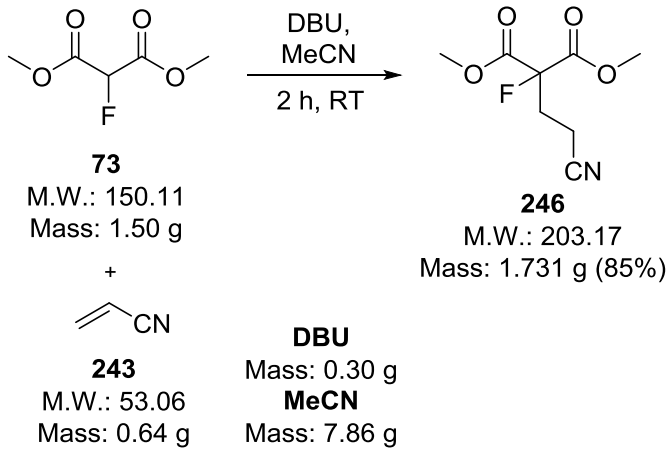

Yield	85.2
Conversion	100.0
Selectivity	85.2
AE	100.0
RME	80.8
PMI total	26.0
PMI Reaction	6.0
PMI Solvents	24.5
PMI Workup	20.0

Materials used for workup and isolation: Conc. HCl (0.11 g), water (15 g), ethyl acetate (13.53 g), brine (6 g).

$$AE = \frac{203.17}{150.11 + 53.06} \times 100 = \mathbf{100.0}$$

$$RME = \frac{1.73}{1.50 + 0.64} \times 100 = \mathbf{80.8}$$

$$MI = \frac{1.50 + 0.64 + 0.30 + 7.86 + 0.11 + 15 + 13.53 + 6}{1.73} = \mathbf{26.0}$$

***Figure 98** - Synthesis of **246** from dimethyl fluoromalonate with selected metric calculations.*

Another benefit to this method over the previous attempts is that acetonitrile is also used in the synthesis of dimethyl fluoromalonate using F_2 methodology. This could potentially lead to a telescoped reaction that uses the same volume of solvent over two steps of the reaction scheme (fluorination and Michael addition). A decrease in total solvent volume for the reaction scheme would lower the total PMI of the reaction.

To determine the feasibility of a one-pot style reaction, DBU and two further 'green' bases (potassium phosphate and 2-methyl pyridine) were screened under two sets of conditions (***Table 12***).

Firstly, the Michael addition reaction between dimethyl fluoromalonate and acrylonitrile was tested for each base in acetonitrile with copper (II) nitrate hemipentahydrate present. Copper (II) nitrate hemipentahydrate is used as a catalyst in the synthesis of dimethyl fluoromalonate from dimethyl malonate and F_2, and so would be present in the crude fluoromalonate solution obtained in a one-pot style synthesis. Secondly, the bases were screened in a solventless reaction between fluoromalonate and acrylonitrile. Since both reactants are liquids, it is possible that no solvent is required for the addition reaction.

Table 12 *– Michael addition reactions using different bases.*

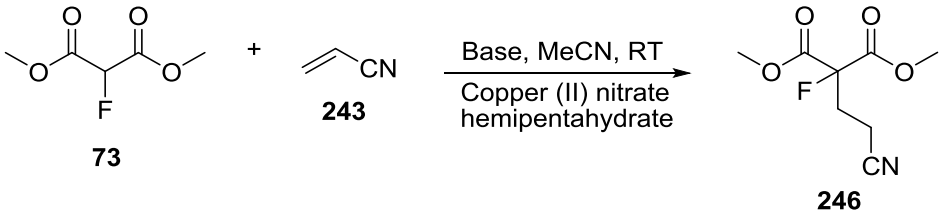

Base	Eq. copper nitrate hemipentahydrate	Eq. base	Conversion* /%
DBU	0	0.2	≥ 99
	0.1	0.25	20
	0.1	0.5	23
	0.1	1.0	≥ 99
Potassium phosphate	0	0.2	≥ 99
	0.1	0.2	0
	0.1	0.5	≥ 99
2-Methyl pyridine	0	0.2	0
	0.1	0.2	0

*Conversion measured by ^{19}F NMR spectroscopy

DBU catalysed the solvent-free reaction to full conversion, though minimal conversion was observed in the reaction mixture containing copper nitrate. A further portion of base was added (up to 1 eq.) and full conversion was observed. Similarly, potassium phosphate catalysed the reaction in absence of the copper catalyst but minimal conversion was observed in the presence of copper nitrate. When additional potassium phosphate was added (up to 0.5 eq.) the reaction went to full conversion. 2-Methyl pyridine did not catalyse the reaction even in the absence of copper nitrate.

It is probable that the organic bases are coordinating to the copper salts and so are unavailable in the reaction solution to catalyse the Michael addition reaction. Although both DBU and potassium phosphate catalysed the reaction with copper present, potassium phosphate was selected as the base for subsequent reactions because it is a solid and so it should be possible to remove this base by filtration and avoid aqueous workup that would likely be necessary if organic bases were used.

These model reactions served to show that it was feasible to avoid a workup to remove the copper catalyst since full conversion was obtained with the copper catalyst still present. Both potassium phosphate reactions in ***Table 12*** were scaled up from the 3 mmol scale used in the screening reactions.

The one-pot fluorination-Michael addition reaction was then carried out on a 160 mmol (21 g) dimethyl malonate **72** scale (**Figure 99**). Following the fluorination reaction using the optimised conditions the system was purged with nitrogen to remove any residual fluorine gas before 0.5 eq. K_3PO_4 was added and the solution stirred. Acrylonitrile **243** was added over 30 min and the solution stirred. After 24 h poor conversion was observed by ^{19}F NMR spectroscopy and so a further 0.5 eq. of K_3PO_4 was added and the reaction stirred for 24 h, after which time conversion had stopped at approximately 30%. The base was then removed by filtration and a further portion of K_3PO_4 (0.2 eq.) was added leading to full conversion after a further 24 h. It is likely that the HF produced in the fluorination reaction hinders the base and so additional base is required to catalyse the Michael addition effectively. After a small aqueous workup and purification by Kugelrohr distillation the product was obtained in 58% isolated yield with an AE value of 91.0, a RME of 49.5 and a PMI of 12.0 over the two reaction steps.

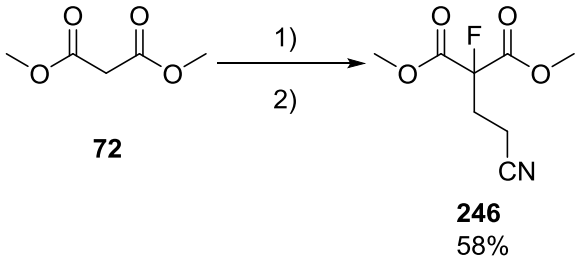

1) 20% F_2/N_2, $Cu(NO_3)_2 \cdot 2.5H_2O$, MeCN, 0-5 ^oC, 4.5 h
2) i) Acrylonitrile, K_3PO_4 (0.5 eq.), MeCN, RT, 24 h
ii) K_3PO_4 (0.5 eq.), 24 h
iii) Filtration to remove K_3PO_4 followed by addition of 0.2 eq. fresh K_3PO_4, 24 h

Figure 99 *– One-pot fluorination/Michael addition reaction of dimethyl malonate in which the crude fluoromalonate is not isolated before alkylation.*

The optimised fluorination method leads to the consumption of all dimethyl malonate **72** leaving only dimethyl 2-fluormalonate **73** and a small quantity of dimethyl 2,2-difluoromalonate (unreactive towards alkylation at the 2-position) so no alkylation products of non-fluorinated malonate are observed. The difluorinated by-product is removed during the distillation following the alkylation reaction.

Subsequent one-pot style reactions followed a method based on this procedure, whereupon the crude fluoromalonate solution was stirred with potassium phosphate and filtered before a further portion of base was added.

The solventless reaction was scaled up to a 30 mmol (4.5 g) dimethyl fluoromalonate scale giving 72% conversion after 3 min, 79% conversion after 30 min and 98% conversion overnight. However, the reaction is very exothermic and heats up significantly upon addition of acrylonitrile which is a significant hazard on the manufacturing scale so it was decided that the reaction should occur with solvent present to enable better thermal control. Also, slow addition of acrylonitrile to allow more time for any heat to dissipate than with a rapid addition of acrylonitrile was achieved with a syringe pump in the following reactions. The effect of temperature on conversion was investigated and the results are shown in ***Table 13***.

***Table 13** - Table displaying reaction conversions using different temperatures.*

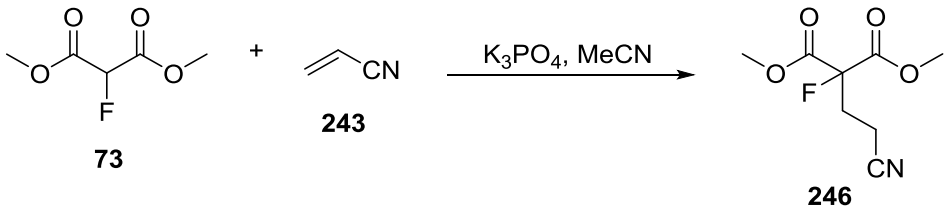

Temp. (^{o}C)	Eq. K_3PO_4	Conversion* /%
25	0.1	33 (1.5 h), 61 (24 h), 80 (144 h)
25	0.2	36 (1.5 h), ≥ 99 (20 h)
55	0.2	97 (1.5 h), ≥ 99 (3 h)
85	0.2	99 (1.5 h)

*Conversion measured by ^{19}F NMR spectroscopy

The reaction attempted at room temperature with 0.1 eq. base showed 61% conversion after 24 h, though conversion peaked at 80% after 6 days (144 h). This rate of reaction was deemed too slow to allow for the reaction to occur in any feasible timeframe.

The reaction was repeated with 0.2 eq. base and full conversion was observed after 20 h. 55 ^{o}C gave 97% conversion after 1.5 h and 85 ^{o}C similarly gave 99% conversion after 1.5 h, the best results achieved. Because there was no significant difference in reaction time between 55 ^{o}C and 85 ^{o}C, all subsequent addition reactions were carried out at 55 ^{o}C.

Subsequently, a scaled up one-pot style reaction (***Figure 100***) was carried out on a 200 mmol dimethyl malonate scale using 2 eq. potassium phosphate (in two portions, as before) and gave full conversion in 3.25 h following the addition of acrylonitrile over 30 min, resulting in 60% isolated yield (following distillation) with a PMI value of 12.3 and a RME value of 51.1.

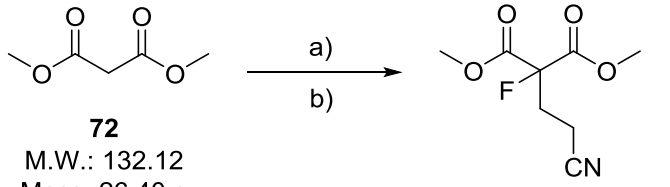

72
M.W.: 132.12
Mass: 26.40 g

246
M.W.: 203.17
Mass: 24.45 g (60%)

Yield	60.2
Conversion	100.0
Selectivity	60.2
AE	91.0
RME	51.1
PMI total	12.3
PMI Reaction	8.7
PMI Solvents	6.7
PMI Workup	3.6

a) 20% F_2/N_2, $Cu(NO_3)_2{\cdot}2.5H_2O$, MeCN, 4.5 h, 0-5 °C
b) Acrylonitrile, K_3PO_4, MeCN, 3.25 h, 55 °C

Materials used in reaction: Fluorine (M.W. 38.00, 8.36 g), $Cu(NO_3)_2{\cdot}2.5H_2O$ (4.65 g), MeCN (86.46 g), K_3PO_4 (84.9 g), acrylonitrile (M.W.: 53.06, 12.7 g).

Materials used for workup and isolation: MeCN (78.60 g).

$$AE = \frac{203.17}{132.12 + 38.00 + 53.06} \times 100 = \mathbf{91.0}$$

$$RME = \frac{24.45}{26.4 + 8.36 + 12.7} \times 100 = \mathbf{51.1}$$

$$MI = \frac{26.4 + 8.36 + 4.65 + 165 + 84.9 + 12.7}{24.45} = \mathbf{12.3}$$

Figure 100 *- Reaction scheme and selected metric calculations for the one-pot style synthesis of* ***246*** *from dimethyl malonate* ***72****.*

In conclusion, the product of the Michael addition reaction between dimethyl fluoromalonate and acrylonitrile has successfully been achieved. A number of variations to the original synthetic route have, along with the use of the green metrics package, developed the process into a greener and more efficient reaction pathway to a one-pot two step sequential process (PMI 12).

3.2.2. Reduction of Nitrile and Cyclisation

The second reaction step involved reduction of the nitrile group to an amino group and subsequent cyclisation to form heterocycle **248**. Reductions of **246** were carried out in a Parr hydrogenator with palladium/carbon in methanol with a catalytic amount of concentrated hydrochloric acid.

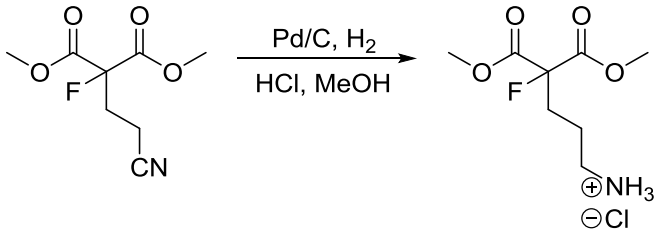

246 **247**

Figure 101 *- Synthesis of 'open-chain' salt* ***247*** *by reduction of* ***246****.*

Upon filtration through celite to remove the palladium/carbon catalyst the solvent was removed *in vacuo*. A solid formed that was insoluble in organic solvents but soluble in water and methanol/ethanol and was suspected to be the 'open-chain' salt **247**. Washing the insoluble salt with an organic solvent such as ethyl acetate provides an easy purification process for the 'open-chain' systems leading to heterocycles.

This reaction was therefore repeated with two amendments (***Figure 102***). The reaction time was increased to 7.5 h and the methanol filtrate from the celite 'plug' was concentrated *in vacuo* in a 50 ^{o}C water bath in order to aid removal of residual water from the crude product. As a result, the crude salt was noticeably drier and more powder-like than with previous attempts and, after an ethyl acetate wash, gave the desired product **247** in 83% yield. The metric calculations for this reaction show that the PMI value is 8.1 and the RME value is 61.

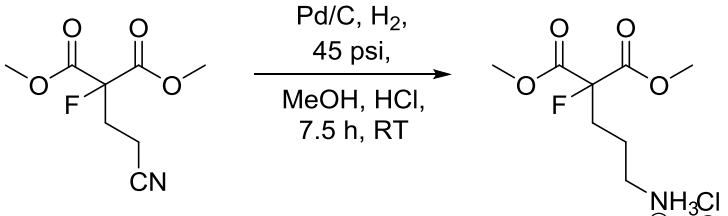

246
M.W.: 203.17
Mass: 10.16 g

247
M.W.: 243.66
Mass: 10.07 (83%)

Yield	82.6
Conversion	100.0
Selectivity	82.6
AE	100.0
RME	61.0
PMI total	8.1
PMI Reaction	3.9
PMI Solvents	6.2
PMI Workup	4.3

Materials used in reaction: Pd/C (2.66 g), hydrogen (M.W.: 2 x 2.00, 0.400 g) conc. HCl (M.W.: 36.46, 5.95 g), MeOH (19.78 g).

Materials used for workup and isolation: MeOH (15.82 g), ethyl acetate (27.06 g).

$$AE = \frac{243.66}{203.17 + 4.00 + 36.46} \times 100 = \mathbf{100.0}$$

$$RME = \frac{10.07}{10.16 + 0.40 + 5.95} \times 100 = \mathbf{61.0}$$

$$MI = \frac{10.16 + 0.40 + 5.95 + 2.66 + 35.60 + 27.06}{10.07} = \mathbf{8.1}$$

Figure 102 *- Synthesis of open chain salt* ***247*** *by reduction of* ***246****, with selected metric calculations.*

After some process development, salt **247** was dissolved in water, neutralised with potassium carbonate (1.1 eq.) and concentrated *in vacuo*. The solid was then washed with ethyl acetate and concentrated *in vacuo* to give the heterocycle **248** in 72% yield but the PMI value for this small scale (3 mmol) reaction was relatively high (52).

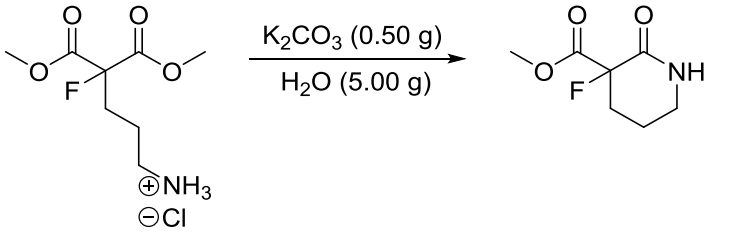

247
M.W.: 243.66
Mass: 0.73 g

248
M.W.: 175.16
Mass: 0.38 (72%)

Yield	72.4
Conversion	100.0
Selectivity	72.4
AE	71.9
RME	52.1
PMI total	52.0
PMI Reaction	16.4
PMI Solvents	48.8
PMI Workup	35.6

Materials used for workup and isolation: Ethyl acetate (13.53 g).

$$AE = \frac{175.16}{243.66} \times 100 = \mathbf{71.9}$$

$$RME = \frac{0.38}{0.73} \times 100 = \mathbf{52.1}$$

$$MI = \frac{0.73 + 0.50 + 5.00 + 13.53}{0.38} = \mathbf{52.0}$$

Figure 103 *- Synthesis and selected metric calculations of heterocycle* ***248*** *from open chain salt* ***247****.*

The salt and the heterocycle were characterised by ^{1}H, ^{19}F and ^{13}C NMR spectroscopy, low and high resolution mass spectrometry, infrared spectroscopy, X-ray crystallography and melting point analysis.

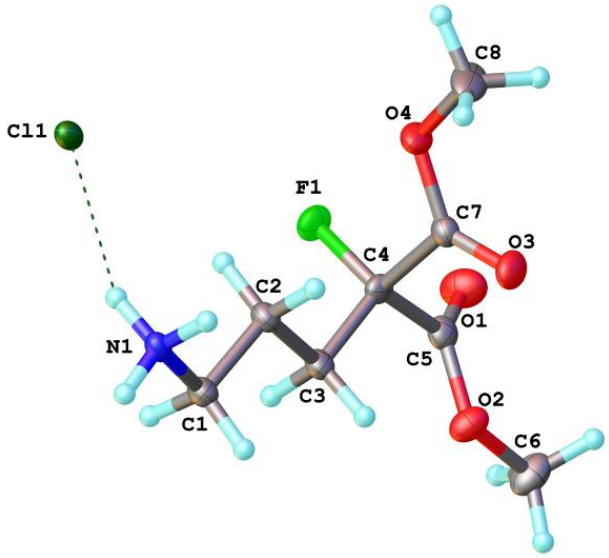

Figure 104 *- Molecular structure of salt* ***247****.*

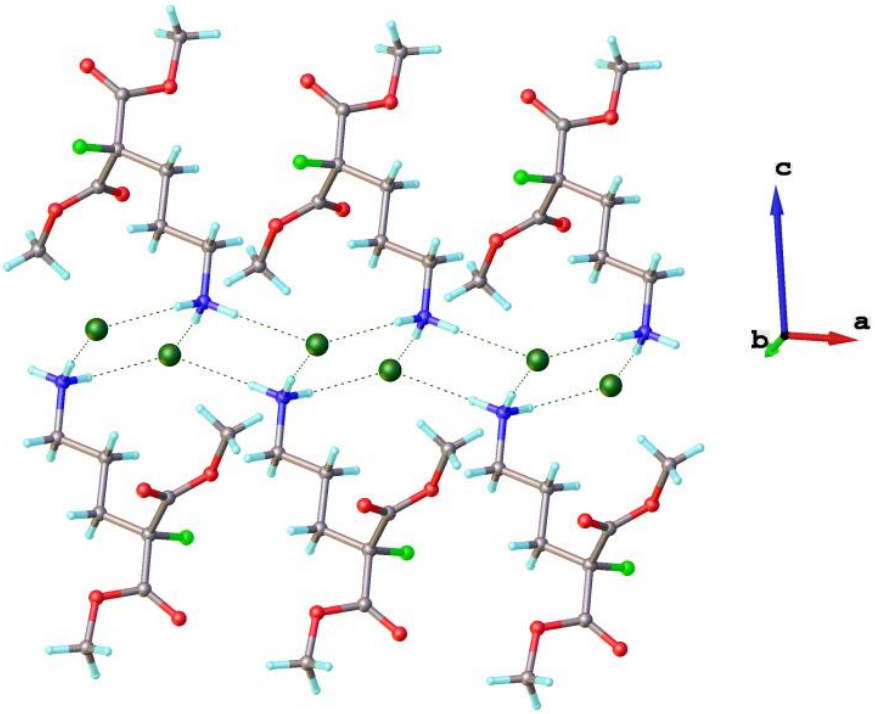

Figure 105 *- Crystal structure of salt* ***247****, as determined by X-ray crystallography.*

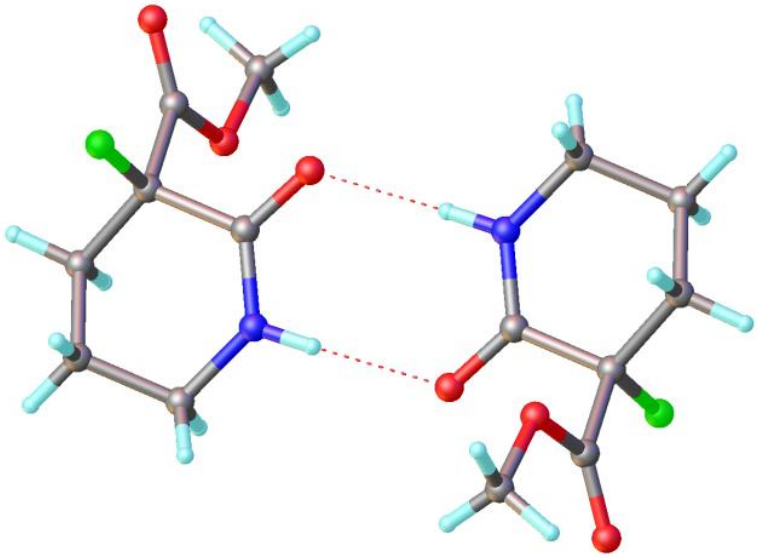

Figure 106 *- Molecular structure of* ***248*** *dimer.*

3.2.3. Biochemical Introduction of Asymmetry

Following the successful synthesis of the racemic fluorolactam **248** and the intermediates **246** and **247** in Durham, the GSK collaborators developed a biocatalytic route to enantiopure heterocycle (*S*)-**248**. The results presented in this section (3.2.3.) were obtained by Dr Nicky J. Willis of GSK. Routes previously published by GSK involving chiral fluorination of the heterocycle are described in appendix section A1.1.4.

The first strategy used hydrolase enzymes with nitrile **246** as a substrate to yield an asymmetric fluoromalonate derivative using a process for a related non-fluorinated reaction (appendix section A1.1.3.).[115] Unfortunately it was discovered that nitrile **246** is unstable to degradation in solution at pH 7.0-7.1 and so the use of **246** as a potential substrate for desymmetrisation was discontinued.

Hydrolysis reactions of salt **247** were then investigated. Gutman *et al*.[116] had previously investigated the use of PLE and other enzymes in the synthesis of lactams by aminolysis of the corresponding aminoesters (appendix section A1.1.3.). Consequently, GSK attempted the amidation reaction of salt **247** using various hydrolase catalysts in anhydrous tertiary amyl alcohol as solvent (***Figure 107***) however, unfortunately no enantioselectivity was detected and the reactions only yielded racemic fluorolactam **248**.

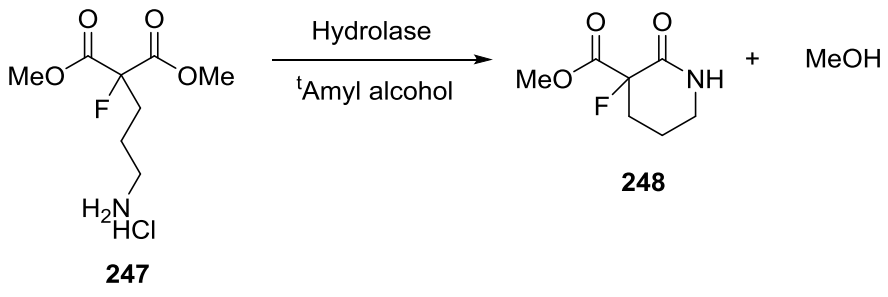

247 **248**

Figure 107 *– Attempted hydrolase catalysed route to enantiopure fluorolactam (S)-**248** from salt **247** yielded only the racemic fluorolactam **248**. (Work carried out by Nicky J. Willis).*

Efforts then turned to chiral resolution of racemic fluorolactam **248** to give enantiomerically pure (*S*)-**248**. The stability of **248** to hydrolysis in aqueous phosphate buffer was first investigated and found to be stable for over 16 h at 20-25 ^{o}C and pH 7.3.

An initial screen of 56 enzymes against **248** in these reaction conditions was then undertaken (Appendix section A1.1.5.). Of the 56 hydrolases, 25 were found to resolve lactam **248** to a reasonable extent (10-60% hydrolysis) and a further five to a greater extent (60-100% hydrolysis) in 8 h and so were selected for further analysis.

A handful of hydrolases showed a high level of enantioselectivity giving both esters ((*S*)-**248** and (*R*)-**248**) and both acids ((*S*)-**249** and (*R*)-**249**) (***Table 14***). Of these, CAL-B 10,000 (*Candida antarctica* lipase B) was selected for scale up because of the high enantioselectivity and reasonable yield it afforded, and the fact that it is available for purchase on large scale at low cost. Additionally, the use of CAL-B 10,000 on large scale syntheses has literature precedent.[117,118]

Table 14 – *The four most promising entries from the screen of 56 hydrolases. (Work carried out by Nicky J. Willis).*

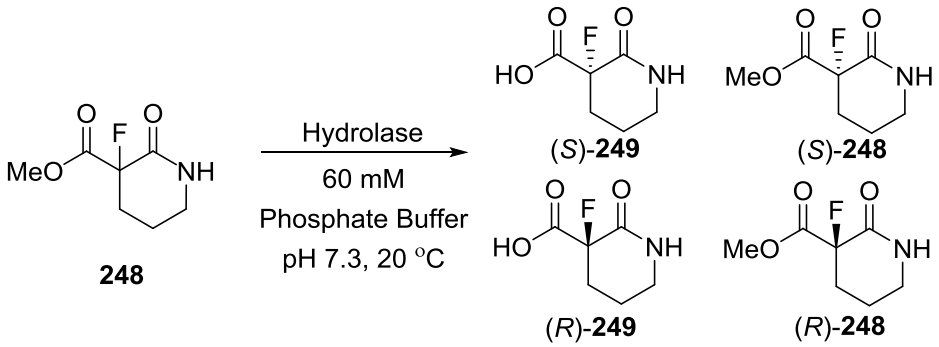

Entry	Hydrolase	Conv. /%[a]	Acid 249 *ee* /%		Ester 248 *ee* /%	
1	JM X14	30	>95	(*S*)-**249**	62	(*R*)-**248**
2	JM X35	19	>95	(*S*)-**249**	19	(*R*)-**248**
3	JM X50	28	>95	(*S*)-**249**	37	(*R*)-**248**
4	CAL-B 10,000	51	>95	(*R*)-**249**	>95	(*S*)-**248**

[a]Calibrated UPLC-MS conversion.

As a result, the two esters (*S*)-**248** and (*R*)-**248** were isolated by preparatory scale chiral HPLC and X-ray crystallographic analysis confirmed their structures and absolute stereochemistries (***Figure 108***). HPLC required the synthesis of the racemic acid **249** as a standard. This was achieved by reaction of the racemic ester **248** with potassium hydroxide based on a literature procedure.[119]

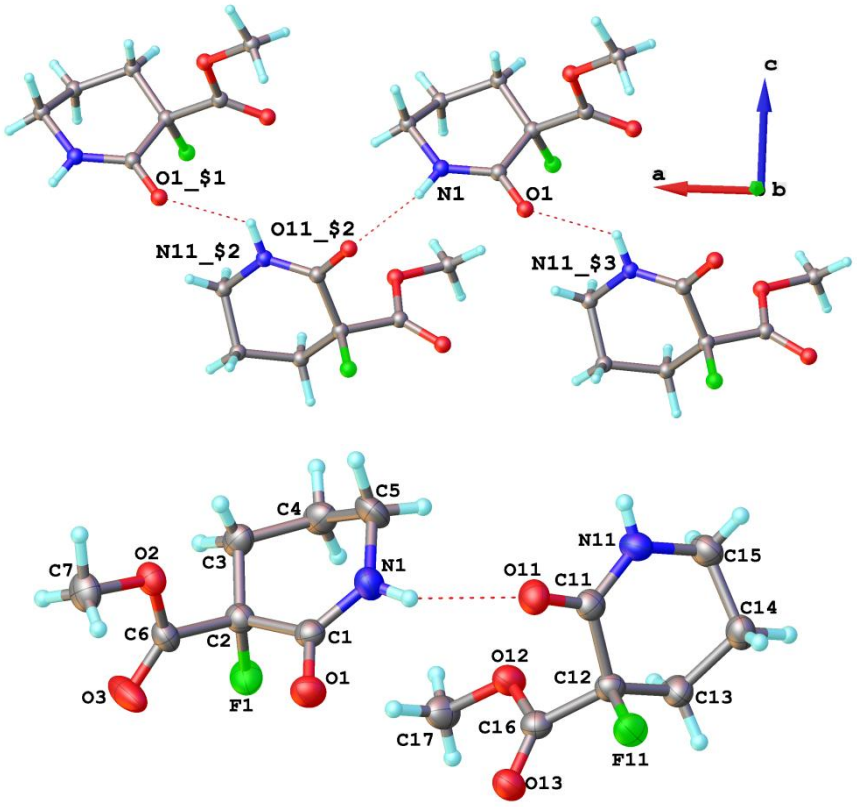

***Figure 108** – Structures of (S)-**248** (top) and (R)-**248** (bottom), recrystallized and analysed by X-ray crystallography in Durham.*

Following the successful synthesis of enantiopure fluorolactam (*S*)-**248** from racemic fluorolactam **248** the possibility of telescoping the formation and resolution of (*S*)-**248** from salt **247** was investigated as this would remove an isolation/work-up if successful.

Salt **247** was added to a buffer solution at room temperature to form a 25 mM solution. After 15 min no degradation or side products were observed but the pH was reduced from 7.3 to 6.7. Upon basification to pH 7.3 (sodium hydroxide solution) ^{19}F NMR spectroscopy and chiral HPLC analysis revealed full conversion to the desired product (*S*)-**248** and, upon work-up, the enantiopure fluorolactam (*S*)-**248** was isolated in 47% yield with 98% *ee* (***Figure 109***).

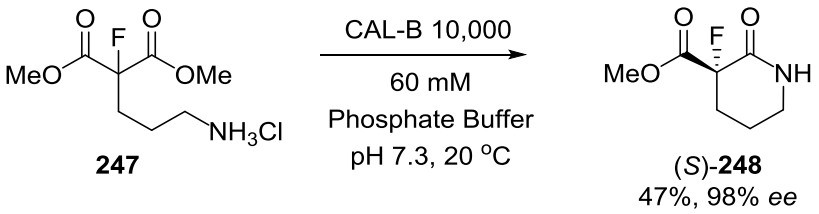

No loss of CAL-B activity after 3 uses

***Figure 109** – The initial telescoped synthesis of fluorolactam (S)-**248** from salt **247**. (Work carried out by Nicky J. Willis).*

Scale-up reactions initially encountered difficulty because when higher concentrations (250 mM) of salt **247** were added to the solution the pH dropped to 4.9 and at this acidic pH hydrolysis side reactions were observed. This difficulty was overcome by the slow addition of the salt and base such that the pH was maintained between 6.8 and 7.3 and a subsequent reaction (257 mM) successfully yielded the desired enantiopure fluorolactam (*S*)-**248** (***Figure 110***). Additionally, the CAL-B enzyme was recovered quantitatively and recycled. No loss of enzyme activity was observed after three subsequent reactions.

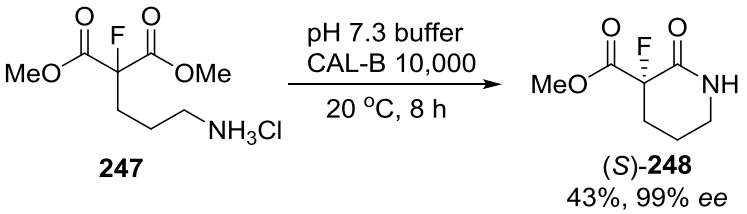

***Figure 110** – The telescoped synthesis of fluorolactam (S)-**248** from salt **247**. (Work carried out by Nicky J. Willis).*

The reduction of nitrile **246** to salt **247** was then optimised by our GSK collaborators. Various parameters were investigated, including catalyst loading, hydrochloric acid stoichiometry, volume of water, volume of methanol, pressure and temperature. A full list of screen reactions and further details are available in appendix section A2. The final optimised process was then scaled up to 10 g (49.2 mmol) **246** scale and gave the desired hydrochloride salt **247** in 84% yield (***Figure 111***).

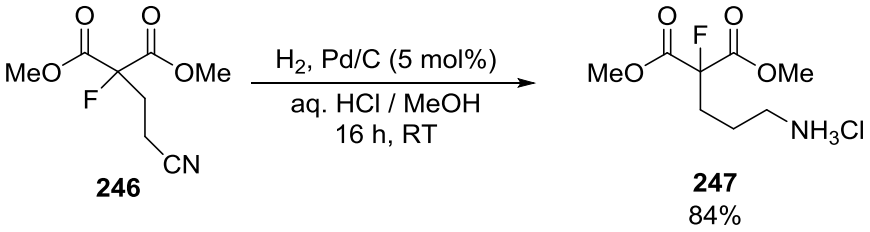

***Figure 111** – The optimised synthesis of hydrochloride salt **247** from nitrile **246**. (Work carried out by Nicky J. Willis).*

Following this optimisation of the syntheses of salt **247** and fluorolactam (*S*)-**248** the processes were analysed by the green metrics package.

3.2.4. Metric Analysis of Further Optimised Hydrogenation and Cyclisation Steps

The metric values for the GSK optimised syntheses of salt **247** and fluorolactam (*S*)-**248** are shown below. Full details and calculations can be found in the appendix of this thesis (section A1.1.6.).

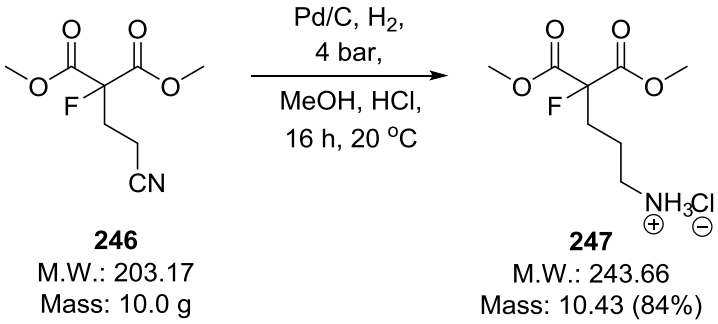

Yield	84
AE	100
RME	73.7
PMI total	12.0
PMI Reaction	5.2
PMI Solvents	10.1
PMI Workup	6.8

Materials used in reaction: Pd/C (2.62 g), hydrogen (M.W.: 2 x 2.02, 1.0 g, assuming 3 L gas volumes (autoclave + storage tank) at 4 bar and 20 °C) conc. HCl (M.W.: 36.45, 5.82 g), MeOH (81.7 g).

***Figure 112**– Optimised synthesis and selected metric calculations of hydrochloride salt **247** from nitrile **246**.*

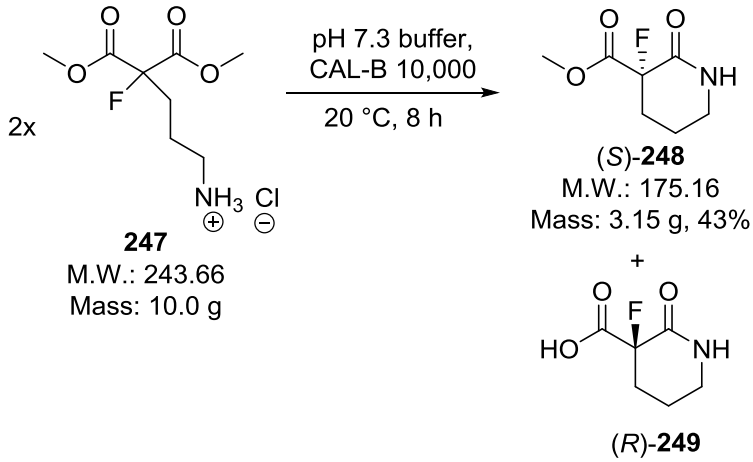

Yield	43
AE	35.9
RME	31.5
PMI total	132.0
PMI Reaction	110.1
PMI Solvents	126.6
PMI Workup	21.9

Materials used in reaction: 0.06 M Na_2HPO_4 : 0.06 M KH_2PO_4 buffer (assume overall 246 mL, assume d = 1.0 g/mL, 246 g), 05 M NaOH solution (assume 1 eq. NaOH, 82 mL, 83.6 g solution), Fermase immobilised CAL-B 10,000 (7.2 g).

Figure 113** – Optimised synthesis and metric calculations of fluorolactam (S)-**248** from hydrochloride salt **247.

3.3 Conclusions

With the telescoped synthesis of nitrile **246** from dimethyl malonate via fluoromalonate **73** optimised in Durham and the syntheses of salt **247** from nitrile **246** and enantiopure fluorolactam (*S*)-**248** from salt **247** developed in collaboration with GSK (specifically Nicky J. Willis), the overall metrics of the optimised process were available for analysis and comparison with the literature process.

The metrics for the Durham/GSK process are as follows. Full details and calculations can be found in the supporting information of the related publication[102] and the appendix of this thesis (section A2.) with further discussion in appendix section A1.1.7.

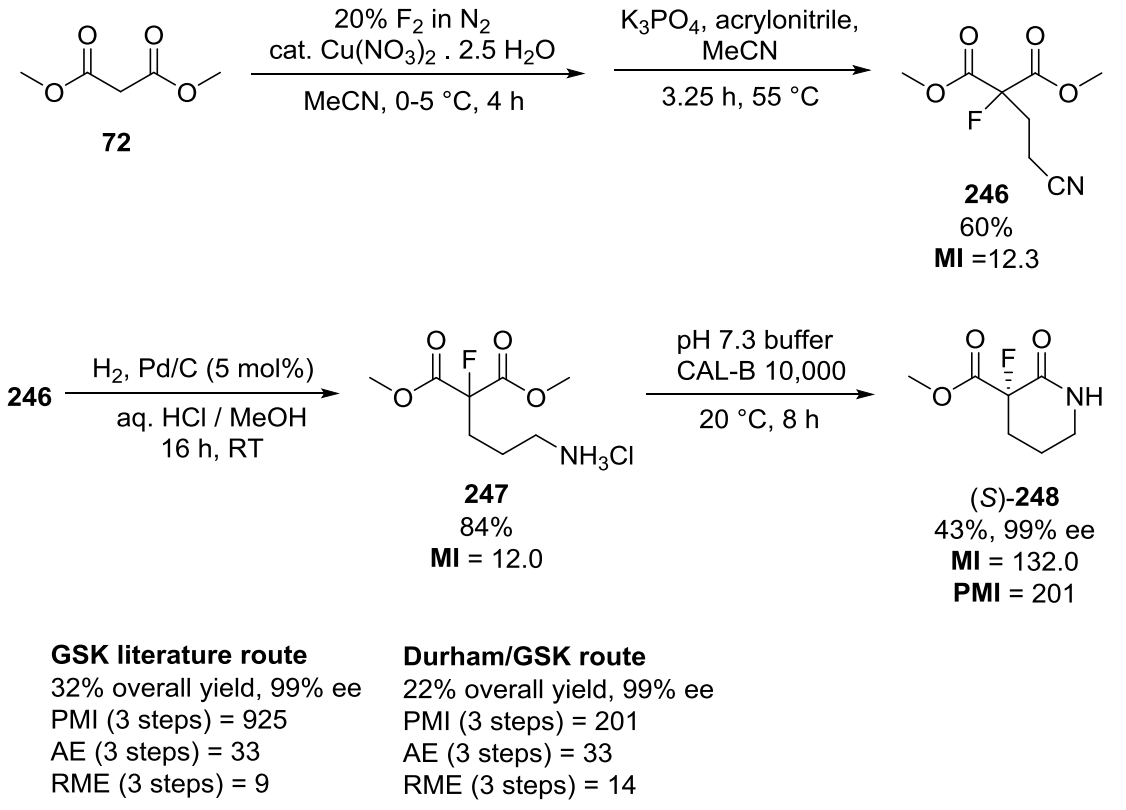

GSK literature route	**Durham/GSK route**
32% overall yield, 99% ee	22% overall yield, 99% ee
PMI (3 steps) = 925	PMI (3 steps) = 201
AE (3 steps) = 33	AE (3 steps) = 33
RME (3 steps) = 9	RME (3 steps) = 14

***Figure 114** – The optimised synthesis of fluorolactam* (*S*)-**248** *from dimethyl malonate.*

Thus, the overall yield for the Durham/GSK optimised process is 22% compared to 32% yield via the GSK literature procedure, primarily due to the fact that the chiral resolution of (*S*)-**248** has a maximum yield of 50% because the 50% undesired enantiomer (*R*)-**249** is lost.

The overall AE of the process is 33, the same as the literature procedure. Again, when 50% of the material is lost in the chiral resolution step this limits the overall AE. The first two steps of the optimised process have good AEs (90 and 100) and the RME of the optimised process is 14, slightly better than the literature 9.

The overall PMI of the optimised process is 201.2, less than a quarter of the literature value of 925. This value is clearly a considerable improvement on the literature procedure. The PMI values for the first two steps (dimethyl malonate to salt **247**) are both around 12, meaning that the bulk of the PMI value comes from the resolution step, specifically the limited yield and AE combined with the relatively high solvent usage. Enzyme reactions typically require a reasonable quantity of water as solvent to function efficiently and though used in higher volumes, water is generally considered to be environmentally benign.

In addition to these quantitative improvements, several more qualitative improvements have been achieved. Expensive NFSI has been eliminated and replaced by cheaper fluorine gas, complex heavy metal catalysts have been replaced by cheaper and non-toxic enzymes and the time-consuming expensive HPLC step has been removed.

Chapter 4. Synthesis of Cyclic Fluorolactam Methyl 3-fluoro-2-oxopyrrolidine-3-carboxylate 250 and Methyl 3-fluoro-2-oxoazepane-3-carboxylate 251

4.1. Introduction

Following synthesis of the 6-membered fluorolactam in the previous chapter we targeted the synthesis of 5- and 7-membered derivatives, methyl 3-fluoro-2-oxopyrrolidine-3-carboxylate **250** and methyl 3-fluoro-2-oxoazepane-3-carboxylate **251** respectively.

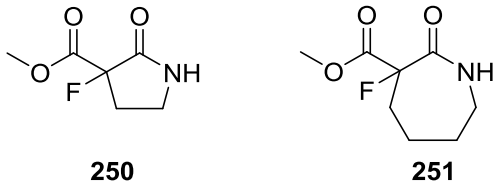

Figure 115 *- Structures of the 5- and 7-membered analogues.*

The 5-membered ring **250** is an intermediate in the synthesis of an αV integrin antagonist developed by GSK (***Figure 116***).[120,121]

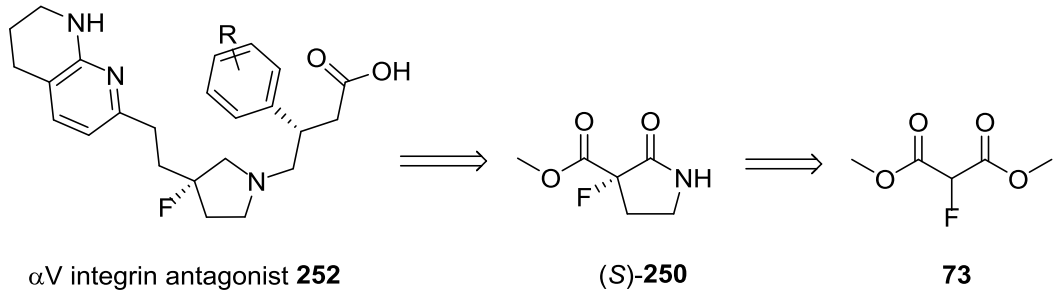

Figure 116 *– Disconnection of an αV integrin antagonist target to dimethyl fluoromalonate via a 5-membered cyclic fluoroamide intermediate.*

Syntheses of the 5- and 7-membered ring systems were attempted using bromoacetonitrile and 4-bromobutyronitrile respectively in alkylation steps followed by reduction and cyclisation in adaption of methodology described in Chapter 3.

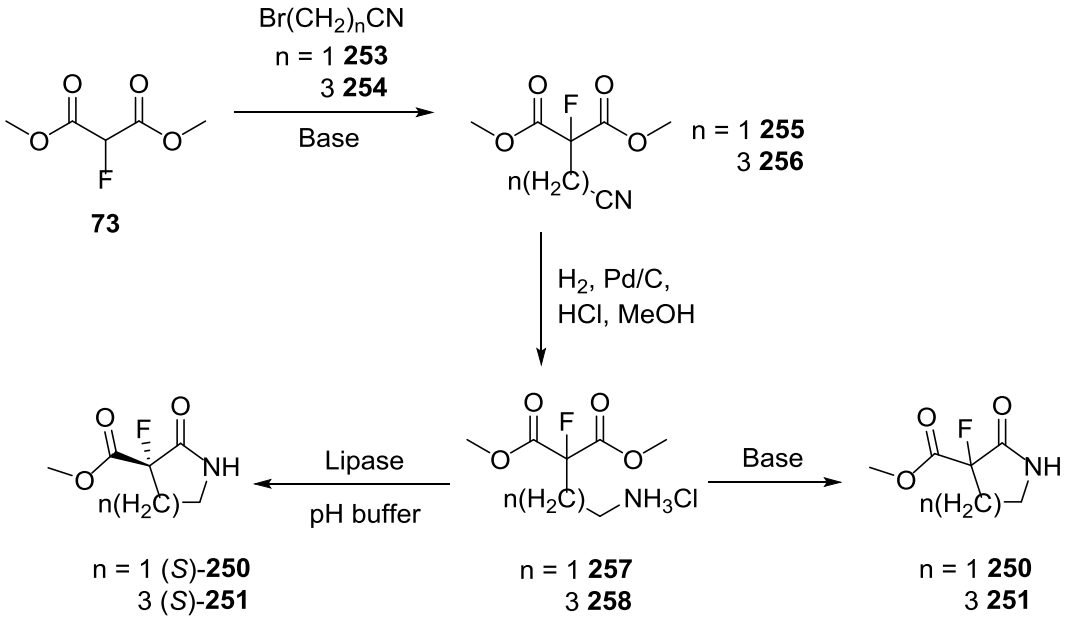

Figure 117 *- Proposed synthetic route to 5- and 7-membered fluorinated heterocycles.*

4.2. Synthesis of 5-Membered Fluorolactam Methyl 3-fluoro-2-oxopyrrolidine-3-carboxylate 250

Reaction of dimethyl fluoromalonate and excess bromoacetonitrile (1.2 eq.) was carried out using excess base and gave the nitrile **255** in 55% yield (3.11 g) after distillation (***Figure 118***).

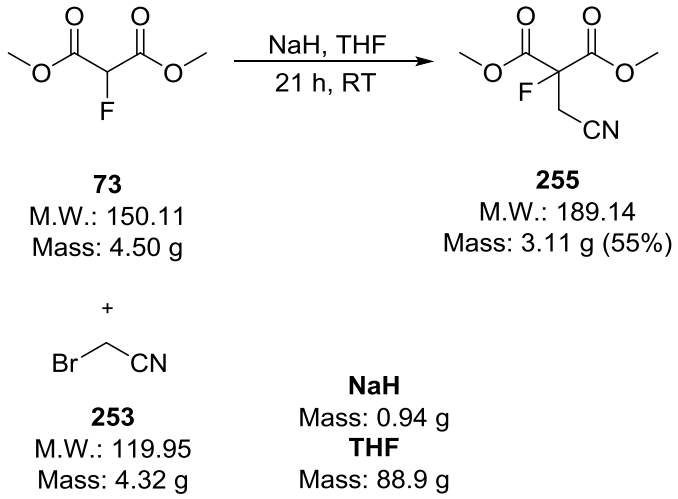

Yield	54.8
AE	70.0
RME	35.3
PMI total	141.5
PMI Reaction	31.7
PMI Solvents	138.0
PMI Workup	109.8

Materials used for workup and isolation: Water (100 g), ethyl acetate (180.4 g), HCl (1.00 g), brine (60 g).

$$AE = \frac{189.14}{150.11 + 119.95} \times 100 = \mathbf{70.0}$$

$$RME = \frac{3.11}{4.50 + 4.32} \times 100 = \mathbf{35.3}$$

$$MI = \frac{4.50 + 4.32 + \ 0.94 + 88.9 + 1 + 100 + 180.4 + 60}{3.11} = \mathbf{141.5}$$

Figure 118 *- The improved synthesis and selected metric calculations of alkylated product **255** from dimethyl fluoromalonate **73** and bromoacetonitrile **253**.*

Metric calculations on this unoptimised reaction show a reasonable AE and RME with a relatively high PMI value, most of which comes from solvent use.

As with the analogous 6-membered fluorolactam synthesis, the nitrile **255** was reduced in a Parr hydrogenator with palladium/carbon and catalytic hydrochloric acid in methanol with hydrogen under 45 psi pressure giving the cyclised fluorolactam **250**.

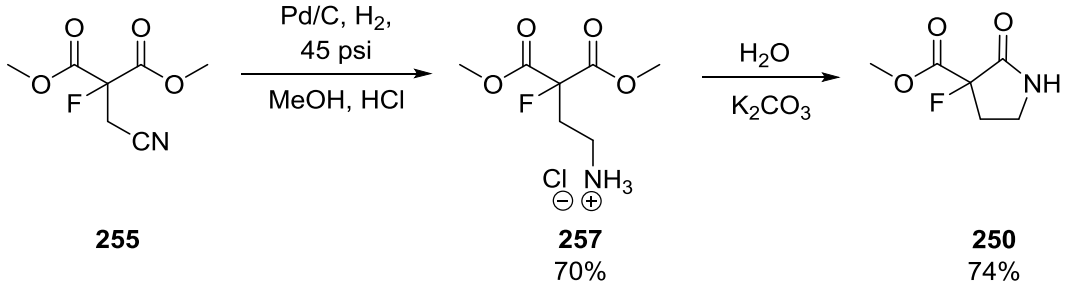

Figure 119 *- Synthesis of the open chain salt **257** and subsequent synthesis of the heterocycle **250** from alkylated product **255**.*

Because of the slight aqueous instability of this system, the salt **257** was isolated before the cyclisation step and each step was performed separately rather than in a telescoped route. Salt **257** was isolated in 70% yield and subsequent basification gave the racemic heterocycle **250** in 74% yield. The hydrogenation reaction has a desirable AE of 100 and a reasonable RME. The PMI is relatively high at 151.9 and can be attributed to the relatively large volume of solvent required for the Parr hydrogenator to give efficient mixing. Similarly, the large PMI of the workup to fluorolactam **250** is attributed to the relatively large solvent usage. The yields in both steps are good.

The salt and heterocycle were analysed by X-ray crystallography and their structures were confirmed.

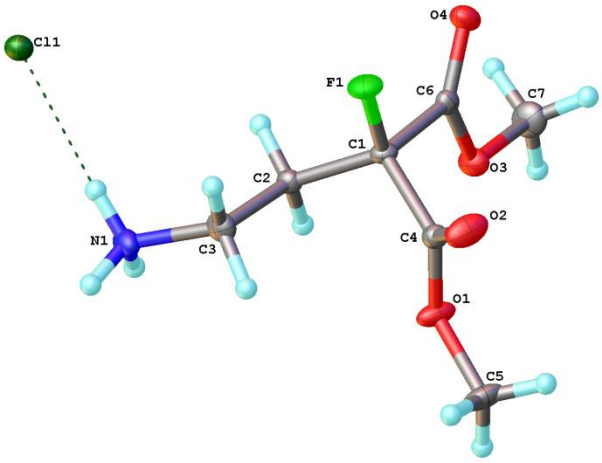

Yield	70.2
AE	100.0
RME	59.2
PMI total	151.9
PMI Reaction	11.8
PMI Solvents	149.9
PMI Workup	140.1

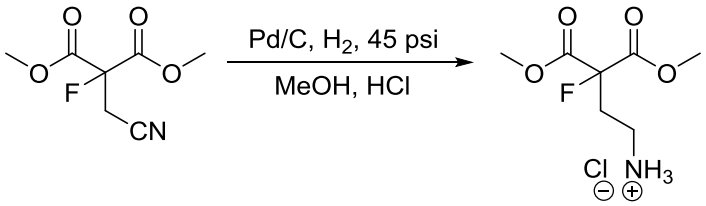

255
M.W.: 189.14
Mass: 189.0

257
M.W.: 229.63
Mass: 1.61 g (70%)

Materials used in reaction: Pd/C (0.52 g), hydrogen (M.W.: 2 x 2.00, 0.400 g) conc. HCl (M.W.: 36.46, 0.43 g), MeOH (15.82 g).

Materials used for workup and isolation: Ethyl acetate (225.5 g).

$$AE = \frac{229.63}{189.14 + 4.00 + 36.46} \times 100 = \mathbf{100.0}$$

$$RME = \frac{1.61}{1.89 + 0.40 + 0.43} \times 100 = \mathbf{59.2}$$

$$MI = \frac{1.89 + 0.40 + 0.43 + 0.52 + 15.82 + 225.5}{1.61} = \mathbf{151.9}$$

Figure 120 *- Molecular structure, showing H-Cl interaction, reaction scheme and selected metric calculations of salt* ***257****.*

Interestingly the 5-membered heterocycle was shown by X-ray crystallography to be a monohydrate, whereas the 6-membered ring analogue was not (***Figure 121***).

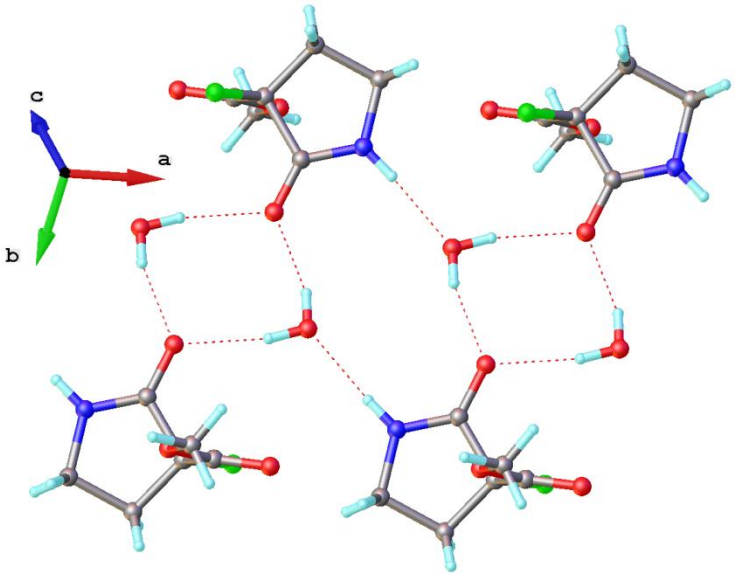

Yield	74.1
AE	70.2
RME	52.0
PMI total	369.8
PMI Reaction	1.9
PMI Solvents	366.0
PMI Workup	367.9

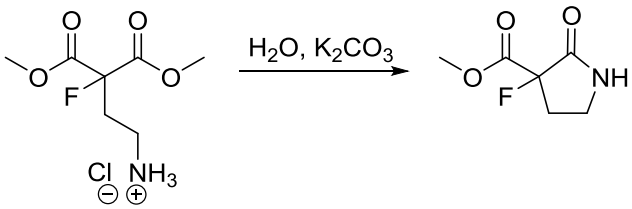

257
M.W.: 229.63
Mass: 1.00 g

250
M.W.: 161.13
Mass: 0.52 (74%)

Materials used for workup and isolation: Water (25 g), K_3PO_4 (1.00 g), ethyl acetate (135.3 g), brine (30 g).

$$AE = \frac{161.30}{229.63} \times 100 = \mathbf{70.2}$$

$$RME = \frac{0.52}{1.00} \times 100 = \mathbf{52.0}$$

$$MI = \frac{1.00 + 1.00 + 25 + 135.3 + 30}{0.52} = \mathbf{369.8}$$

Figure 121 *- Crystal packing structure, showing hydrogen bonding interactions with water molecules, reaction scheme and selected metric calculations of heterocycle* ***250****.*

The synthesis of salt **257** was somewhat optimised by our GSK collaborators by the use of an alternative hydrogenation vessel that allowed the use of only 3.12 mL of methanol for a 0.446 g nitrile **255** scale reaction that gave the salt **257** in 96% yield.

Lipase CAL-B 10,000 was investigated by GSK in the synthesis of (*S*)-**250** but the undesired enantiomer was obtained in this case. Work is ongoing at GSK to find an alternative lipase to give the desired enantiomer (*S*)-**250**.

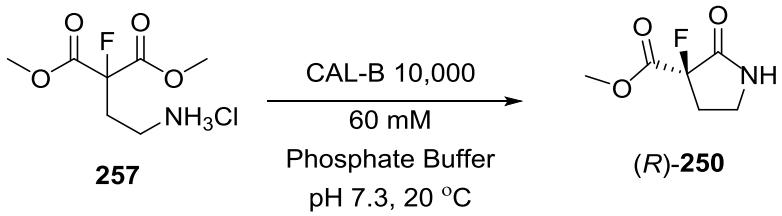

Figure 122 *– Synthesis of chiral fluorolactam (R)-**250** from salt **257**. (Work carried out by Nicky J. Willis).*

4.3. Synthesis of 7-Membered Fluorolactam Methyl 3-fluoro-2-oxoazepane-3-carboxylate 251

As with the 5- and 6-membered ring systems, synthesis of the 7-membered ring system was attempted via an alkylation step from dimethyl fluoromalonate followed by hydrogenation in the presence of hydrochloric acid and a subsequent basic aqueous work-up. Nitrile **256** was synthesised by reaction of dimethyl fluoromalonate **73** with 4-bromobutyronitrile **254** on a 30 mmol scale using sodium methoxide as base, resulting in 64% yield after distillation (***Figure 123***).

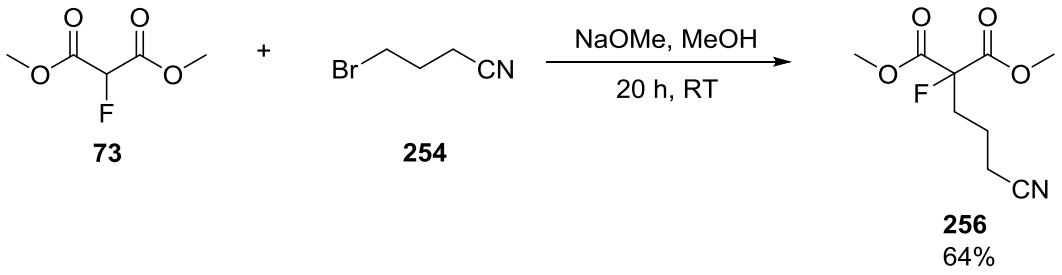

Figure 123 *- Synthesis of alkylation product **256** from dimethyl fluoromalonate **73** and 4-bromobutyronitrile **254** using sodium methoxide as base.*

Nitrile **256** reduced by hydrogenation in a Parr hydrogenator in methanol with catalytic Pd/C and HCl to give the crude salt in 69% yield (***Figure 124***).

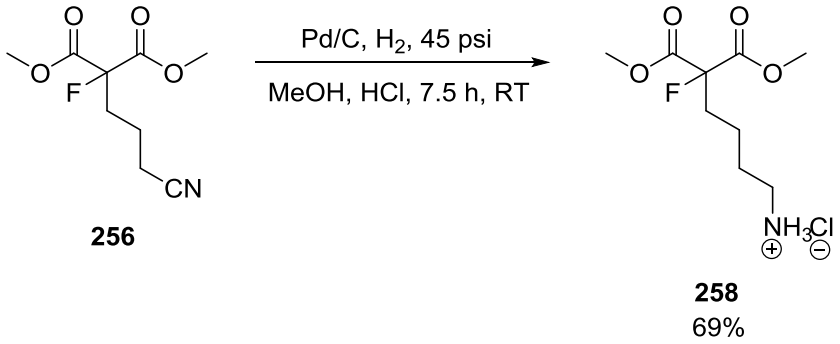

Figure 124 *- Synthesis of hydrochloride salt **258** from nitrile **256**.*

Several recrystallization attempts did not yield crystals with satisfactory properties for analysis by X-ray crystallography. In one instance, due to the hygroscopic nature of methanol, upon evaporation of the methanol solvent residual water hydrolysed the methyl esters of **258** and formed the dicarboxylic acid derivative **259**. This derivative formed analysable crystals that confirmed it to be the zwitterion of the corresponding dicarboxylic acid (***Figure 125***).

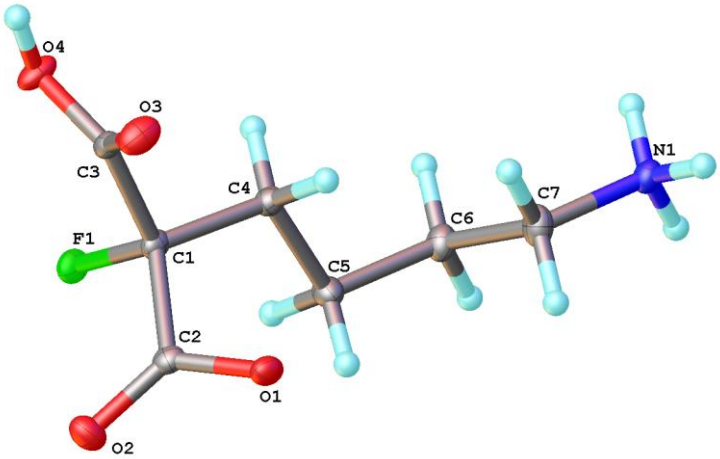

Figure 125 *- X-ray crystallographically determined molecular structure of diacid derivative (**259**) of open chain amine **258**.*

Unfortunately, attempts to form the 7-membered fluorolactam heterocycle by analogous routes described above were unsuccessful, reflecting the difficulty in the synthesis of 7-membered ring systems.

However, heating **258** in a microwave irradiator with one equivalent of DBU gave **251** in 60% crude yield (***Figure 126***).

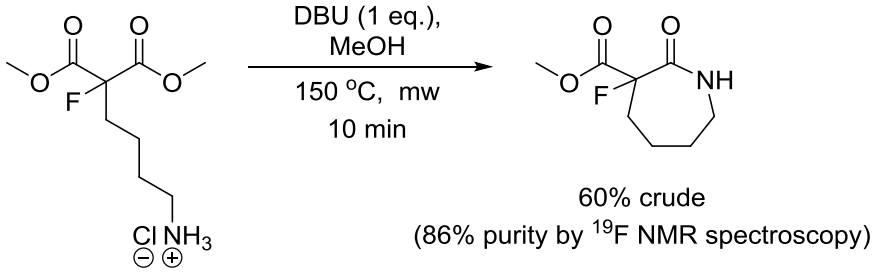

Figure 126 *- Attempted synthesis of 7-membered cyclic fluorolactam **251** from hydrochloride salt **258** using a microwave* reactor.

A small sample of the crude product was recrystallized to give crystals of sufficient quality for X-ray crystallography analysis and confirms the heterocycle's structure (***Figure 127***).

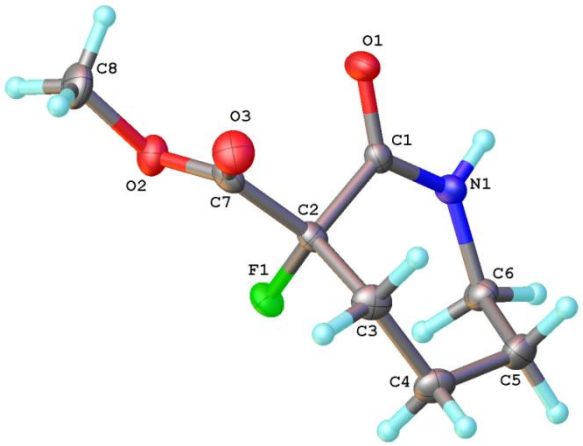

Figure 127 *- Molecular structure of 7-membered cyclic fluorolactam* ***251***.

4.4. Conclusions

A 5-membered analogue **250**, of interest as an intermediate in a potential αV integrin antagonist, and a 7-membered analogue **251** of fluorolactam (*S*)-**248** have been successfully synthesised.

Metric analysis of the racemic 5-membered system showed reasonable AE and RME values and good yields but high PMI values due to the relatively large volumes of solvents used on these small scale, unoptimised reactions. Aqueous instability hindered a telescoped workup of salt **257** to heterocycle **250** from the crude reduction mixture and an attempted lipase reaction of salt **257** yielded the undesired enantiomer of the 5-membered chiral fluorolactam and work is ongoing to reach the desired enantiomer (*S*)-**250**.

Synthesis of the alkylated fluoromalonate derivative **256** was successful and subsequent hydrogenation gave hydrochloride salt **258** in good yield. Basic work-up of salt **258** to heterocycle **251** was considerably less trivial than the corresponding 5- and 6-membered heterocyclic analogues but a crude sample was obtained and its structure confirmed.

Chapter 5. Biocatalytic Synthesis of Ethyl 2-fluoro-3-hydroxy-butanoate Diastereomers

5.1. Aims

Enzymes have the ability to perform stereoselective transformations to yield a single product with the desired stereochemistry that may be difficult to achieve chemically using a large, bulky chiral metal based catalyst. Transition metal based catalysts are often expensive on scale and are not ideal for the pharmaceutical industry due to the toxicity of trace amounts of metal that may remain in the drug. Such catalysts may also be disfavoured from a green chemistry perspective due to the multistep synthesis of the complex ligand system. Another benefit of using enzymes is that reactions are carried out in physiological conditions (atmospheric pressure, close to room temperature etc.) which are simple and inexpensive to maintain.

This project aims to produce a short series of molecules that contain fluorine atoms attached to a stereogenic centre by means of an enzyme based biocatalytic route for fluoroketoester substrates. The following section reviews literature enzymatic reactions of α-fluorocarbonyl species followed by more specific examples of α-fluoroketoesters.

5.2. Literature Examples of Biotransformations of α-Fluorocarbonyl Systems

This brief literature review is in two parts. The first part outlines biotransformations of general α-fluorocarbonyl moieties observed in the literature whilst the second part covers more specific examples of biotransformations involving ketoesters or fluoroketoesters similar in structure to model substrate ethyl 2-fluoroacetoacetate **282**.

This section covers some literature examples of biotransformations that introduce asymmetry to, primarily, α-fluorocarbonyl systems. Whilst a number of non-biologically catalysed syntheses exist, this review focuses on biocatalysed monofluorocarbonyl species and has omitted trifluoro- or difluoro- analogues and non-biocatalysed routes which have been reviewed elsewhere.[122,123]

Lipase P30 has been used to desymmetrise an α-fluoroester in excellent *ee* (***Figure 128***).[124]

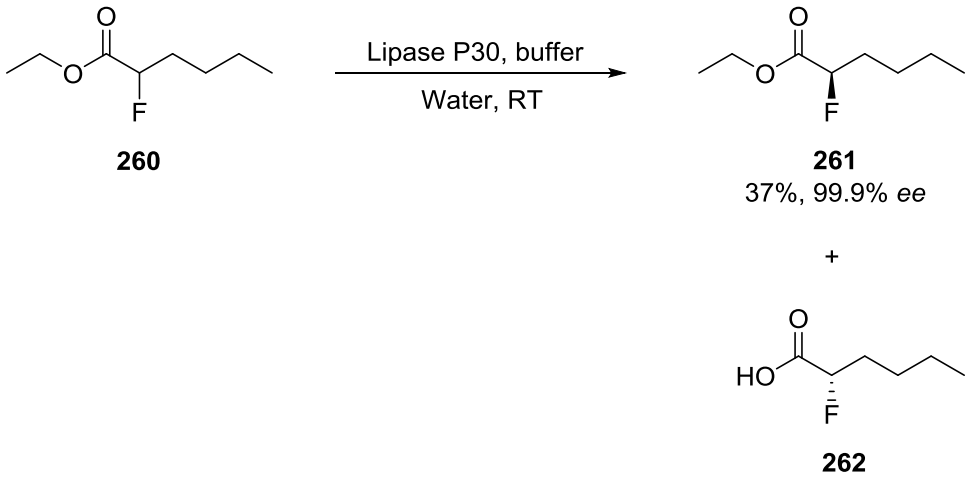

260

261
37%, 99.9% *ee*

+

262

Figure 128– *Lipase catalysed desymmetrisation of ethyl 2-fluorohexanoate.*

Kitazume and co-workers reported the use of immobilised lipase-MY in the stereoselective hydrolysis of diethyl fluoromalonate. Subsequent reduction led to a enantiomerically enriched fluorohydrin in 99% *ee*. The authors also reported similar processes using 2-substituted fluoromalonate derivatives (***Figure 129***).[125,126,127]

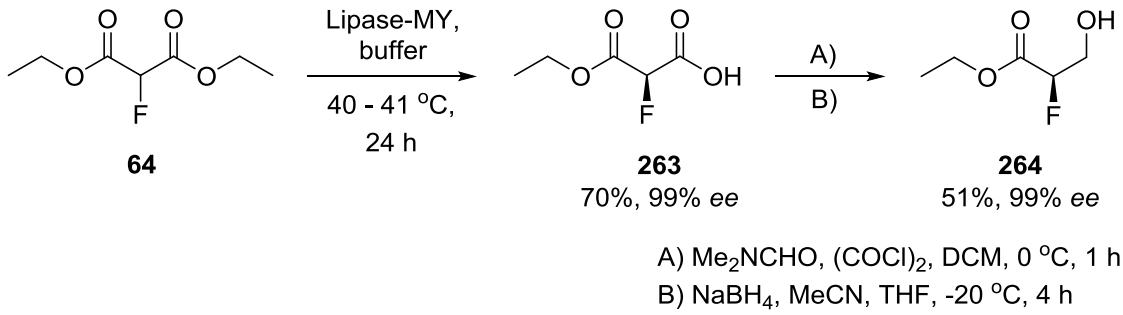

Figure 129 *– Lipase catalysed chiral hydrolysis of diethyl fluoromalonate.*

A 2-phenyl substituted diethyl fluoromalonate derivative was treated with arylmalonate decarboxylase, following hydrolysis of the diester to the dipotassium salt, giving an enantiomerically enriched fluorocarboxylic acid in 99% *ee*.[128]

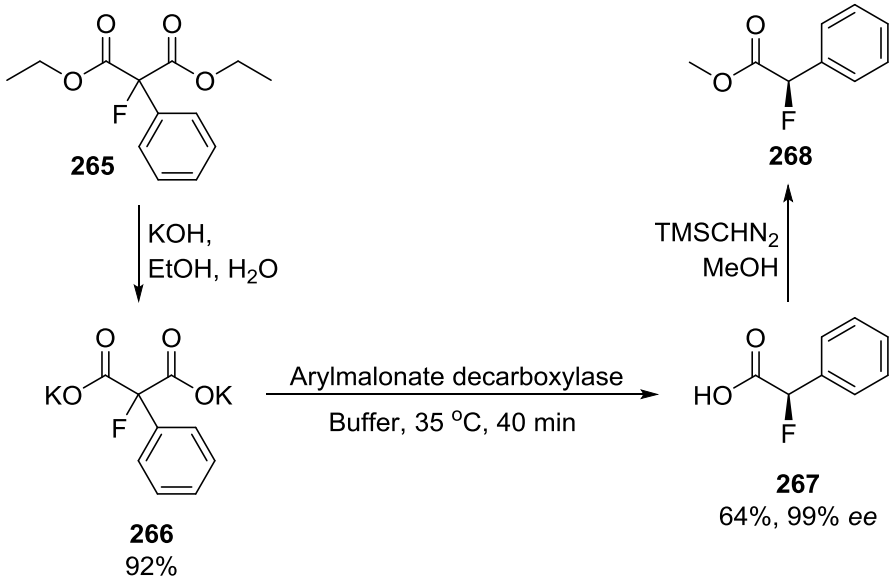

Figure 130 *– Biocatalysed asymmetric decarboxylation of a fluorodiacid derivative.*

Narisano and Riva report a multi-route synthesis of a chiral fluorohydrin from substituted fluoromalonate derivatives. Multiple lipases were screened for each stereoselective step and gave products with excellent *ee* values.

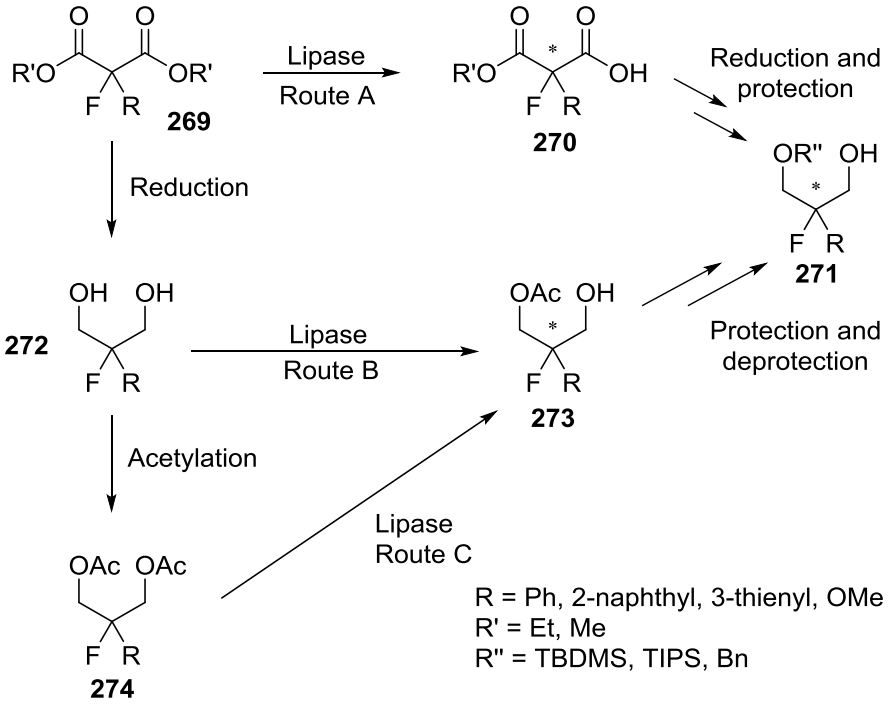

Figure 131 *– Multiple lipase catalysed chiral reactions of substituted diethyl fluoromalonates and derivatives.*

Citrate synthase has been used to stereoselectively deprotonate the pro-*S* proton of a fluoroacetate derivative. This anion then nucleophilically attacked the *Si* face of oxalacetic acid to give diastereomeric (2*R*, 3*R*)-fluorocitric acid with the introduction of two new chiral centres (***Figure 132***).[129,130,122]

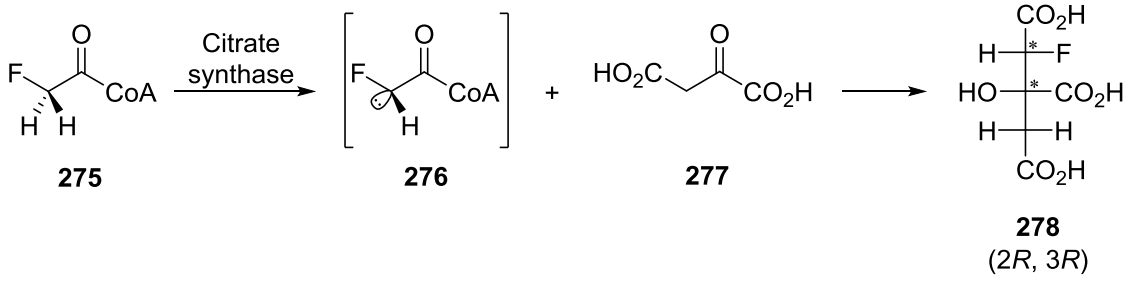

Figure 132 *– The use of citrate synthase to give a diastereomeric fluorocitrate derivative from two achiral molecules.*

A number of syntheses involving chiral reductions of aromatic α-fluorocarbonyl systems have been reported. Using two alcohol dehydrogenases (ADHs) (*E. Coli*/ADH-A and LBADH) was shown to give the *R* and *S* fluoroalcohols respectively in excellent yields and enantioselectivities (***Figure 133***).

A number of derivatives with ring substituents and, additionally, difluoroacetophenone and trifluoroacetophenone were also used successfully as substrates for these reduction reactions.[131]

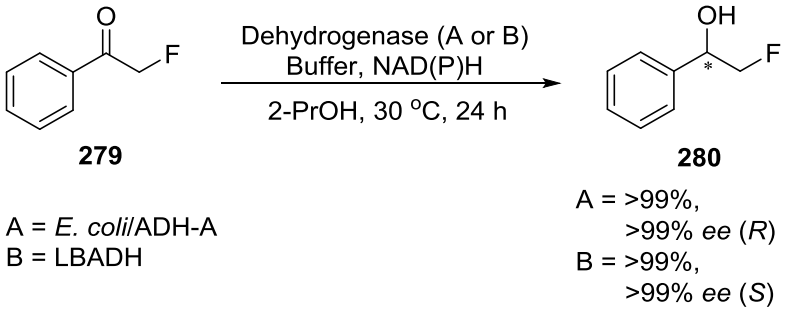

Figure 133 *– Synthesis of both enantiomers of a chiral fluoroalcohol from fluoroacetophenone.*

Similarly, dried cells of the *Geotrichum candidum* IFO 4597 (APG4) fungus (and an isolated enzyme thereof labelled 'B-enz') have been used to catalyse the same reactions of fluoroacetophenone to the two corresponding chiral fluoroalcohols (***Figure 134***).[132,133]

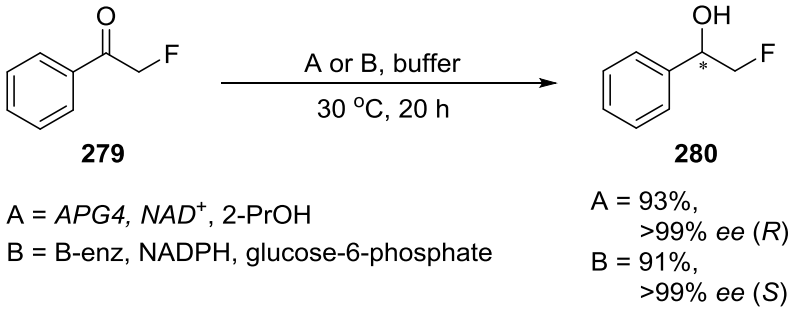

Figure 134 *– Synthesis of both enantiomers of a chiral fluoroalcohol from the analogous fluoroacetophenone.*

Reduction of fluoroacetophenone to the *R* fluoroalcohol has also been effected by the use of the photosynthetic microbe *Synechococcus elongatus* PCC 7942. Whilst whole-cell mediated reactions tend to have poor stereoselectivity due to competing reactions of the multiple enzymes in the cell, it has been found that illuminating this microbe with fluorescent light induces or activates the enzymes responsible for reducing the ketone to the (*R*)-alcohol. Without light the reaction yield is 8.5% with 27% *ee* but with light the yield improves to 35% and the *ee* is increased to 71%. Whilst relatively moderate yields or stereoselectivities are obtained, this novel technique is an interesting approach to biocatalytic desymmetrisation of α-fluorocarbonyl derivatives (***Figure 135***).[134]

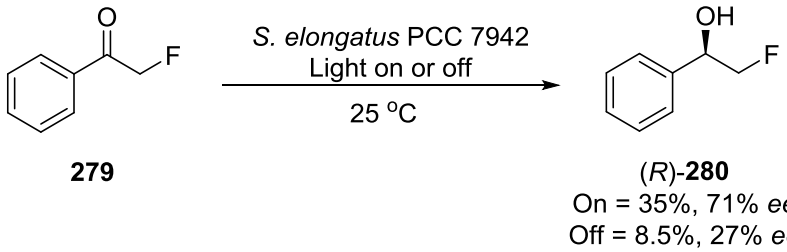

Figure 135 *– Reduction to (R) enantiomer of a chiral fluoroalcohol from fluoroacetophenone in reasonable ee.*

Baker's yeast has also been used in this fluoroacetophenone reduction yielding the (*R*)-fluoroalcohol in 44% yield and 92% *ee* (***Figure 136***).[135]

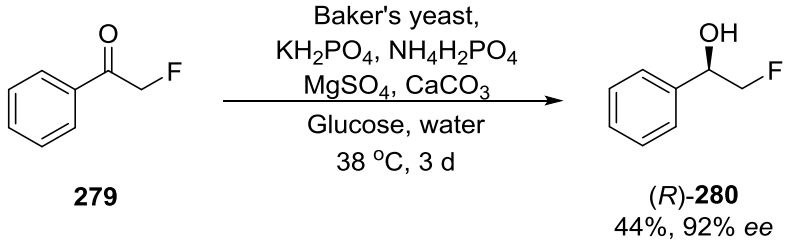

Figure 136 *– Baker's yeast reduction of fluoroacetophenone to the (R) enantiomer of the chiral fluoroalcohol.*

Lipase PS has been used to asymmetrically hydrolyse an isobutyrate derivative to give the chiral fluoroalcohol in 82% *ee* and 47% conversion (***Figure 137***).[122]

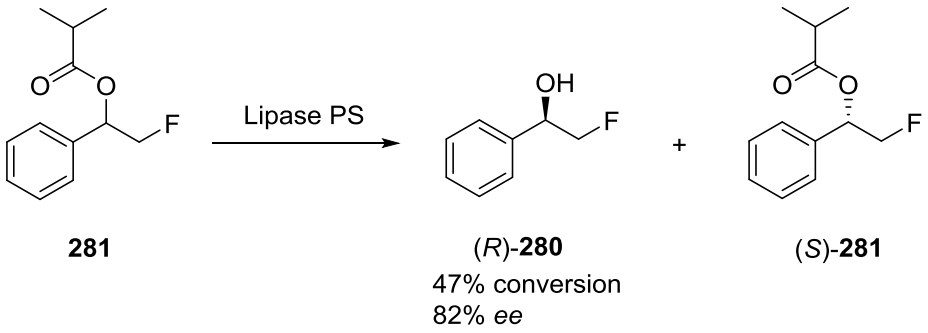

Figure 137 *– Enantioselective hydrolysis of a butyrate derivative to a chiral fluoroalcohol.*

Diastereoselective synthesis of alcohol (2*S*,3*R*)-**283** from racemic ethyl 2-fluoroacetoacetate **282** has been reported with the use of a platinum/aluminium oxide catalysed hydrogenation and a bulky chiral modifier (***Figure 138***). Dynamic kinetic resolution led to the (2*S*,3*R*) diastereomer being the major product.[136]

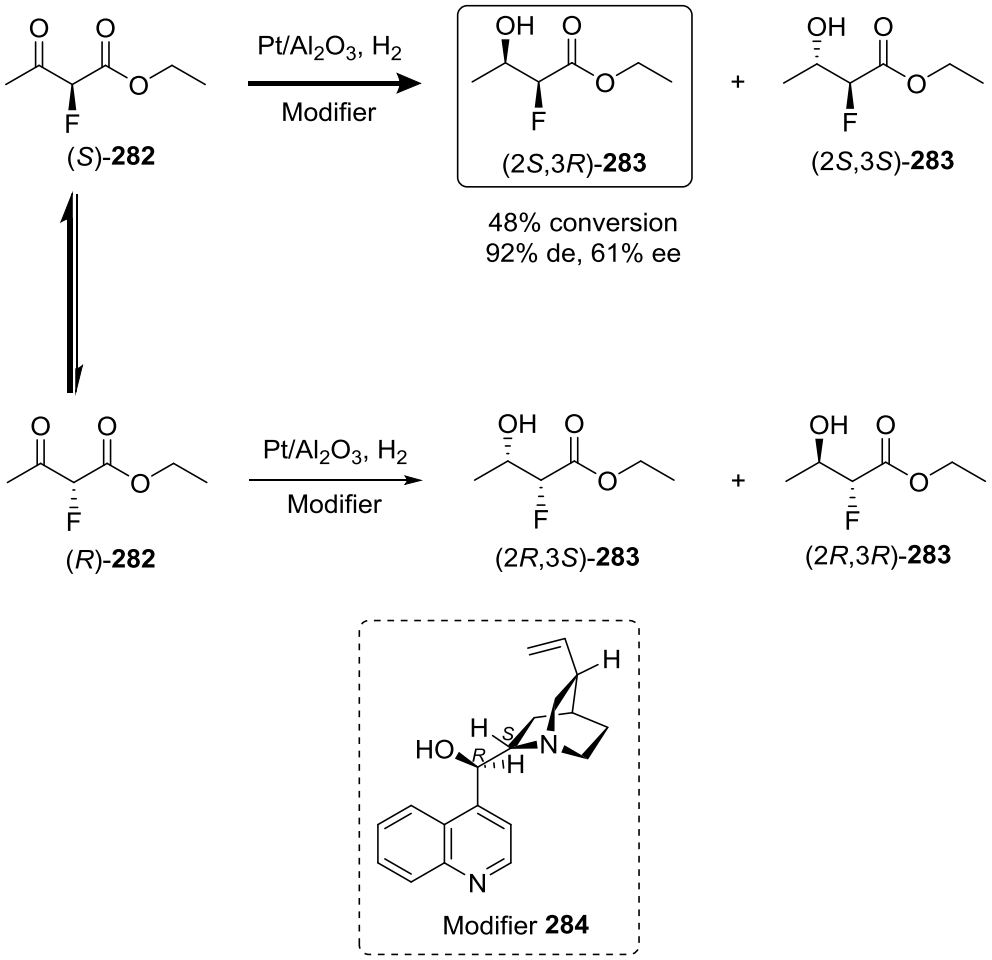

***Figure 138** – Platinum catalysed synthesis of the (2S,3R) diastereomer (2S,3R)-**283** by means of dynamic kinetic resolution with a chiral modifier.*

The (2*R*,3*S*) diastereomer (2*R*,3*S*)-**283** has been synthesised from racemic ethyl 2-fluoroacetoacetate **282** by hydrogenase enzymes. *Saccharomyces cerevisiae* (baker's yeast) enzyme Gcy1 was used under dynamic kinetic resolution conditions to selectively give the diastereomer in a single step (***Figure 139***).[137]

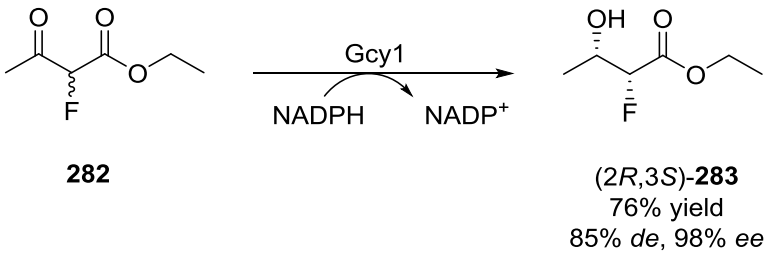

***Figure 139** – Hydrogenase catalysed reduction of ethyl 2-fluoroacetoacetate **282** to yield the diastereomeric alcohol (2R,3S)-**283**.*

Kitazume and co-workers report the reaction of both enantiomers of an enantiomerically enriched methyl substituted fluoromalonic acid monoester to form analogous chiral fluoroketoesters via formation of the acid chlorides of the carboxylic acid moieties. Baker's yeast is then used to enantioselectively reduce the ketones to alcohols to form the two diastereomeric fluorohydroxyesters (***Figure 140***).[138,139]

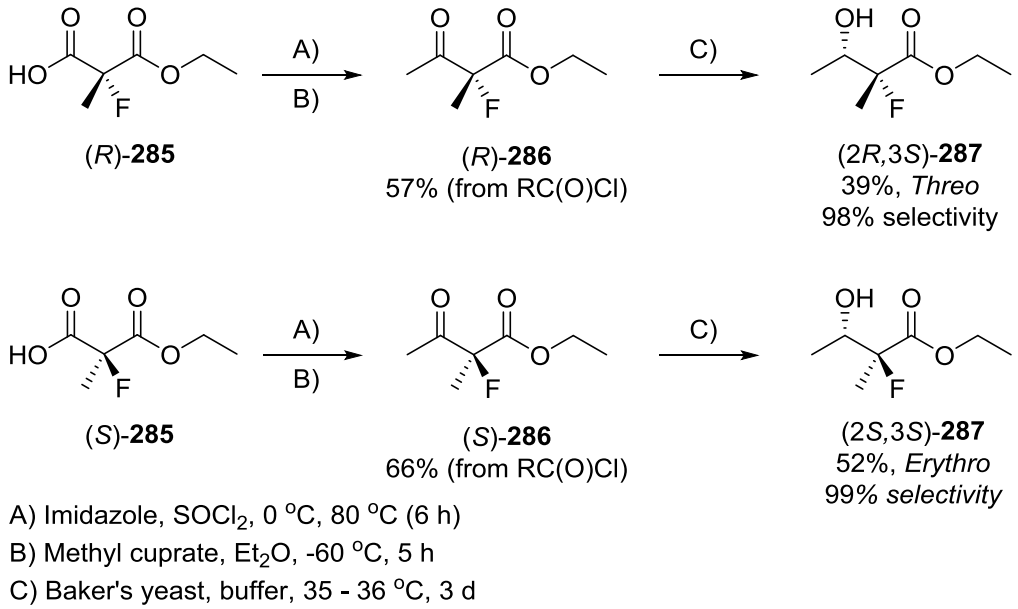

Figure 140 *– Baker's yeast mediated reduction of chiral fluoroketoesters to yield the corresponding diastereomeric fluorohydroxyesters.*

The aim of this project is to react fluoroketoesters with reductase enzymes to yield the corresponding diastereomeric fluorinated alcohol derivatives. In light of this literature and our previous research on related 2-fluoro-1,3-dicarbonyl chemistry, ethyl 2-fluoroacetoacetate **282** was selected as the initial substrate for investigation. Using an appropriate carbonyl reductase (CRED), also known as a ketoreductase (KRED), could lead to the selective production of only one of the possible four diastereomeric alcohols.[140] By screening a series of CREDs it is potentially possible to find different enzymes that selectively give all four diastereomers individually (***Figure 141***).

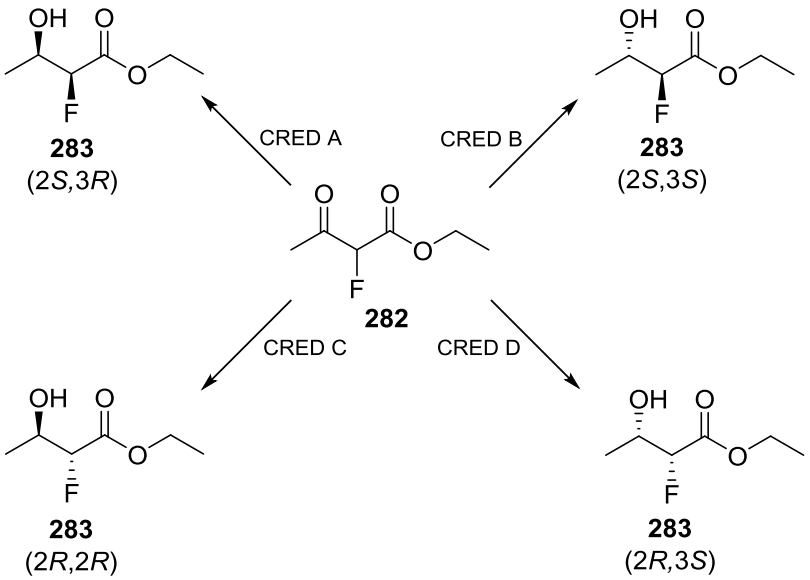

Figure 141 – *Proposed stereoselective reductions of ethyl 2-fluoroacetoacetate* ***282*** *by four different CRED enzymes to yield the four diastereomeric alcohol derivatives* ***283****.*

In order for CREDs to reduce a target carbonyl group they must be provided with a supply of hydride ions. This comes in the form of an enzyme cofactor, for example nicotinamide adenine dinucleotide (NAD) or the phosphate analogue (NADP), the structures of which are shown in ***Figure 142***, along with the structures of their respective reduced forms.

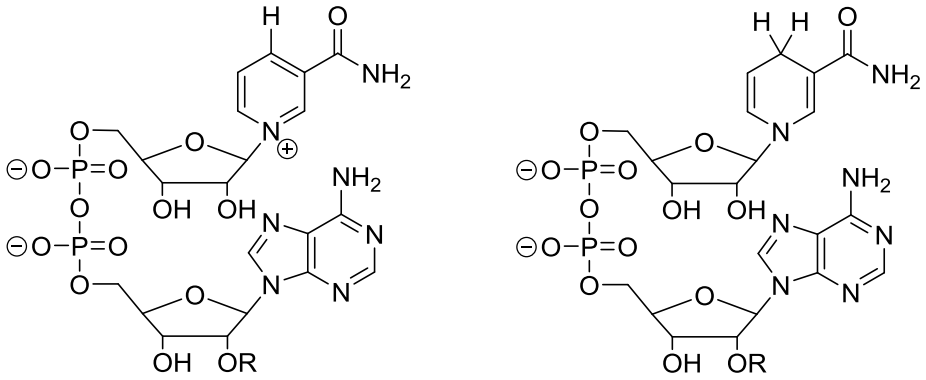

288

NAD^+: R = H

$NAD(P)^+$: R = PO_3^{2-}

289

NADH: R = H

NAD(P)H: R = PO_3^{2-}

Figure 142 – *Structures of NAD and NADP and their reduced forms.*

The reduced forms of these cofactors are a source of hydride to CREDs but these cofactors themselves must be regenerated in order to complete the catalytic cycle. This can be achieved by the addition of glucose dehydrogenase (GDH) and a ready supply of glucose. $NAD(P)^+$ is reduced to NAD(P)H as it oxidises glucose to gluconate. This reduced cofactor then acts as a hydride source for the CRED enzyme which reduces the substrate carbonyl to an alcohol. This process is summarised in ***Figure 143***.

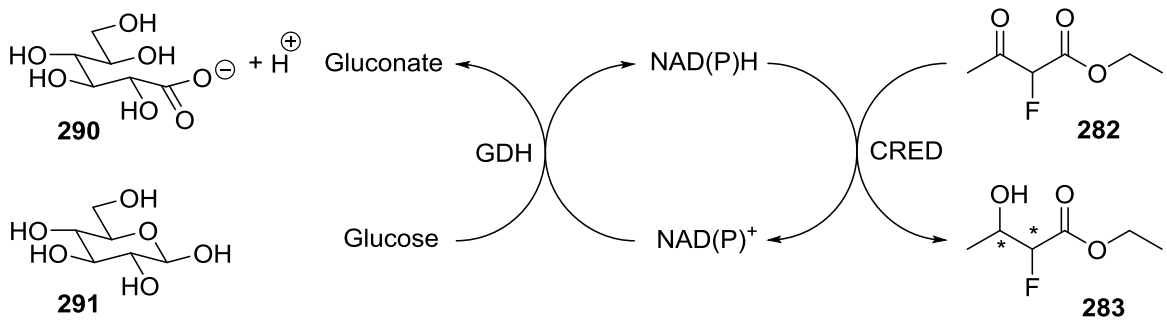

Figure 143 – *Catalytic cycle showing potential reduction of ethyl 2-fluoroacetoacetate* ***282*** *by a CRED enzyme with NAD(P) cofactor and GDH cofactor regenerator. Also shown are the structures of glucose and its oxidised gluconate form.*

Alternatively, isopropyl alcohol can be used instead of glucose since it can be oxidised to acetone by a CRED which, ideally, would be the same CRED that performs the substrate reduction. This is an inexpensive option that may also remove the need for a second enzyme to be present. An additional consideration is that the oxidation of glucose is pH dependent and so a buffer will be used in the screening process.

Whether NAD or NADP will be used as a cofactor for a particular CRED in an enzyme screening process will depend on that particular CRED. While many CREDs will accept either NAD or NADP, many are known to have a preference. CRED screening kits often state the preferred cofactor for each of the enzymes. In order to facilitate the ease and speed of enzyme screening it is also possible to use a 50:50 mix of NAD and NADP for all the enzymes since this should cover all eventualities. At the screening stage it is only important to observe that a reaction has occurred and can be detected by GC or HPLC. The reduction process is subsequently optimised and so the 50:50 mixture of cofactors is perfectly acceptable at this stage of the process development.

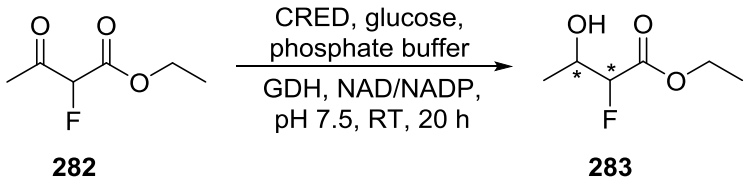

***Figure 144** – Proposed CRED catalysed chiral reduction of ethyl 2-fluoroacetoacetate.*

One issue that faces stereoselective enzymatic transformations is that the yield is often limited to 50%. This is because in a racemic mixture of the starting material only one enantiomer is selected by the enzyme as a substrate to subsequently undergo further transformation. The other enantiomer is not a substrate for the enzyme and so remains unreacted.

One way to overcome this yield limitation is to alter reaction conditions (e.g. pH) to set up a dynamic kinetic resolution (DKR). This occurs when the rate of racemisation of the starting material is comparable with the rate of reaction. Under these conditions the unreactive enantiomer is converted to the reactive enantiomer, the driving force being the removal of the reactive enantiomer by conversion to the product. This could lead to conversions to the product of up to 100%, with no starting material remaining unreacted (***Figure 145***).

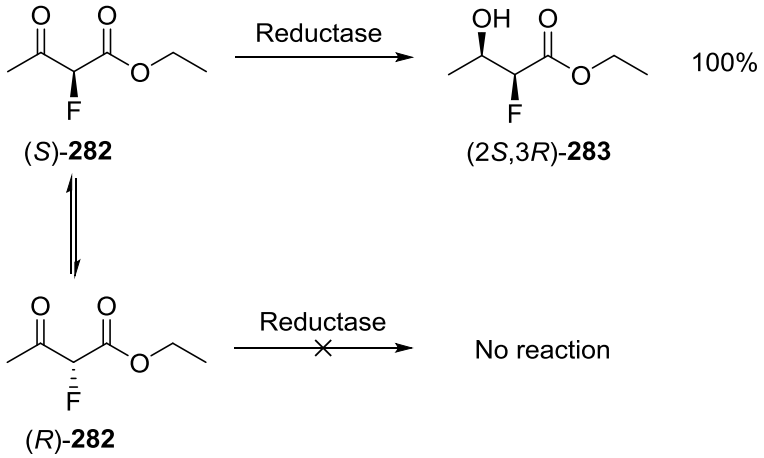

***Figure 145** – A dynamic kinetic resolution (DKR) where an unreactive (R) enantiomer is racemised to the reactive (S) enantiomer and is then converted to the product, leading to conversions of up to 100%.*

In this chapter we describe our initial attempts to prepare all four α-fluoroalcohol diastereomers from CRED catalysed reductions of ethyl 2-fluoroacetoacetate **282**. The enzyme screening experiments were performed by the author while on secondment at Almac (Craigavon, Northern Ireland) under the supervision of Dr. Gareth Brown who carried out optimisation of GC conditions and subsequent GC analysis of the resulting samples.

5.3. Results and Discussion

5.3.1. Chemical Reduction to give Ethyl 2-fluoro-3-hydroxy-butanoate 283 for GC Calibration

Firstly, a sample containing all four fluorohydroxyester stereoisomers was required to calibrate the chiral GC analysis before it could be used with the CRED screen.

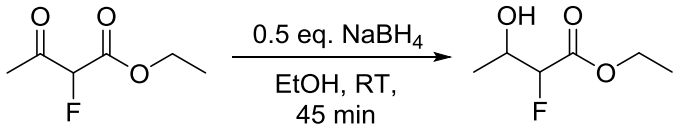

282 **283**

***Figure 146** – Sodium borohydride reduction of ethyl 2-fluoracetoacetate to give the alcoholic product that was used as a GC standard.*

Sodium borohydride reduction was carried out on a 50 mg ethyl fluoroacetoacetate scale to give a mixture of fluoroalcohol diastereomers for which chiral GC conditions were subsequently optimised.

^{19}F NMR spectroscopy of the mix of all fluoroalcohol stereomers **283** showed, as expected, two diastereomer peaks (doublets of doublets) with chemical shifts of approximately -202 ppm and -207 ppm. One signal corresponds to the two *threo* enantiomers and the other to the two *erythro* enantiomers (***Figure 147***).

Our computational calculations (courtesy of Dr. Mark Fox, Durham University) suggest that the *erythro* enantiomers have a smaller ^{19}F NMR shift than do the *threo* enantiomers (relative ^{19}F NMR shifts calculated as -197.9 ppm (*erythro*) and -201.4 ppm (*threo*)). Whilst the calculated values of the shifts themselves vary a little from the reported and observed NMR data the important information is the relative shifts rather than the exact shift values.

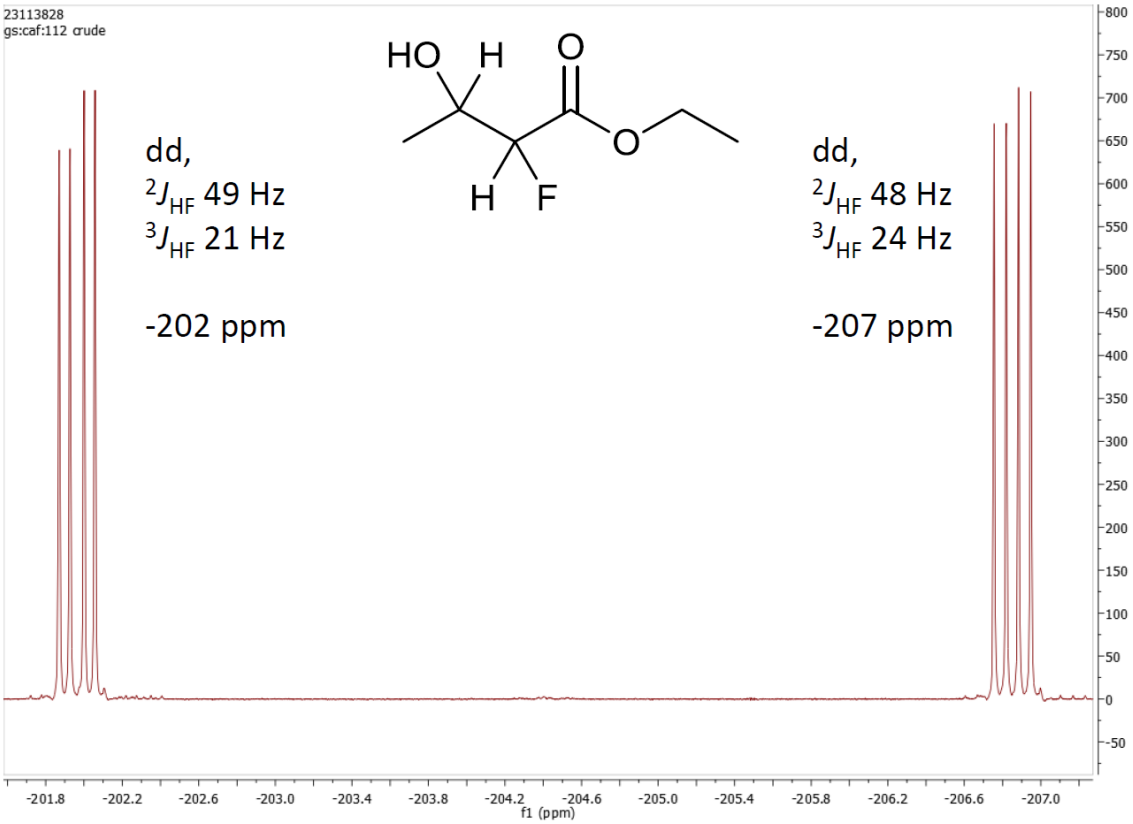

Figure 147 – *^{19}F NMR spectrum of erythro and threo ethyl 2-fluoro-3-hydroxy-butanoate **283** showing two diastereomer peaks.*

5.3.2. CRED Screening of Ethyl 2-fluoroacetoacetate 282

Once the mixture of the four possible diastereomers that act as a GC standard had been produced, Dr Gareth Brown of Almac optimised the column conditions and enzyme screening could commence. 69 CREDs were available at the time of screening and so all were screened against ethyl 2-fluoroacetoacetate **282**. To each enzyme was added 1 mL of a 0.1M phosphate buffer solution of pH 7.5 that contained glucose, GDH, NAD and NADP. A solution of ethyl 2-fluoroacetoacetate dissolved in DMSO was then added.

A 'blank' sample of ethyl 2-fluoroacetoacetate without enzyme was also included as a control sample, giving a total of 70 samples. The vials were agitated for 20 h at room temperature before 1 mL MTBE was added to each and the products were extracted in the organic layer, dried ($MgSO_4$) and analysed by GC. Full results from the screen are available in the appendix of this thesis (section A1.2.) and the following discussions include only the most stereoselective results.

Table 16 shows that 18 entries were observed to give good selectivity of over 70% and have been colour coded according to ***Table 15***. 25 of the entries exhibit isomer excess values of over 50%. Until the absolute stereochemistries of the four products are determined it remains unknown which products are enantiomeric or diastereomeric pairs and so the terms *ee* and *de* are invalid. In the following tables the term 'isomer excess' is used until the absolute conformations are determined. Isomer excess is calculated in a similar manner to *ee* and *de* except it is a ratio of one product to the other three combined.

Table 15 – *Colour coding of entries which display selectivity above 50%.*

Isomer Excess /%	Colour
95-100	
90-94	
80-89	
70-79	

Table 16 – *Colour coded entries exhibiting over 70% isomer excess listed in descending order. (Relative peak area obtained by Dr Gareth Brown of Almac, Isomer Excess calculated by the author).*

CRED	Isomer Excess /%				Conversion /%
	Alcohol 1	Alcohol 2	Alcohol 3	Alcohol 4	
50	88.7				99.5
42	87.0				99.8
32	83.2				99.7
25	80.6				99.7
43	75.1				99.7
59		90.3			99.7
29		70.0			94.7
17			93.4		99.8
44			88.8		99.8
5			84.7		99.7
23			84.0		99.7
12			83.0		99.9
63			77.4		99.8
14			75.4		99.9
18				96.6	99.8
30				92.1	99.9
6				71.1	99.4
24				70.0	98.3

In most of these 18 high isomer excess entries the percentage conversion (calculated by GC) was above 99%, with all above 94%. This implies that dynamic kinetic resolution was observed in all 18 cases. The best CRED candidates for each diastereomeric product will be further investigated by means of scale-up and optimisation of reaction conditions and, subsequently, identification of each diastereomeric fluoroalcohol. Work on this project is still ongoing at Almac.

Although biocatalytic routes to all four diastereomeric alcohols are being developed it remains unknown which CREDs give which diastereomer. The following section describes initial attempts to develop a process of determining the absolute stereochemistries of each product. Upon determination of absolute stereochemistries it would be possible to determine *ee* and *de* for the four biocatalytic routes and compare the final optimised results with the analogous literature routes.

5.3.3. Determination of Absolute Stereochemistries of Ethyl 2-fluoro-3-hydroxy-butanoate Diastereomers

Although it was possible for GC analysis of the CRED screen to determine that all four of the diastereomers had been synthesised depending on the CRED used, it is not possible to deduce the absolute stereochemistries of each diastereomer using chiral GC alone.

It is possible for NMR analysis to determine the diastereomeric excess of any of the products but not the enantiomeric excess. The two *erythro* products share one ^{19}F NMR peak and the two *threo* products share another. It is, therefore, possible to determine the *erythro*:*threo* ratio of a product by NMR but not the ratio between the two *erythro* products (or, conversely the two *threo* products) i.e. the *ee*.

As previously described, Szőri *et al*. used a chiral modifier to give (2*S*,3*R*) ethyl 2-fluoro-3-hydroxy-butanoate (2*S*,3*R*)-**283** in 92% *de* and 61% *ee* (***Figure 138***).[136] The authors assigned the stereochemistries of the products by comparison with literature NMR data to identify diastereomers (Elkik and Imbeaux-Oudotte[141]) and identification of enantiomers by synthesis of two of the alcohols of known stereochemistries (one *erythro* and one *threo*, ***Figure 148***) as GC standards for comparison of retention times with the products.

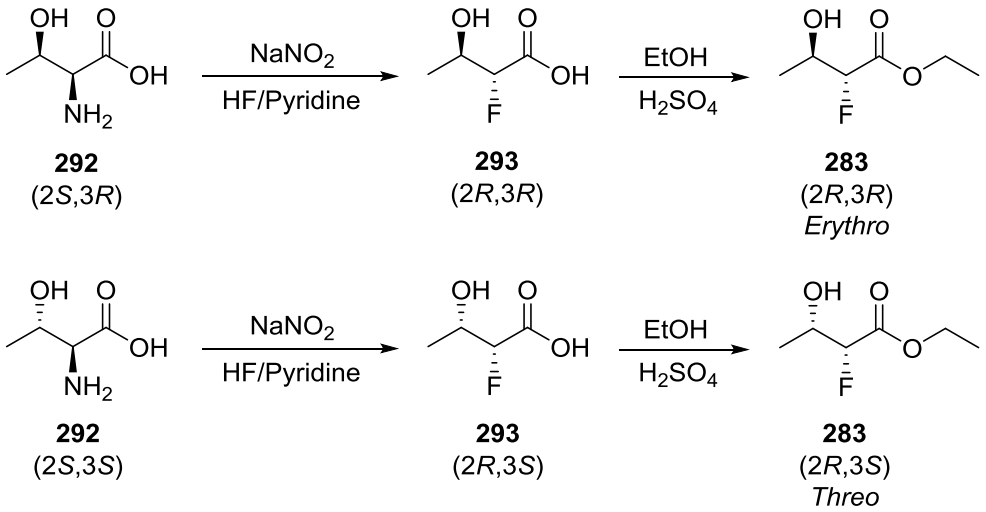

***Figure 148** – Reported syntheses of two stereoisomers of ethyl 2-fluoro-3-hydroxy-butanoate from threonine (top) and L-allo-threonine (bottom).*

The two GC standards were synthesised following procedures described by Olah *et al*.[142,143] Threonine (2*S*,3*R*)-**292**, and analogous L-*allo*-threonine (2*S*,3*S*)-**292**, were reacted with sodium nitrite in a solution of HF and pyridine to give the α-fluorocarboxylic acid via a diazotisation step with subsequent nucleophilic substitution of the fluoride ion. The authors claim that stereochemistry is inverted at this stage, however, upon further inspection of the literature Dascier *et al*. state "Assignments previously reported (Szőri [*et al*.]) were incorrect; diazotization/fluoride substitution of L-threonine and L-*allo*-threonine actually proceeds with retention of configuration."[144] The authors report that the absolute configuration of the (2*R*,3*S*) diastereomer was determined by NMR analysis of the corresponding Mosher ester.

Furthermore, our computational calculations (courtesy of Dr. Mark Fox) support the claim that the *erythro* diastereomer has a smaller ^{19}F NMR shift than does the *threo* diastereomer (relative ^{19}F NMR shifts calculated as -197.9 ppm (*erythro*) and -201.4 ppm (*threo*)) and that the *threo* product had been synthesised.

Thus, it appears that *erythro* corresponds to a resonance at ~ -202 ppm and *threo* corresponds to a resonance at ~ -207 ppm, as supported by the work of Dascier *et al.*[144] in concurrence with our NMR calculations.

Our proposed synthetic route to the α-fluorocarboxylic acid initially followed the reported synthesis of the α-fluorocarboxylic acid using the milder 48:52 HF/pyridine mixture (***Figure 149***).[143]

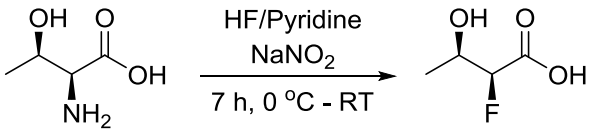

292 (2*S*,3*R*)

293 (2*S*,3*R*) *Threo*

Figure 149 *– Proposed diazotisation/fluorination reaction of threonine.*

Standard extraction of the crude product into diethyl ether proved inefficient, yielding a mixture of products with only trace amounts of the desired product. Subsequently, a continuous extraction apparatus was used to extract the product from the aqueous layer into DCM. Additionally, the volume of ice water used to quench the reaction was reduced in an attempt to aid extraction of the product from the aqueous portion. A small sample of the desired α-fluorocarboxylic acid was obtained.

^{19}F NMR analysis (***Figure 150***) revealed a small number of peaks but, importantly, only one of the two diastereotopic peaks (approximately -207 ppm, *threo*) was observed suggesting that the diastereoselectivity was good and that this crude product should be sufficiently pure for analysis by GC to determine the stereochemistries of two of the diastereotopic products.

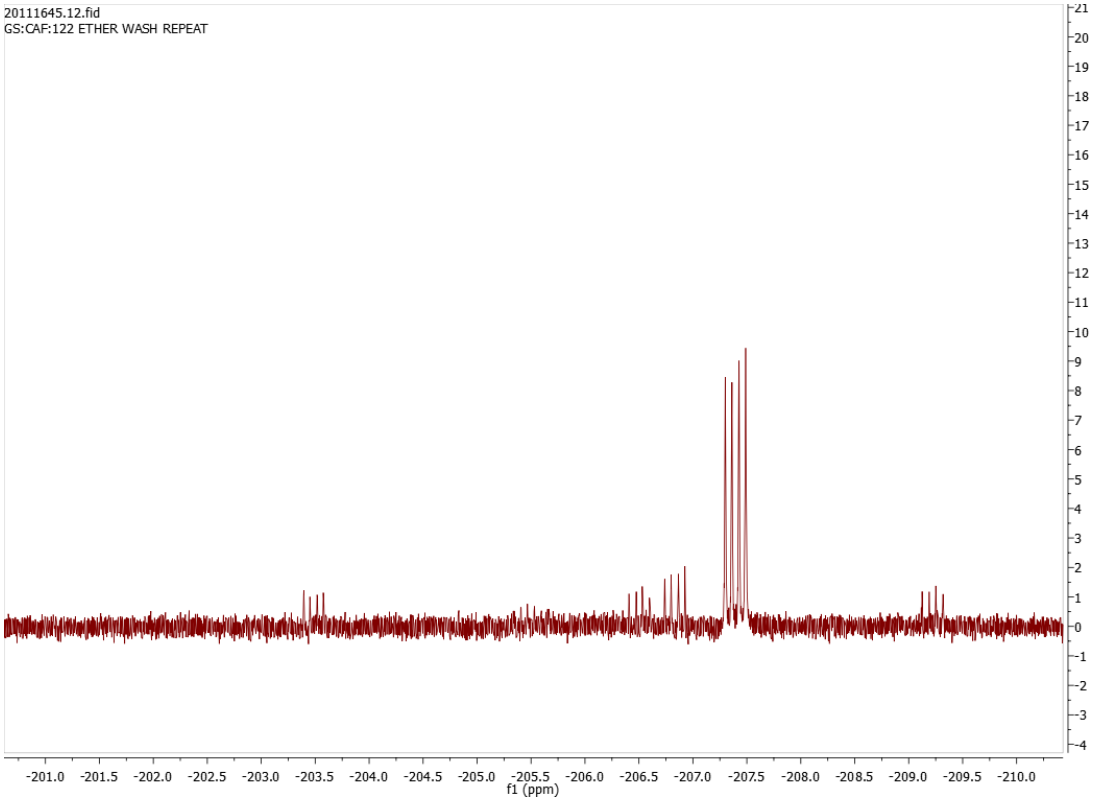

Figure 150 *– ^{19}F NMR spectrum of the crude reaction mixture (following extraction from glass degradation products from continuous extraction) showing good diastereoselectivity.*

Although only a small quantity of this product was isolated it was then carried forward to an esterification reaction to yield a sample of the α-fluoroester for GC analysis (***Figure 151***). ***Figure 152*** shows the ^{19}F NMR spectrum of the α-fluoroester GC sample in good diastereoselectivity (91% pure by ^{19}F NMR spectroscopy, approximately -207 ppm, *threo*). Work is ongoing with regards to GC analysis of this sample.

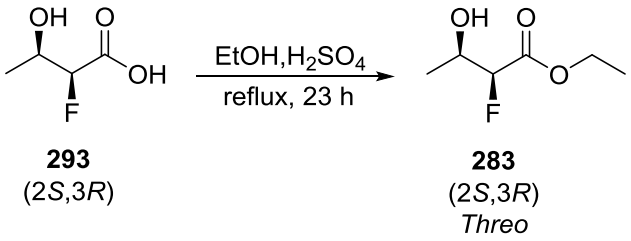

293
(2*S*,3*R*)

283
(2*S*,3*R*)
Threo

Figure 151 – *Esterification reaction of the fluorinated intermediate carboxylic acid to give (2S,3R)-ethyl 2-fluoro-3-hydroxy-butanoate (2S,3R)-**283**.*

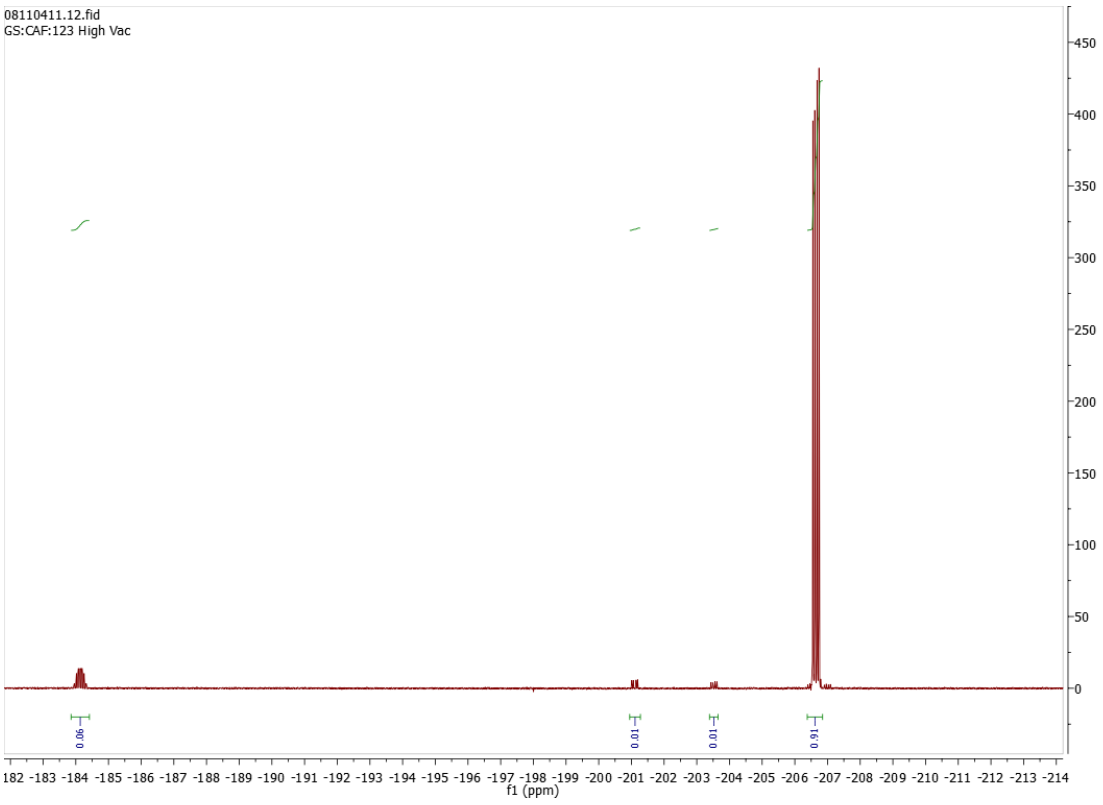

Figure 152 *– ^{19}F NMR spectrum of the α-fluoroester showing good diastereoselectivity.*

Whilst the majority of the literature, and our calculations, agree that the *threo* product is formed in the diazotisation/fluorination reaction of threonine the discrepancy with Szőri *et al*. highlights the use of a more direct approach to determination of the absolute stereochemistries of the four products. In future, derivatisation of the ethyl 2-fluoro-3-hydroxy-butanoate products **283** to form solids would give the opportunity for analysis by X-ray crystallography. This technique would allow direct observation of the molecular conformation without relying on NMR comparisons.

5.4. Conclusions and Future Work

A series of carbonyl reductases (CREDs) were screened against ethyl 2-fluoroacetoacetate **282** in an attempt to develop biocatalytic routes to all four reduced ethyl 2-fluoro-3-hydroxy-butanoate products. Work on this project is ongoing but initial results suggest that CREDs have been found to selectively reduce the fluoroketoester to all four desired diastereomers. Dynamic kinetic resolution is also observed in each case, leading to yields (by GC) of greater than 50%.

Synthesis of an ethyl 2-fluoro-3-hydroxy-butanoate derivative of known absolute stereochemistry (required to determine the absolute stereochemistries of the four products) proved problematic and conflicting literature raised concerns whether the stereochemistry of the standard actually was as reported. This issue could potentially be bypassed by derivatisation and subsequent recrystallization of the diastereomeric products. Analysis of these compounds by X-ray crystallography would allow direct observation of the configurations of the chiral centres. Consequently, future work includes determination of the absolute stereochemistries of the four products and further optimisation of the biosynthetic routes to each. Work on this project is ongoing.

Chapter 6. Conformational Studies of α-Fluorocarbonyl Species

Following the observation of an F-C-C=O *syn* trend in several of our fluoroester X-ray crystal structures (discussed in the relevant sections below) the literature was reviewed to determine the accepted theories of fluorocarbonyl conformational preference and why this may be of interest to the life sciences.

6.1. Literature Review of α-Fluorocarbonyl Conformational Studies

6.1.1. General Effects

Recent reviews by O'Hagan[145] and Hunter[146] outline the use of the C-F bond as a conformational tool in organic and biological chemistry by utilising a number of effects associated with C-F bonds. Among the interactions reviewed are dipole-dipole interactions, hyperconjugation effects and charge-dipole interactions. Hunter discusses examples relevant to the life sciences, including an HIV protease inhibitor[147] **294** where selective introduction of fluorine atoms either reinforces (**295a**) or destabilises (**295b**) the zigzag conformation of the active form of the drug due to the fluorine *gauche* effect (***Figure 153***).[148] The latter analogue (**295b**) results in a 14-fold decrease in potency of the drug.

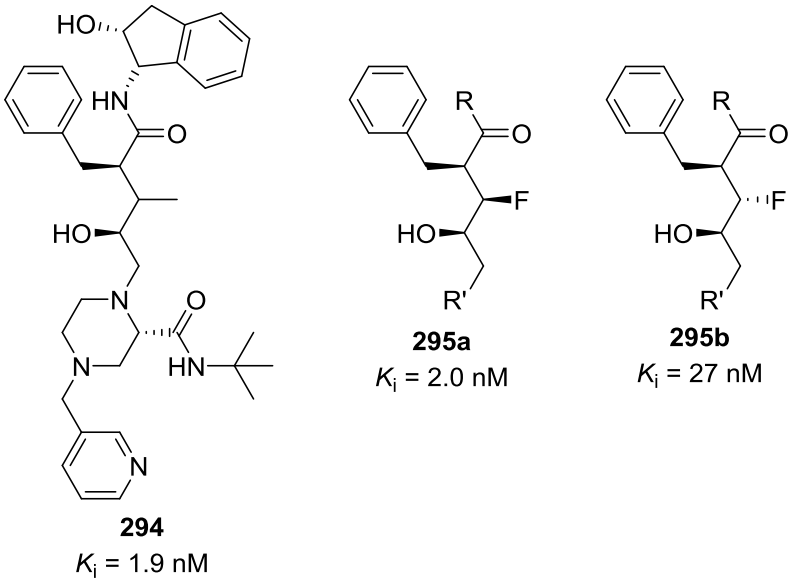

Figure 153– *Fluorination of the HIV protease inhibitor Indinavir results in a change in potency because of the fluorine gauche effect.*

Massa *et al.* describe a cholesteryl ester transfer protein inhibitor that utilises the hyperconjugation effects of the C-F bond to improve binding affinity by forcing the phenoxy ether alkyl group out of plane of the ring (***Figure 154***).[149]

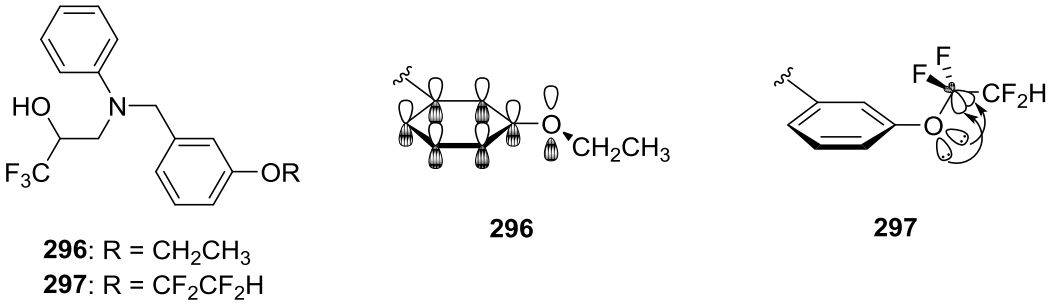

Figure 154 *– Fluorination of ethoxy group of this transfer protein inhibitor leads to an sp^3 hybridised oxygen that disrupts the planarity of the ether moiety.*

Due to the strong electronegativity of the fluorine atom, dipole-dipole effects occur in molecules with adjacent polarised bonds. Fluorine atoms may form electrostatic interactions with partial positive charges, for example to a carbonyl carbon atom.[150,151] Hydrogen bonding interactions with fluorine do occur but the O-H---F-C interaction is only around a quarter as strong as would be expected for a standard hydrogen bond with oxygen.[145] Conversely, repulsive dipole-dipole interactions are observed in 1,3-difluorinated molecules, such as 2,4-difluoropentane, where bonds rotate to increase the distance between the repelling fluorine atoms.[152]

Similarly, α-fluorocarbonyl species, for example fluoroesters, may also exhibit dipole-dipole repulsion between the electronegative fluorine and oxygen atoms, where an F-C-C=O *trans* preference is reported.[145]

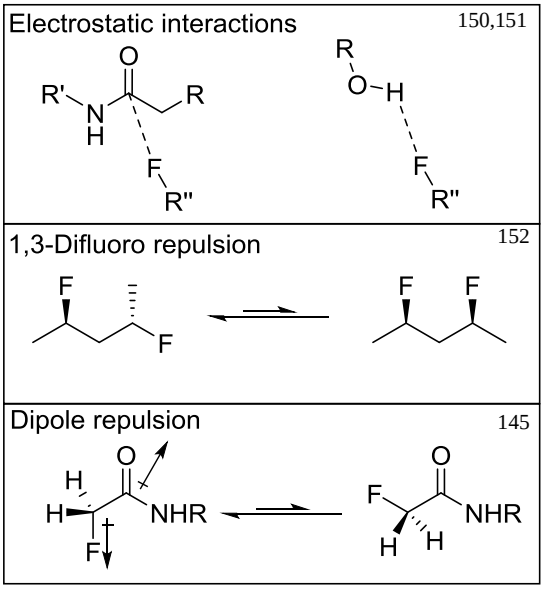

***Figure 155** – The three primary types of dipole-dipole interactions involving the C-F bond.*

Hyperconjugation effects involving C-F bonds have also been reviewed. The *anti* conformation of fluoroamides is proposed to be further stabilised by donation of electron density from the carbonyl oxygen atom to the C-F σ^* antibonding orbital.[153] For 1,2-difluoroalkanes, the C-F σ^* antibonding orbital can be stabilised by donation of electron density from an adjacent C-H bond *trans* to the C-F bond. The preferred *anti* F-C-C-H conformation determines a *gauche* F-C-C-F conformation and so this hyperconjugation effect is known as the fluorine *gauche* effect. Gilmour *et al*. recently reviewed a brief overview of the fluorine *gauche* effect.[154]

Because the molecules studied in the following sections are α-fluorocarbonyl species, no adjacent C-H bonds are available to enact the *gauche* effect and so it is not expected that this effect will be prevalent in our data. Whilst fluoroaldehydes do contain an adjacent C-H bond it is on an sp^2 carbon and so an *anti* F-C-C-H bond would give a *syn* F-C-C=O, rather than a *gauche* F-C-C=O.

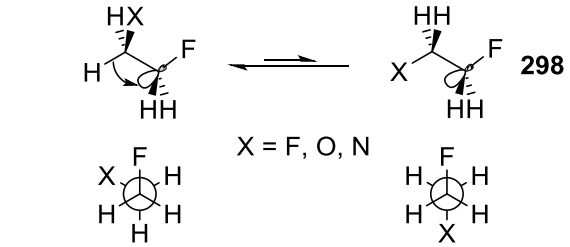

Figure 156– *The fluorine gauche effect stabilised by hyperconjugation of C-H electron density into the C-F σ^* antibonding orbital.*

Charge-dipole effects are also significant. It was observed that where a fluorine atom is vicinal to a positively charged (e.g. protonated) nitrogen or oxygen atom the *gauche* conformation is preferred in order to reduce the distance between the electropositive atom and the partially negative fluorine atom. [155]

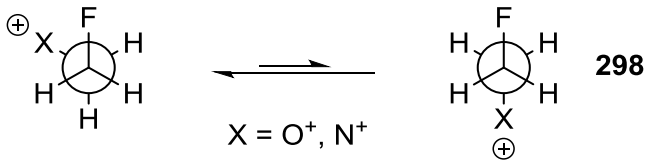

Figure 157 – *The charge-dipole effect.*

6.1.2. α-Fluorocarbonyl Species

Whilst α-fluorocarbonyl systems are subject to some of the conformational effects discussed above and, as such, are generally considered to have an *anti* preference the extent of this preference depends on the nature of the fluorocarbonyl moiety. O'Hagan listed common fluorocarbonyl moieties in order of decreasing *anti* preference as follows: amides, esters, ketones and aldehydes (***Table 17***). The following literature discussions concerning α-fluorocarbonyl systems follow this order.

Table 17 *- F-C-C=O anti preferences for α-fluorinated amides, esters, ketones and aldehydes.* [145]

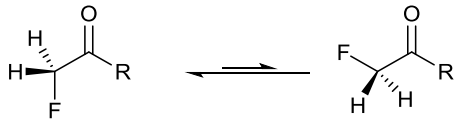

Entry	Compound	R	*Anti* preference /kcal mol^{-1} [145]
1	**299**	-NH_2	7.5
2	**300**	-OMe	4.5
3	**301**	-Me	2.2
4	**302**	-H	1.68

6.1.2.1. α-Fluoroamides

Fluoroamides are predicted to have the strongest *anti* preference of the α-fluorocarbonyl derivatives due to additional effects that stabilise this conformation.[156] For example, favourable hydrogen bonding interactions exist between N-H protons and the fluorine atoms (***Figure 158***).

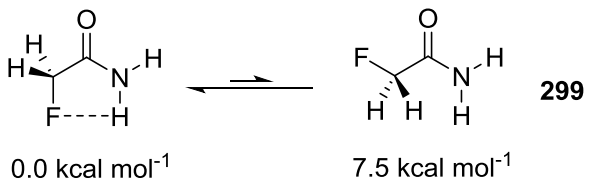

Figure 158 – *Hydrogen bonding interactions have been reported to stabilise the anti conformation leading to a 7.5 kcal mol^{-1} energy difference between the anti and syn conformers.*[145]

Additionally, the *anti* conformation is stabilised by donation of electron density from the carbonyl oxygen atom to the C-F σ^* antibonding orbital (***Figure 159***).[153]

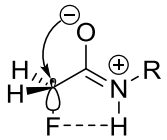

Figure 159 – *Donation of electron density from the amide carbonyl oxygen to the C-F σ^* antibonding orbital.*

O'Hagan *et al*. studied the molecular structures of two related *N*-substituted phenylalanine derived amides (-NH-CO-CH_2-R, where R = Me or F (***Figure 160***)) and reported a more planar, *trans* R-C-C=O conformation observed in the X-ray crystal structure of the fluorinated analogue.[156] To determine if the *anti* conformation is affected by a substituent on the F-C carbon a methyl substituted analogue of a similar α-fluoroamide (*N*-phenyl-2-fluoropropionamide) was synthesised and both *S* and *R* enantiomers were found to exhibit *anti* F-C-C=O conformations in their X-ray crystal structures (***Figure 160***).

Ab initio calculations of a simpler fluoroamide (*N*-methyl-2-fluoropropionamide, NMFP) gave a rotational energy profile with an energy minimum at F-C-C=O = 180°, a maximum at 300° (when the methyl group eclipses the amide hydrogen) and a plateau at around 60° (when both F and CH_3 are *gauche* to the C=O bond) (***Figure 160***). Natural bond orbital (NBO) analysis[156,157] led to the conclusion that the F---HN interaction is not the dominant effect in determining the *anti* conformation. Instead, the leading stabilising effect is the interaction between fluorine lone pairs and the N-H σ* orbital and, to a lesser extent, the alignment between the C-F σ orbital and both the *anti* C=O σ* orbital and the *anti* methyl C-H σ* orbital.

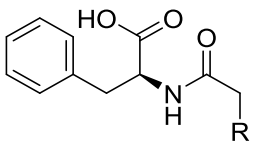

303
R = F, Me

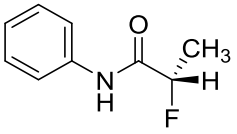

304

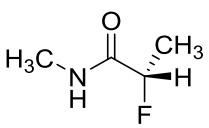

305

Figure 160 – *Left – The structures of the two initial amides studied. Centre – The structure of the related methyl substituted fluoroamide. Right – The simpler fluoroamide structure analysed by computational chemistry.*[156]

Furthermore, O'Hagan *et al*. combined two conformational effects of C-F bonds to gain additional control of a small difluorinated amide derivative.[158] The molecule in ***Figure 161*** features a F-C-C=O fluorocarbonyl moiety which would be expected to exhibit *anti* conformation and a F-C-C-N moiety that would be expected to have a *gauche* conformation, rather than *anti*, due to the fluorine *gauche* effect. The predictions were confirmed by X-ray crystal analysis which revealed an *anti* fluorocarbonyl conformation and a *gauche* β-fluoroethylamide conformation.

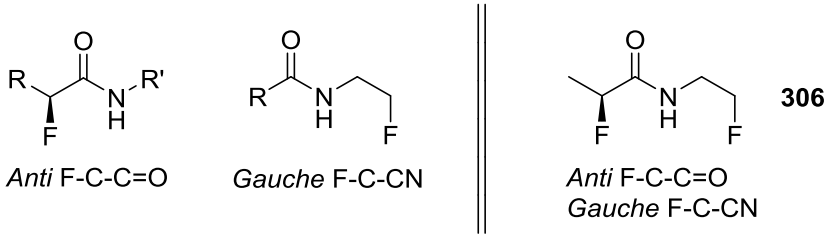

Figure 161 – *The predicted cumulative C-F bond effects were confirmed by X-ray crystallography.*

March *et al.*[159] and Peddie *et al*.[160] utilise this effect further in short peptidic compounds using one fluorine atom to direct the adjacent amide and amine moieties and provide a level of conformational control over the secondary structure of the peptide backbone (***Figure 162***).

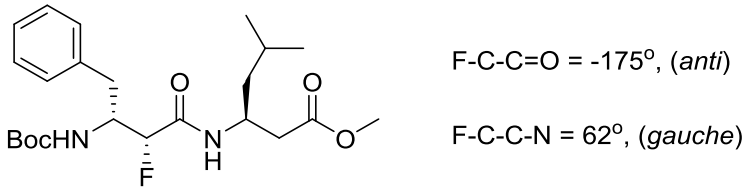

307

Figure 162 – *The cumulative C-F bond effects behave as predicted for this peptidic compound.*

This effect has also been observed in longer peptide fragments such as the β-peptide shown in ***Figure 163***.[146,161] In molecule **308a** the fluorine lies *anti* to the amide C=O bond and *gauche* to the vicinal nitrogen and so the helical secondary structure is reinforced. In molecule **308b**, however, this conformational preference destabilises the helix.

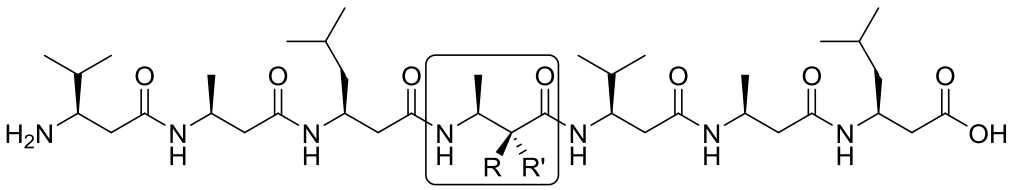

308a: R = H, R' = F
308b: R = F, R' = H

Figure 163 *– A β-peptide fragment whose secondary helical structure can either be stabilised or destabilised by C-F bond effects depending on the absolute stereochemistry of the C-F bond on the chiral centre.*

Abraham *et al*. noted a lack of solution state data for the α-fluoroamide derivatives and the reliance on solid state data (X-ray crystallography) and computational predictions in the literature. Consequently, NMR studies, FTIR studies and further *ab initio* and DFT computational analysis of the previously reported simple fluoroamide (NMFP) and a related structure (N-methyl-2-fluoroacetamide, NMFA) were conducted.[162] Rittner recently reviewed the use of NMR spectroscopy as a tool for conformational analysis.[163]

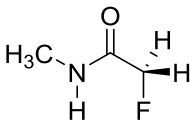

309
NMFA
N-Methyl-2-fluoroacetamide

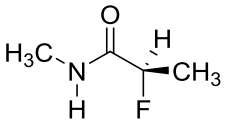

310
NMFP
N-Methyl-2-fluoropropionamide

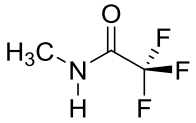

311
MTFA
N-Methyltrifluoroacetamide

Figure 164 *– The structures of NMFA, NMFP and MTFA.*

The rotational energy profile was reproduced and the *gauche* plateau around 60^{o} was observed. A plateau, however, is not defined as a stable energy minimum and so the question remained as to whether the *gauche* conformer actually exists in solution state. Abraham and co-workers conducted IR studies in various solvents that indicated two carbonyl absorption bands (one *anti*, one *gauche*) and further computational calculations revealed that the plateau becomes a minimum with increasing solvent relative permittivity confirming that the *gauche* conformer does indeed exist in solution.

NMR studies of NMFA and NMFP in solvents of increasing polarity showed significant changes in coupling constants that were attributed to the decreasing *anti* preference in the solution state. In order to determine whether this change in coupling constant was due to change in conformational preference or simply intrinsic solvent effects (increasing polarity) a trifluorinated analogue (MTFA) was analysed because it only contains very few conformations in solution so is, theoretically, independent of conformational effects. Any change in coupling constant observed with increasing solvent polarity is, therefore, due to intrinsic solvent polarity effects.

The NMR data for NMFA and MTFA are reproduced below.[162] The minimal change in $^{1}J_{CF}$ coupling constant with increase in solvent polarity in the trifluorinated analogue MTFA suggests that the relatively larger changes in coupling constant for NMFA and NMFP were, therefore, related to conformational changes and not simply a product of intrinsic solvent effects.

Table 18 - *Chemical shifts (δ ppm) and coupling constants (Hz) for NMFA.*

Solvent	**H_4**	**H_2**	**H_3**	**C_1**	**C_2**	**C_3**	**$^{3}J_{HH}$**	**$^{2}J_{HF}$**	**$^{1}J_{CF}$**	**$^{2}J_{CF}$**
$CDCl_3$	6.38	4.80	2.91	168.2	80.4	25.5	5.00	47.22	185.4	17.3
CD_2Cl_2	6.43	4.77	2.84	168.3	81.0	25.6	4.96	47.06	183.9	17.2
Acetone-d_6	7.48	4.77	2.78	168.4	81.1	25.4	-	47.42	183.1	18.3
CD_3CN	6.84	4.73	2.74	168.6	81.0	25.2	4.85	47.06	181.6	17.2
DMSO-d_6	8.26	4.92	2.78	167.5	80.1	25.2	4.69	47.00	180.2	18.1

Table 19 - *Chemical shifts (δ ppm) and coupling constants (Hz) for MTFA.*

Solvent	**H_3**	**H_4**	**C_1**	**C_2**	**C_3**	**$^{3}J_{HH}$**	**$^{5}J_{HF}$**	**$^{1}J_{CF}$**	**$^{2}J_{CF}$**
$CDCl_3$	2.96	6.73	158.1	115.9	26.4	4.97	0.65	286.1	36.9
CD_2Cl_2	2.91	6.74	158.1	116.4	26.6	4.93	0.65	286.2	35.5
Acetone-d_6	2.87	8.39	157.8	117.0	26.3	4.76	0.65	285.6	35.9
DMSO-d_6	2.92	9.34	156.4	115.8	25.8	4.65	0.65	285.9	36.0

Computations involving these data concluded that NMFA moved towards the *syn* conformer and NMFP moved towards the *gauche* conformer as solvent polarity increased. *Gauche* is favoured over *syn* in NMFP as the *syn* conformer is destabilised by steric repulsion between the 2-methyl group and the $NH(CH_3)$ groups. The *anti* conformer, however, was still preferred in all solvents and in vapour phase calculations, though to a lesser extent in more polar solvents.

This is possibly because as the solvent polarity increases, the more polar (i.e. *syn*) conformation becomes more energetically stable than the less polar conformer (*anti*) as the overall dipole aligns with the polar solvent (***Figure 165***).

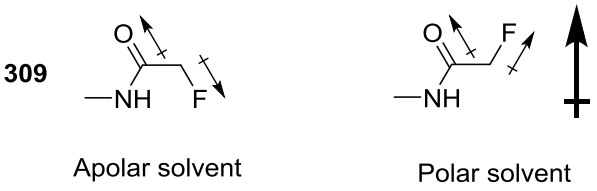

***Figure 165** – In more polar solvents it is proposed that the more polar syn conformation is preferred due to dipole alignment.*

This evidence suggests that the inherent amide F-C-C=O *anti* preference can be reduced by the use of polar solvents and so the use of the C-F bond as a conformational tool in polar environments *in vivo* may be weakened.

Issues regarding the ability of environmental effects (e.g. solvent effects, crystal packing, steric effects, inter/intramolecular interactions) to override the predicted C-F conformational effects have been discussed throughout this section. Quoting research by O'Hagan *et al*.[156] and Abraham *et al*.[162] as a basis for their study, a 2012 paper by Jones *et al*. further probed the concept of overriding the fluoroamide *anti* preference. They incrementally 'built' upon a simple fluoroamide such that a carbonyl oxygen atom was directed towards the fluoroamide moiety.

They indeed found that the new oxygen atom 'overrode' the NH---F-C hydrogen bond that stabilised the *anti* conformation and, instead, formed a stronger NH---O=C hydrogen bond which resulted in *syn* F-C-C=O conformations being observed in the X-ray crystal structures (***Figure 166***).[164] The same result was also observed in a series of difluoroamides.

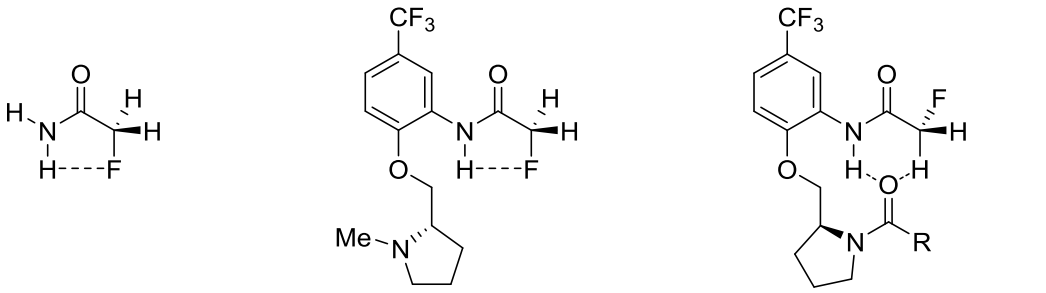

299
F-C-C=O = 179°

312
F-C-C=O = 180°
F-C-C=O = 179°

313a-c
R = O^{t}Bu, F-C-C=O = 4°
R = O^{i}Bu, F-C-C=O = -20°
R = H, F-C-C=O = 23°

***Figure 166** – The inherent anti conformation of the fluoroamide was overridden by interactions with an adjacent oxygen atom, leading to a syn conformation.*

6.1.2.2. α-Fluoroesters

A 1993 paper by van der Veken *et al*.[165] stated that the simplest fluoroester (methyl fluoroacetate, MFA, ***Figure 167***) has a 4.0 kJ mol^{-1} (0.96 kcal mol^{-1}) *anti* preference and so the value appears to have been misquoted in subsequent papers and reviews.

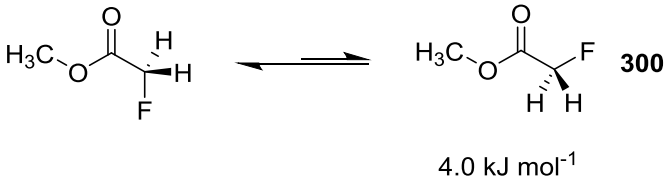

Figure 167 *– The two conformers of methyl fluoroacetate.*

Subsequently, Abraham *et al*. reported combined NMR, IR and DFT studies of methyl fluoroacetate (MFA) and methyl difluoroacetate (MDFA).[166] MFA clearly exhibits two stable conformers in DFT and IR analysis (*syn* and *anti*) and the more polar *syn* conformer is the preferred conformer in the five most polar solvents of the seven solvent systems analysed, with *anti* the preferred conformer in only carbon tetrachloride and chloroform. MDFA, has two stable conformers, *syn* and *gauche*, with the more polar *gauche* conformer favoured in medium to high polarity solvents. As with the fluoroamide analogues, a trifluorinated derivative was also analysed to confirm that changes in NMR shifts and coupling constants were a result of conformational effects rather than intrinsic solvent polarity effects. The results for MFA and MTFA are reproduced in ***Table 20*** and ***Table 21***.

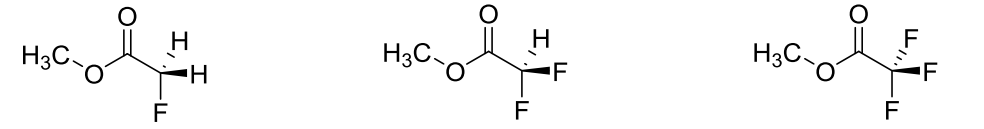

300
MFA
Methyl fluoroacetate

314
MDFA
Methyl difluoroacetate

315
MTFA
Methyl trifluoroacetate

Figure 168 *– The structures of MFA, MDFA and MTFA.*

Table 20 *- Chemical shifts (δ ppm) and coupling constants (Hz) for MFA.*[166]

Solvent	H_1	H_3	C_1	C_2	C_3	$^2J_{HF}$	$^1J_{CF}$	$^2J_{CF}$
CCl_4	4.76	3.77	77.1	167.4	51.5	47.22	185.3	21.8
$CDCl_3$	4.86	3.82	78.2	169.3	52.7	47.01	182.9	21.8
CD_2Cl_2	4.85	3.78	78.5	169.2	52.6	46.96	181.2	21.9
Acetone-d_6	4.95	3.75	78.7	169.6	52.3	46.84	178.6	21.9
Pure Liquid	4.91	3.78	79.2	170.5	52.8	46.71	178.3	21.8
CD_3CN	4.88	3.74	79.2	170.1	52.8	46.69	177.7	21.8
DMSO-d_6	5.03	3.72	78.0	168.9	51.9	46.43	176.6	21.8

Table 21 *- Chemical shifts (δ ppm) and coupling constants (Hz) for MTFA.*[166]

Solvent	H_1	C_1	C_2	C_3	$^1J_{CF}$	$^2J_{CF}$
CCl_4	3.96	115.1	158.0	54.3	284.9	42.6
$CDCl_3$	3.98	114.5	158.0	54.3	285.1	42.4
Acetone-d_6	4.03	115.6	158.4	55.2	284.5	41.8
CD_3CN	3.95	115.4	158.3	55.3	284.5	41.7

Abraham *et al*. also reported a study of some slightly more complex fluoroesters.[167] Methyl 2-fluoropropionate (MFP) was found to have an *anti* conformational preference in the vapour phase, roughly equal *anti* and *syn* energies in CCl_4 and a *syn* preference in more polar solvents. By increasing the bulk of the substituent on the F-C carbon the *syn* preference can be further increased (***Figure 169***).

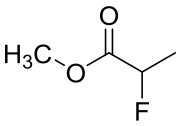

MFP
Methyl 2-fluoropropionate, **316**

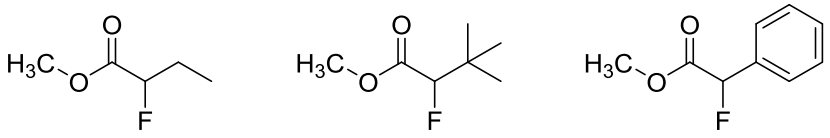

317 **318** **319**

Assorted analogues of MFP

Figure 169 *– The structures of MFP and three bulkier analogues.*

Abraham and co-workers computed F-C-C=O torsion angles, conformer energies and dipole moments for the four α-fluoroester derivatives (***Table 22***) and offered rationalisations of the observed conformational preferences of these systems (***Figure 170***), summarised below, though no NMR analysis was carried out on these derivatives.

In the *anti* conformation there is a repulsive interaction between the electronegative fluorine and methoxy oxygen atoms (A) which destabilises this conformation. There is a calculated distortion away from the 180^{o} F-C-C=O torsion angle (***Table 22***). This is rationalised by a proposed stabilising *gauche* effect between the C-H σ orbital and the C-O σ* orbital that prefers an *anti* H-C-C-OMe torsion angle. This, in turn, rotates the C-F bond away from the ideal 180^{o} F-C-C=O torsion angle (C). This distorted conformation away from *anti* F-C-C=O also leads to increased stabilisation by $n_F \rightarrow \pi^*_{C=O}$ hyperconjugation (D). Abraham *et al*. conclude that the latter attractive interactions are more important than the repulsive interaction as evidenced by the *anti* conformation predicted for **316**-**318** in the vapour phase and non-polar solvents. The *t*-butyl analogue **318** has a stronger *anti* preference (0.30 kcal mol^{-1}) and this is rationalised by hydrogen bonding interactions between the carbonyl oxygen and the alkyl protons of the butyl moiety (B).

The *syn* conformation similarly has a repulsive interaction between the electronegative fluorine atom and the carbonyl oxygen atom (E) which decreases in progressively more polar solvents. Slight distortion away from the ideal *syn* F-C-C=O dihedral angle of 0^{o} is also observed and the rationale offered is that the C-H bond aligns into a more *anti* conformation with regard to the C=O bond to increase the stabilising *gauche* effect (G). Additionally, this distorted conformation would aid donation from lone pairs of the fluorine to the carbonyl antibonding orbital (H). The phenyl derivative **319** is found to be more stable in the *syn* conformation even in the vapour phase due to electrostatic repulsion of the carbonyl oxygen atom and the bulky, high electron density of the phenyl group when the F-C-C=O moiety is in the *anti* conformation (F).

Table 22 – *Computed compound parameters for the four α-fluoroester derivatives.*[167]

Compound parameters	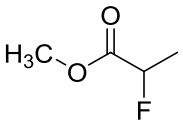 **316**		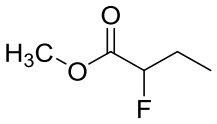 **317**		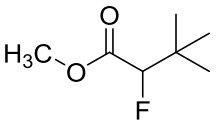 **318**		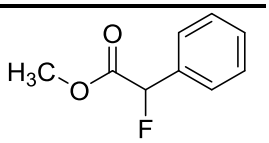 **319**	
	Syn	***Anti***	***Syn***	***Anti***	***Syn***	***Anti***	***Syn***	***Anti***
F-C-C=O torsion angle /^{o}	16	168	18	167	39	157	28	1.49
E_{rel} /kcal mol^{-1}	0.15	0.00	0.17	0.00	0.30	0.00	0.00	0.24
Dipole moment /D	3.75	0.89	3.67	0.90	3.31	1.16	3.66	1.67

The authors concluded that the *syn* conformation is expected to be the most stable conformation in polar solvents for any α-fluoroester.

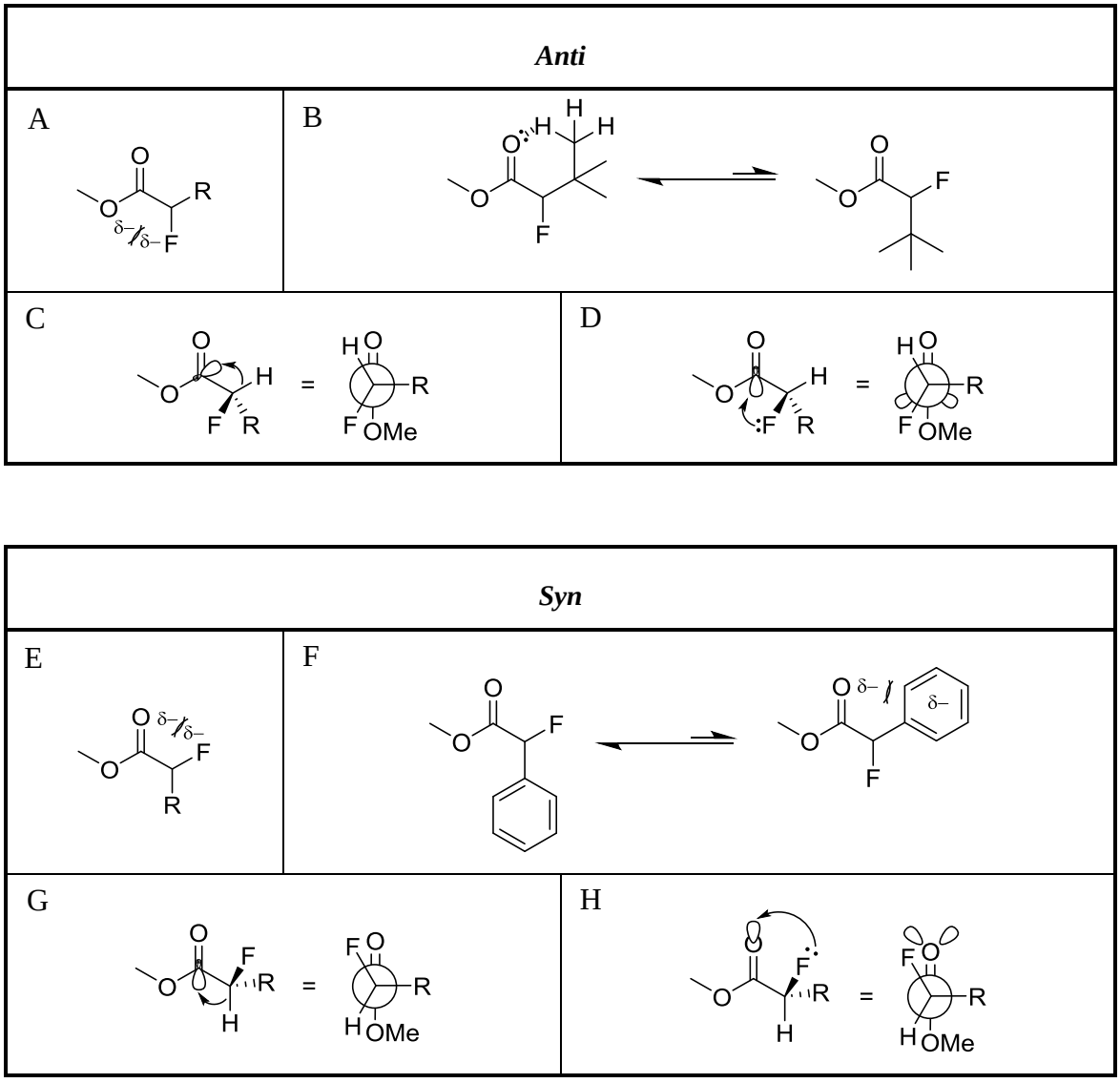

Figure 170 – *The interactions reported by Abraham et al. to rationalise the conformational preferences of α-fluoroesters.*

Takeuchi *et al*. report ester derivatives of α-cyano-α-fluoro-*p*-tolylacetic acid (CFTA, ***Figure 171***, a derivatising agent similar to Mosher's agent) exhibiting *syn* F-C-C=O conformations in X-ray crystal structures.[168] The ester 'R' groups R' and R'' show a chemical shift change in NMR when they are eclipsed by the large *p*-tol group due to shielding effects. Since the absolute stereochemistry of the chiral C-F carbon is known, by measuring whether R' or R'' exhibits a chemical shift difference, the authors claim that the conformation of the chiral carbon (of known configuration) can be derived and, hence, the conformation of the C-F bond relative to the C=O bond. Complementary computations are also described.

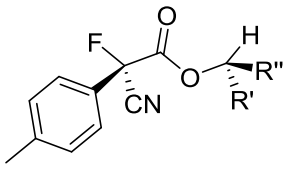

320

Figure 171 *– The generic structure of a CFTA derivative.*

In the example in ***Figure 171*** the *p*-tol group will shield the R'' group and indicate a syn F-C-C=O conformation. If the F-C-C=O bond were to rotate such that shielding is observed in R' then it would be implied that the fluorine has rotated to give a torsion angle of around 120^{o}. This technique relies on the assumption that the ester alkyl carbon (CR') has known conformation i.e. the C-H bond is always *syn* to the C=O bond. It also relies on the shielding effect to be strong enough such that it is observed in atoms five bonds away (*p*-tol-C*-C(O)-O-C-R').

Takeuchi and co-workers have also reported an *ab initio* molecular orbital study of the conformational preference in a CFTA ester[169] and a study on the substituent effects on conformational preference (i.e. replacing the cyano substituent).[170]

March *et al.*[159] describe deviations from the predicted conformations for fluoroester analogues, proposing that the weaker conformational preference of fluoroesters (c.f. fluoroamides) is often overridden by steric or crystal packing interactions. The authors suggest that whilst X-ray crystallographic studies are very useful in determining the configuration and conformation of a molecule in the solid state, the conformational preferences can, however, be heavily influenced or overridden by steric and crystal packing effects. NMR studies may provide a greater insight into conformation in the solution state which is potentially of more use for *in vivo* systems (e.g. biochemistry, medicine, pharmacology).

In comparison with the fluoroamides, the fluoroesters appear to have a considerably reduced *anti* preference and, in more polar solvents as Abraham *et al.* indicated,[166] the fluoroester *syn* conformation is actually preferred instead.

6.1.2.3. α-Fluoroketones

Abraham *et al*. reported a relatively low *anti* preference of 2.2 kcal mol^{-1} for the fluoroketones.[171] This 2.2 kcal mol^{-1} value is for fluoroacetone (FA) in the vapour phase and decreases to 1.0 kcal mol^{-1} in CCl_4 and further to -0.6 kcal mol^{-1} (i.e. a 0.6 kcal mol^{-1} *syn* preference) in the pure liquid. As with the corresponding α-fluoroesters, the assumed *anti* preference depends on the solvent polarity which, *in vivo*, is likely to be high leading to more *syn* preference.

Difluoroacetone (DFA) was also analysed and found to have a 0.8 kcal mol^{-1} *syn* preference in the vapour phase decreasing to 0.1 kcal mol^{-1} in CCl_4. A further decrease in the liquid phase favours the more polar conformation of F-C-C=O = 104° by 0.9 kcal mol^{-1}. The *syn*/*gauche* preference (and lack of *anti* preference) of the difluorinated ketone is similar to that of the difluorinated ester.

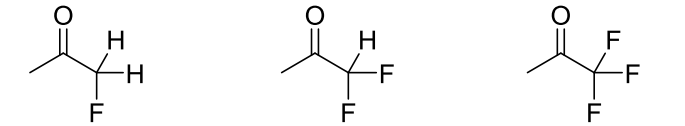

301 FA Fluoroacetone | **321** DFA Difluoroacetone | **322** TFA Trifluoroacetone

Figure 172 *– The structures of FA and DFA.*

The NMR data reported by Abraham *et al.* for fluoroacetone and trifluoroacetone are reproduced below. Minimal change in $^4J_{HF}$ coupling constant with increase in solvent polarity in the trifluorinated analogue TFA was observed. This suggests that the relatively larger changes in coupling constant for FA (4.7 to 3.5 Hz) and, to a lesser extent, DFA (1.3 to 1.7 Hz) were, therefore, related to conformational changes and not simply a product of intrinsic solvent effects. A similar trend is observed in the $^1J_{CF}$ data though the TFA $^2J_{CF}$ coupling shows some intrinsic solvent dependence (36.3 to 34.7 Hz). However, this change in $^2J_{CF}$ coupling constant is much less than is observed in FA (22.1 to 16.2 Hz) and slightly less than for DFA (27.7 to 24.5 Hz).

Table 23 *- Chemical shifts (δ ppm) and coupling constants (Hz) for FA.*[171]

Solvent	H_1	H_3	C_1	C_2	C_3	$^2J_{HF}$	$^4J_{HF}$	$^1J_{CF}$	$^2J_{CF}$
CCl_4	4.656	2.218	84.58	203.01	25.24	48.19	4.68	185.7	22.10
$CDCl_3$	4.792	2.253	85.70	205.62	26.42	47.74	4.32	184.9	20.42
CD_2Cl_2	4.801	2.183	85.28	204.44	25.33	47.60	4.03	184.1	19.32
Acetone-d_6	4.931	2.135	85.77	203.99	25.31	47.45	3.76	181.0	18.01
CD_3OD	4.891	2.150	86.08	206.43	25.25	47.41	3.77	181.7	18.00
DMSO-d_6	4.986	2.079	84.94	203.54	25.06	47.13	3.53	179.4	16.23

Table 24 *- Chemical shifts (δ ppm) and coupling constants (Hz) for TFA.*[171]

Solvent	H_3	C_1	C_2	C_3	$^4J_{HF}$	$^1J_{CF}$	$^2J_{CF}$
CCl_4	2.388	115.35	186.70	23.10	0.94	291.3	36.3
$CDCl_3$	2.431	116.07	189.33	24.40	0.95	291.3	36.4
CD_2Cl_2	2.421	116.28	189.60	24.45	0.97	291.4	36.0
Acetone-d_6	2.510	116.49	189.77	24.08	0.98	291.3	35.2
CD_3NO_2	2.475	116.99	191.19	24.22	1.00	291.3	35.4
DMSO-d_6	2.487	115.19	189.32	24.12	0.99	292.3	34.7

Plots of variables were also described as an alternative method of isolating changes in couplings due to population changes, finding that the $^4J_{HF}$ and $^2J_{CF}$ coupling constants appeared to strongly correlate with conformer population changes as, to a lesser extent, did the $^1J_{CF}$ coupling constants. The ^1H and ^{13}C chemical shift values did not correlate strongly with the coupling constants suggesting that factors other than conformer population changes were more important. Variable temperature NMR studies were also carried out as it had been shown that the $^4J_{HF}$ coupling constants varied depending on temperature and solvent. These combined studies gave the predicted conformer energy values stated at the beginning of this α-fluoroketone section.

Abraham and co-workers also studied slightly more complex fluoroketones.[172] 3-Fluoro-3-methyl-2-butanone (FMB) favoured *anti* by 3.8 kcal mol^{-1} in the vapour phase, with a reduced preference of 2.6 kcal mol^{-1} in CCl_4 and a negligible preference of 0.27 kcal mol^{-1} in DMSO. 1-Fluoro-3,3-dimethyl-2-butanone (FDMB) was also studied and determined to have a lower *anti* preference of 1.80 kcal mol^{-1} in the vapour phase, a 0.47 kcal mol^{-1} *anti* preference in CCl_4 and a 1.25 kcal mol^{-1} *syn* preference in DMSO. The introduction of the methyl group to the F-C carbon resulted in a higher *anti* preference than for the unsubstituted fluoroacetone. Addition of methyl groups to the non-fluorinated carbon resulted in no significant change.

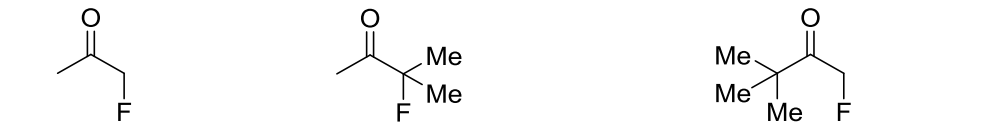

301 FA Fluoroacetone

323 FMB 3-Fluoro-3-methyl-2-butanone

324 FDMB 1-Fluoro-3,3-dimethyl-2-butanone

Figure 173 *– The structures of FA, FMB and FDMB.*

Table 25 *- Computed energy differences (E_{syn} - E_{anti} / kcal mol^{-1}) for FMB and FDMB in solvents of increasing polarity (positive values indicate an anti preference, negative values a syn preference).*[172]

Solvent	FMB	FDMB
Vapour phase	3.80	1.80
CCl_4	2.59	0.47
$CDCl_3$	1.77	-0.22
CD_2Cl_2	1.28	-0.62
Acetone-d_6	0.77	-1.00
CD_3CN	0.42	-1.19
DMSO-d_6	0.27	-1.25
Pure liquid	1.40	-0.91

Thus, fluoroketones appear to have similar trends in conformational preference to the analogous fluoroesters (generally tending toward *syn* preference in more polar environments).

6.1.2.4. α-Fluoroaldehydes

Phan and Durig reported an *anti* preference of 1.68 kcal mol^{-1} for fluoroacetaldehyde.[173] They note the instability of fluoroacetaldehyde at ambient temperature and that, as such, no experimental data was obtained. Additionally, the computations were limited to the vapour phase and so no solvent polarity effects were taken into account. Given that increasing solvent polarity overcame the reasonably stronger *anti* preferences of the fluoroketones and fluoroesters it would seem likely that the small 1.68 kcal mol^{-1} fluoroaldehyde preference could be readily overridden *in vivo*.

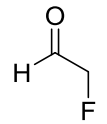

302
Fluoroacetaldehyde

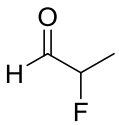

325
2-Fluoropropanal

Figure 174 *– The structures of fluoroacetaldehyde and 2-fluoropropanal.*

Similarly, Cee, Cramer and Evans reported a 1.27 kcal mol^{-1} *anti* preference for fluoroacetaldehyde at B3LYP/6-31G(d) level of computational theory, in general agreement with related computations at three other levels of computational theory.[174] A rotational energy profile for 2-fluoropropanal was also calculated to give an *anti* (189^{o}) preference over *syn* (354^{o}) by 1.9 kcal mol^{-1}. The authors note that the presence of a stable *anti* conformer of a substituted aldehyde is unusual and appears to be limited to aldehyde derivatives with highly electronegative substituents.

Given the instability of fluoroaldehydes considerably less research has been conducted into the preferred F-C-C=O torsion angle.

6.1.3. Summary of Literature Review of α-Fluorocarbonyl Conformational Studies

Several effects involving the C-F bond have been reported and examples of how the C-F bond can be used as a conformational tool have been discussed. The predictive power of these effects is promising but the F-C-C=O conformational preference may be limited to moieties that exhibit stronger preferences, such as fluoroamides.

Whilst the literature reports fair to strong F-C-C=O *anti* preferences these calculations are often performed in the vapour phase which provide an unrealistic molecular environment. For potential *in vivo* applications such as medicine and biochemistry a more polar environment is likely and, when a polarised continuum solvent model was applied to calculations, the fluoroesters and fluoroketones generally turned from *anti* preference to *syn* preference as solvent polarity increased.

This is possibly because as the solvent polarity increases the more polar (i.e. *syn*) conformation becomes more energetically stable than the less polar conformer (*anti*) as the overall dipole aligns with the polar solvent (***Figure 175***).

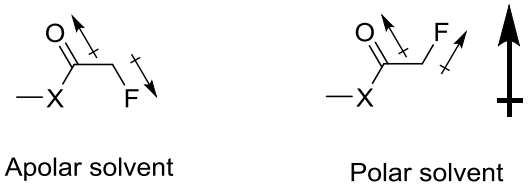

Figure 175 – *In more polar solvents it is proposed that the more polar syn conformation is preferred due to dipole alignment.*

The fluoroamides were predicted to have the strongest *anti* preference (due primarily to hyperconjugation and hydrogen bonding arguments) and it seems that solvent polarity effects alone are often not quite enough to overcome the *anti* preference. However, this *anti* preference has been intentionally overcome by the introduction of stronger C=O---H-N hydrogen bonding to override the C-F---H-N interaction (***Figure 166***, pg. 131) which may potentially be overcome in more complex, polar environments *in vivo*.

Fluoroesters and fluoroketones were predicted to have less of an *anti* preference and, in some cases, a *syn* preference was predicted even in the gas phase. Combined NMR/computational studies suggest that the *anti* conformation is increasingly disfavoured in solvents of increasing polarity. ***Table 26*** summarises the calculated energy differences of the *syn* and *anti* conformers of three simple α-fluorocarbonyl species reported by Abraham and co-workers (positive values indicate an *anti* preference, negative values a *syn* preference).

Table 26 *- Computed energy differences (E_{syn} - E_{anti} / kcal mol^{-1}) for α-fluorocarbonyl species in solvents of increasing polarity (α-fluoroamide data originally published in kJ mol^{-1} and here converted to kcal mol^{-1}).*[162,166,171]

Solvent	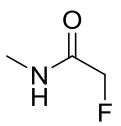 **309**	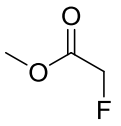 **300**	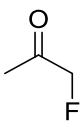 **301**	
Vapour phase	5.09	0.90	2.2	
CCl_4	-	0.41	1.04	Positive values are *anti*
$CDCl_3$	2.20	0.05	0.25	
CD_2Cl_2	1.53	-0.19	-0.24	Negative values are *syn*
Pure liquid	-	-	-0.63	
Acetone-d_6	0.86	-0.46	-0.75	
Pure liquid	-	-0.48	-	
CD_3CN	0.38	-0.65	-1.12	
DMSO-d_6	0.18	-0.71	-1.27	

The assumption that fluorocarbonyl systems have an inherent *anti* preference may be oversimplified and even if this is the case, there is no guarantee that this F-C-C=O torsion angle preference will actually have any effect in determining the conformation of the molecule if it is likely to be overridden by other competing factors including solvent and other functionality present in the system.

6.2. Search of Cambridge Structural Database for α-Fluorocarbonyl Species

To further our understanding of F-C-C=O conformations, a search of the Cambridge Structural Database (CSD) was conducted on a series of fluorocarbonyl systems, namely α-fluoro-esters, carboxylic acids, amides, ketones (including an acetophenone subcategory) and aldehydes. X-ray crystallography plays a vital role in conformational determination but is limited to providing conformational information about a compound in the solid state. Additionally, other environmental effects (such as crystal packing interactions) may influence the conformation of the molecule in such a way that it differs from solution state conformation as discussed above.

For solution state information, we have performed computational modelling and NMR studies in the α-fluoroesters category since this category is one most frequently used throughout this thesis. Further work on solution state conformations of α-fluoroketones (α-fluoroacetophenones, in particular) is currently being carried out within the research group. These techniques can provide a very useful insight and, when combined with X-ray crystallography, offer a complete approach to fluorocarbonyl conformational studies.

For comparison, some of our structures have been analysed along with the CSD data in the discussion section of this report. The final statistics for the CSD searches, however, exclusively contain CSD entries.

Molecules were analysed and then categorised according to their structural types in order to aid interpretation of the data and to eliminate any unusable entries. The F-C-C=O dihedral angle values were then separated into one of four angle ranges (defined below). Where secondary F-C-C=O torsion angles exist in the event of a 1,3-dicarbonyl system, unless the two fluorocarbonyl moieties are of the same species (e.g. a diester or a ketone), the secondary torsion angle is labelled to indicate its species. Esters are labelled ‘(E)’, amides are labelled ‘(A)’, ketones are labelled ‘(K)’ and acetophenones are labelled ‘(AcPh)’.

The angle values were then separated into one of four angle ranges, defined as *syn* (0-30^{o}), *gauche* (31-90^{o}), *eclipsed* (91-150^{o}) and *anti* (151-180^{o}). These ranges were derived from 0^{o} ± 30^{o} (*syn*), 60^{o} ± 30^{o} (*gauche*), 120^{o} ± 30^{o} (*eclipsed*) and 180^{o} ± 30^{o} (*anti*). The ranges were colour coded as an additional aid to interpretation (***Table 27***).

***Table 27** – Definitions of F-C-C=O dihedral angle ranges with their assigned colours.*

	Syn	*Gauche*	*Eclipsed*	*Anti*
Dihedral angle φ **(°)**	0-30	31-90	91-150	151-180

The dihedral angles are assigned either a '+' or a '-' sign according to the direction of rotation of the F-C-C=O bond. When viewed in a Newman projection along the C-C bond, '+' denotes the rear bond (F-C, in the example of ***Figure 176***) rotating in a clockwise direction relative to the O=C bond and, conversely, '-' denotes anticlockwise rotation of the rear atom.

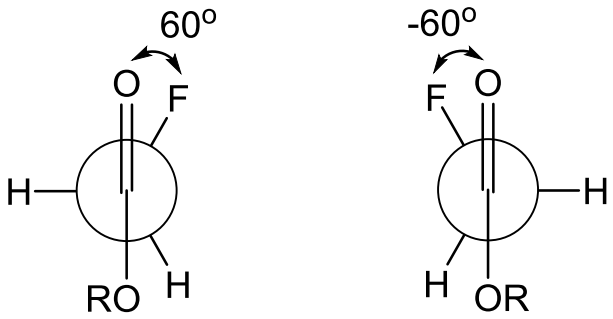

***Figure 176** – Newman projections of the F-C-C=O bond showing clockwise (+) and anticlockwise (-) rotation of the F-C bond relative to the O=C bond.*

Although these signs were recorded in the data tables, they were ultimately excluded when the angles were analysed due to symmetry. The analysis focussed primarily on the magnitude of the dihedral angles rather than in which direction the F-C-C=O bonds were rotated. It is also of note that due to symmetry, the *syn* and *anti* ranges span 30^{o} whereas the *gauche* and *eclipsed* categories each span the full 60^{o} range (***Figure 177***).

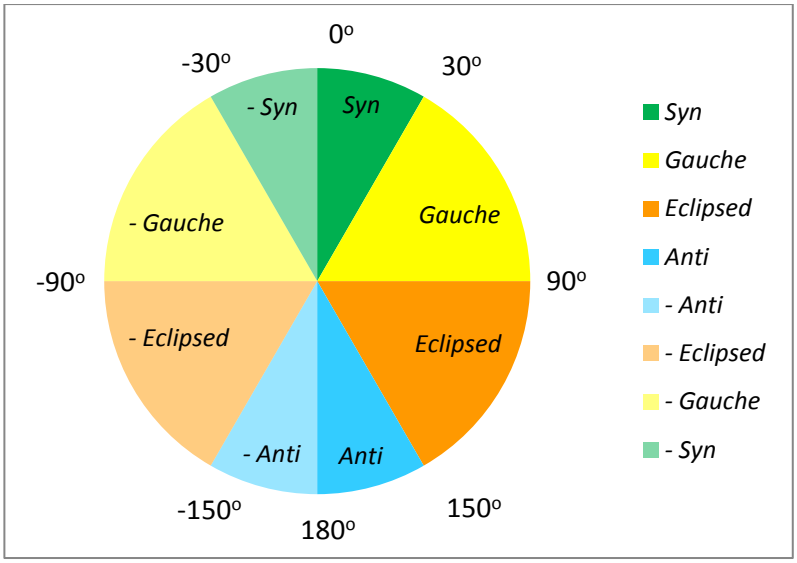

***Figure 177** – Definitions of the dihedral angle ranges.*

6.3. α-Fluoroesters

6.3.1. Simplest α-Fluoroesters

This category describes the simpler α-fluoroester entries in the CSD and excludes cyclic fluoroesters, acyclic fluoroesters adjacent to ring systems that may hinder free rotation of the FC-CO bond and polycarbonyl derivatives. These exclusions are described in the subsequent section.

6.3.1.1. CSD Search

Due to the minor discrepancies between search results using CCDC's online WebCSD search function and CCDC's ConQuest software, both of these search functions were utilised and the resulting two data sets were combined into one definitive list of structures to be analysed.

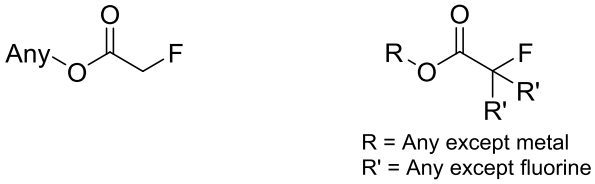

***Figure 178** – The substructure specifications for the initial (left) and amended (right) CSD searches.*

The initial substructure search (***Figure 178***, left) returned approximately 1,500 hits, many of which were organometallic compounds bound directly to a metal atom through the ester oxygen. Additionally, a large number of trifluoromethyl derivatives were observed that are of minimal value in investigating any F-C-C=O bond conformational preference. Subsequently, the search was refined to only include organic compounds with one fluorine atom adjacent to the ester moiety (***Figure 178***, right). As of January 2016, this substructure search returned 143 hits, a number of which were fluorocarboxylic acid derivatives excluded here and discussed in a later section (***Table*** 28). Appendix section A1.3.1. gives additional notes on exclusions to this category.

Table 28 *– The CSD Refcodes for the 143 hits from the combined WebCSD/ConQuest search of the refined substructure*

AWULOT	HALPER	MOWCEG	PAVDAR01	UDEHER
AWULUZ	HIJXEE	MUNZEC	PIWVIC	UGOCIE
BAGREG	HODBAD	MUQBAD	PIWVUO	UGOCOK
BAKWUG	HODBEH	MUQBEH	PUCROV	UNAJOJ
BARBAX	HOXNUE	MUQBIL	PULJIR	UNAJUP
BAWHAI	HOXNUE01	MUQQAS	QALBIP	VAGCOV
BIZMAY	IBACAR	MUQQEW	QALBOV	VAJYUB
BOJPUN	IQAFIQ	MUQQIA	QALCEM	VATDAX
BUTXET	IWIRIQ	MUQQOG	QAMPIF	VATDEB
BUTXET10	IWIROW	MUQQUM	QIVYEB	VEKLUT
CAXBEJ	IWIRUC	MUQRAT	QUKHOT	VEVSIZ
CFAPCH	JETJIC	NAGVUM	QUKHUZ	VEVSUL
DAJTEN	JUTBUX	NALFEL	RABBUN	VEVTAS
DIYJIF	KORXUM	NOTNAL	RADKIT	VIGPOQ
DOCVAS	LALPUL	NOTNEP	RAWJOQ	VIGQAD
DOZWEV	LIQNEF	NOTNIT	RFMALC	VOJSIW
DUWPAM	LIQNIJ	ODOPAZ	RUXZAM	VURBAN
EJETUJ	LIQNOP	OGIBUB	RUXZEQ	VURKUQ
ERAHEK	LIQNUV	OHIJAR	SELMIH	WOLGAF
EWIMEC	LISMOQ	OHIJAR01	SELMON	WUJBEK
EWIMIG	LOWCOR	OHIJAR02	SEQPIN	XEFQIK
FACETC01	MABBEY	OHIJAR03	SICRIG	XOHFUV
FACETC10	MAWBET	OHIJAR04	SIKYEQ	YEBSIJ
FLCTRT	MAWBIX	OKODAT	SIRGAD	YUMKEX
FMALON20	MAWBOD	OMECAK	SUHBUT	ZURWAK
FMALON21	MAWBUJ	OMILOM	SURKIZ	ZUWYAT
FUGDOC	MEGSUN	OYAGUR	TEFVEF	ZZZKZO
FUMPAE	MEKLIX	OYAHAY	TEFVEF10	
GIZNEI	MOWCAC	PAVDAR	TORPOH	

6.3.1.2. Exclusions

The 143 structures were categorised according to structure and only the acyclic monofluoroester category is included in this section.

Nine of the structures had no 3D data available for analysis and so these entries were excluded from this study. Six crystal structures had significant disorder that affected the fluoroester moiety and so these too were excluded. The example in ***Figure 179*** is QIVYEB, which exhibits disorder in the -CO_2Et moiety.

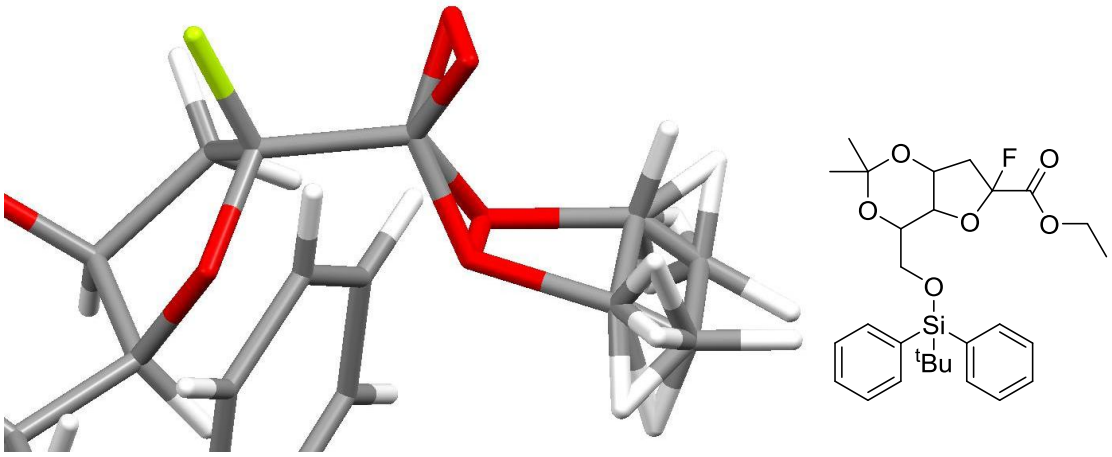

Figure 179 – *The -CO_2Et moiety of QIVYEB exhibits disorder that resulted in the exclusion of this structure from this study.*

Three entries (e.g. BUTXET) displayed no hydrogen atoms in the crystal structure due to high R-factors (e.g. 10.1 % for BUTXET) and were excluded. A further six of the 143 structures are duplicates that are identical to other entries in chemical structure but often differ in crystal packing arrangement. In the event of duplication only one entry for a structure (the one with the lowest R-factor) was included in the study. 16 of the structures were cyclic esters (i.e. fluorolactam derivatives) and were excluded from this study because the conformational restraints of being in a ring system would significantly impede rotation of the F-C-C=O bond and overpower any *syn*/*anti* preferences. As expected, the vast majority of the cyclic esters are assigned *gauche* conformations. OMECAK (***Figure 180***) is an example of a cyclic fluoroester. The F-C-C=O torsion angle is 60^{o} due to the conformational restraints of the heterocyclic ring system.

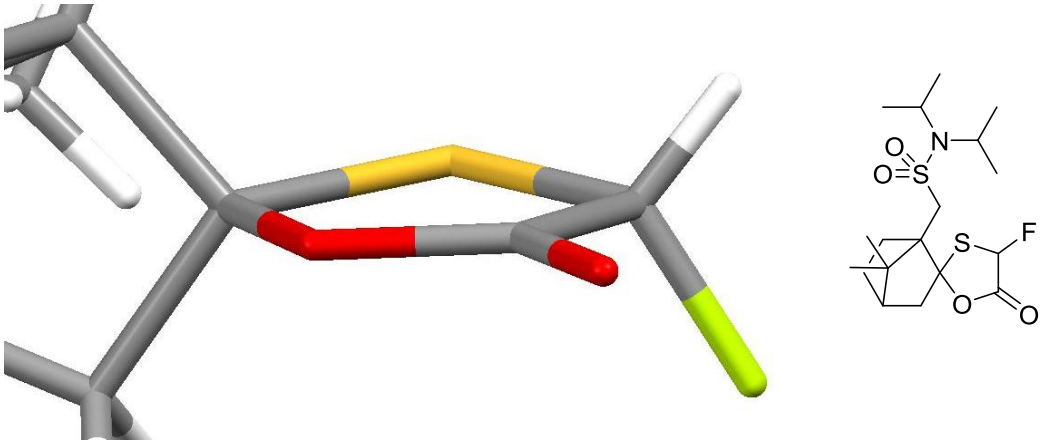

Figure 180 – *The crystallographically derived molecular structure of OMECAK – an example of a fluorolactam derivative that has a significant barrier to rotation of the F-C-C=O bond.*

A further 29 structures are acyclic fluoroesters, however, the fluorine atoms are directly bonded to a cyclic structure which could also potentially impose a barrier to rotation and so these structures have also been excluded from this section. Nine structures are fluorodiesters and a further five structures were fluorinated 1,3-dicarbonyl or tricarbonyl derivatives that include ketone F-C-C=O bonds in addition to the ester moiety which are reviewed later.

It is of note that XEFQIK has an additional amide F-C-C=O bond involving a separate fluorine atom. Thus this entry is not a 1,3-dicarbonyl system and so has been included here.

The remaining entries are acyclic monofluoroesters that are not directly bonded to a ring system, a total of 39 structures. Because several of the entries, like QALBIP, have multiple independent molecules in their crystal structures, the initial 39 entries are increased to 46 independent fluoroester moieties in total which have been analysed below.

6.3.1.3. Acyclic α-Fluoroesters

The 46 acyclic α-fluoroesters identified for this study are listed in ***Table 29*** in ascending F-C-C=O torsion angle.

Table 29 *– The 46 CSD structure Refcodes of acyclic α-fluoroesters, as defined above, ordered by their increasing F-C-C=O torsion angles.*

CSD Refcode	Torsion angle /°	CSD Refcode	Torsion angle /°
IBACAR	0	MAWBOD	18
VATDEB (A)	1	MOWCEG	18
VATDEB (B)	1	MAWBIX	20
UDEHER (A)	2	IQAFIQ	21
UDEHER (B)	2	MEKLIX	-27
VATDEB (C)	-2	QALBOV (A)	-30
AWULOT	3	EWIMIG	-47
VOJSIW	3	VAGCOV (A)	91
QAMPIF	-3	AWULUZ	127
VURBAN	5	VAGCOV (B)	128
GIZNEI	-5	LOWCOR	-140
DAJTEN	-6	EWIMEC	-148
MAWBUJ	-7	XEFQIK	155
UGOCOK	-7	QALBOV (B)	-160
VATDEB (D)	-8	HALPER	-167
VEVTAS (A)	-10	UNAJUP	-170
VEVTAS (B)	-11	VURKUQ	173
OYAGUR	12	UNAJOJ	-173
OMILOM	-12	QALBIP (A)	-175
MAWBET	13	EJETUJ	-176
FLCTRT	-13	YUMKEX	-177
CFAPCH	-14	CAXBEJ	-178
XOHFUV	-17	SURKIZ	-180

Of the 46 entries, 29 (63%) are *syn*, one (2%) is *gauche*, five (11%) are *eclipsed* and 11 (24%) are *anti*. These data are represented in the pie chart in ***Figure 181***.

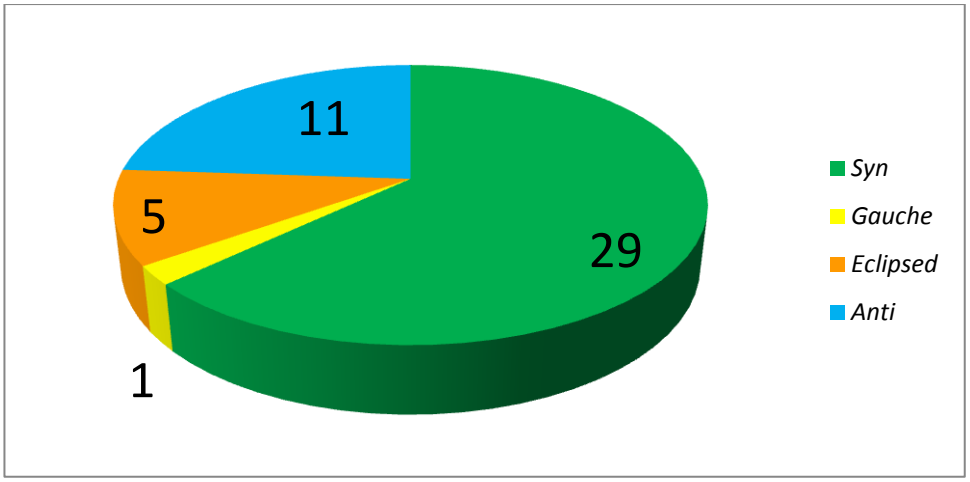

Figure 181 *– A pie chart to display the distribution of torsion angles into the four angle ranges*

Figure 182 *shows the cumulative totals for each angle, regardless of whether the angle is positive or negative.*

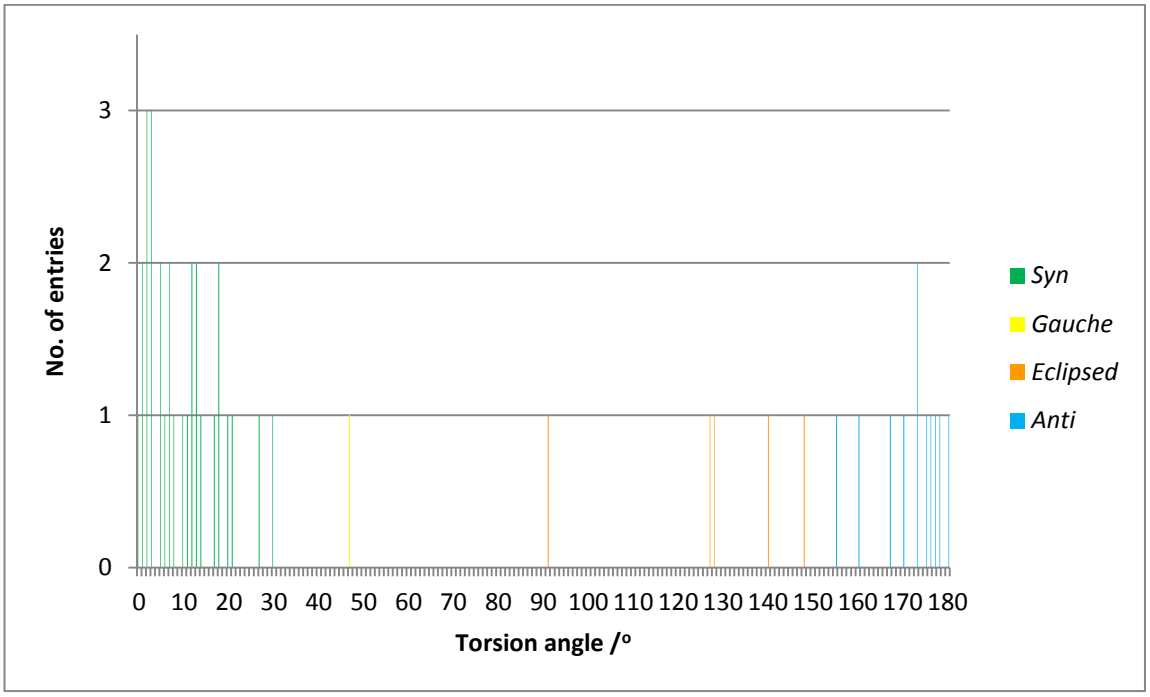

Figure 182 *– The cumulative distribution of torsion angles, independent of direction of rotation.*

These data have been projected onto a circle in ***Figure 183***. This diagram can essentially be viewed as a Newman projection with the oxygen atom at 0^{o} and the fluorine atom at the end of one of the radial lines. This projection offers a more visual interpretation of the data.

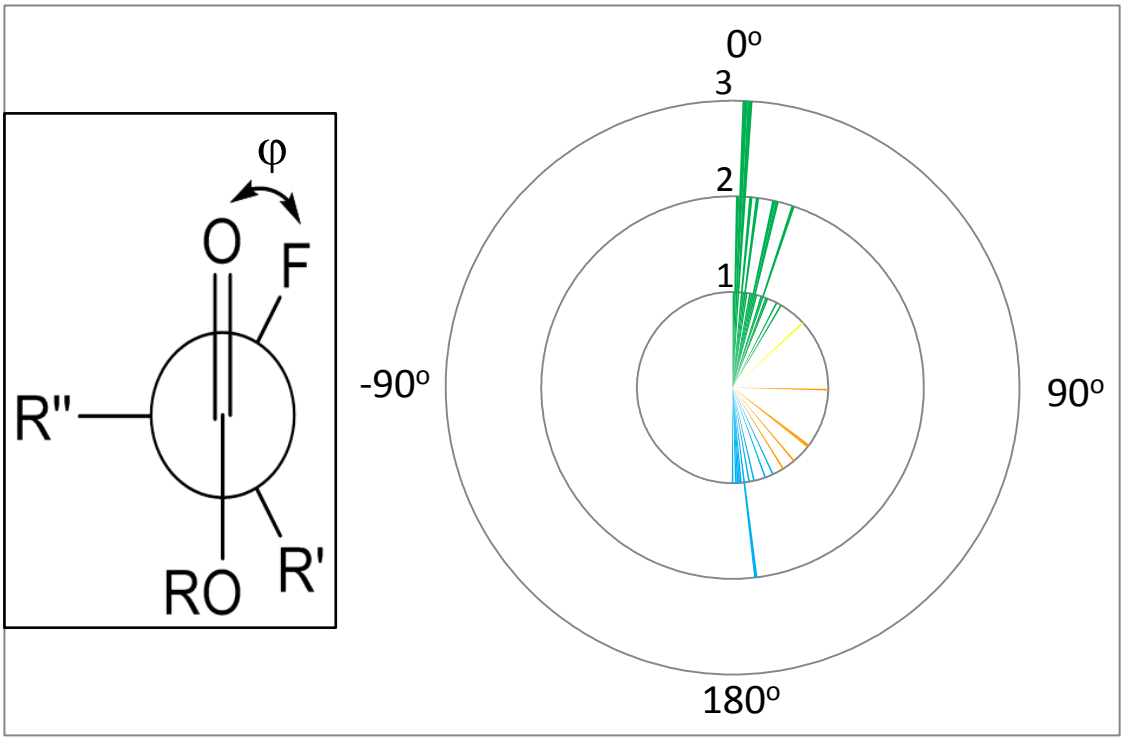

Figure 183 *– The cumulative distribution of torsion angles, independent of direction of rotation.*

Therefore, there is a clear indication that *syn* angles are the most populous angles in these data, accounting for nearly two thirds of all of the F-C-C=O moieties studied, a category around three times larger than the *anti* category. However, it may be erroneous to assume that there is a strong *syn* preference in fluoroester F-C-C=O bond conformation based purely on these data because there are still a significant number of examples (37%) that are not *syn*.

6.3.1.4. Examples of Interactions in Crystals of α-Fluorocarbonyl Derivatives

It is likely, therefore, that any inherent conformational preferences are often weak enough to be overpowered by external effects such as intermolecular or intramolecular interactions. A number of the key intermolecular and intramolecular interactions are discussed below.

F---H interactions – QAMPIF (***Figure 184***) is an example of a structure that exhibits multiple interactions between the fluorine atom and -CH protons. The interactions distances in this example are 2.314, 2.458 and 2.556 Å.

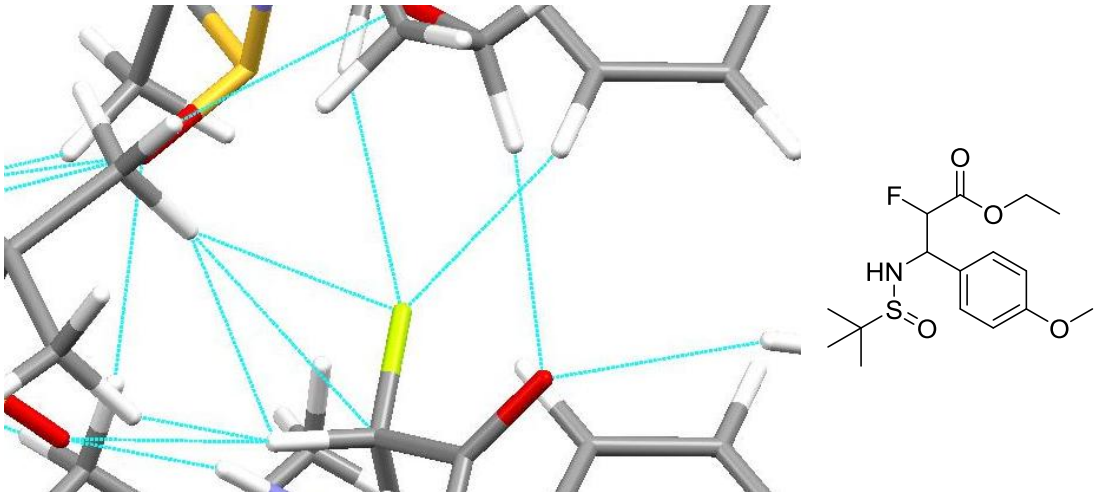

Figure 184 *– QAMPIF exhibits intermolecular F---H interactions.*

C=O---H-O interactions – Intermolecular hydrogen bonding between the ester carbonyl oxygen atom and a hydroxyl hydrogen is exhibited in GIZNEI (***Figure 185***). GIZNEI also features intermolecular F---H interactions with the proton geminal to the hydroxyl oxygen which may strengthen the *syn* preference for this structure. GIZNEI has a F-C-C=O torsion angle of only -5^{o}. The interaction distances are 1.942 Å (C=O---H-O) and 2.498 Å (F---H).

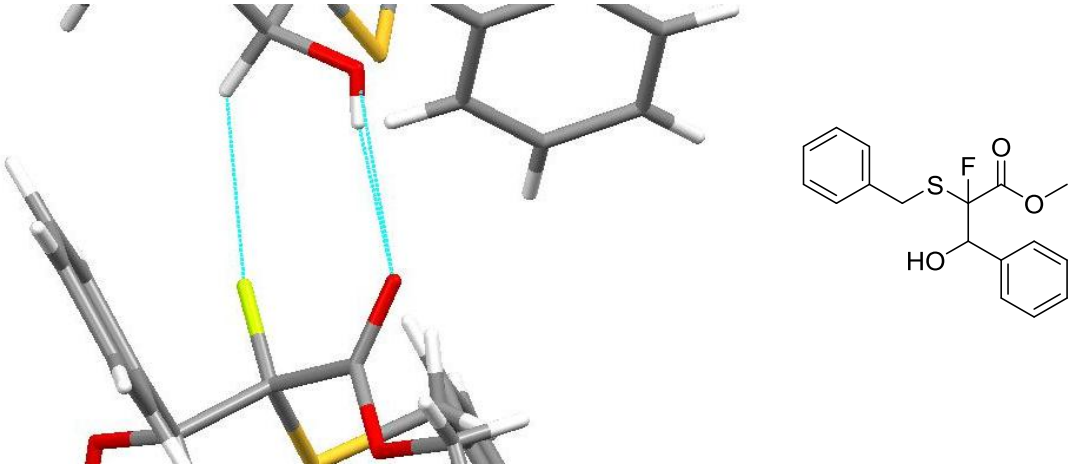

Figure 185 – *GIZNEI exhibits hydrogen bonding involving the ester carbonyl oxygen.*

F---H-O interactions – FLCTRT (***Figure 186***) is an example of hydrogen bonding involving the fluorine atom. The F---H-O interaction distance is 2.266 Å. This bond distance is shorter than most standard F---H interactions but longer than most C=O---H-O interactions, perhaps indicating a bond strength somewhere between the two.

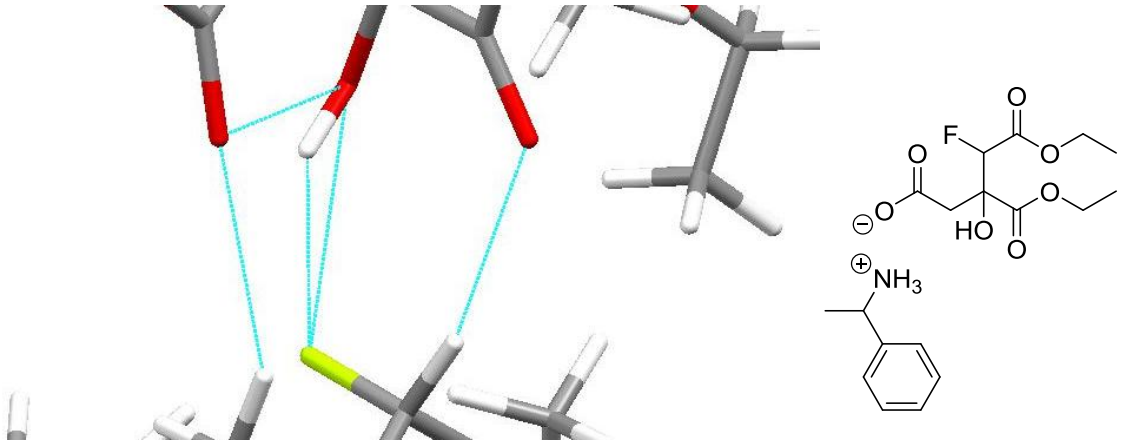

Figure 186 – *FLCTRT exhibits F---H-O hydrogen bonding.*

C=O---H interactions – CFAPCH (***Figure 187***) exhibits both C=O---H and C=O---H-O interactions. The interaction distances are 2.513 Å and 2.118 Å respectively.

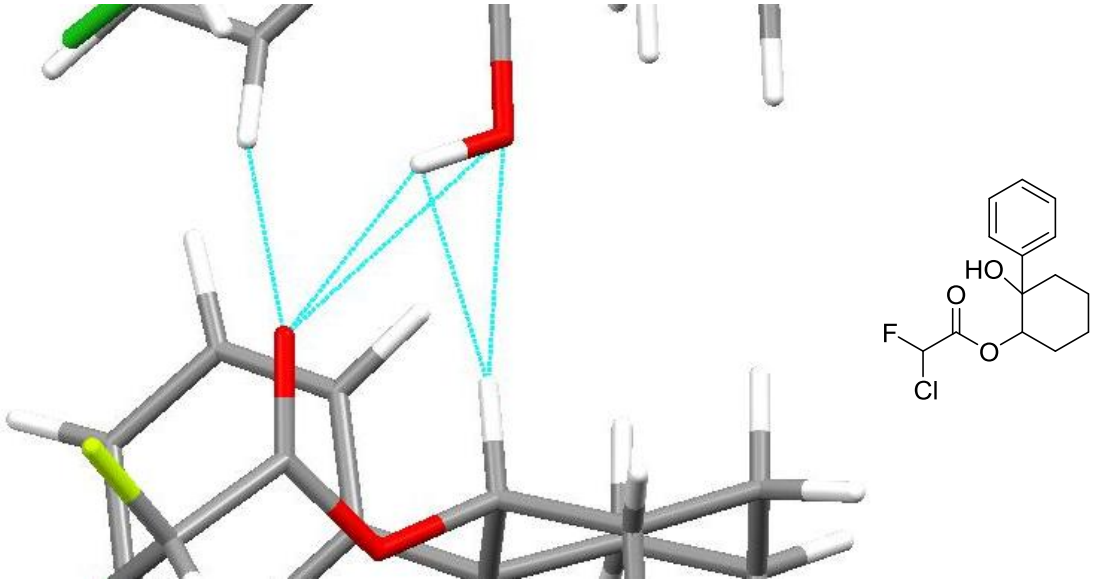

Figure 187 *– CFAPCH exhibits intermolecular C=O---H interactions.*

COO---H interactions – A number of the structures exhibit intermolecular interactions involving the other ester oxygen C-O atom. SURKIZ (***Figure 188***) has two COO---H interactions involving this oxygen with interaction distances of 2.697 and 2.717 Å.

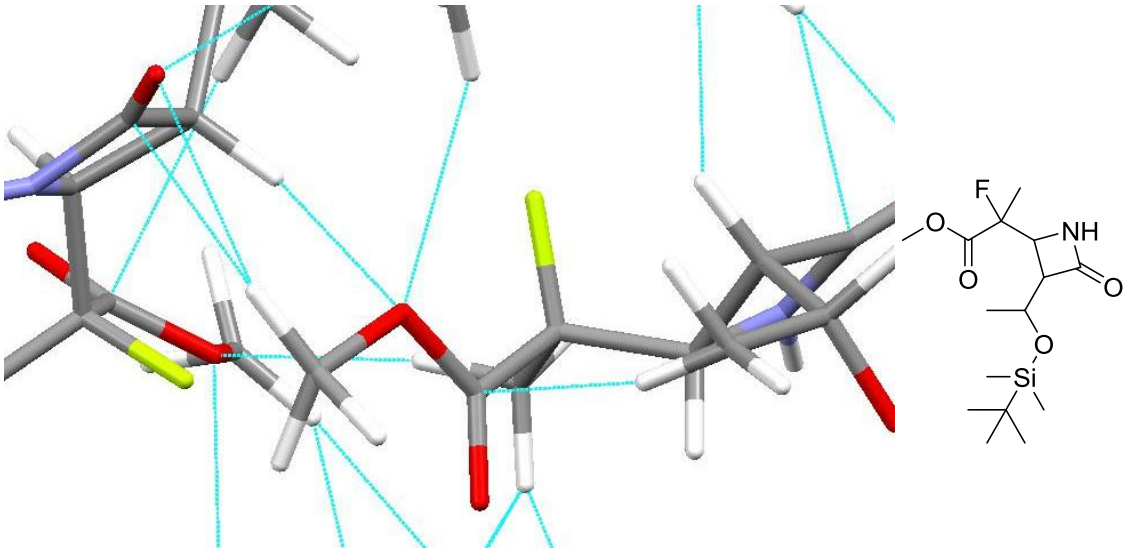

Figure 188 *– SURKIZ exhibits COO---H interactions.*

Ester alkyl interactions – The protons of ester alkyl groups are often involved in interactions which would contribute to determining the conformation of the nearby O=C-C-F bond. QAMPIF (***Figure 189***) is a simple example of a hydrogen bond between an ethyl ester proton and the carbonyl oxygen of another molecule with interaction distance 2.633 Å.

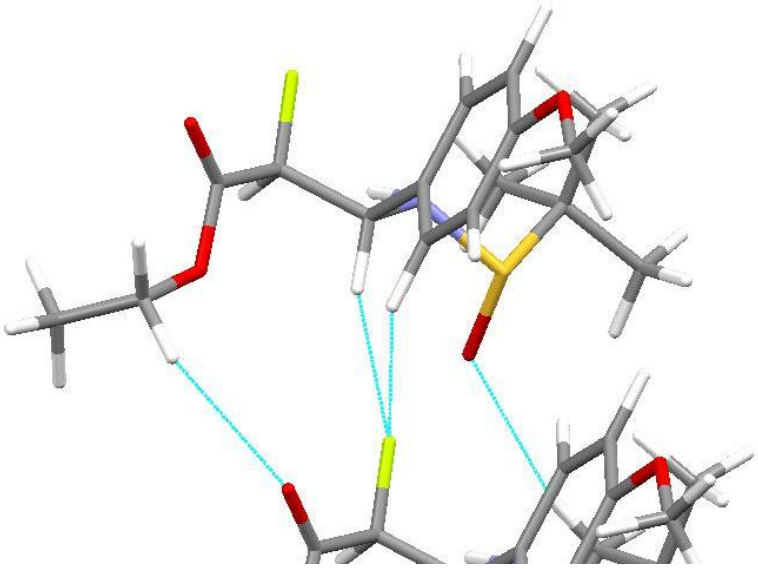

Figure 189 – *QAMPIF exhibits an intermolecular interaction between the ethyl group of the ester moiety and a carbonyl oxygen of another molecule.*

Amide interactions – Amide moieties often exhibit intermolecular hydrogen bonding. VATDEB (***Figure 190***) consists of four independent molecules with C=O---H-N bond distances ranging from 2.037 Å to 2.077 Å.

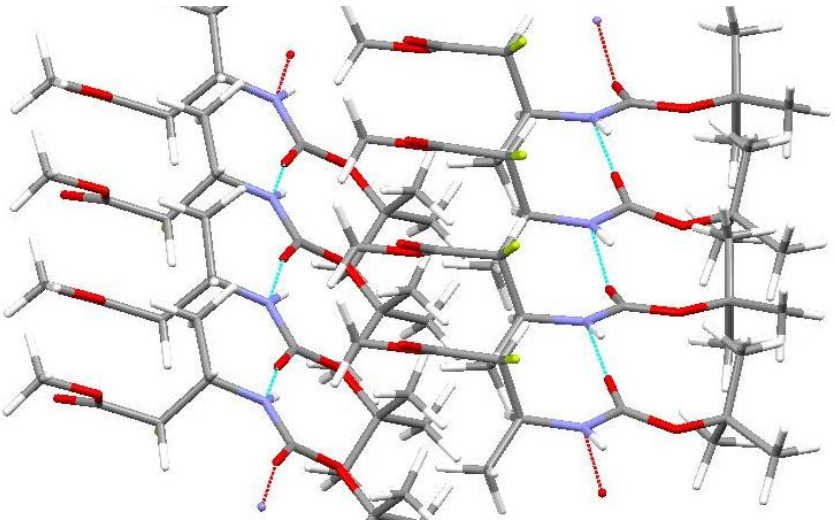

Figure 190 – *VATDEB is an example of an amide containing structure which exhibits extensive intermolecular hydrogen bonding interactions.*

Heteroatomic interactions – Many structures feature a variety of heteroatoms that may become involved in intermolecular interactions. For example, XOHFUV (***Figure 191***) has a bromine atom geminal to the fluorine atom. This bromine exhibits intermolecular interactions with the benzene rings in the co-crystal structure. Additionally, the geminal hydrogen and ester carbonyl oxygen atom are involved in hydrogen bonding with a hydroxyl group. The Br---H interaction distances are 2.773 and 3.044 Å and the Br---C distance is 3.517 Å.

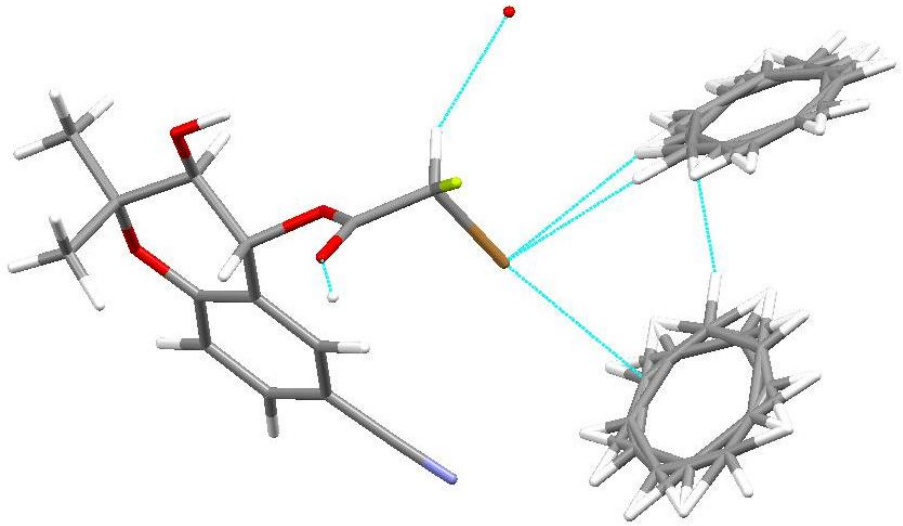

Figure 191 *– XOHFUV exhibits heteroatomic interactions through the bromine atom.*

CN and NO_2 interactions – Several of the entries' structures contain either nitrile or, more commonly, nitro groups and these nitrogen containing moieties are often involved in various interactions. EWIMIG (***Figure 192***) is an example of a nitrile group undergoing extensive intermolecular interactions. It is plausible that the F-C-C=O bond has been rotated such that these intermolecular interactions are maximised and this would account for the unusual *gauche* torsion angle of -47^{o}. The N---C=O interaction distances are 3.010 and 3.234 Å, the N---H interaction distance is 2.739 Å and the N---C interaction distance is 3.111 Å.

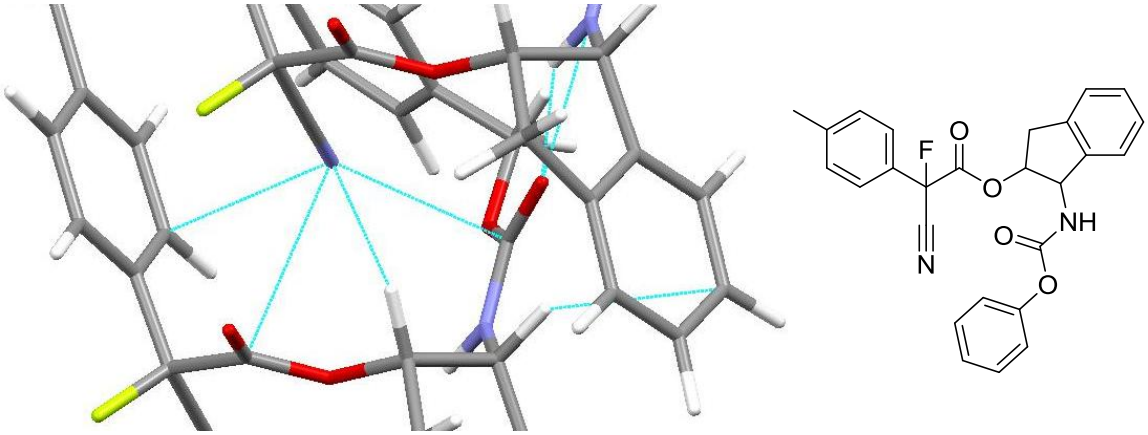

***Figure 192** – EWIMIG exhibits extensive FC-CN--- interactions.*

Stacking interactions – Entries that include either nitro groups, aromatic rings or both, frequently stack in the crystal structure. This stacking interaction has the potential to override any conformational preferences of the fluoroester moiety. UGOCOK (***Figure 193***) is an example that shows significant Ar-NO_2 stacking interactions.

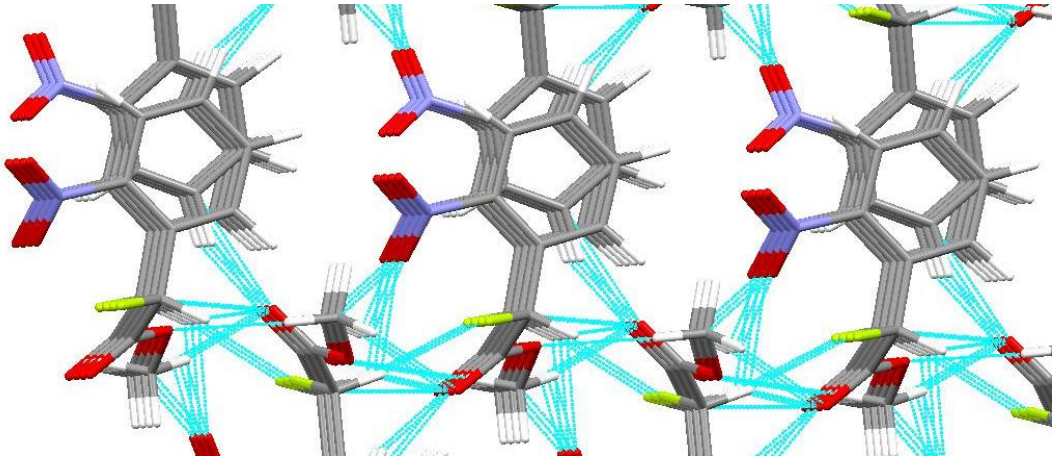

***Figure 193** – UGOCOK exhibits extensive Ar-NO_2 stacking.*

Observations of CN/NO_2 structures – Seven of the 46 entries contain nitrile or nitro groups. It is interesting to note that these account for all but one of the structures with *gauche* or *eclipsed* conformations. Two are *syn*, one is *gauche* and four are *eclipsed* (***Table 30***). It is unlikely a coincidence that all but one of the non-planar F-C-C=O moieties contain either nitrile or nitro groups.

Table 30 – *The seven CSD structures containing nitro or nitrile moieties.*

CSD Refcode	Torsion angle /°	Moiety
EWIMEC	-148	CN
EWIMIG	-47	CN
LOWCOR	-140	NO_2 x 2
MEKLIX	-27	CN
UGOCOK	-7	NO_2
VAGCOV (A)	91	NO_2
VAGCOV (B)	128	NO_2

The one remaining non-planar entry (AWULUZ, ***Figure 194***) does have a tertiary amine vicinal to the fluorine atom but appears to lack any interactions involving this nitrogen.

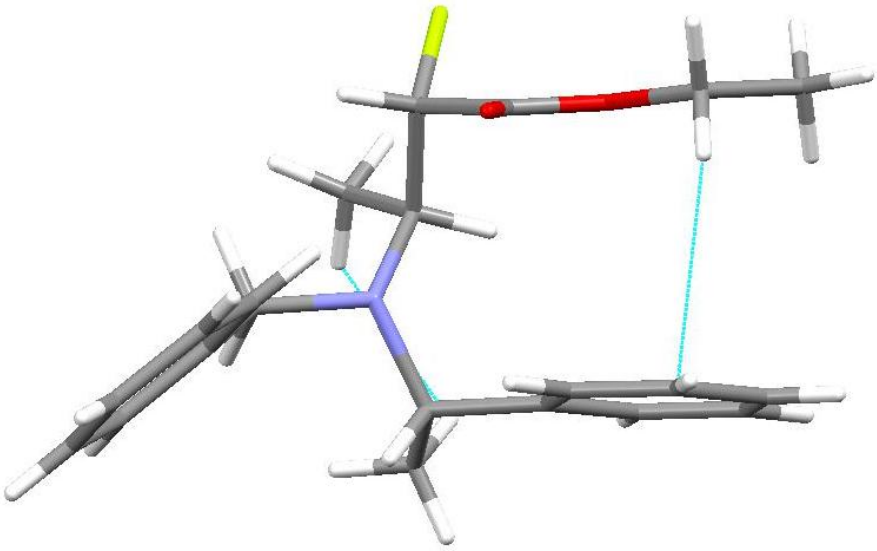

Figure 194 – *The crystallographically determined molecular structure of AWULUZ.*

Steric interactions - It is interesting to note that the ester moiety in AWULUZ (***Figure 194***) is in a near-parallel plane to the benzyl ring and only an H---C interaction (2.746 Å) is observed. This structure appears to have some level of steric hindrance to the rotation of the F-C-C=O bond due to the nearby phenyl ring.

Summary

The F-C-C=O moieties in CSD crystal structures of these simple α-fluoroesters are mainly *syn* (63%). 24% are *anti* and the remaining entries often show other interactions with heteroatoms that override this conformational preference in the solid state.

6.3.1.5. Solution-State Conformational Studies of α-Fluoroesters

Whilst analysis of X-ray crystal structures provides a valuable insight to the conformations of fluorocarbonyl species in the solid state, other means of analysis must be used to gain information on conformations in solution, which is an important consideration when physiological conditions are relevant, such as in drug design. The following section outlines both literature studies of solution state fluoroester conformations and our own research. All our computational calculations were performed by Dr. Mark Fox (Durham University).

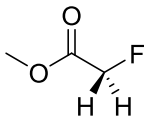

300

Figure 195 *– The structure of methyl fluoroacetate.*

A 1993 paper by van der Veken *et al.*[165] states a 4.0 kJ mol^{-1} (0.96 kcal mol^{-1}) *anti* preference for the simplest fluoroester (methyl fluoroacetate). Upon further investigation the 4.0 kJ mol^{-1} appears to be erroneous due to a mistake in the paper when assigning dipole moments. Our calculations to reproduce the original computations with the same level of computational theory (HF/4-21G) led instead to a 1.70 kcal mol^{-1} *syn* preference. Additionally the dipole moments were recomputed (HF/6-31G) to be 4.4. D (*syn*) and 1.0 D (*anti*).

It is unfortunate that a small gas phase *syn* preference was erroneously reported as a small *anti* preference (0.96 kcal mol^{-1})) by van der Veken *et al.* (1993).[165] Consequently, recent reviews by O'Hagan (2008)[145] and Hunter (2010)[146] quoted that *anti* is the preferred conformation of α-fluoroesters by 4.5 kcal mol^{-1}. In contrast, Abraham and coworkers[166] (2001) reported a *syn* preference for methyl fluoroacetate in the five most polar of the seven solvents simulated. Our further calculations at a higher level of theory (MP2/6-31+G**) lead to a negligible *syn* preference of 0.08 kcal mol^{-1} in the gas phase which was confirmed at MP2/aug-cc-pVTZ level giving a 0.04 kcal mol^{-1} *syn* preference.

Since gas phase calculations do not take into account solvent polarity which affects fluorocarbonyl conformational preferences, we applied a polarised continuum solvent model to rotational energy profile computations. Larger *syn* preferences were observed: 0.22 kcal mol^{-1} for apolar cyclohexane and 0.61 kcal mol^{-1} for polar water, with various solvents producing values between these two extremes (***Figure 196***).

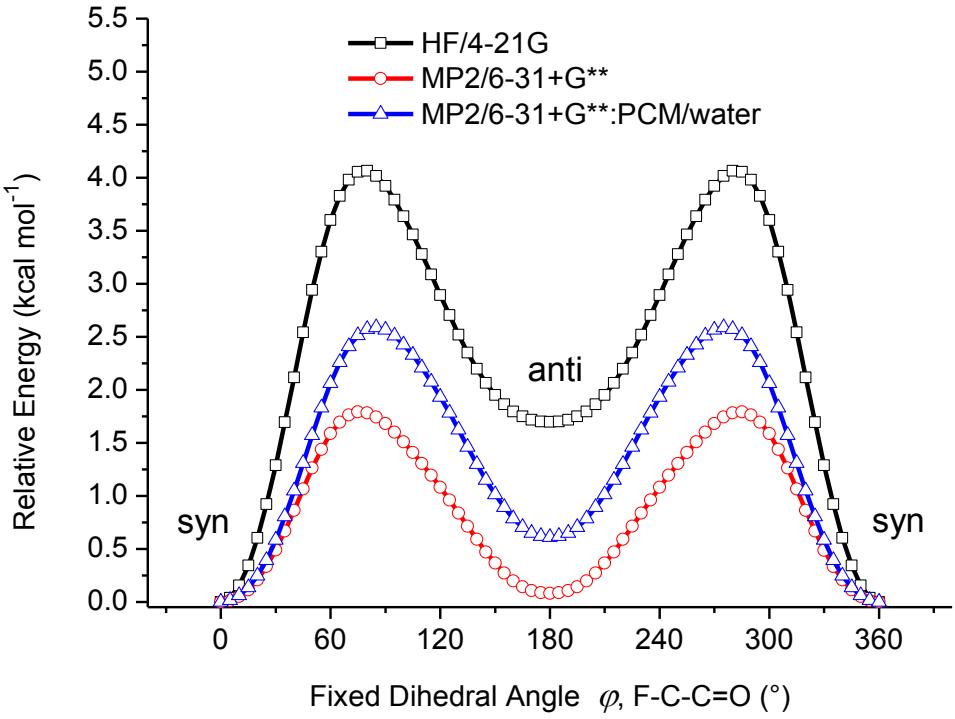

Figure 196 – *The rotational energy profiles for gas phase and solvent environments for methyl fluoroacetate.*

As discussed above, Abraham *et al*. reported combined NMR, Raman, IR and DFT studies of methyl fluoroacetate (MFA) and methyl difluoroacetate (MDFA).[166] MFA clearly exhibits two stable conformers in DFT and IR analysis (*syn* and *anti*) and the more polar *syn* conformer is the preferred conformer in the five most polar solvents of the seven solvent systems analysed, with *anti* the preferred conformer in only carbon tetrachloride and chloroform. MDFA, has two stable conformers, this time *syn* and *gauche*, with the more polar *gauche* conformer favoured in medium to high polarity solvents.

300
MFA
Methyl fluoroacetate

314
MDFA
Methyl difluoroacetate

Figure 197 *– The structures of MFA and MDFA.*

The Raman spectrum reported by Abraham *et al*. observed two CC stretch peaks of 843 (*anti*) and 787 (*syn*) cm^{-1}. These assignments are based on the erroneous calculated dipole moments reported by van der Veken *et al*. Our recalculated (MP2/ 6-31+G**) Raman data gave CC stretch peaks at 829 (*syn*) and 791 (*anti*) cm^{-1}, in contrast to the reported data. Experimentally determined Raman spectra reported by van der Veken *et al.* confirmed that crystalline (neat) methyl fluoroacetate at 204 K is only in one of the two conformations (*syn*) since only the peak at 843 cm^{-1} is observed. At higher temperatures (293 K) both conformers are observed with a 5:2 ratio of *syn* to *anti*. These data are consistent with our calculations (***Figure 198***) where the same 5:2 ratio was observed at 293 K.

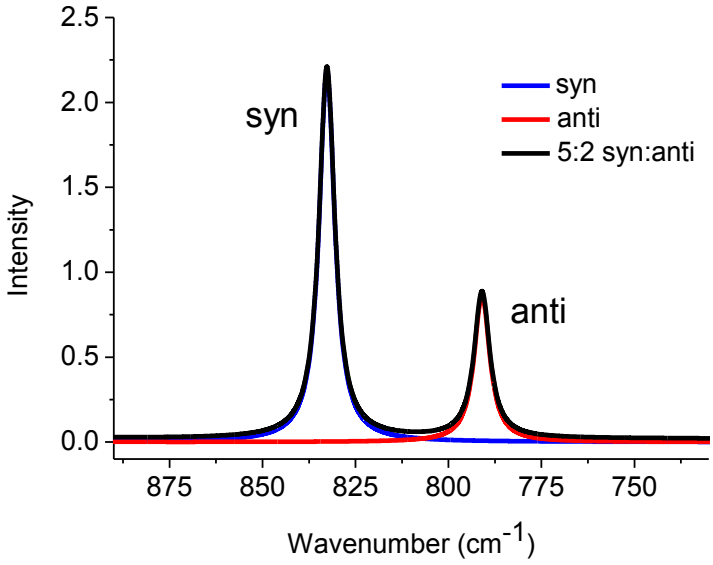

Figure 198 *–Simulated Raman spectrum (MP2/6-31+G**:PCM/water) of methyl fluoroacetate at 293 K. The two CC stretching bands are observed in a 5:2 ratio of syn:anti.*

Laato *et al*. report[175] that the IR spectrum of methyl fluoroacetate has two C=O stretching bands at 1790 and 1759 cm-1 which were assigned to *syn* and *anti* respectively on account of MP2/ 6-31+G** level computations predicting peaks at 1791 (*syn*) and 1760 (*anti*). The relative intensity of the *anti* band decreases with increasing solvent polarity suggesting a stronger *syn* preference in more polar solvents. Our simulated IR spectrum strongly agrees with the IR spectrum reported by Laato *et al*. where a 3:2 ratio of *syn*:*anti* conformers is observed in hexane at 293 K. The simulated IR spectrum is shown in ***Figure 199***.

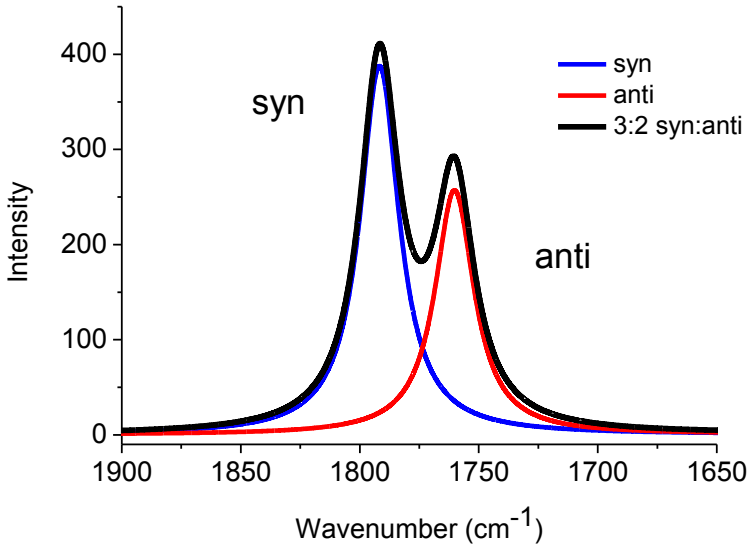

Figure 199 *–Simulated IR spectrum (MP2/6-31+G**:PCM/n-hexane) of methyl fluoroacetate at 293 K. The two C=O stretching bands are observed in a 3:2 ratio of syn:anti.*

Abraham *et al*. report an *anti*:*syn* energy difference of 0.90 kcal mol^{-1} (*anti* preference) and predicted the $^{1}J_{CF}$ coupling constants to be 172.3 (*syn*) and 192.4 (*anti*) Hz in the vapour phase based on solvent theory of NMR data. The $^{1}J_{CF}$ coupling constants in solvents of varying polarities were recorded and extrapolated into the vapour phase. Our computed (MP2/6-31+G**) $^{1}J_{CF}$ coupling constants are 191 (*syn*) and 206 (*anti*) Hz for the vapour phase but decrease to 178 (*syn*) and 196 (*anti*) Hz when acetonitrile is used in a solvation model. ***Table 31*** compares our optimised geometries with experimental data reported by Abraham *et al*.

Table 31 *– Comparison of our computed NMR data with reported experimental data.*[166]

Solvent	Conformation	Coupling Constants /Hz			Chemical Shifts /ppm		
		$^1J_{CF}$	$^2J_{CF}$	$^2J_{HF}$	δ(CF)	δ(CO)	δ(Me)
Gas	*Anti*	206.2	13.9	54.3	78.5	168.0	51.7
Gas	*Syn*	190.7	22.8	54.3	77.5	166.2	51.2
CCl_4	*Anti*	200.9	13.4	54.1	79.2	168.7	52.4
CCl_4	*Syn*	184.5	22.2	54.3	78.3	167.4	51.9
CCl_4	Experimental	185.3	21.8	47.2	77.1	167.4	51.5
CH_2Cl_2	*Anti*	196.3	12.9	53.9	79.9	169.4	52.9
CH_2Cl_2	*Syn*	178.7	21.6	54.3	79.3	168.7	52.5
CH_2Cl_2	Experimental	181.2	21.9	47.0	78.5	169.2	52.6
MeCN	*Anti*	195.7	12.9	53.8	80.0	169.4	53.0
MeCN	*Syn*	177.9	21.6	54.2	79.4	168.7	52.6
MeCN	Experimental	177.7	21.8	46.7	79.2	170.1	52.8

Abraham *et al*. compared these results to a trifluorinated analogue to confirm that the change in coupling constants with solvent polarity wasn't simply a result of inherent solvent dependency, as previously discussed with the α-fluoroamides.

The *anti*/*syn* difference of 0.90 kcal mol^{-1} is very small given that the $^1J_{CF}$ coupling constants vary considerably between the vapour and solvent models and so is somewhat inappropriate and means it is not particularly valid as a prediction when considering fluoroesters more complex in structure than methyl fluoroacetate. As such, we computed (MP2/6-31+G**) FC-CO bond rotation barriers and relative energy values of some more complex fluoroester moieties in both the 'gas-phase' and in a 'polar solvent' model using water as the solvent (***Table 32***).

Table 32 *– Computed FC-CO bond rotation barriers and relative energy values (kcal mol^{-1}) of some fluoroester moieties.*

Entry	Cpd	Fluoroester	Gas		Rotation Barrier /kcal mol^{-1}	Water		Rotation Barrier /kcal mol^{-1}
			Anti	*Syn*		*Anti*	*Syn*	
1	**300**	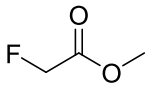	0.08	0.00	1.79	0.61	0.00	2.59
2	**319**	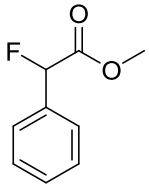	0.16	0.00	2.97	0.61	0.00	2.91
3	**326**	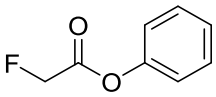	0.23	0.00	2.10	0.68	0.00	2.85
4	**316**	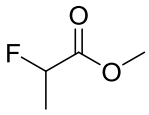	0.00	0.04	2.04	0.57	0.00	2.30
5	**327**	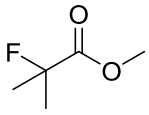	0.00	0.18	1.40	0.57	0.00	2.03
6	**328**	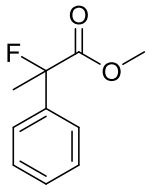	0.00	0.48	3.19	0.49	0.00	2.77
7	**329**	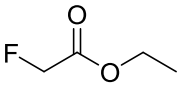	0.00	0.01	1.77	0.58	0.00	2.58

In the gas phase, esters with Me-CF moieties (entries 4 and 5) preferred the *anti* conformation, as did the phenyl methyl substituted entry 6. The other phenyl substituted analogues (entries 2 and 3) preferred the *syn* conformation while the ethyl ester (entry 7) showed little change. However, when a polar solvent model was applied (water), all structures, to a larger extent, favour the *syn* conformation.

The conformational preferences here are, again, relatively small and it cannot be stated with any certainty that *syn* is the preferred conformation of fluoroester F-C-C=O moieties in polar solvents. When considered with the low energy rotation barriers it can be expected that either conformation could be present in X-ray crystal structures of fluoroester derivatives since other factors (e.g. crystal packing or intermolecular interactions) could override any inherent F-C-C=O conformational preference.

The X-ray crystal structure of ethyl fluoroacetate **329** (a less toxic derivative of the methyl ester) was obtained (***Figure 200***) and the F-C-C=O torsion angle was determined to be *syn* (1^{o}). As previously discussed, 63% of 46 simple F-C-C=O fluoroester torsion angles available in the CSD are *syn*. It could perhaps be considered that a crystal is a polar lattice of other fluoroester molecules surrounding the fluoroester molecule and, as such, the observed conformational preference trend in the CSD is somewhat comparable to the polar solvent models in solution.

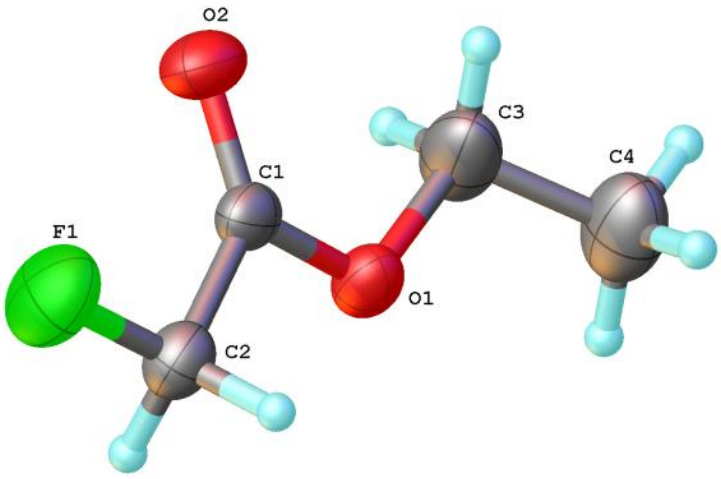

Figure 200 *–The molecular structure of ethyl fluoroacetate, as determined by X-ray crystallography.*

6.3.2. Miscellaneous α-Fluoroesters

Having analysed the simpler α-fluoroester structures in the CSD there now follows discussions of more complex systems excluded from the initial study. These include cyclic fluoroesters, acyclic fluoroesters adjacent to ring systems that may hinder free rotation of the FC-CO bond and polycarbonyl derivatives.

6.3.2.1. Cyclic α-Fluoroesters

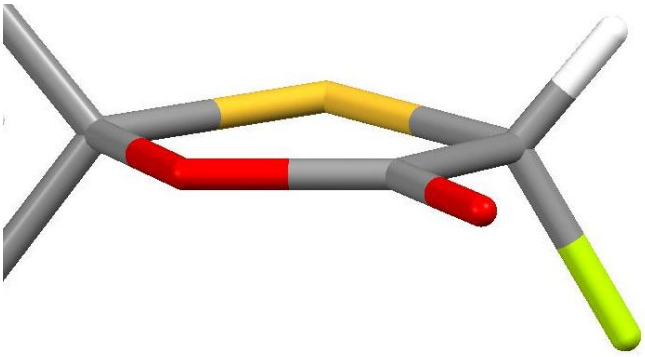

Figure 201 *– OMECAK has a F-C-C=O bond torsion angle of 60° due to the rotational restraints of the sp^3 carbon atom in a flat, planar ring system.*

Table 33 *– The 16 CSD structure Refcodes for the lactone derivatives.*

CSD Refcode	Torsion angle /°
BAKWUG	-38
BOJPUN	-89
LIQNEF	-49
LIQNIJ	62
LIQNOP	-51
LIQNUV	54
MEGSUN	-89
NOTNAL	38
NOTNEP	38
NOTNIT	78
OMECAK	60
PAVDAR	39
PIWVUO	-35
SIKYEQ	42
VEKLUT	44
ZUWYAT	-11

16 of the α-fluoroester entries in the CSD are cyclic esters (lactones) that exhibit severe inhibition of F-C-C=O bond rotation due to the restraints of the ring system (e.g. ***Figure 201***). ***Table 33*** shows that all but one of these structures (94%) have *gauche* torsion angles, as would be expected. Further examples can be found in appendix section A1.3.2.

6.3.2.2. α-Fluoroesters on a Ring System

15 structures are acyclic fluoroesters but the F-C carbon atoms are part of a cyclic moiety that could potentially restrict rotation of the F-C-C=O bond. SELMON is an example (***Figure 202***). ***Table 34*** displays the Refcodes for these 15 derivatives.

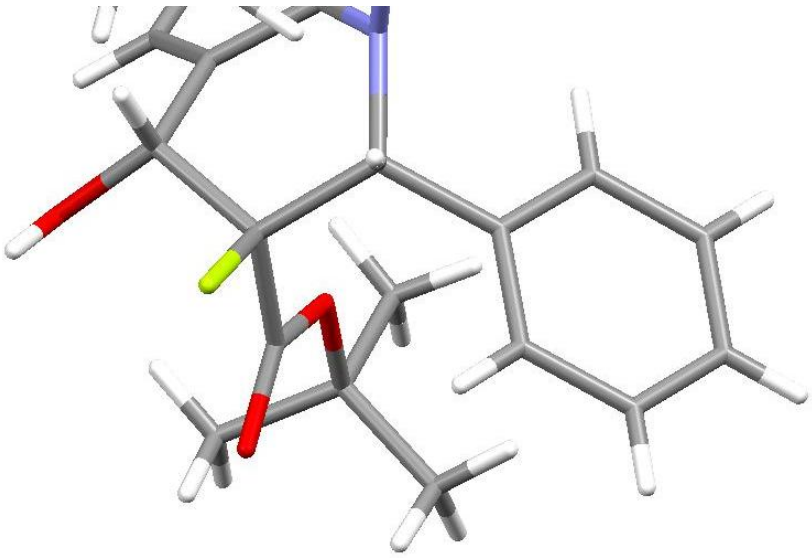

Figure 202 – *The molecular structure of SELMON shows the fluoroester moiety adjoined to the substituted heterocyclic ring moiety.*

Table 34 – *The CSD Refcodes for the 15 structures in which the fluoroester moiety is attached to a ring system.*

CSD Refcode	Torsion angle /°
DUWPAM	-5
JETJIC	0
KORXUM	-166
LISMOQ	-133
OKODAT	7
PIWVIC	142
PUCROV	-4
RADKIT	-24
RAWJOQ	-43
RUXZAM	-175
RUXZEQ	-177
SELMON	3
TORPOH	11
WOLGAF	-162
WUJBEK	17

53% of the fluoroester F-C-C=O torsion angles in these entries are *syn*, 7% are *gauche*, 13% are *eclipsed* and the remaining 27% are *anti*.

RAWJOQ exhibits unusual *gauche* fluoroester conformation. Analysis of the structure revealed an apparent repulsion between the ester oxygen atom and an adjacent heterocyclic amide carbonyl oxygen that could account for the rotation of the F-C-C=O bond to -43° (***Figure 203***).

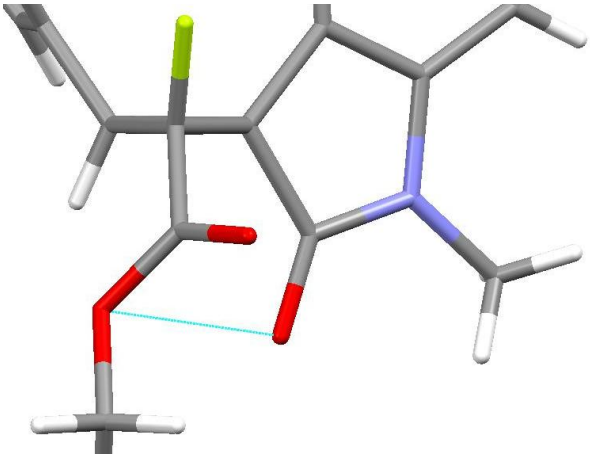

Figure 203 – *The molecular structure of RAWJOQ.*

Other examples of intermolecular interactions observed in these systems are given in the appendix (section A1.3.3.)

6.3.2.3. α-Fluorodicarbonyls on a Ring System

A further 14 entries are fluoroesters adjoining ring systems that feature either a cyclic fluoroamide or fluoroketone. We've also included here one of our own previously unpublished structures for discussion (16srv117, the 7-membered α-fluorolactam **251** described in Chapter 4) though the overall reported statistics of the CSD search only include entries published in the CSD. These compounds are classified as cyclic fluorodicarbonyls in which the fluoroester moiety is acyclic. Two of these entries had more than one independent molecule in their crystal structures and so the total number of fluoroester moieties is increased to 16 (***Table 35***). An additional example is given in appendix section A1.3.4.

MUQQOG is an example that features a *syn* acyclic fluoroester F-C-C=O bond torsion angle (-3^{o}) and a *gauche* cyclic fluorolactam F-C-C=O torsion angle (-71^{o}) (***Figure 204***).

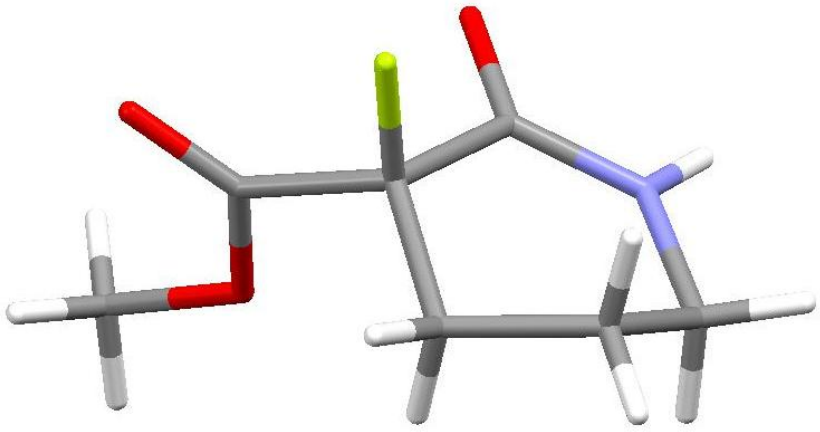

Figure 204 *– The molecular structure of MUQQOG.*

Table 35 – *The CSD Refcodes and Durham code for the 16 dicarbonyl structures in which the fluoroester moiety is attached to a heterocyclic ring system.*

CSD Refcode	Torsion angle 1 /°	Torsion angle 2 /°
16srv117	147	125
BIZMAY	158	-27 (A)
DOZWEV	-169	39 (K)
HIJXEE	14	47 (K)
MUQBIL	26	27 (A)
MUQQAS (A)	-7	70 (A)
MUQQAS (B)	9	63 (A)
MUQQEW (A)	7	-70 (A)
MUQQEW (B)	-9	-64 (A)
MUQQOG	-3	-71 (A)
MUQRAT	6	48 (A)
ODOPAZ	11	45 (K)
PULJIR	175	77 (A)
SELMIH	18	88 (K)
SEQPIN	153	-169 (K, macrocyclic)
SUHBUT	170	-36 (K)
YEBSIJ	-178	-166 (K, macrocyclic)

59% of the esters are *syn*, 6% are *eclipsed* and 35% are *anti*. PULJIR exhibits intermolecular hydrogen bonding interactions between the fluoroester carbonyl oxygen atoms and amide hydrogen atoms. These interactions may lead to an increased *anti* fluoroester conformational preference in this structure (***Figure 205***).

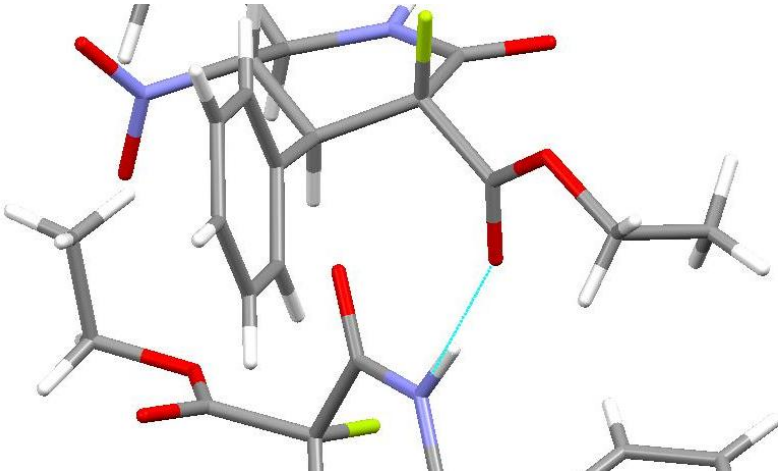

Figure 205 – *The molecular structure of PULJIR.*

Of the secondary torsion angles, 71% are *gauche*, as would be expected for a cyclic system. One entry (6%) is *eclipsed* and two examples (12%) are assigned as *syn* (but only 4^{o} from the *gauche* range) and appear to have interesting ring puckering conformations that could account for the lower torsion angles, as was seen with the lactone derivatives. MUQBIL is an example (***Figure 206***). Two of the entries (12%) have *anti* secondary, cyclic fluorocarbonyl moieties. Both of these examples are macrocyclic and so the conformational restraints are significantly lower than had the ring system been smaller. YEBSIJ is an example of a 14-membered macrocyclic ring system (***Figure 207***).

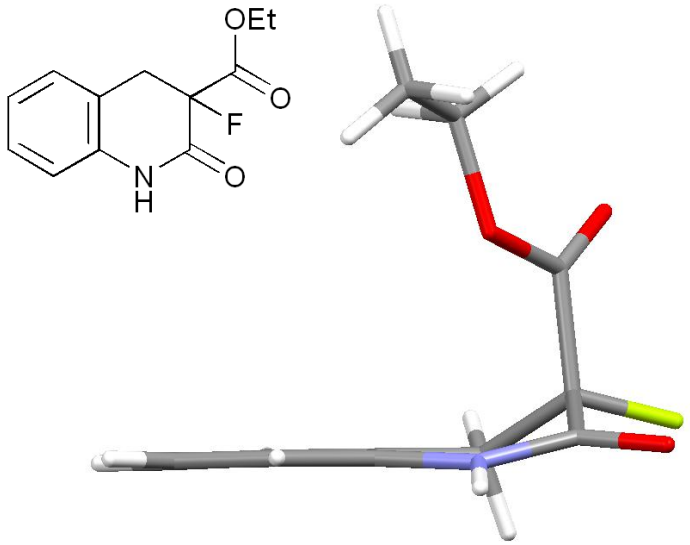

Figure 206 – *The molecular structure of MUQBIL.*

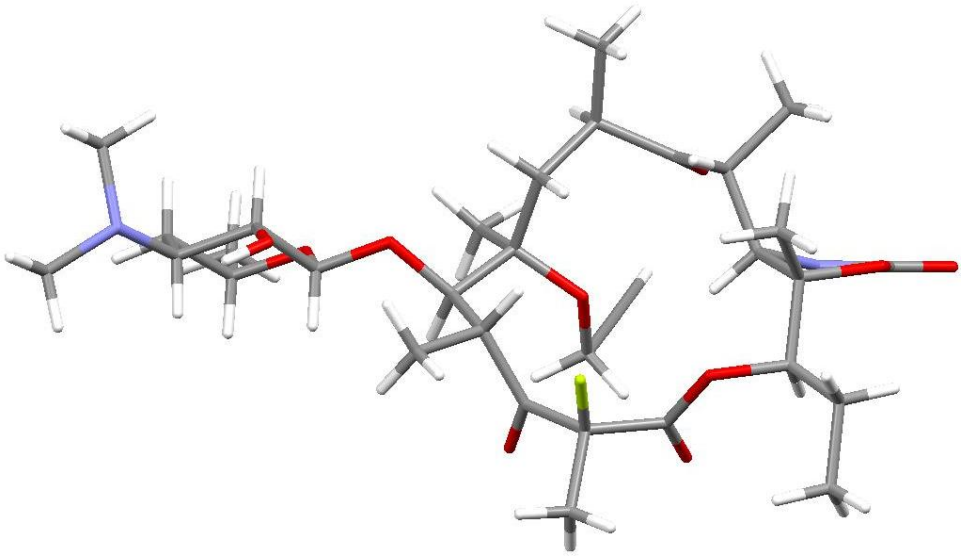

Figure 207 – *The molecular structure of YEBSIJ.*

The reason why the ester torsion angle of 7-membered fluorolactam 16srv117 is *eclipsed* (and only 4^{o} away from *anti* classification) is less clear but interactions are observed between the amide bonded dimers and the ester ether oxygen atoms that may result in the unusual *eclipsed* torsion angle. 16srv117 also has an unusual *eclipsed* fluoroamide torsion angle which is likely because the slightly larger 7-membered ring allows for more flexibility and rotation of bonds than the analogous 6-membered systems. The 7-membered ring system exhibits interesting ring puckering (***Figure 208***).

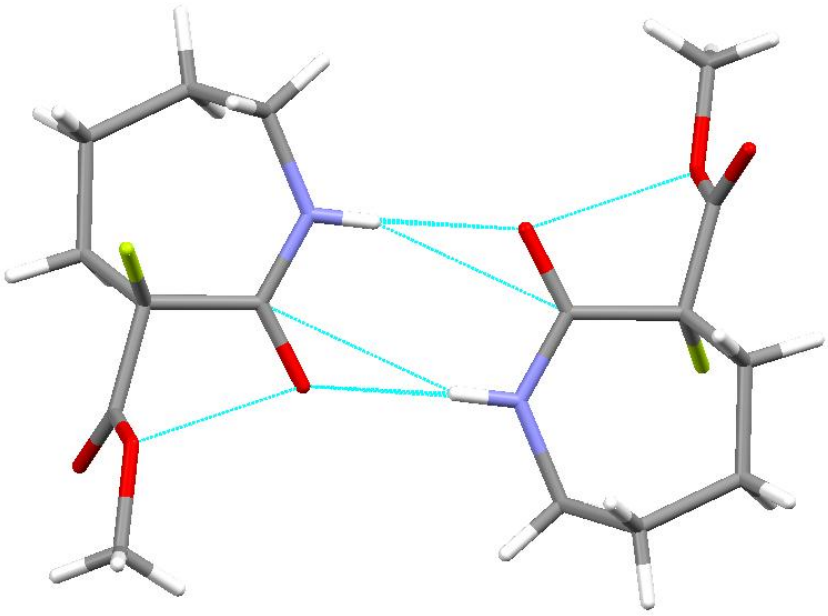

Figure 208 – *The crystal structure of 7-membered lactam 16srv117 exhibits dimeric amide hydrogen bonding.*

6.3.2.4. Axial/Equatorial Fluorine Conformations

As part of our initial investigation into the structural preferences of our α-fluorocarbonyl systems our fluorolactams were also investigated to determine whether the fluorine atoms are equatorial or axial. In our previous work[54] it was noted that the fluorine atom in MUQBIL is in the equatorial position and the ester group axial. This is perhaps unexpected because it is common for the large, bulky ester group to go in the equatorial position to minimise steric hindrance.

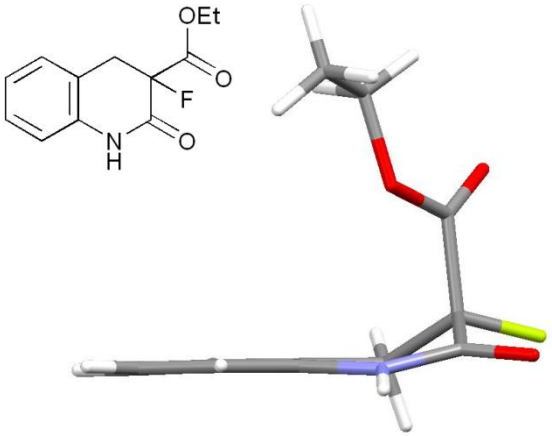

***Figure 209** – The molecular structure of MUQBIL.*

Our reasoning was that the majority of the molecule was flat and sp^2 hybridised and so had no axial protons (in red in ***Figure 210***) to encounter steric hindrance with an axial ester group. Additionally, if the ester group was equatorial it may encounter steric hindrance with the adjacent amide carbonyl group.

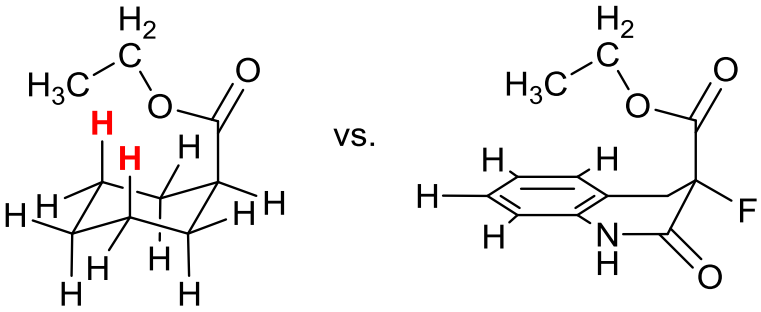

***Figure 210** – The comparison of fluorolactam MUQBIL with a cyclohexyl analogue.*

However, subsequent work by the Durham group[176] yielded the decarboxylated heterocycle and an equatorial fluorine atom was still observed (***Figure 211***).

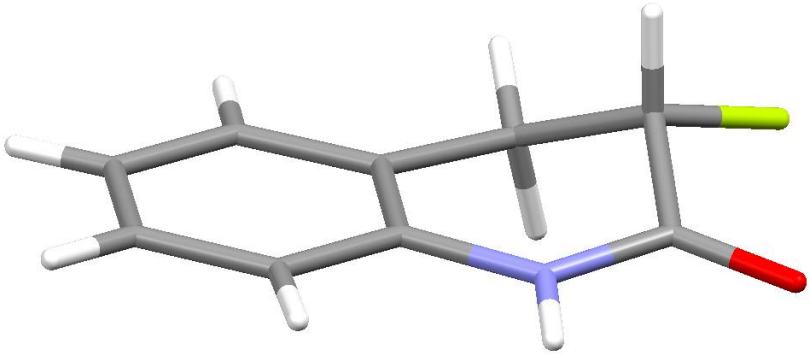

***Figure 211** – 15srv090, the decarboxylated analogue of MUQBIL, still exhibits an equatorial fluorine atom.*

Given that fluorine is a very small atom it usually has a preference for the axial position if only because whatever is in the equatorial position is usually larger than fluorine and so has a stronger equatorial preference. However, when the other substituent is only a proton (as in the case of 15srv090) there can't be much of a steric preference either way.

Removing the benzyl ring of MUQBIL gives the structure of the analogous 6-membered fluorolactam **248** (MUQQOG). Analysis of this structure reveals an axial fluorine atom, in contrast with MUQBIL. Although the two structures are very similar, the lack of adjacent benzyl ring means that the heterocycle exhibits more 'cyclohexane character' and so appears to behave more as a cyclohexyl derivative would be expected to behave (***Figure 212***).

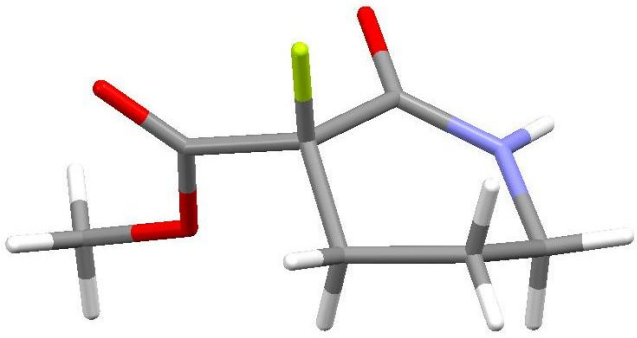

***Figure 212** – The molecular structure of MUQQOG (fluorolactam **248**).*

This might suggest that the aromatic ring attached to MUQBIL affects the equatorial preference of the fluorine atom, since aside from the ethyl ester (rather than methyl) the only difference between the two molecules is the aromatic ring attached.

The 5-membered analogue **250** is less trivial since the ring is smaller and has a relatively high sp^2 character (***Figure 213***). Measuring various torsion angles round the ring and the fact that the adjacent CH_2 carbon puckers downwards, it appears that the 5-membered analogue is more equatorial than axial. However, the dihedral angles between the amide carbonyl oxygen and the fluorine and ester groups (i.e. O=C-C-F and O=C-C-C) are both approximately 45^o and so the axial/equatorial preference of fluorine in this system is perhaps minimal, if not entirely invalid.

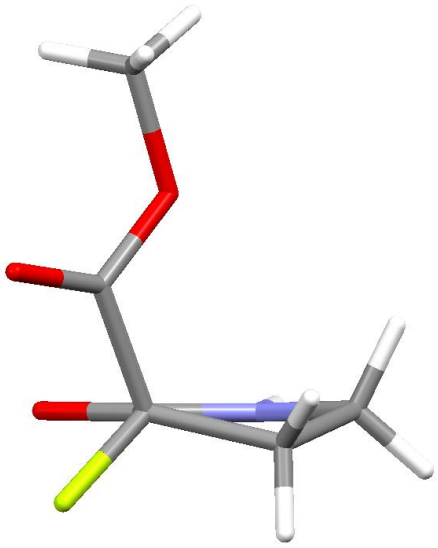

Figure 213 – *The molecular structure of 5-membered heterocycle* ***250*** *(MUQRAT).*

The 7-membered ring analogue 16srv117 exhibits a stronger axial fluorine atom with the bulkier ester group in the equatorial position away from the ring (***Figure 214***). This is consistent with the 6-membered system.

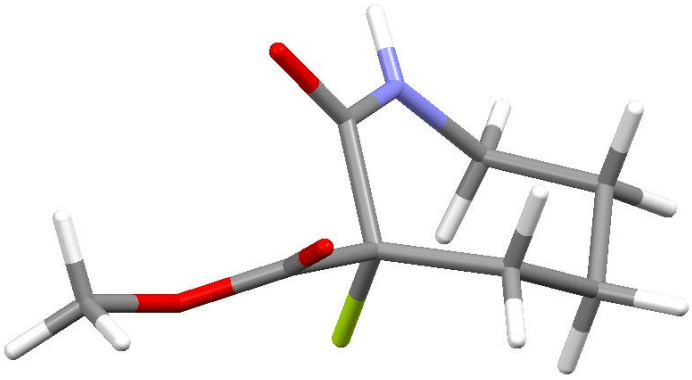

Figure 214 – *The crystal structure of 7-membered lactam* ***251*** *(16srv117) exhibits an axial fluorine atom.*

It is also possible that no distinct preference exists for these systems and that with so few data points it is unreasonable to draw conclusions regarding a preference.

6.3.2.5. Acyclic α-Fluorodicarbonyl Systems

Five entries (***Table 36***) are acyclic dicarbonyl systems in which only one of the carbonyl oxygens is part of a fluoroester moiety. Four of the structures are published and available in the CSD. 15srv201 is one of our previously unpublished crystal structures that have been included in this study, the structure of which is shown in ***Figure 215***.

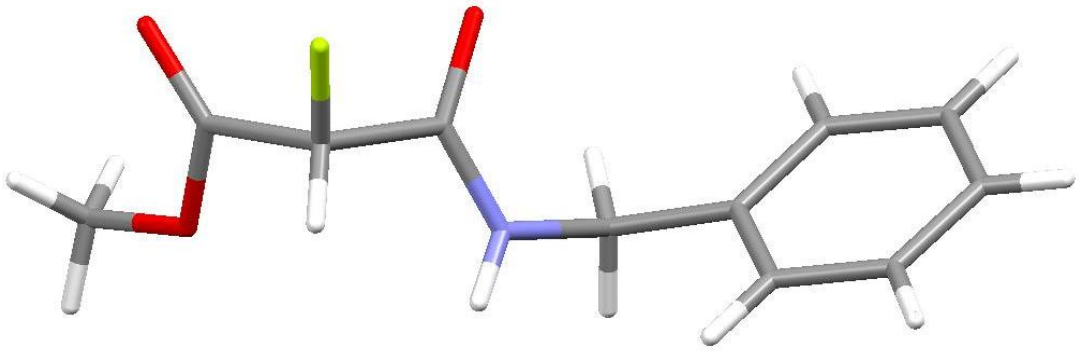

Figure 215 *– The molecular structure of 15srv201 showing a fluoroamide moiety in addition to the fluoroester group.*

Table 36 *– The CSD Refcodes and Durham code for the five acyclic dicarbonyl structures.*

CSD Refcode	Torsion angle 1 /°	Torsion angle 2 /°
15srv201	17	-42 (A)
MABBEY	-10	-21 (K)
MUNZEC	156	180 (K)
SICRIG	-144	178 (K)
VAJYUB	9	-15 (K)

Three of the fluoroester torsion angles are *syn*¸ one (SICRIG) is *eclipsed* and one (MUNZEC) is *anti*. SICRIG exhibits few interactions involving the fluoroester moiety but stacking of adjacent –SO_2- moieties and phenyl rings leads to the fluoroester groups on the exterior of the crystal (***Figure 216***). Whether this packing arrangement directly contributes to the *eclipsed* conformation of the F-C-C=O moiety is not immediately obvious. Interactions between the two carbonyl moieties may also affect the conformation of the F-C-C=O bonds.

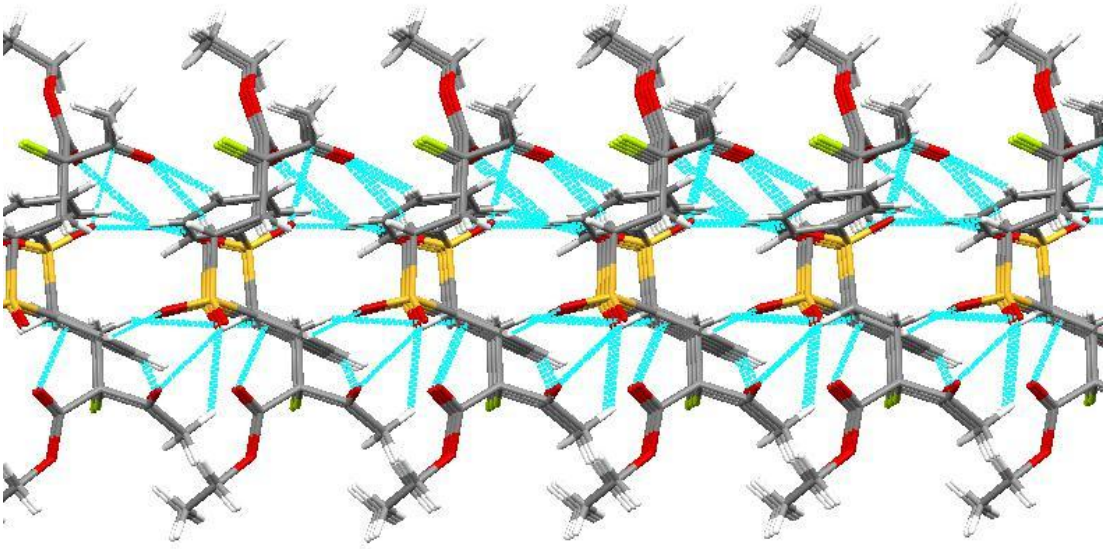

Figure 216 – *The molecular structure of SICRIG.*

In addition to stacking of the phenyl ring systems and nitro groups, MUNZEC exhibits two intermolecular interactions between the ester alkyl moiety and the oxygen atoms of a nitro group. The carbonyl oxygen atom also exhibits intermolecular interactions (***Figure 217***).

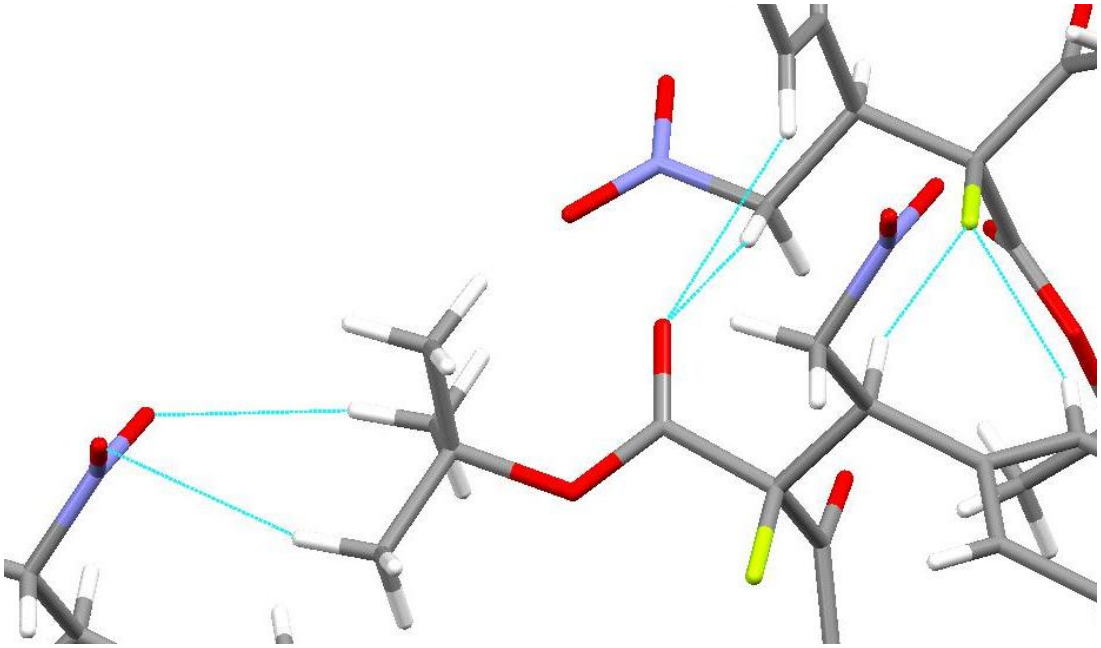

Figure 217 – *The molecular structure of MUNZEC.*

Of the fluoroketone moieties, half are *syn* and half are *anti*. The remaining entry (15srv201) has a *gauche* fluoroamide torsion angle. Given that *gauche* torsion angles are rare outside of cyclic systems, it is possible that intermolecular amide hydrogen bonding is responsible for an increased torsion angle. ***Figure 218*** shows an intermolecular hydrogen bonding interaction between two of the fluoroamide moieties. It seems plausible that the top F-C-C=O bond is rotated to maximise this favourable interaction, leading to an increased torsion angle.

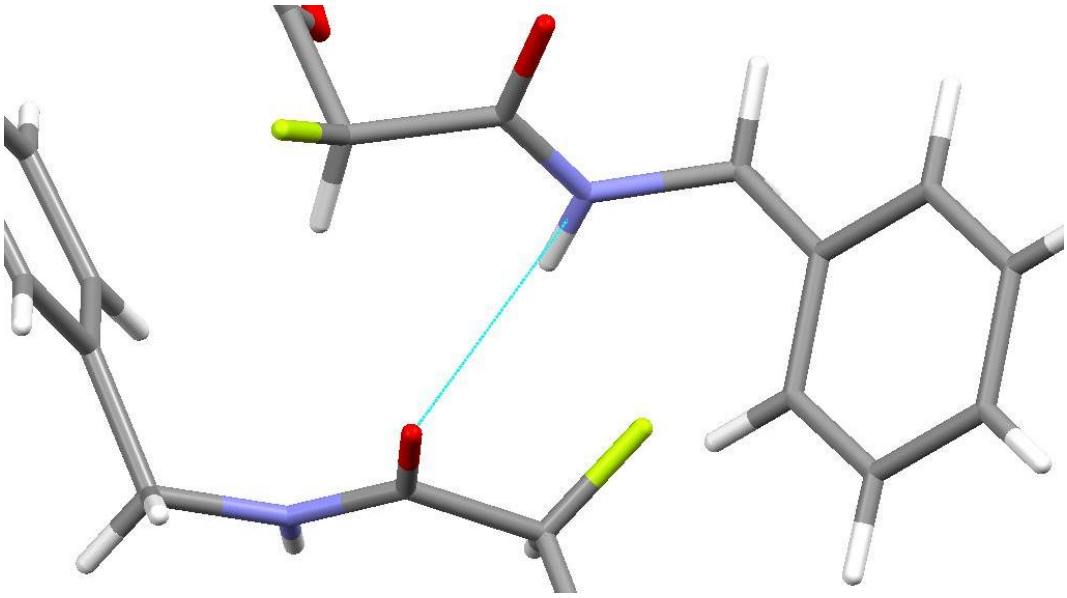

Figure 218 – *The molecular structure of 15srv201 showing a hydrogen bonding interaction between fluoroamide moieties that may lead to an increased F-C-C=O torsion angle.*

6.3.2.6. α-Fluorotricarbonyl System

There is only one example of a tricarbonyl system (***Figure 219***) in which the fluorine atom is adjacent to one ester and two ketone moieties. The fluoroester F-C-C=O torsion angle is *syn* and both the fluoroketone moieties have *eclipsed* F-C-C=O bond torsion angles. With two adjacent benzoyl derivatives it is likely that steric hindrance has a key role in determining the three F-C-C=O torsion angles.

Table 37 *– The CSD Refcode for the fluorotricarbonyl structure.*

CSD Refcode	Torsion angle 1 /°	Torsion angles 2 /°
TEFVEF10	19	-126 (K), -134 (K)

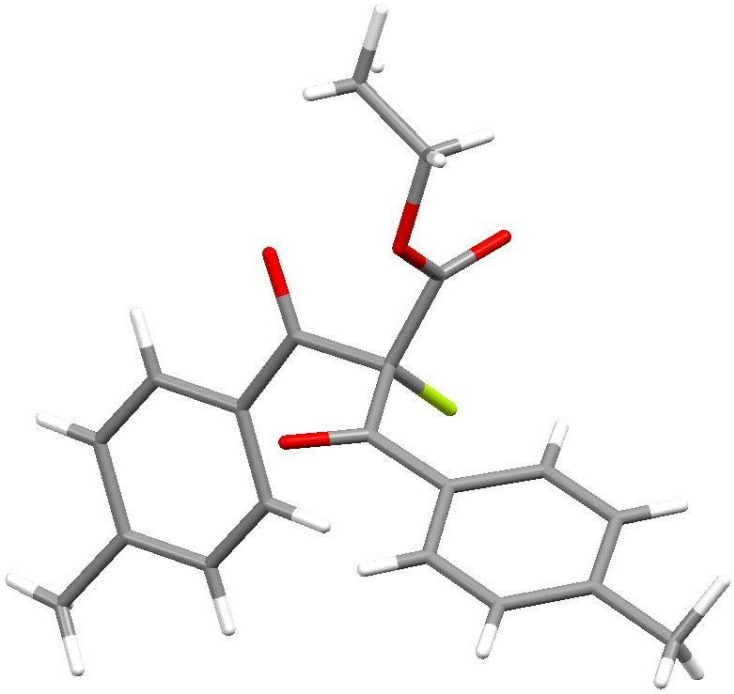

Figure 219 *– The molecular structure of TEFVEF10.*

6.3.3. α-Fluorodiesters

Following our CSD, DFT, NMR and X-ray analysis of α-fluorinated monoesters we turned to analysis of α-fluorodiesters. These systems are of particular interest to our research group as several examples of fluoromalonate derivatives have been synthesised and crystallised in this thesis and in previous work. Examples of these structures and their notable interactions are given in appendix section A1.3.12.

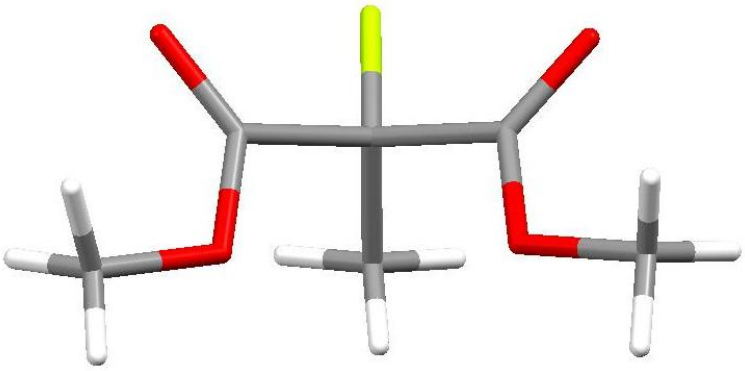

***Figure 220** – The molecular structure of 15srv211.*

6.3.3.1. Solid-State Conformational Studies of α-Fluorodiesters

Nine entries in the CSD are α-fluorodiesters and have been analysed alongside three of our previously unpublished structures. MUQBEH contained two independent molecules in the crystal structure. While identical in configuration, these two molecules differ in conformation and have both been included in this study. In this case, the two molecules have very similar torsion angles. Overall, 13 entries are analysed here and their structures are given in ***Figure 221*** and their dihedral angles are given in ***Table 38***. 15srv211, 15srv034, 15srv036, MUQQUM and MUQQIA have all been discussed in this thesis. Four of the remaining structures were obtained at Durham in previous research projects.[54,55,112]

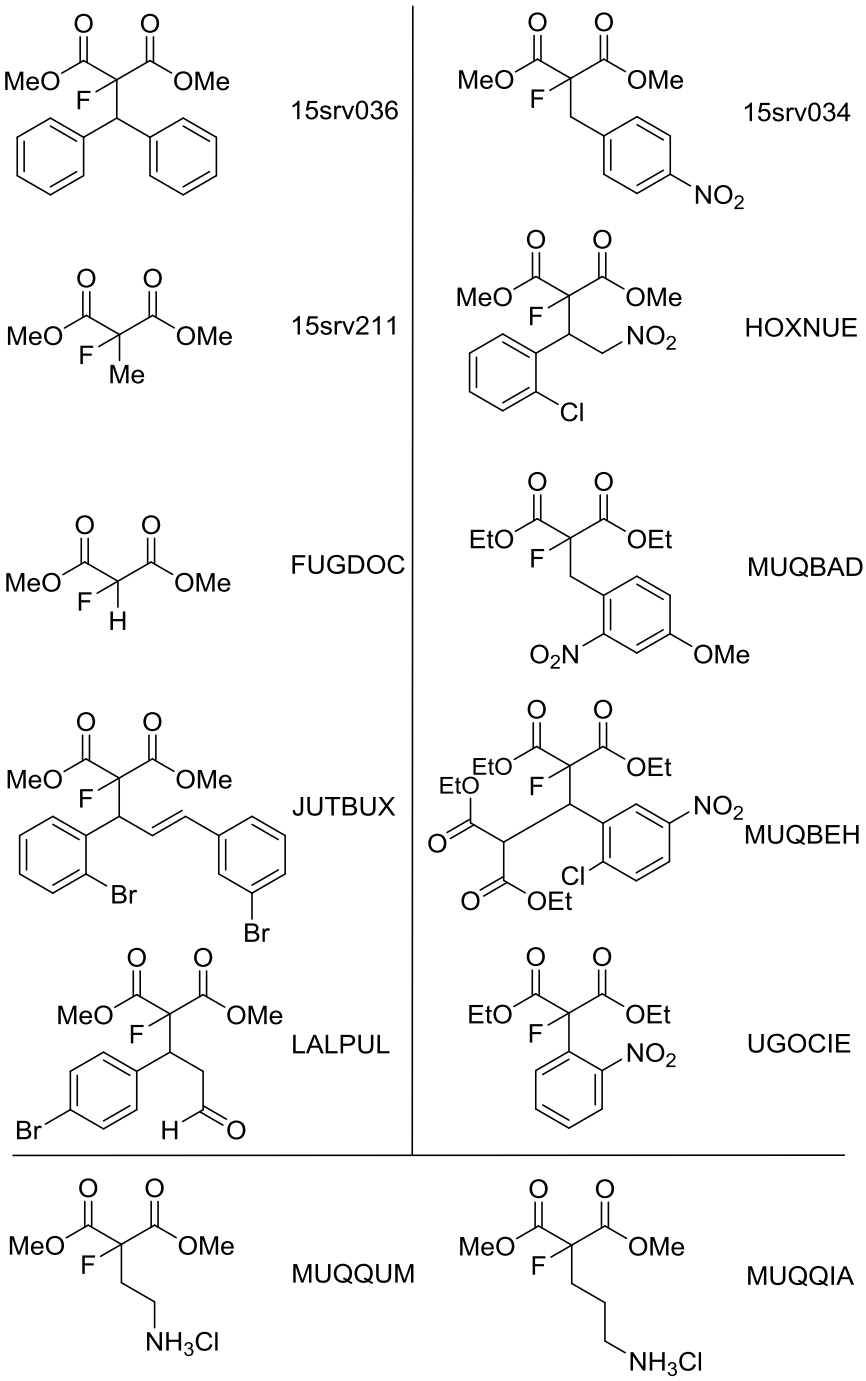

Figure 221 *– The structures of the fluoromalonate categorised by non-nitrogen containing (left), nitro compounds (right) and amine hydrochloride salts (bottom).*

Table 38 *– The CSD Refcodes and Durham Codes for the 13 fluorodiester structures arranged by structure.*

Moiety	CSD Refcode	Torsion angle 1 /°	Torsion angle 2 /°	Conformations
-	15srv036	4	17	*Syn,syn*
-	15srv211	-1	-6	*Syn,syn*
-	FUGDOC	-1	6	*Syn,syn*
-	JUTBUX	3	5	*Syn,syn*
-	LALPUL	-14	-7	*Syn,syn*
Nitro	15srv034	-10	130	*Syn,eclipsed*
Nitro	HOXNUE	4	-141	*Syn,eclipsed*
Nitro	MUQBAD	-12	139	*Syn,eclipsed*
Nitro	MUQBEH (A)	-25	136	*Syn,eclipsed*
Nitro	MUQBEH (B)	-27	137	*Syn,eclipsed*
Nitro	UGOCIE	-29	-33	*Syn,gauche*
Amine salt	MUQQIA	31	-176	*Gauche, anti*
Amine salt	MUQQUM	-7	-14	*Syn,syn*

All but one (92%) of the structures contained at least one *syn* F-C-C=O torsion angle, and the remaining structure has a torsion angle of 31°, only 1° away from the *syn* classification. Of the secondary torsion angles, six (46%) are *syn*, one (8%) is *gauche*, five (38%) are *eclipsed* and one (8%) is *anti*. It is also interesting to note that the only *gauche* torsion angle in this category is only 3° away from *syn* classification. Of all 26 fluoroester moieties, 69% are *syn*, 8% are *gauche*, 19% are *eclipsed* and 4% are *anti*.

As a general overview, six *syn,syn* structures (plus UGOCIE with *syn,gauche* conformation), five *syn,eclipsed* structures and one *syn,anti* structure are observed. All of the structures containing *eclipsed* F-C-C=O torsion angles contain nitro groups. The two *gauche* torsion angles belong to structures containing either a nitro group or an amine salt. The one *anti* torsion angle belongs to a structure containing an amine salt moiety. As such, ***Figure 221*** and ***Table 38*** show the division of entries according to structure, based on whether a nitrogen moiety is present.

The five structures that contained no nitrogen moieties exhibited all *syn* F-C-C=O torsion angles. Of the six nitro group containing structures, five were *syn,eclipsed* and one was *syn,gauche* (with a very low *gauche* angle). The three unusually large *syn* torsion angles (-25°, -27° and -29°) are also in this category.

The nitro groups exhibit stacking interactions within the crystal structures and often exhibit intermolecular or intramolecular interactions with the fluoroester moieties that could account for their unusual *gauche* conformations. For example, MUQBAD exhibits intermolecular interactions between the nitro group and the alkyl moiety of the *eclipsed* fluoroester group (***Figure 222***).

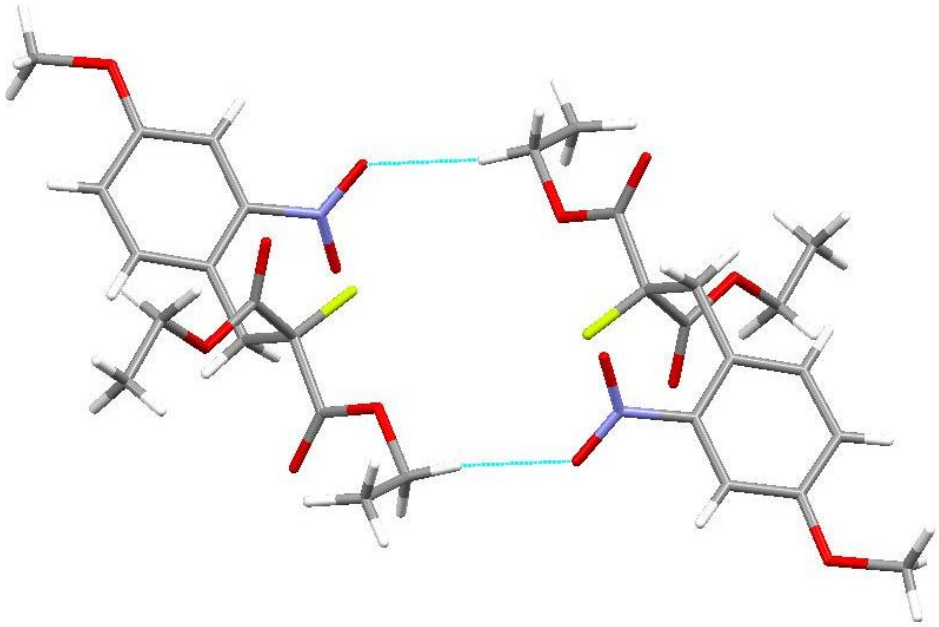

Figure 222 – *The molecular structure of MUQBAD.*

Of the amine salt containing entries prepared in Chapter 3, it is interesting to observe that MUQQIA (the only *anti* fluoroester) is a close analogue of MUQQUM, which has *syn,syn* conformations (***Figure 223***, ***Figure 224***).

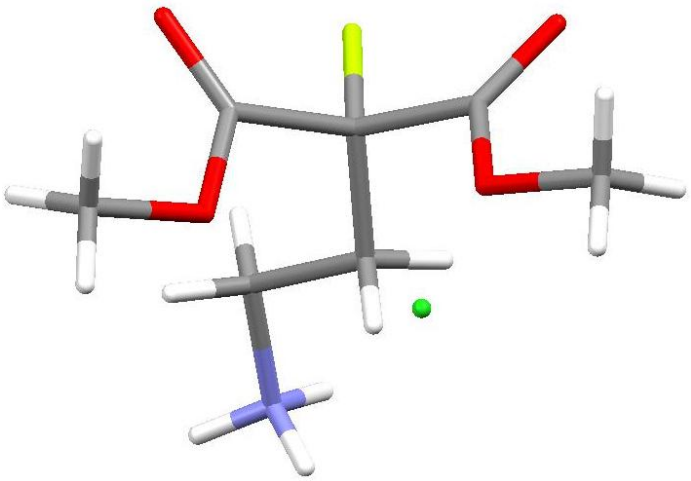

Figure 223 *– The molecular structures of MUQQUM, as determined by X-ray crystallography (syn,syn).*

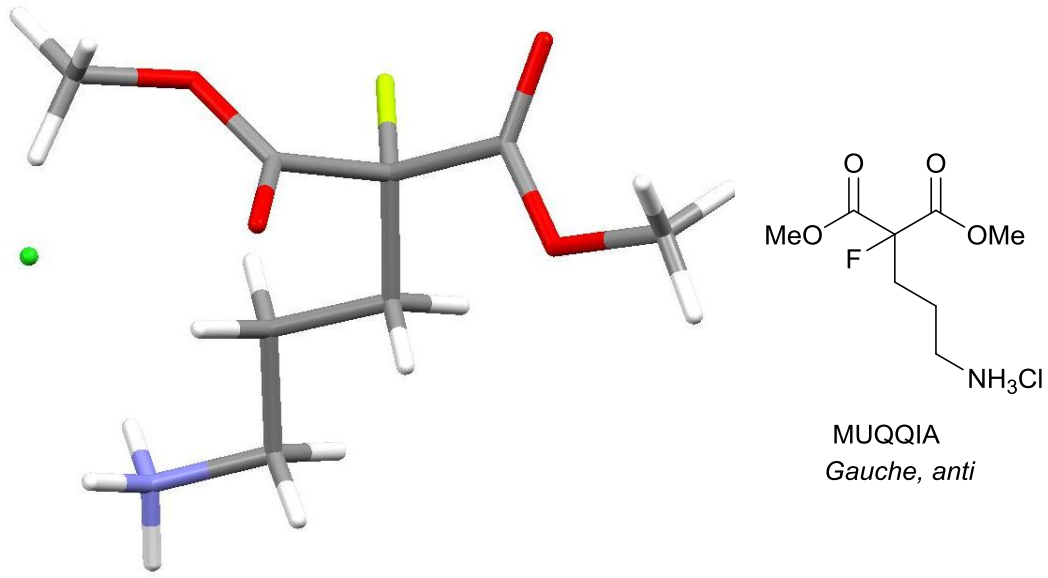

Figure 224 *– The molecular structures of MUQQIA, as determined by X-ray crystallography (gauche,anti).*

6.3.3.2. Solution-State Conformational Studies of α-Fluorodiesters

In a similar fashion to the computational/NMR studies reported on the fluoroesters, the following section discusses some of our new investigations into solution-state conformations of fluorodiesters. The NMR data for dimethyl fluoromalonate was measured by Anne Lückener (Erasmus student in Durham).

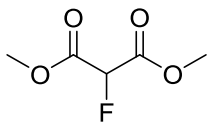

73
FUGDOC

Figure 225 *– The structure of dimethyl fluoromalonate.*

Rotational energy profile calculations (B3LYP 6-31G(d)) were carried out on dimethyl fluoromalonate using water as a solvent model and found that there is a small energy preference for *syn,syn* relative to *syn,anti* and *anti,anti*. The rotational energy barriers are not particularly high (***Table 39***).

Table 39 *– Computed relative energy values of three dimethyl fluoromalonate conformations.*

Conformation		Relative Energy /kcal mol^{-1}	Rotational Energy Barrier /kcal mol^{-1}
Syn,syn	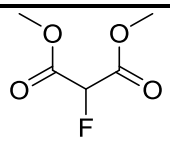	0.0	2.1 (to *syn,anti*)
Syn,anti	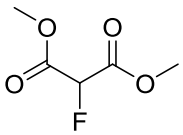	0.4	2.3(to *anti,anti*)
Anti,anti	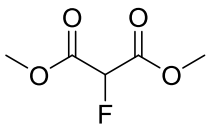	1.0	2.6 (to *syn,syn*)

A rotational energy profile for the 2-methyl substituted fluoromalonate derivative was also calculated (B3LYP 6-31G(d)) using methanol as a solvent model (***Figure 226***, ***Table 40***). All the fluorodiester crystal structures in the CSD (except dimethyl fluoromalonate) are substituted in the 2-position and so this computational model may provide more relevant data. A 2-methyl group leads to *syn,eclipsed* being the lowest energy minimum, presumably due to steric interactions with the substituent whilst *syn,syn* is the next lowest energy minimum. *Anti,eclipsed* is not a minimum due to steric hindrance and is a peak of relative energy 0.7 kcal mol^{-1}flanked by two approximately *anti,eclipsed* conformer energy troughs of relative energy 0.5 kcal mol^{-1}.

Energy differences of conformational preferences for both dimethyl 2-fluoromalonate and dimethyl 2-fluoro-2-methylmalonate the substituted derivative are very low ≥ 1.0 kcal mol^{-1}.

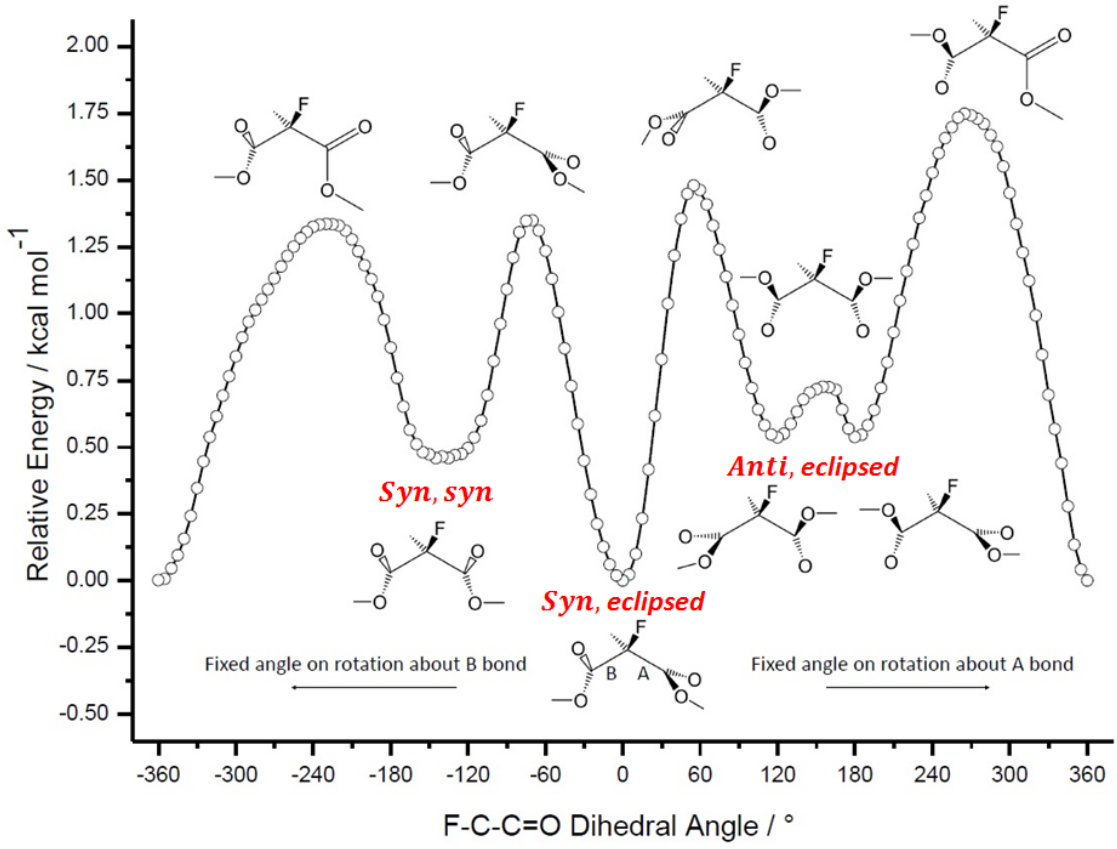

Figure 226 – *The rotational energy profile calculated for dimethyl fluoromalonate.*

Table 40 *– Computed relative energy values of three dimethyl fluoromethylmalonate conformations.*

Conformation	Relative Energy /kcal mol^{-1}	Rotational Energy Barrier /kcal mol^{-1}
Syn,eclipsed	0.0	1.3
Syn,syn	0.4	1.3
Syn,eclipsed	0.0	1.5
Approx. *anti,eclipsed*	0.5	0.7
Approx. *anti,eclipsed*	0.5	1.7
Syn,eclipsed	0.0	-

As with the simplest fluoroesters, experimental NMR and computationally predicted (GIAO-NMR B3LYP/6-31+G**//MP2/6-31G*) NMR data were obtained in a range of solvents and compared for dimethyl fluoromalonate. The calculated $^{1}J_{CF}$ coupling constants are 199 (*syn*) and 225 (*anti*) Hz for the 'gas-phase' and 188 (*syn*) and 228 (*anti*) Hz when DMSO is used in a solvation model (***Table 41***).

Table 41 *– Comparison of our computed NMR data with experimental data for dimethyl fluoromalonate.*

Solvent	Conformation	Coupling Constants /Hz			Chemical Shifts /ppm		
		$^{1}J_{CF}$	$^{2}J_{CF}$	$^{2}J_{HF}$	δ(CF)	δ(CO)	δ(Me)
Gas	*Anti*	224.8	18.1	51.9	87.8	164.3	52.4
Gas	*Syn*	199.1	24.8	51.1	85.1	163.2	52.1
CCl_4	*Anti*	223.3	17.8	51.3	88.0	164.7	53.2
CCl_4	*Syn*	198.4	24.8	50.6	85.3	162.9	52.3
CCl_4	Experimental	197.6	24.1	48.0	84.9	163.7	52.7
$CHCl_3$	*Anti*	228.9	18.0	48.4	88.4	164.4	53.8
$CHCl_3$	*Syn*	191.5	24.5	50.1	86.1	164.0	53.3
$CHCl_3$	Experimental	196.6	24.1	48.0	85.2	164.4	53.4
CH_2Cl_2	*Anti*	228.2	17.8	48.3	88.5	164.5	54.1
CH_2Cl_2	*Syn*	190.0	24.4	50.1	86.3	164.3	53.6
CH_2Cl_2	Experimental	194.9	24.2	47.9	85.2	164.2	53.2
Acetone	*Anti*	227.7	17.7	48.2	88.5	164.6	54.2
Acetone	*Syn*	188.9	24.3	50.1	86.5	164.5	53.8
Acetone	Experimental	192.1	24.2	47.3	86.2	165.3	53.5
MeCN	*Anti*	227.5	17.7	48.2	88.5	164.7	54.3
MeCN	*Syn*	188.5	24.3	50.1	86.5	164.5	53.8
MeCN	Experimental	191.9	24.2	47.4	86.4	165.5	54.0

DMSO	*Anti*	227.5	17.7	48.2	88.6	164.7	54.3
DMSO	*Syn*	188.4	24.3	50.1	86.5	164.5	53.9
DMSO	Experimental	190.7	24.2	46.4	85.1	164.4	53.1
H_2O	*Anti*	227.4	17.6	48.2	88.6	164.7	54.3
H_2O	*Syn*	188.3	24.3	50.1	86.6	164.6	53.9

Dimethyl difluoromalonate was also investigated to confirm that conformational changes were not instead due to inherent solvent effects, as previously discussed (***Table 42***).

The coupling constants and chemical shifts of dimethyl difluoromalonate do not change drastically with increasing solvent polarity. Since this structure is considerably more complex than methyl trifluoroacetate and more distinct conformations are possible with the two ester moieties and the two fluorine atoms it may be expected that some level of conformational change would be observed in addition to inherent solvent effects for this system. However, the changes in coupling constants and shifts are insignificantly small as to suggest that the changes in NMR data for the monofluoro system are primarily due to conformational changes and so are valid.

Table 42 *– Experimentally determined NMR data for dimethyl difluoromalonate in solvents of increasing polarity.*

Solvent	**Coupling Constants /Hz**		**Chemical Shifts /ppm**		
	$^1J_{CF}$	$^2J_{CF}$	**δ(CF)**	**δ(CO)**	**δ(Me)**
CCl_4	261.0	31.1	106.51	161.13	54.07
CH_2Cl_2	260.2	31.0	107.06	161.89	55.04
MeCN	259.1	30.8	107.34	161.96	55.26
DMSO	259.6	30.8	106.63	161.39	55.17

For ease of interpretation the $^1J_{CF}$ coupling constant data for dimethyl fluoromalonate is presented again in ***Table 43***. $^1J_{CF}$ data shows a general trend of decreasing coupling constant with increasing solvent polarity. NMR shows a 6.9 Hz decrease from CCl_4 to DMSO and suggests a shift towards a *syn* conformational preference in more polar solvents, consistent with α-fluoroester derivatives discussed previously.

Table 43 *– Comparison of computed NMR data with experimental data for dimethyl fluoromalonate $^{1}J_{CF}$ coupling constants.*

Solvent	$^{1}J_{CF}$ Coupling Constant /Hz		
	Computational		**Experimental**
	Anti	***Syn***	**NMR**
CCl_4	223.3	198.4	197.6
$CDCl_3$	228.9	191.5	196.6
CD_2Cl_2	228.2	190.0	194.9
Acetone	227.7	188.9	192.1
MeCN	227.5	188.5	191.9
DMSO	227.5	188.4	190.7

Changes in $^{2}J_{CF}$ coupling constants in dimethyl fluoromalonate are negligible and $^{2}J_{HF}$ coupling constants are small (1.6 Hz difference between experimental coupling constants between carbon tetrachloride and DMSO) (***Table 44*** and ***Table 45***).

Table 44 *– Comparison of computed NMR data with experimental data for dimethyl fluoromalonate $^{2}J_{CF}$ coupling constants.*

Solvent	$^{2}J_{CF}$ Coupling Constant /Hz		
	Computational		**Experimental**
	Anti	***Syn***	**NMR**
CCl_4	17.8	24.8	24.1
$CDCl_3$	18.0	24.5	24.1
CD_2Cl_2	17.8	24.4	24.2
Acetone	17.7	24.3	24.2
MeCN	17.7	24.3	24.2
DMSO	17.7	24.3	24.2

Table 45 *– Comparison of computed NMR data with experimental data for dimethyl fluoromalonate $^2J_{HF}$ coupling constants.*

Solvent	$^2J_{HF}$ Coupling Constant /Hz		
	Computational		Experimental
	Anti	*Syn*	NMR
CCl_4	51.3	50.6	48.0
$CDCl_3$	48.4	50.1	48.0
CD_2Cl_2	48.3	50.1	47.9
Acetone	48.2	50.1	47.3
MeCN	48.2	50.1	47.4
DMSO	48.2	50.1	46.4

The CF, CO and CH_3 ^{13}C NMR chemical shift values do not vary significantly with solvent polarity but do tend to follow the same non-linear trend, perhaps suggesting an inherent solvent polarity effect. The trend increases the shift from CCl_4 to chloroform and then decreases the shift to DCM (or plateaus in the case of the CF moiety). Subsequently the shift increases through acetone to acetonitrile before decreasing again to DMSO.

The coupling constant trends are comparable in magnitude to the fluoromonoesters investigated, with $^1J_{CF}$ coupling constant values changing only slightly more than in the diester analogue (7.6 Hz vs. 5.7 Hz respectively, CCl_4 to MeCN). Likewise, the CF chemical shift values change slightly more in the case of the monoester (***Table 20***, pg. 133) than the diester (2.2 ppm vs. 1.5 ppm respectively, CCl_4 to MeCN) but the CO and CH_3 values change by around the same extent.

The rotational energy profiles for dimethyl fluoromalonate and 2-methyl dimethyl fluoromalonate predict *syn,syn* for the former and *syn,eclipsed* for the latter to be the lowest energy minima. The energy differences are, however, small and so may be easily overridden by other interactions such as crystal packing and intermolecular interactions in the solid state. The crystal structures of both have been determined by X-ray crystallography and both are observed to be *syn,syn*. It is interesting to note that of the fluorodiesters reported in the CSD the two major conformations are also *syn,syn* and *syn,eclipsed*.

6.3.4. Statistical Analysis of α-Fluoroesters

Table 46 displays the distribution of all CSD α-fluoroester structures (including diesters, lactones etc.) into the four torsion angle ranges for comparison, excluding the unpublished structures that were included in the discussion sections.

Table 46 *– The distribution of F-C-C=O torsion angles into the four categories of syn, gauche, eclipsed and anti.*

	Syn	***Gauche***	***Eclipsed***	***Anti***	**Total**
Initial Fluoroesters	29	1	5	11	46
Lactones	1	15	-	-	16
Esters on a ring	8	1	2	4	15
Dicarbonyls on ring	10	-	-	6	16
Dicarbonyls	2	-	1	1	4
Tricarbonyls	1	-	-	-	1
Diesters	13	2	4	1	20
Total	64	19	12	23	118
%	54	16	10	19	100

Table 47 shows the percentage distribution of torsion angles for the acyclic esters with the exclusion of the lactones. The 'Entries' column denotes the total number of F-C-C=O moieties in each category.

Table 47 *– The percentage distribution of torsion angles within the data as a whole, and with the exclusion of cyclic entries.*

	Syn	***Gauche***	***Eclipsed***	***Anti***	**Entries**
All Esters	54	16	10	19	118
Excluding lactones	62	4	12	23	102

This information has been projected onto circles, as before, in ***Figure 227*** for a more direct representation of these data, also taking into account whether the torsion angle is positive or negative. Negative angles are on the left hand side of the diagram.

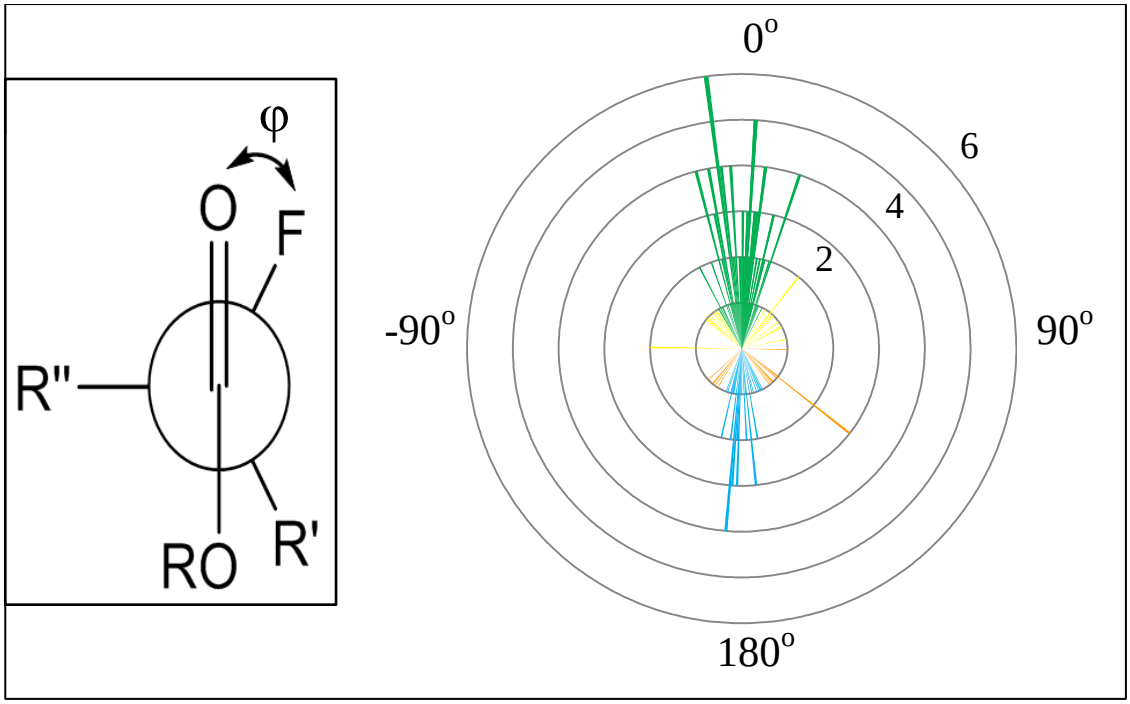

***Figure 227** – The cumulative distribution of torsion angles from all 165 data points. Negative torsion angles are displayed on the left hand side of the diagram.*

As previously discussed, the lactone category consists of primarily *gauche* torsion angles due to the conformational restraints of the ring systems. Excluding this category decreases the overall '*gauche*' percentage from 12% to 3%. It slightly increases the '*syn*' percentage from 58% to 63%, the '*anti*' percentage from 22% to 24%, and the '*eclipsed*' percentage from 9% to 10%. By additionally removing the carboxylic acid structures, 109 acyclic esters remain. Within the acyclic esters category 63% of torsion angles are *syn*, compared to 58% of the total esters. Only 4% are *gauche*, compared to 15% when the lactones are included. The number of *eclipsed* torsion angles increases slightly from 10% to 12%, and the number of *anti* torsion angles increases from 18% to 21%.

In all cases (except lactones) it is clear that *gauche* and *eclipsed* angles are disfavoured. When the lactones category is excluded, 87% of the remaining 149 F-C-C=O moieties are either *syn* or *anti*, i.e. have torsion angles within 30° of being planar or antiplanar. The remaining 13% lie between ±30° and ±150°. Even if the lactones are included, 79% of all the F-C-C=O moieties studied are *syn* or *anti*.

6.3.5. Summary of α-Fluoroesters and Comparison with Literature Studies

Of the 118 F-C-C=O moieties analysed in this study 16 were cyclic lactones and so had strong rotational restraints leading to primarily *gauche* conformations. Of the remaining 102 acyclic structures over three quarters of the structures (77%) are not *anti* in conformation with *syn* conformations being the most common conformation observed in solid state (62%).

A combination of computational, NMR, IR and Raman studies of the simple fluoroester and fluorodiester categories suggest a small *syn* preference in solution. Reported relative energy values for methyl fluoroacetate are[a] 0.90 kcal mol^{-1} (gas phase) *anti* preference to 0.71 kcal mol^{-1} (DMSO-d_6) *syn* preference,[166] and 0.08 kcal mol^{-1} (gas phase) to 0.61 kcal mol^{-1} (water) *syn* preferences (this work).

These preferences, however, are relatively small as are the calculated FC-CO rotation barriers and so other factors may override any inherent F-C-C=O conformational preference in crystal structures and, indeed, a mix of conformations are observed in the CSD. Despite this, the predominant fluorodiester conformations observed in the CSD agree with the calculated rotational energy profiles.

It is important to consider solvent effects on conformational preference as 'gas-phase' models do not accurately simulate physiological conditions and so it is difficult to use this analysis to predict fluoroester conformations in more complex molecules in solution.

[a] The value of 0.96 kcal mol^{-1} (4.0 kJ mol^{-1}) *anti* preference reported by van der Veken *et al.*[165] was proven to be miscalculated and later misquoted as 4.5 kcal mol^{-1} *anti* preference by O'Hagan,[145] with the error then duplicated by Hunter[146] and so these literature values are not valid for comparison in this section.

6.4. α-Fluorocarboxylic Acids

Exclusions to this category and further examples can be found in appendix section A1.3.5.

37 entries in the CSD are monofluorocarboxylic acids. 24 (65%) are *syn*, two (5%) are *eclipsed* and 11 (30%) are *anti*. *Gauche* and *eclipsed* angles are barely observed and it is interesting to note that all but two *syn* angles are within 15° of 0° and all but one *anti* angles are within 15° of 180°.

***Table 48** – The CSD Refcodes for the 37 fluorocarboxylic acid structures.*

CSD Refcode	Torsion angle /°	CSD Refcode	Torsion angle /°
BAGREG	14	QUKHUZ (B)	128
BARBAX	-19	QUKHUZ (C)	-175
DIYJIF	-176	QUKHUZ (D)	-175
DOCVAS	-167	RABBUN (A)	5
ERAHEK	-168	RABBUN (B)	167
FACETC10	0	VATDAX (A)	161
HODBAD (A)	8	VATDAX (B)	165
HODBAD (B)	-178	VEVSIZ (A)	-7
HODBEH (A)	170	VEVSIZ (B)	-11
HODBEH (B)	174	VEVSUL (A)	-6
NAGVUM (A)	3	VEVSUL (B)	-6
NAGVUM (B)	-19	VIGPOQ (A)	-3
OHIJAR03 (A)	13	VIGPOQ (B)	-3
OHIJAR03 (B)	13	VIGQAD (A)	4
OYAHAY (A)	174	VIGQAD (B)	-4
OYAHAY (B)	174	VIGQAD (C)	10
QUKHOT (A)	7	VIGQAD (D)	-10
QUKHOT (B)	7	ZURWAK	2
QUKHUZ (A)	128		

All the carboxylic acid derivatives exhibit strong hydrogen bonding interactions that appear to have a large effect on determining the F-C-C=O bond conformations such as in ***Figure 228*** which shows hydrogen bonding interactions exhibited in FACETC10.

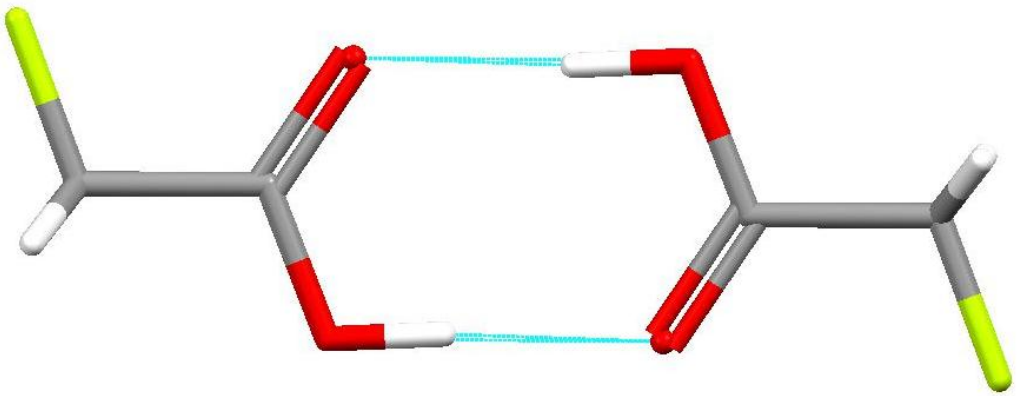

***Figure 228** – The molecular structure of FACETC10 showing intermolecular hydrogen bonding interactions.*

Two entries are diacids, for example FMALON21 (***Figure 229***) and, like the monoacids, the diacids also exhibit strong hydrogen bonding interactions.

***Table 49** – The CSD Refcodes for the two fluorodicarboxylic acid structures.*

CSD Refcode	Torsion angle 1 /°	Torsion angle 2 /°
BAWHAI	18	-
FMALON21	177	177

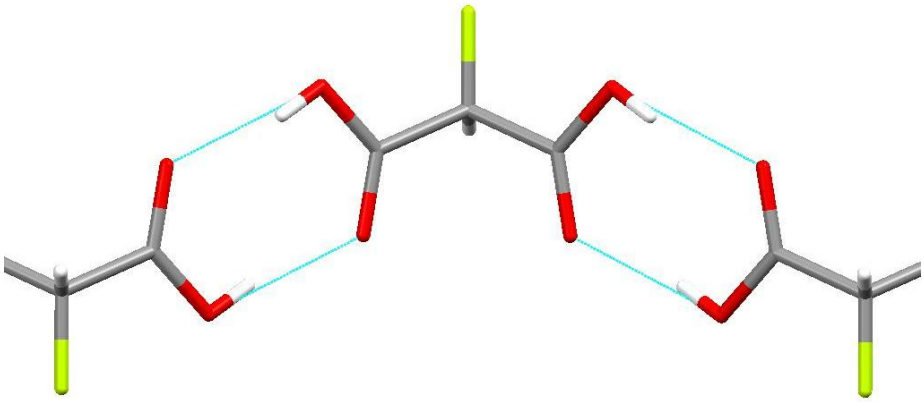

***Figure 229** – The molecular structure of FMALON21 exhibits two anti F-C-C=O bond conformations and hydrogen bonding interactions.*

BAWHAI is a diacid but exhibits disorder in one of the two acid hydrogen atoms. As such, one of the torsion angles is indeterminate and has been omitted.

The 40 α-fluorocarboxylic acid and diacid F-C-C=O moieties are predominantly either *syn* (63%) or *anti* (33%) with one *eclipsed* torsion angle being exhibited in two independent molecules of one structure. These data and the respective torsion angle distributions are exhibited in ***Figure 230*** and ***Figure 231***.

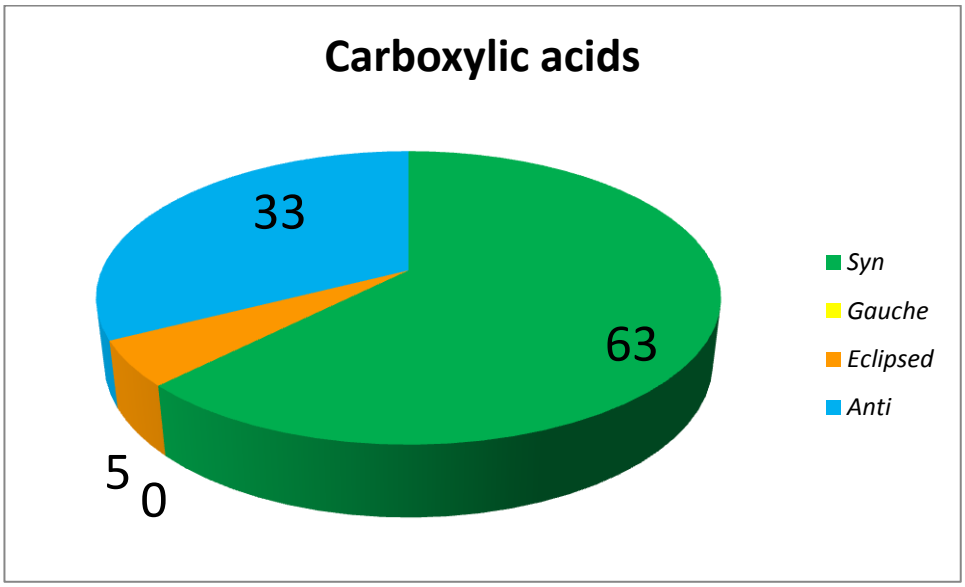

Figure 230 *– A pie chart to illustrate the percentage distribution of the torsion angles from the 40 carboxylic acid F-C-C=O moieties.*

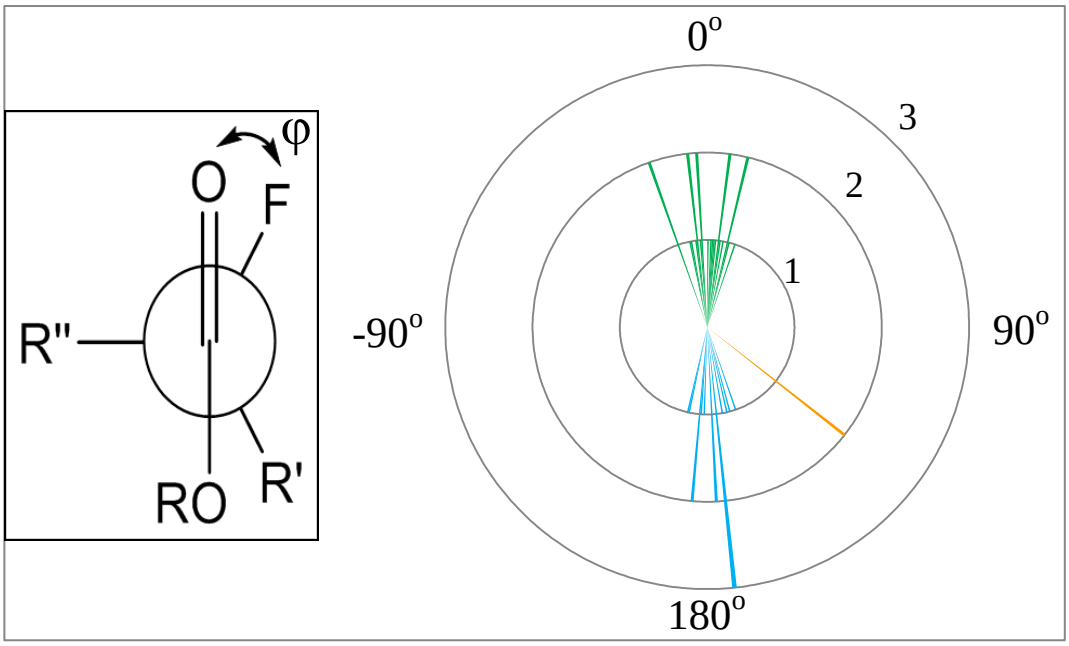

Figure 231 *– The cumulative distribution of torsion angles from the 40 carboxylic acid F-C-C=O moieties.*

In the solid state, therefore, *syn* is the by far the most favoured conformer for the F-C-C=O unit.

6.5. α-Fluoroamides

6.5.1. CSD Search

As with the α-fluoroesters, a CSD search was limited to organic monofluoroamides to exclude the large number of organometallic compounds and trifluoromethyl derivatives giving 149 structures for analysis. The search parameters are displayed in ***Figure 232*** and details of exclusions are given in appendix section A1.3.6.

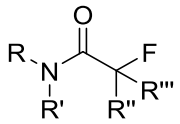

R, R' = Non metal
R'', R''' = Non fluorine

Figure 232 – *The structure entered into the CCDC's ConQuest software and the online WebCSD search functions.*

As discussed above, the literature[145] suggests that the *anti* conformation is the preferred conformation for fluoroamide moieties.

6.5.2. Simplest α-Fluoroamides

This *anti* conformation is confirmed by analysis of the simplest α-fluoroamides (categories derived as with the fluoroesters, discussed further in appendix section A1.3.7., along with additional examples) as shown in ***Table 50***, ***Table 51*** and ***Table 52***.

Table 50 *– The four CSD structure Refcodes for the primary amide derivatives.*

CSD Refcode	Torsion angle /°
CLFLAC	180
FACETA	179
UXOQII	168
UXOQOO	-168

Table 51 *– The 58 CSD structure Refcodes for the secondary amide derivatives.*

CSD Refcode	Torsion angle /°	CSD Refcode	Torsion angle /°
CEXPAW	165	OYEHEG	173
CEXPOK (B)	-173	SEHDAK	175
FALSER	-29	TUWWOX	-177
FOSXOB	175	UXOQAA (A)	-169
GERNAS	-155	UXOQAA (B)	-172
JAXBIU (A)	155	UXOQEE (A)	170
JAXBIU (B)	166	UXOQEE (B)	172
JAXBOA (A)	-169	VAGCEL	-179
JAXBOA (B)	-176	VAGCIP	-179
JAXBOA (C)	-177	VATCUQ	-177
JAXBOA (D)	-178	VEXPIY (A)	-172
JIXHON	-167	VEXPIY (B)	-173
KAVWEJ	-4	VEXPIY (C)	-173
MAWBAP	-177	VEXPIY (D)	-176
MAWCAQ	174	WEFGEV (A)	-178
NELYAF	-172	WEFGEV (B)	180
NERMUT	169	WEFGIZ	4
NEYMEL (A)	-170	WEFGOF	23
NEYMEL (B)	172	WEFGUL (C)	-20
NUNQAQ (A)	-151	WEFGUL (D)	21
NUNQAQ (B)	-155	XEFQIK	177
NUNQAQ (C)	156	XEFQOQ (A)	-172
NUNQAQ (D)	-158	XEFQOQ (B)	180
NUNQAQ (E)	-165	XEFQUW (A)	-175
NUNQAQ (F)	-175	XEFQUW (B)	-175
ONEMEA (A)	169	XEFROR (A)	177
ONEMEA (B)	-176	XEFROR (B)	179
ONEMIE (A)	-171	XUQSOT	-178
ONEMIE (B)	-175	XUQTAG	-177

Table 52 *– The 12 CSD structure Refcodes for the tertiary fluoroamide derivatives.*

CSD Refcode	Torsion angle /°	CSD Refcode	Torsion angle /°
EFIJOS	28	PUQNEU	92
IBIFOP (A)	174	PUQNIY	173
IBIFOP (B)	-178	RAGNUI (A)	164
ISAFAJ (A)	-126	RAGNUI (B)	169
ISAFAJ (B)	131	VASXIX	176
NOKSUB	110	ZOGREU	-29

The primary amide structures exclusively exhibit *anti* torsion angles. It is worth noting that this category is relatively small (four entries) and so care must be taken when drawing conclusions.

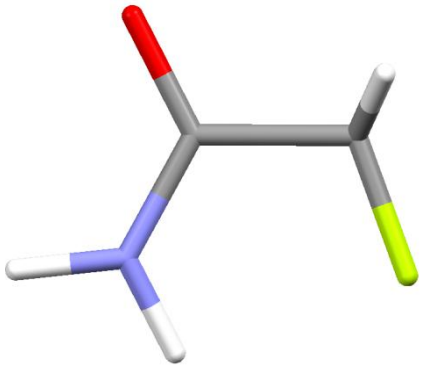

***Figure 233** – FACETA has a F-C-C=O bond torsion angle of 179 ^{o} and is typical of the anti conformations observed in the primary amide category.*

Of the 58 secondary α-fluoroamide structures analysed, 52 (90%) are *anti* and six (10%) are *syn*. Although a strong *anti* preference is observed, it appears to be slightly reduced when compared to the (small number of) primary fluoroamide derivatives. The secondary amide category is the most populated category observed in this study.

Of the 12 tertiary α-fluoroamide structures analysed, six (50%) are *anti*, none are *gauche*, four (33%) are *eclipsed* and two (17%) are *syn*. Again, a slight *anti* preference is observed though it appears to be reduced when compared to the secondary fluoroamide derivatives.

6.5.3. α-Fluorolactams

Ten entries in the CSD are secondary α-fluorolactams. This category contains structures in which cyclic amides (lactams) are secondary amides with respect to the nitrogen atom. They all contain an N-H proton. Some examples of the subsections below are included in appendix section A1.3.8.

Table 53 – *The ten CSD structure Refcodes for the secondary lactam derivatives.*

CSD Refcode	Torsion angle /°	Torsion angle /°
BIZMAY	-27	158 (E)
DOMJUM	74	
MFXHUR	-13	
PULJIR	77	175 (E)
QEKLEX	25	
ULACEQ	-49	
VOXKAU	-22	
XINKEM	-58	
ZOQZIQ	-21	
ZOQZUC	33	

BIZMAY and PULJIR are both fluorodicarbonyl derivatives with adjacent fluoroester moieties.

Five structures in this category are classified as *syn* and five are *gauche*. Due to the conformational restraints of the cyclic ring system there is a larger proportion of *gauche* torsion angles when compared to the acyclic fluoroamide derivatives. This was also observed to be the case with the cyclic lactone derivatives when compared to the acyclic fluoroesters. Four of the five *syn* angles are higher than 20°. MFXHUR has a F-C-C=O torsion angle of 13°, though this is possibly due to puckering of the heterocycle due to the mix of sp^2 and sp^3 atoms on the ring. Similar instances were observed in the ester analogues.

23 entries in the CSD are tertiary α-fluorolactams. This category contains structures in which cyclic amides are tertiary amides with respect to the nitrogen atom. They all contain an N-R substituent.

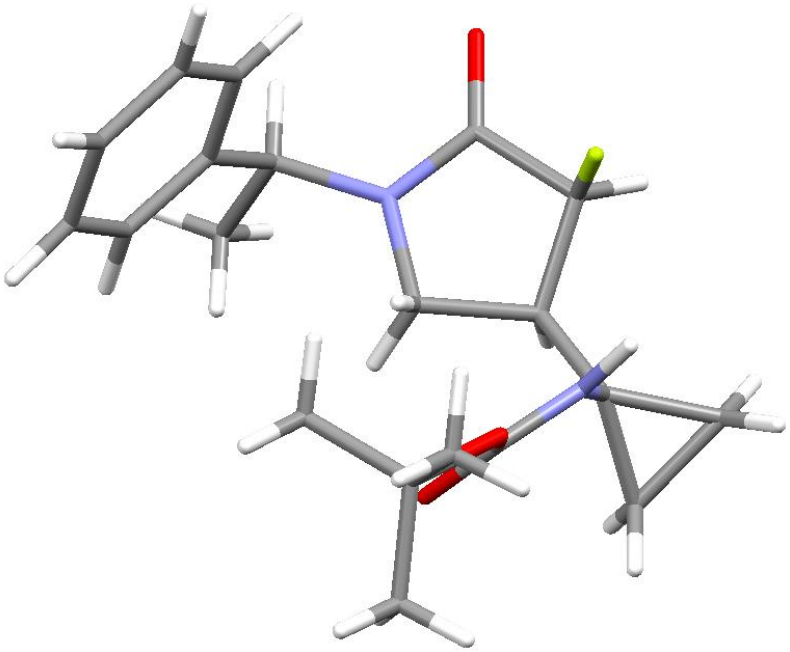

Figure 234 *– BEKBEZ is an example of a tertiary fluorolactam derivative. It has a F-C-C=O bond torsion angle of 80 °.*

Table 54 *– The 23 CSD structure Refcodes for the tertiary lactam derivatives.*

CSD Refcode	Torsion angle /°	CSD Refcode	Torsion angle /°
ACUYIG	-37	HURTOF	-59
BEKBEZ	80	QUKDAD (A)	22
CBUMUR10	-51	QUKDAD (B)	24
CONBAI (A)	31	QUKDEH	-19
CONBAI (B)	-57	RAKTIH	82
FDMUPD10 (A)	40	RECTOK	62
FDMUPD10 (B)	-41	RIDLEX	46
FDMUPD11 (A)	51	VACYAA	40
FDMUPD11 (B)	65	VORDAJ	60
FILQOI	48	VORDEN	-68
HARWEE (A)	55	YIWGEQ	-48
HARWEE (B)	57		

Of the 23 tertiary lactam derivatives, three (13%) are *syn* and the remaining 20 (87%) are *gauche*. Again, due to the conformational restraints of the ring systems it is expected that *gauche* is the dominating torsion angle range.

6.5.4. α-Fluorodiamides

This category contains structures in which the fluorine atom is adjacent to two amide moieties (an additional example is given in appendix section A1.3.9.).

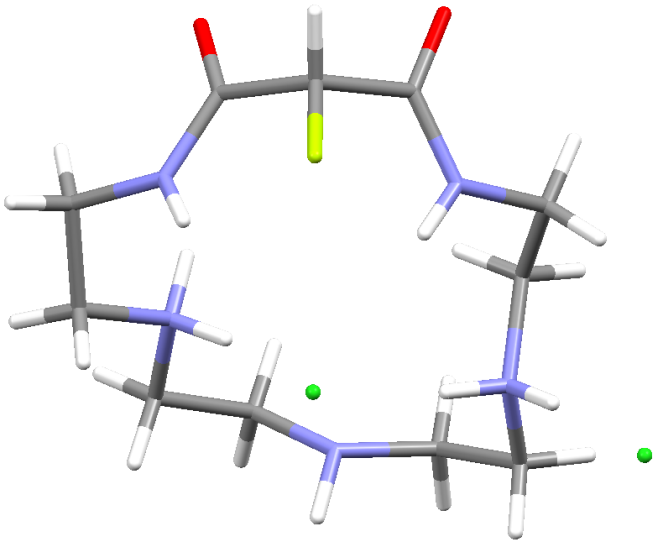

***Figure 235** – CANLOT is an example of a fluorodiamide derivative. It has two F-C-C=O bond torsion angles of -155° and 171°.*

***Table 55** – The nine CSD structure Refcodes for the tertiary lactam derivatives.*

CSD Refcode	Torsion angle 1 /°	Torsion angle 2 /°
CANKUY	-148	157
CANLEJ	151	-159
CANLIN	153	-157
CANLOT	-155	171
CANLUZ	161	-161
HEKTOG	41	-42
PANCEO	160	-162
PANCIS (A)	149	-159
PANCIS (B)	-153	154

14 (78%) of the 18 fluoroamide torsion angles are *anti*, two (11%) are *eclipsed*, and two (11%) are *gauche*. It is interesting to note that the two *eclipsed* angles are only one or two degrees away from being classified as *anti*, given that the *eclipsed*/*anti* border is 150°. It is also interesting to note that all of the structures are cyclic. Whilst eight of the nine structures are macrocyclic (with minimal conformational restraints), HEKTOG is cyclic and the restrains of the 6-membered heterocyclic ring lead to *gauche* F-C-C=O torsion angles of 41° and -42°.

6.5.5. Secondary α-Fluoroamides on Rings

Eight entries in the CSD contain molecules in which the fluorine atom of a secondary fluoroamide is directly bonded to a ring system. This ring system could potentially restrict rotation of the F-C-C=O bond and so affect the torsion angles of these structures. All eight of the entries in this category have *anti* F-C-C=O torsion angles.

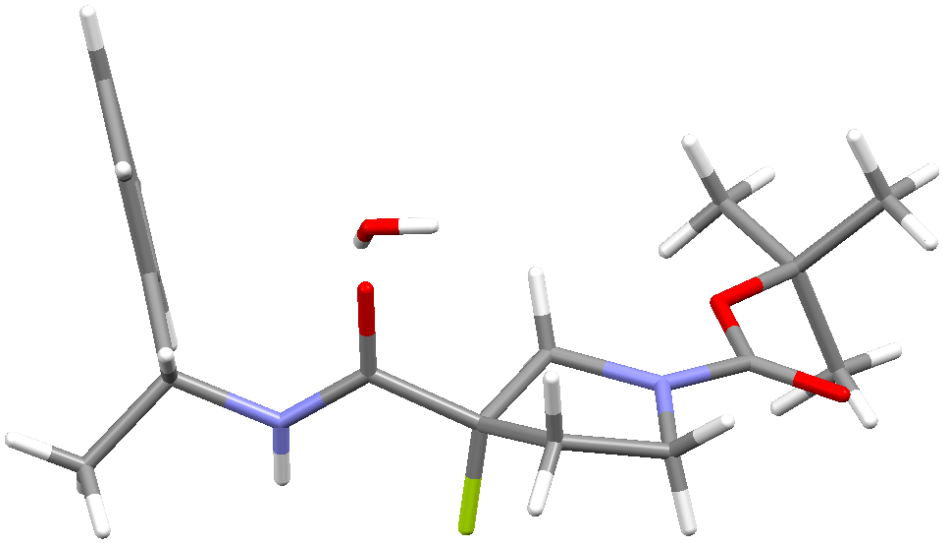

Figure 236 *– ROHQOW is an example of a secondary fluoroamide derivative with the fluorine atom on a ring system. It has an F-C-C=O bond torsion angle of 171°.*

Table 56 – *The eight CSD structure Refcodes for the secondary fluoroamides with fluorine atoms on rings.*

CSD Refcode	Torsion angle /°
CUCHIT	-174
DILDAF (A)	171
DILDAF (B)	-174
ROHQOW	171
TORPIB	-170
TORPOH (A)	156
TORPOH (B)	160
TORPOH (C)	164

6.5.6. Tertiary α-Fluoroamides on Rings

Two entries in the CSD contain molecules in which the fluorine atom of a tertiary fluoroamide is directly bonded to a ring system. One structure (HIRJID, -151^{o}) is *anti* and one (AXUCAX, 100^{o}) is *eclipsed*. An example structure is given in appendix section A1.3.10.

6.5.7. Tertiary α-Fluoroamides with Nitrogen Atoms on Rings

This category contains molecules in which the fluoroamide nitrogen is part of an N-heterocycle. By definition these systems can only be tertiary fluoroamide derivatives. Again, this ring system could potentially restrict rotation of the F-C-C=O bond and so affect the torsion angles of these structures.

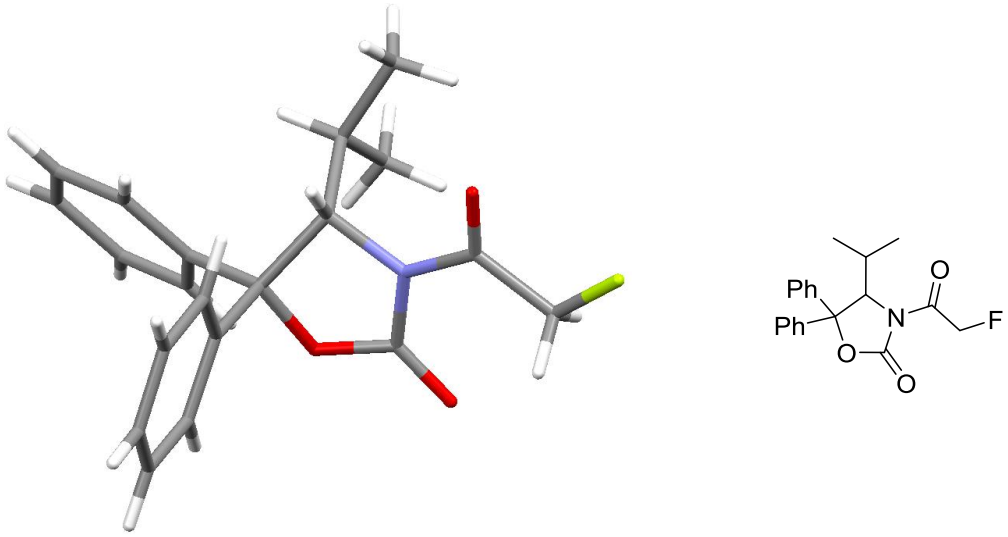

***Figure 237** – BAXCEJ is an example of a tertiary fluoroamide derivative with a heterocyclic nitrogen atom. It has two independent molecules with F-C-C=O bond torsion angles of -2^{o} and -5^{o}.*

***Table 57** – The 14 CSD structure Refcodes for the tertiary fluoroamides with heterocyclic nitrogen atoms.*

CSD Refcode	Torsion angle /°	CSD Refcode	Torsion angle /°
BAXCEJ (A)	-2	IHESOE	17
BAXCEJ (B)	-5	JENTIF	-22
EACXEL	-11	RUCFEC (A)	-24
EACYEM	40	RUCFEC (B)	-32
FADBAQ	-31	RUCFIG	27
FADBEU	33	SEYSIA	138
FADBOE	-163	XINSIX	-155

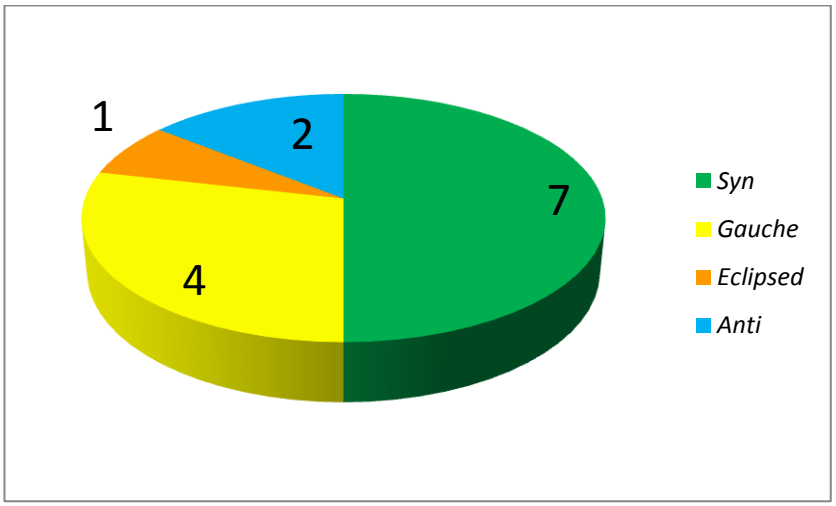

***Figure 238** – Pie chart of N-heterocyclic fluoroamide F-C-C=O bond torsion angles.*

This category exhibits a larger range of torsion angles. Of the 14 entries, seven (50%) are *syn*, four (29%) are *gauche*, one (7%) is *eclipsed* and only two (14%) are *anti*. This decreased *anti* prevalence is consistent with the theory that tertiary fluoroamides lack N-H protons to hydrogen bond to the fluorine atoms and so the *anti* conformation is less stabilised. Tertiary fluoroamides may also experience more significant steric interactions.

6.5.8. Statistical Analysis of α-Fluoroamides

Of the 149 fluoroamide derivatives studied, 87 (58%) are *anti*, eight (5%) are *eclipsed*, 31 (21%) are *gauche* and 23 (15%) are *syn*. These data show a slight *anti* preference of 58%. However, this dataset includes cyclic structures in which conformation restraints restrict rotation of the F-C-C=O bond and lead to a higher number of *gauche* torsion angles. Of the 98 acyclic fluoroamides 73 (74 %) are *anti*, six (6%) are *eclipsed*, four (4%) are *gauche* and 15 (15%) are *syn*.

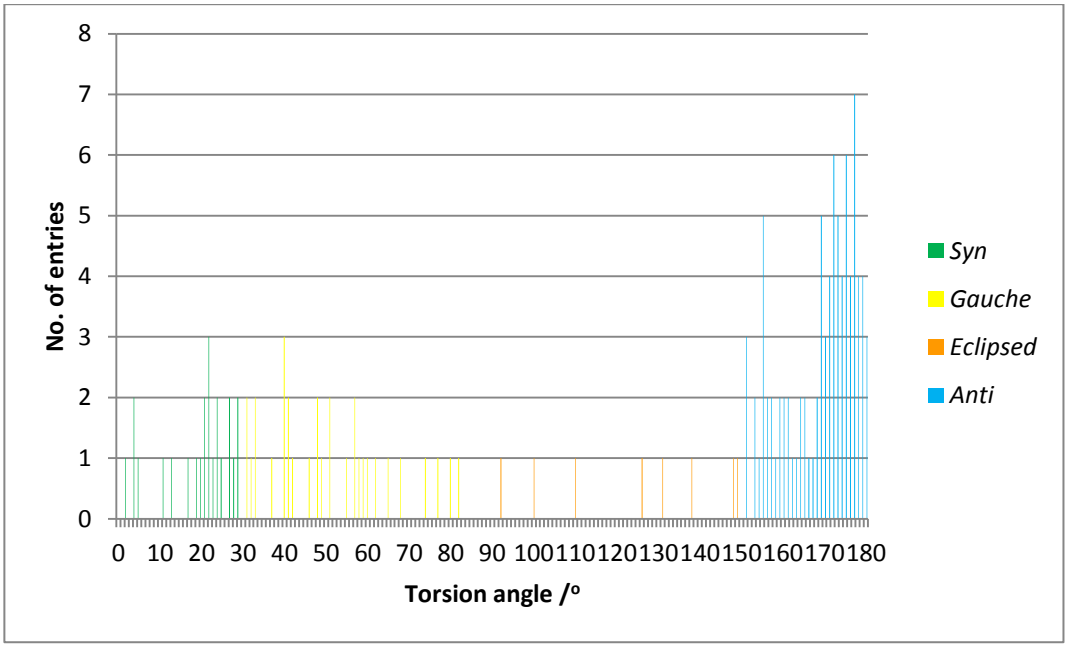

Figure 239 *– The cumulative distribution of torsion angles from all 149 data points, independent of direction of rotation.*

6.5.9. Summary of α-Fluoroamides and Comparison with Literature Studies

When rotationally constrained cyclic and macrocyclic structures are excluded 74% of acyclic fluoroamides are *anti* and this is generally in concurrence with the literature prediction.

The *anti* prevalence decreases from primary amides through to tertiary amides insofar that the tertiary amides with heterocyclic nitrogen atoms have only 14% *anti* structures. This is also concurrent with the theory that N-H protons hydrogen bond with the fluorine atoms to stabilise the *anti* conformation.

When compared to the fluoroester analogues, the fluoroamides have significantly more *anti* prevalence in the CSD, a result that is generally concurrent with the literature understanding. The reported *anti* preferences are 7.5 kcal mol^{-1} for fluoroacetamide,[156] and 5.09 kcal mol^{-1} (gas phase) to 0.18 kcal mol^{-1} (DMSO-d_6) for N-methyl-2-fluoroacetamide.[162] Note, however, that even in the category with the strongest predicted *anti* preference 1 in 4 of the acyclic crystal structures don't have *anti* conformations.

6.6. α-Fluoroketones

The search of the CSD for fluoroketone moieties identified 108 hits that, following the usual exclusions and expansions, yielded 143 fluoroketone moieties to be analysed, as of September 2016. Further details of the CSD search and exclusions are given in appendix section A1.3.11.

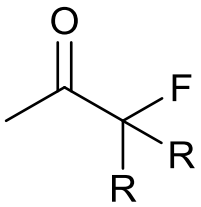

R = Non metal, non fluorine

Figure 240 *– The substructure specifications for the CSD search.*

α-Fluoroacetophenone structures (making up around a third of the 143 fluoroketone moieties) have been categorised separately from the bulk of the esters.

6.6.1. Acyclic α-Fluoroketones (Excluding α-Fluoroacetophenones)

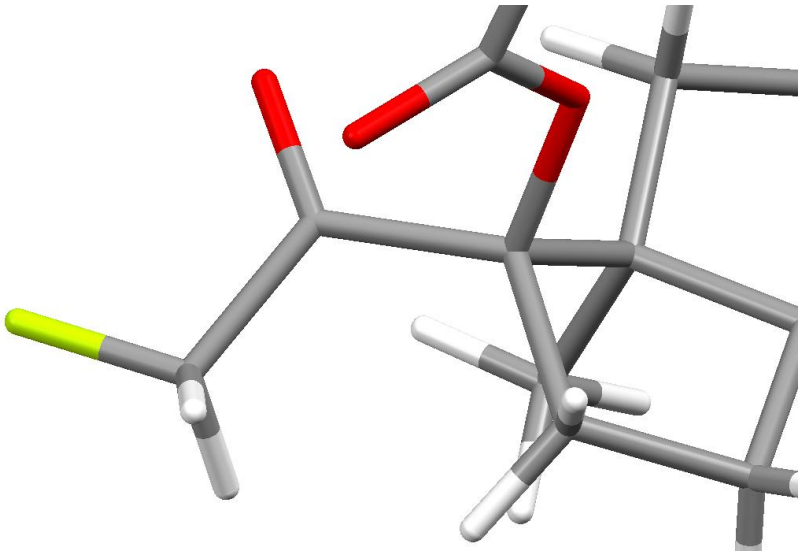

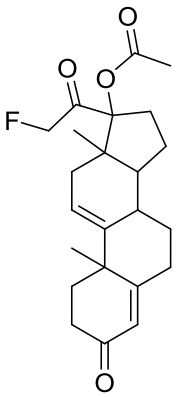

Figure 241 *– The structure of BUYYEZ10.*

11 entries were identified for this category, excluding those identified in subsequent categories. Of the 11 entries, seven (64%) are *syn* and four (36%) are *anti* (***Table 58***).

Table 58 *– The 11 CSD structure Refcodes for the simple acyclic fluoroketone category.*

CSD Refcode	Torsion angle /°
BUJNID	-3
BUYYEZ10	-3
CFAMPR	0
DAFSAF	171
HISRAD	2
PIJRUX	-1
RIQCAV	10
RISCOL	171
SUQQIG	171
VUVVAL	176
YIXQOM	-7

6.6.2. α-Fluoroketones with Fluorine Atoms on Rings

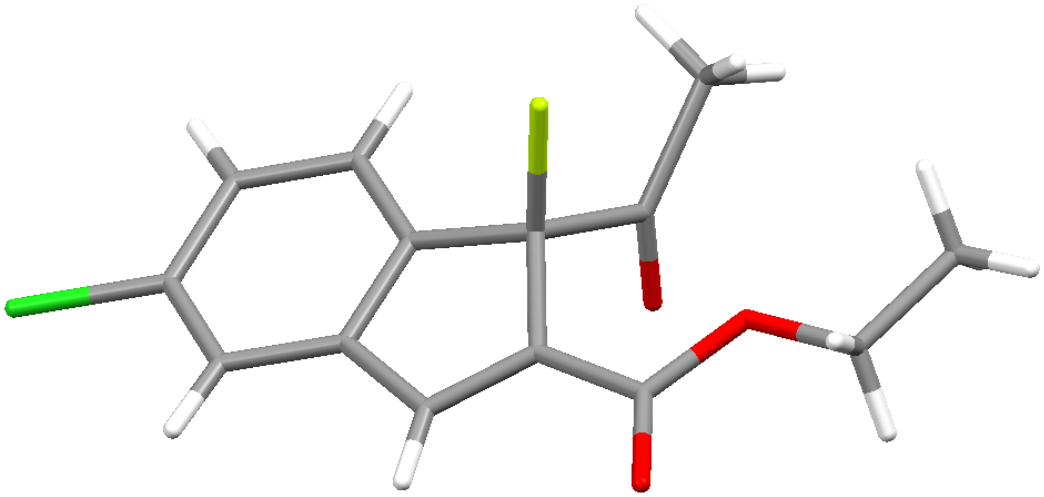

Figure 242 *– The structure of MEXPEO.*

This category consists of two entries with their fluorine atoms directly bonded to a ring system. Both entries exhibit *anti* F-C-C=O conformations (***Table 59***).

Table 59 *– The two CSD structure Refcodes for the fluoroketones with fluorine atoms bonded to ring systems.*

CSD Refcode	Torsion angle /°
DUFQIF	164
MEZPEO	171

6.6.3. Cyclic α-Fluoroketones

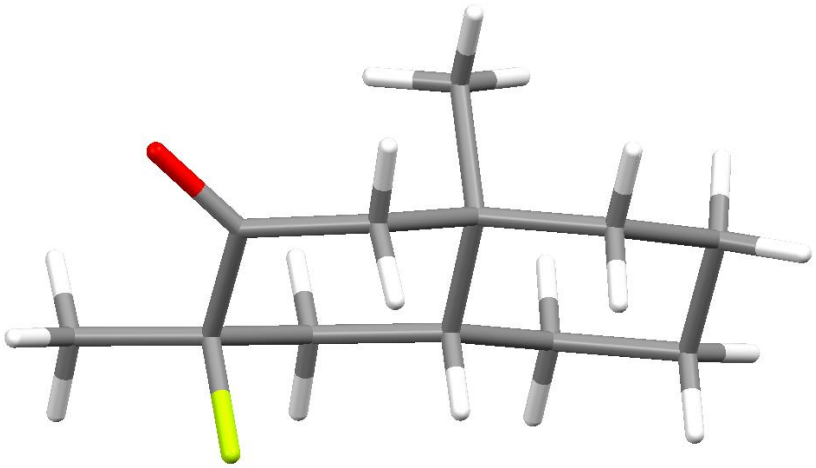

Figure 243 – *The structure of FEMKOY.*

75 cyclic fluoroketone moieties were identified in the CSD (***Table 60***). 49 (65%) moieties are *syn*, 18 (24%) are *gauche*, five (7%) are *eclipsed* and three (4%) are *anti*. The relatively large *syn* prevalence in this category is of note. Cyclic fluorocarbonyl torsion angles have generally been observed to have a *gauche* prevalence in other analogues (e.g. esters, amides etc.). This lack of *gauche* prevalence could possibly be attributed to the prevalence of more complex, fused polycyclic systems in these data. Additionally, these polycycles are often more highly fluorinated and so appear in the data multiple times, further increasing the lack of *gauche* prevalence. XOPMOE (***Figure 244***) is an example of the polyfluorinated fused polycyclic systems in these data.

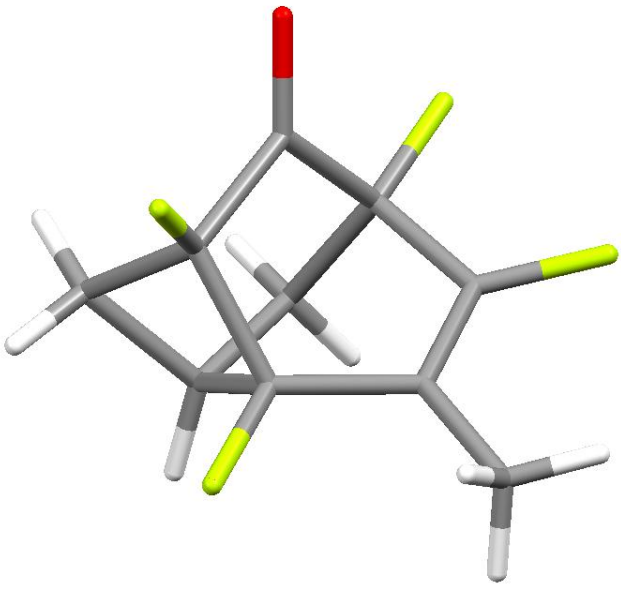

Figure 244 – *The fused polycyclic structure of XOPMOE.*

Table 60 *– The 75 CSD structure Refcodes for the cyclic fluoroketones.*

CSD Refcode	Torsion angle /°	CSD Refcode	Torsion angle /°
AKOYAA (A)	-10	RADZEB (A)	-4
AKOYAA (B)	11	RADZEB (B)	-63
BALCOH	-103	RADZIF (A)	4
BAQYAT (A)	9	RADZIF (B)	58
BAQYAT (B)	25	RADZOL (A)	-4
BAQYEX (A)	-5	RADZOL (B)	-57
BAQYEX (B)	9	RIZGAK	110
BAQYEX (C)	42	UFOTIS (A)	-5
BAQYEX (D)	-48	UFOTIS (B)	-8
CAXQIC	-37	UFOTIS (C)	-18
EQOLAX	178	UFOTIS (D)	-24
EQOLEB	178	UQEJUX (A)	37
EQOLIF	179	UQEJUX (B)	-40
FEMKOY	-117	WEGZOZ	-17
FLESTR	-14	WEGZUF	-21
GADTEL (A)	123	XAJXOY (A)	13
GADTEL (B)	123	XAJXOY (B)	43
HFXBCO (A)	-13	XOPMOE (A)	-9
HFXBCO (B)	14	XOPMOE (B)	-25
IFIWUR (A)	-13	XOPNEV (A)	10
IFIWUR (B)	-64	XOPNEV (B)	38
JAPYOO	-3	XOPNIZ (A)	-5
MEBBUQ (A)	32	XOPNIZ (B)	-13
MEBBUQ (B)	58	YELRIQ (A)	-11
MEBCAX (A)	16	YELRIQ (B)	-24
MEBCAX (B)	-29	YELVEQ (A)	25
NEXQOW	28	YELVEQ (B)	-26
NIJPOL (A)	1	YELZAQ (A)	7
NIJPOL (B)	-1	YELZAQ (B)	29
RADYEA (A)	-10	YEMDOJ (A)	26
RADYEA (B)	-50	YEMDOJ (B)	-26
RADYIE	-5	YEMKOQ (A)	-14
RADYOK (A)	3	YEMKOQ (B)	-34
RADYOK (B)	59	YEMQAI (A)	-6
RADYUQ (A)	5	YEMQAI (B)	-19
RADYUQ (B)	57	ZORPUR (A)	0
RADZAX (A)	-7	ZORPUR (B)	-2
RADZAX (B)	-53		

6.6.4. α-Fluorodicarbonyl Systems

Six entries are 1,3-dicarbonyl systems. Five of these contain one ketone and one ester moiety and the sixth entry (FULBUL) contains an *eclipsed* ketone moiety and an *anti* acetophenone entry. Four (67%) of the entries are *anti*, one (17%) is *syn* and one (17%) is *eclipsed* (***Table 61***).

Table 61 *– The 6 CSD structure Refcodes for the 1,3-dicarbonyl systems.*

CSD Refcode	Torsion angle 1 /°	Torsion angle 2 /°
FULBUL	-140	-168 (AcPh)
MUNZEC	180	156 (E)
SEQPIN	-169	153 (E)
SICRIG	178	-144 (E)
VAJYUB	-15	9 (E)
YEBSIJ	-166	-178 (E)

This category contains macrocycles and other bulky structures, often containing phenyl rings and nitro groups (e.g. FULBUL) that may have influences on the F-C-C=O conformations.

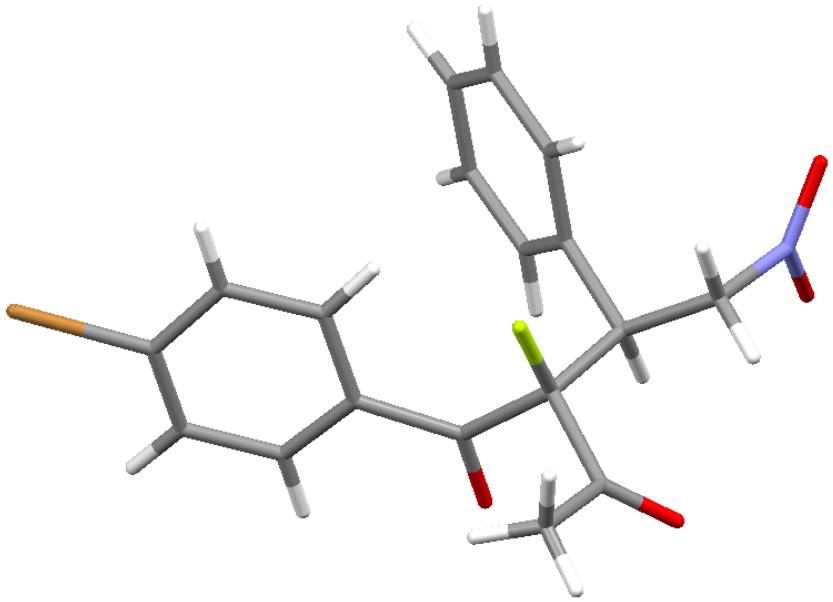

Figure 245 *– The structure of FULBUL.*

6.6.5. α-Fluoroacetophenones

6.6.5.1. Cyclic α-Fluoroacetophenones

While a large proportion of the 49 fluoroacetophenone moieties exhibit *gauche* conformation, this can largely be attributed to the relatively high number of cyclic ketones in the data set – 24 out of 49 (49%). Of the 24 cyclic structures 21 (88%) are *gauche*, one (4%) is *syn* and two (8%) are *eclipsed*, though both of the latter are very similar angles and are observed in the same CSD structure. As expected, it appears that the cyclic configurations of these structures generally force the F-C-C=O bonds into *gauche* conformations.

Table 62 – *The 24 CSD structure Refcodes for the cyclic fluoroacetophenone derivatives.*

CSD Refcode	Torsion angle 1 /°	Torsion angle 2 /°
AHEXUI	-89	
ASIXUX00	-68	
BUKTUY	-39	
COZFAZ (A)	-99	
COZFAZ (B)	-100	
CUCHIT	53	-174 (A)
CUNKON (A)	-46	
CUNKON (B)	-62	
DOZWEV	39	-169 (E)
FAFYUJ	-70	
HIJXEE	47	14 (E)
IHODUG	-57	
IHOHAQ	-57	
IREQAZ	89	
LUZSUW	79	
LUZTAD	-58	
ODOPAZ	46	11 (E)
QUDVUI	15	
QUDWAP	-66	
SELMIH	88	18 (E)
SUHBUT	-36	170 (E)
ZOGYEB	-45	
XOXGOG (A)	47	
XOXGOG (B)	47	

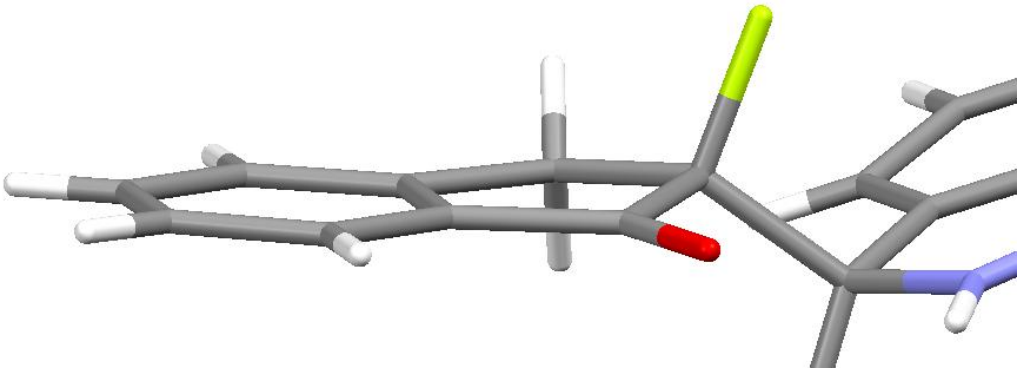

Figure 246 *– FAFYUJ is an example of a cyclic fluoroacetophenone derivative. It has a F-C-C=O bond torsion angle of -70 °.*

6.6.5.2. α-Fluorodiacetophenone Derivative

One structure (TEFVEF10) contained a fluorodiketone moiety. Both fluoroketone torsion angles exhibited *eclipsed* conformations. TEFVEF10 is in fact a fluorotricarbonyl species as it also contains a fluoroester moiety with *syn* conformation. It is likely that steric interactions have a large effect on determining the conformation of the three fluorocarbonyl torsion angles in this bulky structure.

Table 63 *– The CSD Refcode for the fluorodiacetophenone derivative.*

CSD Refcode	Torsion angle 1 /°	Torsion angle 2 /°	Torsion angle 3 /°
TEFVEF10	-126	-134	19 (E)

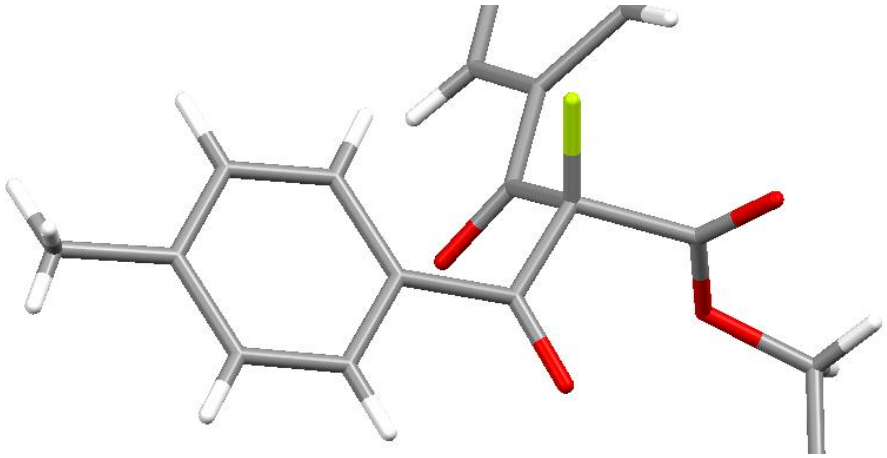

Figure 247 *– The structure of TEFVEF10.*

6.6.5.3. α-Fluorodicarbonyls

Two structures contained fluorodicarbonyl moieties in which one F-C-C=O group is a fluoroacetophenone. FULBUL contains a fluoroacetyl ketone derivative of *eclipsed* conformation and MABBEY contains a fluoroester of *syn* conformation. Again, steric effects may be one of the dominating factors in determining the conformation of fluoroacetophenone F-C-C=O torsion angles.

Table 64 *– The CSD Refcodes for the dicarbonyl derivatives.*

CSD Refcode	Torsion angle 1 /°	Torsion angle 2 /°
FULBUL	-168	-140 (K)
MABBEY	-21	-10 (E)

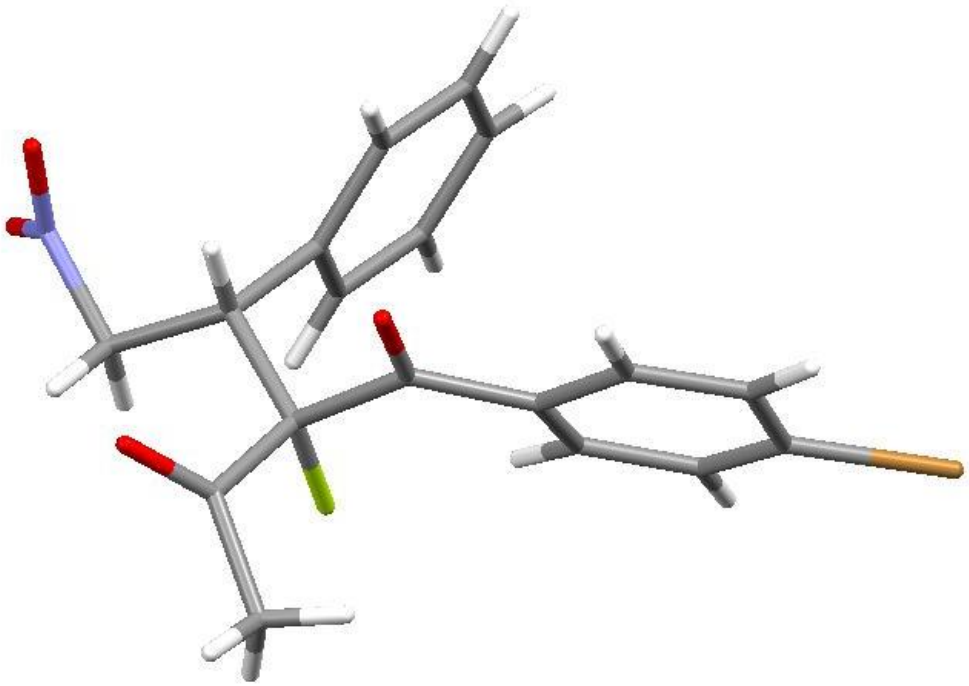

Figure 248 *– The structure of FULBUL.*

6.6.5.4. Acyclic Mono-α-fluoroacetophenones

The remaining 21 α-fluoroacetophenone structures are acyclic and contain only monofluorocarbonyl moiety. 13 (62%) are *syn*, one (5%) is *gauche*, three (14%) are *eclipsed* and four (19%) are *anti* (***Table 65***). It is worth noting that ten of the 13 *syn* F-C-C=O torsion angles are from the same four structures and so may artificially inflate the *syn* precedence in this data. REVPOY (***Figure 249***) is one of the simplest acetophenone structures observed in the CSD and so is likely to be the least sterically hindered of the structures. All four F-C-C=O torsion angles are *syn* and have very low angles of either $\pm 1^{o}$ or $\pm 5^{o}$. Similarly, UVEBOO00 and UVECIJ00 (***Figure 250***) are relatively simple fluoroacetophenone derivatives that all exhibit *syn* torsion angles.

This supports the observation that *anti* is not the preferred conformation in fluoroacetophenone derivatives, though the data set is relatively small.

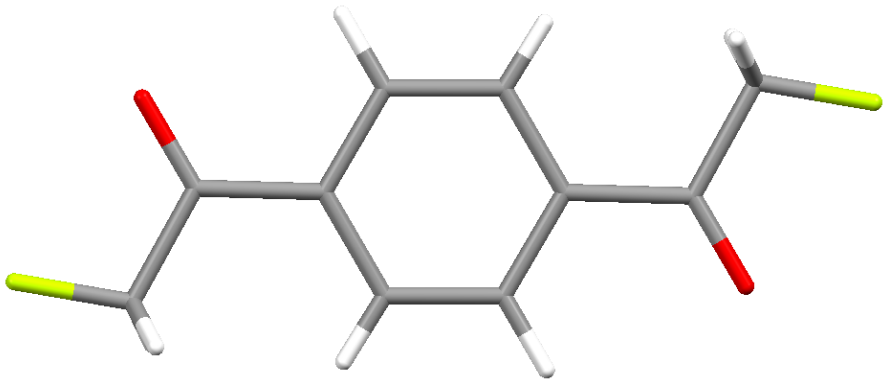

Figure 249 *– The structure of REVPOY is a relatively simple and shows little steric hindrance to rotation of the F-C-C=O bond.*

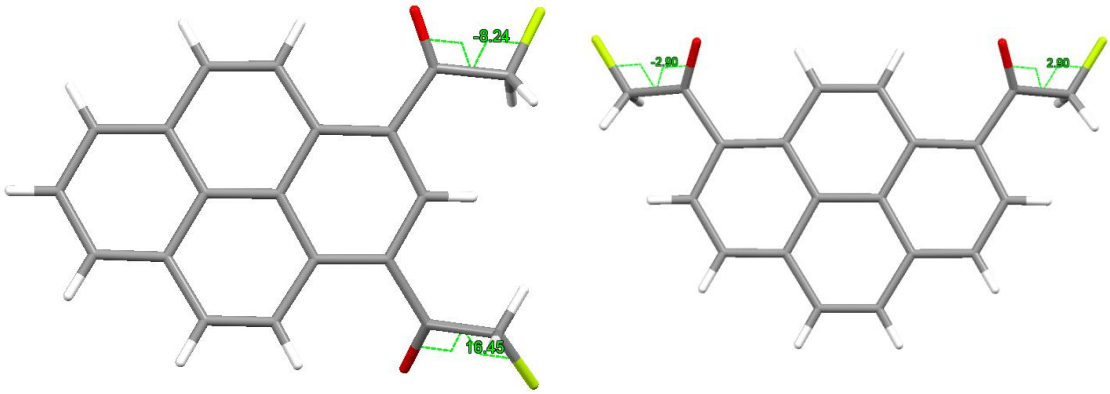

Figure 250 *– The structures of UVEBOO00 (left) and UVECIJ00 (right).*

***Table 65** – The CSD Refcodes for the 21 acyclic monofluoroacetophenone derivatives.*

CSD Refcode	Torsion angle /°
GEXTUA	44
ITALOG	18
PAJCOU	176
PELHIZ	162
RENTOV	-138
REVPOY (A)	1
REVPOY (B)	-1
REVPOY (C)	5
REVPOY (D)	-5
REYNEQ	25
RIYMUJ	-135
RIYNAQ	141
RODPIL (A)	29
RODPIL (B)	-167
UVEBOO00 (A)	-8
UVEBOO00 (B)	16
UVECIJ00 (A)	3
UVECIJ00 (B)	-3
VANCEU	170
WALXUF (A)	-13
WALXUF (B)	-13

The distribution of torsion angles is shown in ***Figure 251***.

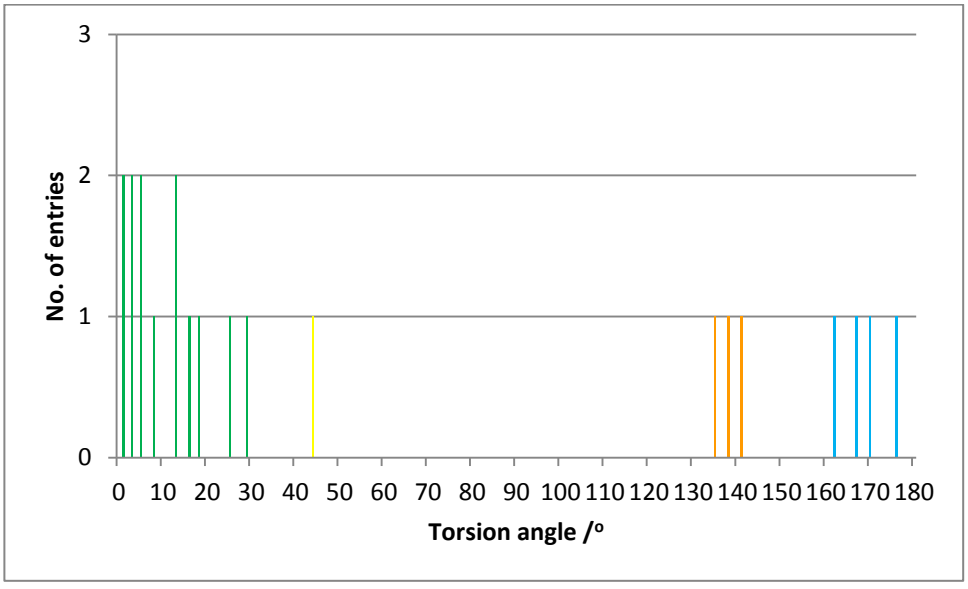

***Figure 251** – The distribution of torsion angles.*

Overall, of all the 49 fluoroacetophenones examined, 31% are *syn*, 45% are *gauche*, 14% are *eclipsed* and 10% are *anti*. When conformationally restrained cyclic structures are excluded, of the remaining 25 structures 14 (56%) are *syn*, one (4%) is *gauche*, five (20%) are *eclipsed* and five (20%) are *anti*.

6.6.6. Summary of α-Fluoroketones and Comparison with Literature Studies

Of the 143 fluoroketone moieties studied, including fluoroacetophenones, 44 were acyclic and 99 were cyclic. Of the 44 acyclic moieties 22 (50%) were *syn*, one (2%) was *gauche*, six (14%) were *eclipsed* and 15 (34%) were *anti*. Of the 99 cyclic entries 50 (51%) were *syn*, 39 (39%) were *gauche*, seven (7%) were *eclipsed* and three (3%) were *anti*. Overall, of the 143 entries, 72 (50%) were *syn*, 40 (28%) were *gauche*, 13 (9%) were *eclipsed* and 18 (13%) were *anti*.

Fluoroacetone was reported to have an *anti* preference of 2.2 kcal mol^{-1} (gas phase) switching to a 0.63 kcal mol^{-1} *syn* preference (pure liquid) and a stronger *syn* preference of 1.27 kcal mol^{-1} in DMSO-d_6.[171] The CSD data are not at odds with the predicted conformational preference of a polar system, though the dataset is relatively smaller than the previous analogues.

6.7. α-Fluoroaldehydes

Only two fluoroaldehyde entries were identified using the search parameters below (***Figure 252***), as of October 2016. When the F-C-*R* groups were defined as non-metal and non-fluorine only VEKLUT was identified, despite the fact that VAKLOL is also a non-metal monofluoride.

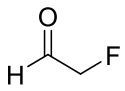

Figure 252 *– The substructure specifications for the CSD search.*

Both fluoroaldehyde entries are, by definition, acyclic. VAKLOL is a relatively simple fluoroaldehyde and exhibits a *syn* conformation of 0^{o} (***Figure 253***).

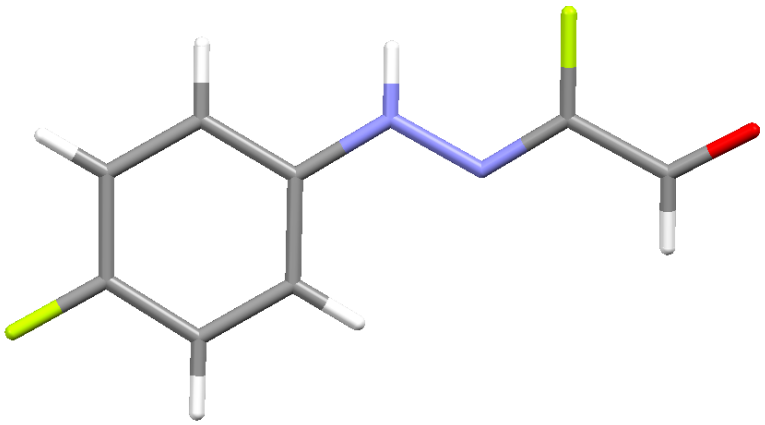

Figure 253 *– The structure and F-C-C=O torsion angle of VAKLOL.*

VEKLUT is a more complex dicarbonyl system as the fluorine atom is bonded directly to a fused lactone ring system. The resulting fluoroaldehyde conformation is *eclipsed* (***Figure 254***).

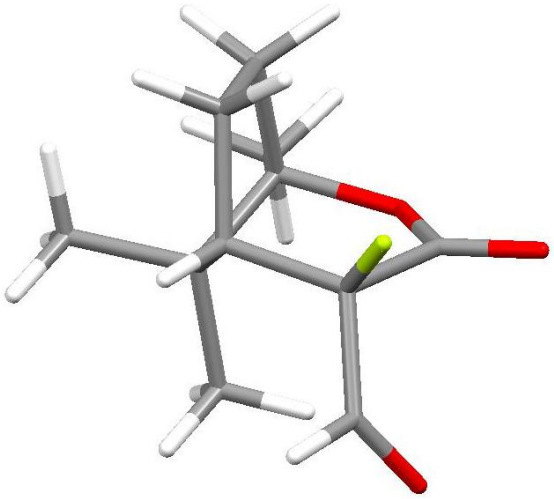

Torsion angle 1 /°	Torsion angle 2 /°
-114	44 (E)

Figure 254 – *The molecular structure and torsion angles of VEKLUT, which also contains a fluoroester moiety.*

Fluoroacetaldehyde is reported to have a small *anti* preference of 1.68 kcal mol^{-1} (Phan and Durig)[173] and 1.27 kcal mol^{-1} (Cee *et al*.).[174] Whilst the simple fluoroaldehyde exhibits a strong *syn* conformation of 0^{o} and the complex dicarbonyl system exhibits an *eclipsed* fluoroaldehyde moiety it is clear that there are not enough examples of fluoroaldehyde moieties in the CSD to draw any reasonable conclusions about the preferred F-C-C=O torsion angle.

6.8. Summary of the Conformational Preference of α-Fluorocarbonyl Systems

6.8.1. Statistical Analysis of CSD Searches

118 esters, 40 carboxylic acids, 149 amides, 143 ketones and two aldehydes moieties give a total of 452 F-C-C=O moieties analysed in the CSD studies. These entries are 41% *syn*, 20% *gauche*, 8% *eclipsed* and 31% *anti* (***Table 66***). With the exclusion of 166 cyclic entries, primarily from ketones and amides, 286 acyclic F-C-C=O moieties remain. Of these 286 moieties 44% are *syn*, 3% are *gauche*, 9% are *eclipsed* and 43% are *anti* (***Table 67***).

There are roughly equal numbers of acyclic *syn* and *anti* entries. *Syn* is the largest region in all categories except the amides where *anti* is by far the largest. It is clear that planar F-C-C=O conformations are preferred in the CSD data since 87% of the fluorocarbonyl moieties have torsion angles within 30^{o} of *syn* (0^{o}) and *anti* (180^{o}). Only 13% of the torsion angles appear in the range of 31^{o}-150^{o}.

Table 66 *– Table displaying the total number of entries (left) and percentages (right) in each angle range for all entries studied.*

Total Entries	Number of Entries					Percentage				
	Syn	***Gauche***	***Eclipsed***	***Anti***	**Total**	***Syn***	***Gauche***	***Eclipsed***	***Anti***	**Total**
Esters	64	19	12	23	118	54	16	10	19	100
Carboxylic Acids	25	-	2	13	40	63	-	5	33	100
Amides	23	31	8	87	149	15	21	5	58	100
Ketones	72	40	13	18	143	50	28	9	13	100
Aldehydes	1	-	1	-	2	50	-	50	-	100
Total	185	90	36	141	452					
%	41	20	8	31	100					

Table 67 *– Table displaying the total number of entries (left) and percentages (right) in each angle range for the acyclic entries.*

Acyclic Entries	Number of Entries					Percentage				
	Syn	***Gauche***	***Eclipsed***	***Anti***	**Total**	***Syn***	***Gauche***	***Eclipsed***	***Anti***	**Total**
Esters	63	4	12	23	102	62	4	12	23	100
Carboxylic Acids	25	-	2	13	40	63	-	5	33	100
Amides	15	4	6	73	98	15	4	6	74	100
Ketones	22	1	6	15	44	50	2	14	34	100
Aldehydes	1	-	1	-	2	50	-	50	-	100
Total	126	9	27	124	286					
%	44	3	9	43	100					

6.8.2. Comparisons of CSD Data with Literature Theory

The literature generally discusses that α-fluorocarbonyl species have an *anti* conformational preference with respect to the F-C-C=O torsion angle. This preference is strongest in α-fluoroamides and sequentially decreases through ester, ketone and aldehyde analogues. However, additional research into solution state conformational preference (primarily computational predictions and NMR studies) asserts that for any given analogue the conformational preference depends rather strongly on the polarity of the surrounding medium, with an increase in *syn* preference in more polar solvents.

74% of the acyclic α-fluoroamide F-C-C=O torsion angles found in the CSD show *anti* conformations, generally in keeping with the literature theory (7.5 kcal mol^{-1} for fluoroacetamide (Banks *et al.*),[156] 5.09 kcal mol^{-1} (gas phase) to 0.18 kcal mol^{-1} (DMSO-d_6) for N-methyl-2-fluoroacetamide (Abraham and co-workers).[162]

The analogous esters in the CSD had only 23% *anti* conformations with 62% *syn* conformations. The reported relative energy values for methyl fluoroacetate were[b] 0.90 kcal mol^{-1} (gas phase) *anti* preference to 0.71 kcal mol^{-1} (DMSO-d_6) *syn* preference (Abraham and co-workers)[166] and 0.08 kcal mol^{-1} (gas phase) to 0.61 kcal mol^{-1} (water) *syn* preferences (our own work). The 2/3 *syn* majority in the CSD is in general agreement with the literature and our own calculations, though they only predict a relatively negligible *syn* preference. The fluorocarboxylic acid entries in the CSD give similar results with 63% *syn* and 33% *anti* conformations.

Fluoroacetone was reported to have a lower *anti* preference of 2.2 kcal mol^{-1} (gas phase) switching to a 0.63 kcal mol^{-1} *syn* preference (pure liquid) and a stronger *syn* preference of 1.27 kcal mol^{-1} in DMSO-d_6 (Abraham and co-workers).[171] The acyclic α-fluoroketone entries exhibit 50% *syn* and 34% *anti* conformations which, again, arguably exhibits a higher *syn* preference than would be expected from the predictions.

[b] The value of 0.96 kcal mol^{-1} (4.0 kJ mol^{-1}) *anti* preference reported by van der Veken *et al.*[165] was proven to be miscalculated and later misquoted as 4.5 kcal mol^{-1} *anti* preference by O'Hagan,[145] with the error then duplicated by Hunter[146] and so these literature values are not valid for comparison in this section.

It has been previously discussed that any inherent *anti* preference in F-C-C=O moieties could be potentially overcome by a variety of factors including intermolecular or intramolecular interactions or crystal packing interactions. This would perhaps explain why no strong preference is observed in the CSD if a large variety of F-C-C=O torsion angles were observed in these data. However, only 13% of acyclic entries observed have torsion angles of between ±31–150^{o} meaning that there must be some factors in effect that lead to 87% of these entries being planar. Of these planar entries *syn* is generally by far more preferred than *anti* in all acyclic CSD categories except the α-fluoroamides. So why the apparent *syn* preference in the solid state?

It is possibly linked to the observation that in the solution state the F-C-C=O conformations tend towards *syn* in solvents of increasing polarity. Whilst there may be significant differences between a molecule in the solution state and in the solid state, all the data in the CSD, and our own data, comes from crystal structures. A crystal is a very ordered structure surrounding the polar α-fluorocarbonyl molecule and so it could perhaps be considered that the molecule is in a very polar environment of 'itself'. This would suggest that the polar environment of a crystal is comparable to the polar environment of the molecule dissolved in a polar solvent such as water or DMSO in which the more polar *syn* conformation becomes more energetically stable as the overall dipole aligns with the polar solvent (***Figure 255***).

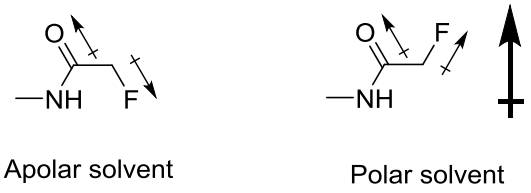

***Figure 255** – In more polar solvents it is proposed that the more polar syn conformation is preferred due to dipole alignment.*

If so, this solid state CSD study would nicely complement existing literature solution state conformational studies that use computational calculations and variable-solvent NMR techniques. It would add strength to the overall conclusion that environmental polarity is a significant factor to consider when using the F-C-C=O moiety as a conformational tool in drug design and that an *anti* conformation should not necessarily be assumed in polar physiological conditions.

In any case, the *anti* and *syn* conformer populations would be subject to a range of competing interactions that would affect the overall conformational preference. As discussed in the literature review of this chapter Abraham *et al.* reported a selection of these interactions for simple α-fluoroesters. The examples are given in ***Figure 256*** and are briefly summarised below.

(A) – Repulsion between electronegative fluorine and oxygen atoms
(B) – Hydrogen bonding between oxygen and R-group protons
(C) – Stabilising *gauche* effect between the C-H σ orbital and the C-O σ* orbital
(D) – Stabilising $n_{F} \rightarrow \pi^*_{C=O}$ hyperconjugation
(E) - Repulsion between electronegative fluorine and oxygen atoms
(F) – Electrostatic repulsion between C=O and bulky, electron dense phenyl group
(G) – Stabilising *gauche* effect between the C-H σ orbital and the C=O σ* orbital
(H) - Donation from fluorine lone pairs to C=O antibonding orbital

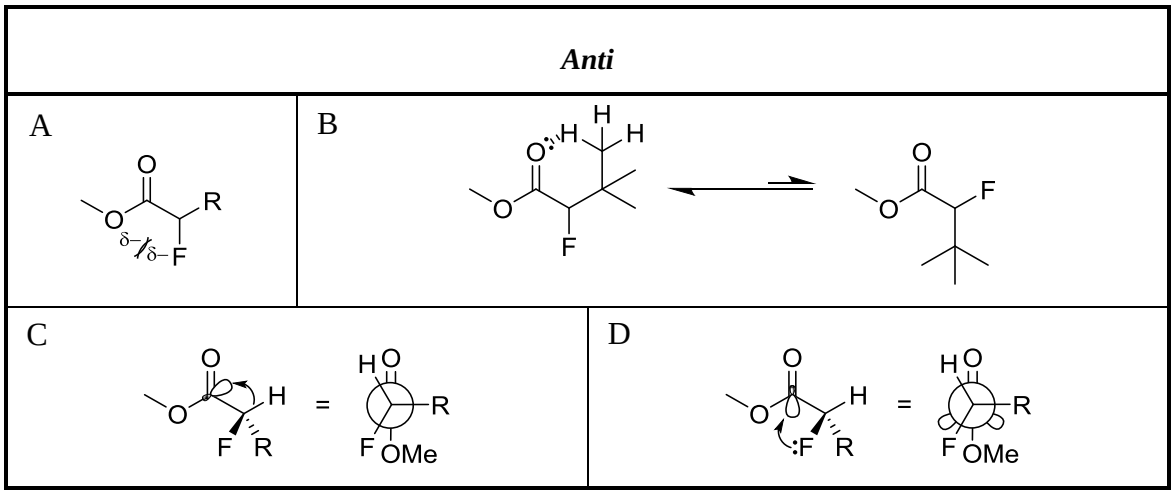

G	H
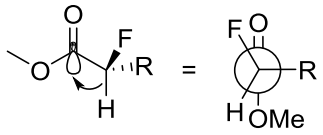	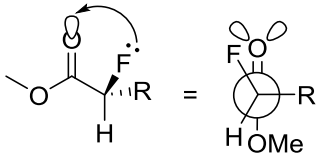

Figure 256 – *The interactions reported by Abraham et al. to rationalise the conformational preferences of α-fluoroesters.*

It is proposed that hydrogen bonding interactions between the fluorine atom and the N-H protons stabilise the *anti* conformer and, indeed, the CSD study found that the *anti* preference decreased from primary through to tertiary amides as the N-H protons were removed. Additionally, the *anti* conformation may be stabilised by donation of electron density from the carbonyl oxygen atom to the C-F σ^* antibonding orbital, as in the case of the α-fluoroamide in ***Figure 257***.[153]

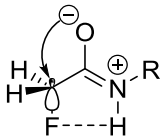

Figure 257 *– Donation of electron density from the amide carbonyl oxygen to the C-F σ^* antibonding orbital.*

Conversely, it may be possible that the *syn* conformation is stabilised if this donation came from the nitrogen or, in the example of the α-fluoroester in ***Figure 258***, the 'ether' oxygen as opposed to the carbonyl oxygen atom.

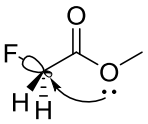

Figure 258 *– Donation of electron density from the 'ether' oxygen to the C-F σ^* antibonding orbital.*

In more polar environments the interactions that destabilise the *syn* conformation tend to be, to an extent, reduced or overcome such that there is a general *syn* preference in more polar environments.

6.9. Conclusions

Whilst the use of the F-C-C=O moiety as a conformational tool in drug design may be valuable, computational calculations of F-C-C=O torsion angle preferences of very simple molecules may prove to be of limited use if certain effects are not accounted for. That is to say that polar (physiological) solvent models must be considered instead of unrealistic gas-phase models and it must be considered that any inherent F-C-C=O torsion angle preferences are energetically similar to a large number of other competing effects such as hydrogen bonding interactions and steric interactions. These interactions may override and 'scramble' any conformational preferences *in vivo*, outside of the simplistic gas-phase model, particularly in larger, more complex molecules with multiple functional groups.

The use of the F-C-C=O moiety in drug design must, therefore, be used with caution and assessed on a case-by-case basis.

Chapter 7. Conclusions and Future Work

This thesis comprises of four related synthetic chapters pertaining to the use of simple yet polyfunctional 2-fluoro-1,3-dicarbonyl ‘building blocks’ to reach more complex, pharmaceutically relevant fluorinated products. The fifth chapter investigates the structural preferences of these systems along with analogous structures available in the Cambridge Structural Database.

First, dimethyl 2-fluoromalonate was reacted with a short series of alkyl halides and gave corresponding 2-alkyl derivatives (methyl, allyl, 4-nitrobenzyl) in moderate to very good yields. Analytical samples of the diphenylmethyl derivative and a monodecarboxylated by-product were obtained. Future work could involve reaction with a wider variety of alkylating agents or the monodecarboxylation reaction could perhaps be investigated further to yield a series of α-fluoromonoester derivatives.

Reaction of dimethyl 2-fluoromalonate with benzylamine proceeded readily at room temperature, though the presence of a fluorodiamide by-product and, hence, unreacted fluoromalonate in the crude product led to difficulty in isolation of the acyclic fluoroamidoester product, though analytical samples of both products were obtained. Subsequently a patent was published describing the synthesis of the ethyl ester analogue in good yield. Future work could include the use of chiral amine derivatives to disrupt potential planarity of the products, enzyme catalysed desymmetrisation of the α-carbon or perhaps both of these steps to yield acyclic diastereomeric fluoroamidoesters.

Building upon these reactions, in collaboration with GSK, we then reacted dimethyl malonate in a combined alkylation-amidation strategy using direct fluorination methodology, and a subsequent lipase catalysed desymmetrisation step yielded the desired enantiomerically enriched fluorolactam pre-clinical candidate spleen tyrosine kinase (Syk) inhibitor intermediate. The process was optimised, quantitatively analysed by a ‘green metrics’ package developed by the EU IMI Chem21 consortium and determined to be considerably less wasteful than the existing strategy. Further work could include substituted or oxygen based Michael addition reagents.

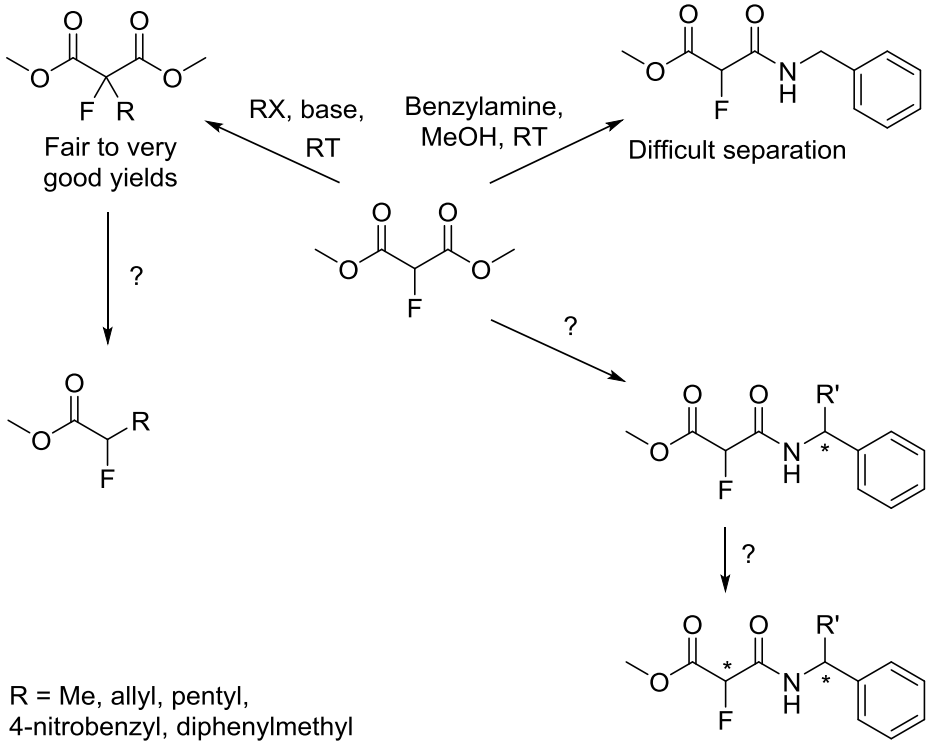

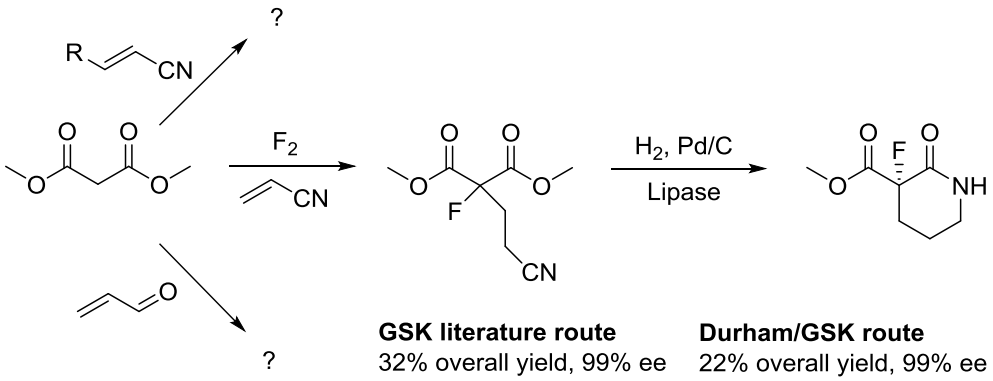

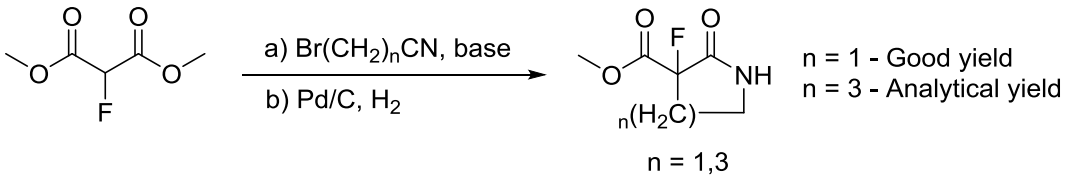

5- and 7-membered fluorolactam analogues were also investigated. The 5-membered analogue was synthesised in good yield though lipase desymmetrisation using the optimised conditions for the 6-membered system gave the opposite enantiomer. Cyclisation of the 7-membered fluorolactam proved more difficult though an analytical sample was obtained for structural confirmation. Further work could include lipase screening to obtain the desired enantiomer and using derivatised Michael acceptors.

Following work with 2-fluorodiesters a 2-fluoroketoester was investigated as a substrate for enzymatic reduction to the corresponding diastereomeric hydroxyl derivatives. Following CRED screening, in collaboration with Almac Group, initial results suggest that biocatalytic routes to all four diastereomers, utilising dynamic kinetic resolution to improve yields, have been found. Work is ongoing and includes determination of the absolute stereochemistry of each product, followed by scaled-up reactions. Possible future work could include substrates that are substituted adjacent to the ketone moiety.

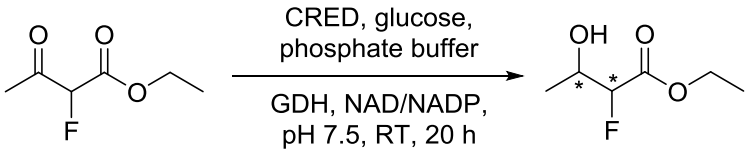

Having collected X-ray crystal structures for several of the products in this thesis we analysed the data, along with analogous structures in the Cambridge Structural Database, to determine if a trend was observed in the F-C-C=O torsion angle. This research was coupled with NMR experiments and computational calculations, from the literature and our own work, of these species in the solution state to determine that there is a greater *syn* F-C-C=O preference in more polar environments, such as water, which is a more realistic representation of physiological conditions relevant to drug design than simple gas-phase calculations. The calculated preferences are, however, small enough that they may potentially be 'overridden' by a number of competing factors. The assumption that *anti* is the preferred conformation of α-fluorocarbonyl species must, therefore, be treated with caution. Further work could include additional solution state analysis of α-fluoroketones and α-fluoroacetophenones.

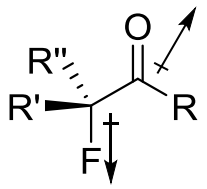

R = OC, OH, C, Ph, H, N

Chapter 8. Experimental Section

Chemicals were purchased from Acros Organics, Apollo Scientific, Fluorochem, Manchester Organics or Sigma Aldrich and, unless otherwise stated, were used without any further purification. General solvents were obtained from Fisher Scientific. Dry solvents were obtained using an Innovative Technology Inc. Solvent Purification System. All column chromatography was carried out using Silicagel LC60A (40–63 micron) purchased from Fluorochem.

Proton, carbon and fluorine nuclear magnetic resonance spectra (^{1}H NMR, ^{13}C NMR and ^{19}F NMR) were recorded on a Bruker 400 Ultrashield (^{1}H NMR at 400 MHz; ^{13}C NMR at 100 MHz; ^{19}F NMR at 376 MHz) spectrometer with residual solvent peaks as the internal standard (^{1}H NMR, $CHCl_3$ at 7.26 ppm; ^{13}C NMR, $CDCl_3$ at 77.36 ppm; ^{19}F NMR). ^{1}H, ^{13}C and ^{19}F spectroscopic data are reported as follows: chemical shift (ppm), integration, multiplicity (s = singlet, d = doublet, t = triplet, q = quartet, m = multiplet), coupling constant (Hz) and assignment.

Accurate mass analysis was achieved with a Xevo QtoF mass spectrometer (Waters Ltd, UK) equipped with an atmospheric solid analysis probe (ASAP). Infra-red (IR) spectra were recorded on a Perkin Elmer 1600 Series FTIR fitted with an ATR probe. Crystallographic data was recorded with a Rigaku R-Axis SPIDER IP diffractometer equipped with a Cryostream (Oxford Cryosystems) low temperature device at 120 K. Melting points were measured with a Gallenkamp apparatus at atmospheric pressure and are uncorrected.

MestReNova software was used to analyse NMR and mass spectrometry data.

Experimental Section for Chapter 2

Dimethyl 2-fluoro-2-methylmalonate 232

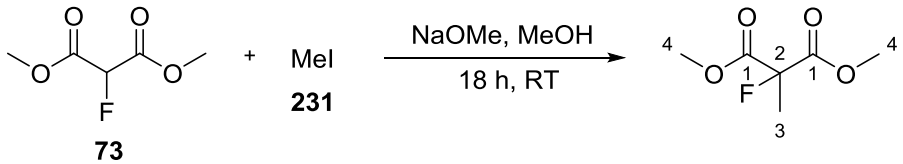

73 **232**
58%

Dimethyl fluoromalonate **73** (4.50 g, 30 mmol) was added to a solution of sodium methoxide in methanol (0.90 g sodium, 39 mmol, in 50 mL methanol) and the solution stirred in a room temperature water bath for 30 min. Methyl iodide **231** (4.68 g, 33 mmol) was added dropwise over 15 min and the solution stirred. After 18 h the solvent was removed *in vacuo*, the residue was taken up in water (25 mL), acidified (1 M HCl, 5 mL) and extracted with ethyl acetate (3 x 25 mL), washed with sodium bicarbonate (25 mL, saturated) and brine (25 mL), dried ($MgSO_4$) and concentrated *in vacuo*. The brown oil was then taken up in ethyl acetate (25 mL) and washed with an aqueous sodium thiosulfate solution (25 mL) and brine (25 mL), dried ($MgSO_4$) and concentrated *in vacuo* to yield *dimethyl 2-fluoro-2-methylmalonate* **232** (2.88 g, 58% yield) as a yellow oil; ^{1}H NMR (400 MHz, chloroform-*d*) δ 3.83 (6H, s, OCH_3), 1.79 (3H, d, $^{3}J_{HF}$ 22.0, CH_3). ^{19}F NMR (376 MHz, chloroform-*d*) δ -157.37 (q, $^{3}J_{HF}$ 22.0). ^{13}C NMR (101 MHz, chloroform-*d*) δ 167.2 (d, $^{2}J_{CF}$ 25.4, C=O), 92.4 (d, $^{1}J_{CF}$ 195.1, CF), 53.4 (s, OCH_3), 20.9 (d, $^{2}J_{CF}$ 23.1, CH_3). *m/z* (ASAP) 165.1 (100%, $[M + H]^+$), 133.1 (76%, $[M - OCH_3]^+$). ($[M + H]^+$, 165.0563. $C_6H_{10}FO_4$ requires $[M + H]^+$, 165.0563). IR (neat, cm^{-1}) 2962, 1751, 1447, 1294, 1258, 1121, 975.

Dimethyl 2-allyl-2-fluoromalonate 234

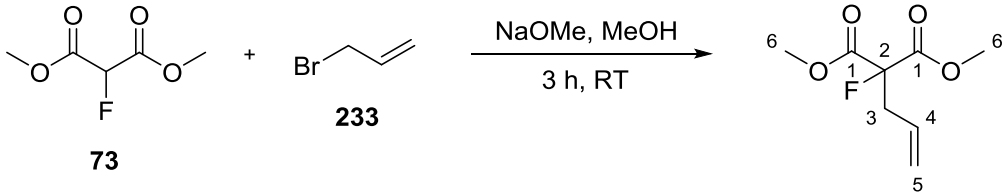

73 **234**
85%

Dimethyl fluoromalonate **73** (4.50 g, 30 mmol) was added to a solution of sodium methoxide in methanol (0.83 g sodium, 36 mmol, in 50 mL methanol) and the solution

stirred in a room temperature water bath for 30 min. Allyl bromide **233** (3.99 g, 33 mmol) was added dropwise over 20 min and the solution stirred. After 3 h the solvent was removed *in vacuo*, the residue was taken up in water (25 mL), acidified (1 M HCl, 5 mL) and extracted with ethyl acetate (3 x 25 mL), washed with sodium bicarbonate (25 mL, saturated) and brine (25 mL), dried ($MgSO_4$) and concentrated *in vacuo* to yield *dimethyl 2-allyl-2-fluoromalonate* **234** (4.87 g, 85% yield) as an off-white oil; ^{1}H NMR (400 MHz, chloroform-*d*) δ 5.61 (1H, ddt, $^4J_{HF}$ 17.3, $^3J_{HH}$ 10.2, $^3J_{HH}$ 7.1, C**4**H), 5.11 – 5.03 (2H, m, C**5**H_2), 3.69 (6H, s, OCH_3), 2.76 (2H, ddt, $^3J_{HF}$ 23.8, $^3J_{HH}$ 7.1, $^4J_{HH}$ 1.1, C**3**H_2). ^{19}F NMR (376 MHz, chloroform-*d*) δ -166.30 (t, $^3J_{HF}$ 23.8). ^{13}C NMR (101 MHz, chloroform-*d*) δ 166.0 (d, $^2J_{CF}$ 25.6, C=O), 129.0 (d, $^3J_{CF}$ 3.0, C**4**), 120.7 (s, C**5**), 94.1 (d, $^1J_{CF}$ 199.5, CF), 53.1 (s, OCH_3), 38.6 (d, $^2J_{CF}$ 21.3, C**3**). *m/z* (ASAP) 191.1 (100%, $[M + H]^+$), 171.1 (76%, $[M – F]^+$). ($[M + H]^+$, 191.0720. $C_8H_{12}FO_4$ requires $[M + H]^+$, 191.0723). IR (neat, cm^{-1}) 2961, 1751, 1438, 1308, 1256, 1221, 1140, 1038.

Dimethyl 2-fluoro-2-(4-nitrobenzyl)malonate 236

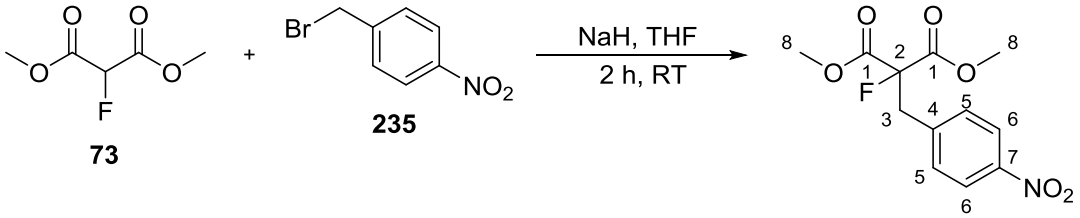

236
84%

Dimethyl fluoromalonate **73** (4.73 g, 31.5 mmol) was added to a solution of sodium hydride (0.86 g, 36 mmol) in THF (50 mL) in a room temperature water bath over 10 min and the solution stirred for a further 5 min. 4-Nitrobenzyl bromide **235** (6.48 g, 30 mmol) was added over 5 min and the solution stirred. After 2 h the solvent was removed *in vacuo*, the residue was taken up in water (25 mL), acidified (1 M HCl, 5 mL) and extracted with ethyl acetate (3 x 25 mL), washed with sodium bicarbonate (25 mL, saturated) and brine (25 mL), dried ($MgSO_4$) and concentrated *in vacuo*. The solid was recrystallized from hexane and ethyl acetate to yield *dimethyl 2-fluoro-2-(4-nitrobenzyl)malonate* **236** (7.20 g, 84% yield) as a pale yellow solid; Mp 89-90 ^{o}C. ^{1}H NMR (400 MHz, chloroform-*d*) δ 8.13 (2H, d, $^3J_{HH}$ 8.7, C**6**H), 7.41 (2H, d, $^3J_{HH}$ 8.4, C**5**H), 3.79 (6H, s, OCH_3), 3.57 (2H, d, $^3J_{HF}$ 24.5, C**3**H_2). ^{19}F NMR (376 MHz, chloroform-*d*) δ -164.78 (t, $^3J_{HF}$ 24.4). ^{13}C NMR (101 MHz, chloroform-*d*) δ 165.7 (d,

$^{2}J_{CF}$ 25.3, C=O), 147.6 (s, C**7**), 140.5 (s, C**4**), 131.3 (d, $^{4}J_{CF}$ 1.3, C**5**), 123.7 (s, C**6**), 94.2 (d, $^{1}J_{CF}$ 203.2, CF), 53.7 (s, OCH_3), 39.9 (d, $^{2}J_{CF}$ 20.6, C**3**). *m/z* (ASAP) 286.1 (100%, $[M + H]^+$), 238.1 (7%, $[M - NO_2]^+$), 214.1 (23%), 167.1 (34%). ($[M + H]^+$, 286.0727. $C_{12}H_{13}FNO_6$ requires $[M + H]^+$, 286.0724). IR (neat, cm^{-1}) 1749, 1520, 1349, 1302, 1254, 1210, 1046.

Dimethyl 2-diphenylmethyl-2-fluoromalonate 238 and Methyl 2-fluoro-3,3-diphenylpropanoate 239

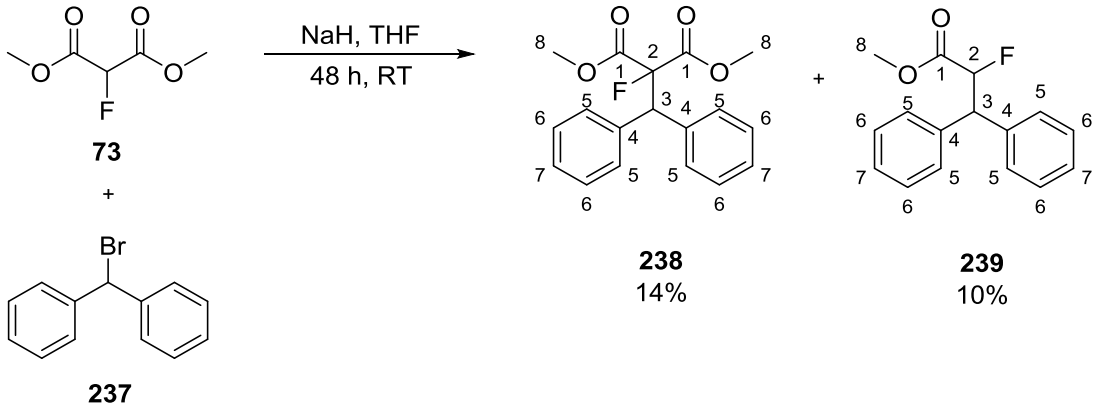

Dimethyl fluoromalonate **73** (4.73 g, 31.5 mmol) was added to a solution of sodium hydride (0.86 g, 36 mmol) in THF (50 mL) in a room temperature water bath over 10 min and the solution stirred for a further 5 min. Bromo diphenylmethane **237** (7.41 g, 30 mmol) was added over 5 min and the solution stirred. After 24 h the solution was heated to 50 ^{o}C for 3 h. A further portion of sodium hydride (1.44 g of unwashed 60% NaH in mineral oil, 36 mmol) was added and the room temperature reaction solution stirred. After 19 h the solvent was removed *in vacuo*, the residue was taken up in water (25 mL), acidified (1 M HCl, 5 mL) and extracted with ethyl acetate (3 x 25 mL), washed with sodium bicarbonate (25 mL, saturated) and brine (25 mL), dried ($MgSO_4$) and concentrated *in vacuo*. Silica column chromatography with hexane and ethyl acetate yielded *dimethyl 2-diphenylmethyl-2-fluoromalonate* **238** (1.34 g, 14% yield) as a pale cream coloured solid*;* Mp 95-96 ^{o}C. ^{1}H NMR (400 MHz, chloroform-*d*) δ 7.43 – 7.39 (4H, m, C**5**H), 7.31 – 7.25 (4H, m, C**6**H), 7.25 – 7.20 (2H, m, C**7**H), 5.09 (1H, d, $^{3}J_{HF}$ 35.2, C**3**H), 3.67 (6H, s, OCH_3). ^{19}F NMR (376 MHz, chloroform-*d*) δ -173.87 (d, $^{3}J_{HF}$ 35.1). ^{13}C NMR (101 MHz, chloroform-*d*) δ 165.8 (d, $^{2}J_{CF}$ 25.9, C=O), 137.9 (s, C**4**), 129.3 (4C, d, $^{4}J_{CF}$ 2.4, C**5**), 128.7 (4C, s, C**6**), 127.6 (s, C**7**), 97.9 (d, $^{1}J_{CF}$ 212.2, CF), 55.5 (d, $^{2}J_{CF}$ 17.8, C**3**), 53.6 (s, OCH_3). *m/z* (ASAP) 317.1 (27%, $[M + H]^+$), 296.1

(46%), 265.1 (57%), 236.1 (28%), 167.1 (100%, $[HC(Ph)_2]^+$). ($[M + H]^+$, 317.1164. $C_{18}H_{18}FO_4$ requires $[M + H]^+$, 317.1189). IR (neat, cm^{-1}) 2958, 1769, 1450, 1276, 1221, 1143, 1043.

and *methyl 2-fluoro-3,3-diphenylpropanoate* **239** (0.79 g, 10% yield) as a clear oil; ^1H NMR (400 MHz, chloroform-*d*) δ 7.36 – 7.21 (10H, m, ArH), 5.56 (1H, dd, $^2J_{HF}$ 48.6, $^3J_{HH}$ 4.6, C**2**H), 4.62 (1H, dd, $^3J_{HF}$ 30.1, $^3J_{HH}$ 4.6, C**3**H), 3.64 (3H, s, OCH_3). ^{19}F NMR (376 MHz, chloroform-*d*) δ -194.39 (dd, $^2J_{HF}$ 48.6, $^3J_{HF}$ 30.1). ^{13}C NMR (101 MHz, chloroform-*d*) δ 169.2 (d, $^2J_{CF}$ 23.8, C=O), 139.7 (d, $^3J_{CF}$ 2.7, C**4**), 138.3 (s, C**4**), 129.2 (d, $^4J_{CF}$ 1.6, C**5**), 128.8 (s, C**6**), 128.7 (s, C**6**), 128.6 (d, $^4J_{CF}$ 1.2, C**5**), 127.5 (s, C**7**), 127.4 (s, C**7**), 91.3 (d, $^1J_{CF}$ 192.8, CF), 53.3 (d, $^2J_{CF}$ 19.7, C**3**), 52.5 (s, OCH_3). *m/z* (ASAP) 259.1 (38%, $[M + H]^+$), 238.1 (49%), 207.1 (60%), 178.1 (40%), 167.1 (80%, $[HC(Ph)_2]^+$). ($[M + H]^+$, 259.1138. $C_{16}H_{16}FO_2$ requires $[M + H]^+$, 259.1134). IR (neat, cm^{-1}) 3030, 2954, 1759, 1496, 1452, 1210, 1097, 696.

Methyl 2-fluoro-3-(benzylamino)-3-oxopropanoate 240 and Dibenzyl 2-fluoromalonamide 241

Screening reactions – General procedure;

Benzylamine **143** ((0.21 g, 2 mmol) in methanol (2 mL)) was added to dimethyl fluoromalonate **73** ((0.30 g, 2 mmol) in methanol (2 mL)) and the solution was stirred before being sealed in a microwave reactor vessel. The reaction mixture was heated to the desired temperature for the stated time before being cooled to room temperature and analysed by ^{19}F NMR spectroscopy.

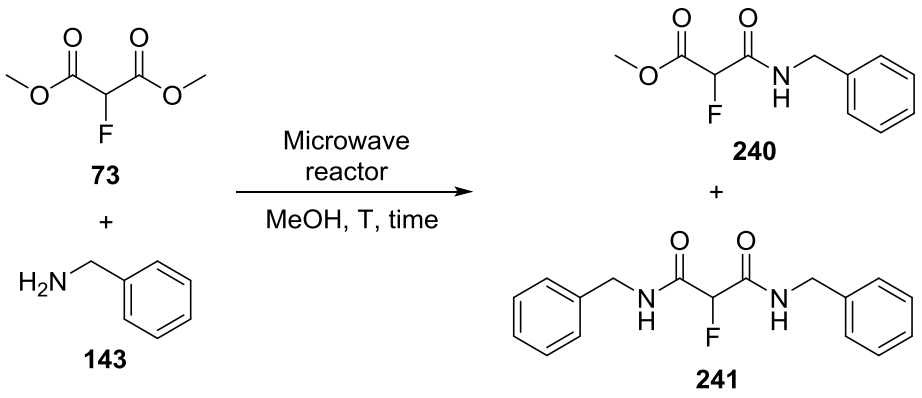

Temp. /°C	Time /min	Compounds present* /%			
		Amidoester 240	Diamide 241	Fluoromalonate 73	Other
150	20	41	17	27	14
150	10	46	16	25	11
100	20	51	20	27	4
100	10	51	19	27	4
60	20	52	17	29	2
60	10	51	14	33	2
25	10	46	6	48	<1
25	20	53	10	36	<1
25	30	57	12	31	<1
25	40	58	15	27	<1

*As determined by ^{19}F NMR spectroscopy

Slow addition reaction;

Benzylamine **143** ((0.21 g, 2 mmol) in methanol (2 mL)) was added over 10 min to dimethyl fluoromalonate **73** ((0.30 g, 2 mmol) in methanol (2 mL)) with vigorous stirring at room temperature. The reaction solution was stirred for a further 30 min before being analysed by ^{19}F NMR spectroscopy.

Stoichiometric screening reactions – General procedure;

Benzylamine **143** ((0.21 g, 2 mmol) in methanol (2 mL)) was added over 5 min to dimethyl fluoromalonate **73** (in methanol (2 mL)) with vigorous stirring at room temperature. The reaction solution stirred for a further 30 min before being analysed by ^{19}F NMR spectroscopy.

Equiv. Fluoromalonate 73	Product ratio* /%	
	Amidoester 240	Diamide 241
1	79	21
2	89	11
3	90	10†

*As determined by ^{19}F NMR spectroscopy

Scaled-up reaction;

Benzylamine **143** ((1.61 g, 15 mmol) in methanol (20 mL)) was added over 5 min to dimethyl fluoromalonate **73** ((4.50 g, 30 mmol) in methanol (20 mL)) and stirred at room temperature. After 1.5 h the solvent was removed *in vacuo* to give a white solid. ^{19}F NMR spectroscopy determined that the mixture contained the amidoester **240**, the diamide **241** and fluoromalonate **73** in a ratio of 0.89 : 0.11 : 1.00. From this crude product, analytical samples of both the monoamide and the diamide were isolated;

Methyl 2-fluoro-3-(benzylamino)-3-oxopropanoate 240

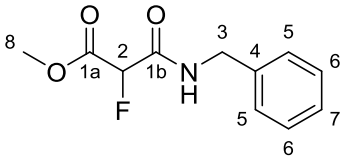

240

A portion of the crude product was washed with hexane until ^{19}F NMR spectroscopy showed that all the excess dimethyl fluoromalonate had been removed. The solid was then stirred with 200 mL hexane and filtered through cotton wool. The solution was concentrated *in vacuo* to yield a pure sample of *methyl 2-fluoro-3-(benzylamino)-3-oxopropanoate* **240** as a white solid which was then recrystallized from ethyl acetate to give clear crystals; Mp 85-86 ^{o}C. ^{1}H NMR (400 MHz, chloroform-*d*) δ 7.44 – 7.18 (5H, m, Ar-H), 6.76 (1H, s, broad, NH), 5.31 (1H, d, $^{2}J_{HF}$ 48.8, HCF), 4.49 (2H, qd, *J* = 14.7, 5.8, CH_2), 3.86 (3H, s, OCH_3). ^{19}F NMR (376 MHz, chloroform-*d*) δ -192.67 (dd, $^{2}J_{HF}$ 48.8, $^{5}J_{HF}$ 2.9). ^{13}C NMR (101 MHz, chloroform-*d*) δ 165.3 (d, $^{2}J_{CF}$ 23.9, O-C=O), 163.3 (d, $^{2}J_{CF}$ 20.1, N-C=O), 137.0 (s, C**4**), 128.9 (s, C**5**), 128.0 (s, C**7**), 127.9 (s, C**6**), 87.1 (d, $^{1}J_{CF}$ 198.9, CF), 53.5 (s, OCH_3), 43.5 (s, CH_2). *m/z* (EI^+) 225.8 (100%, $[M + H]^+$). ($[M + H]^+$, 226.0879. $C_{11}H_{13}FNO_3$ requires $[M + H]^+$, 226.0883). IR (neat, cm^{-1}) 3291, 2964, 1761, 1652, 1562, 1434, 1210, 1103.

Dibenzyl 2-fluoromalonamide 241

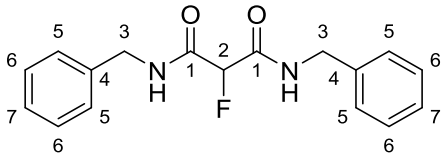

241

A portion of the crude product was stirred with ethyl acetate such that only a small amount of the solid remained undissolved. The solution was then filtered to yield *dibenzyl 2-fluoromalonamide* **241** as a white solid; Mp 154-156 ^{o}C. ^{1}H NMR (400 MHz, chloroform-*d*) δ 7.39 – 7.21 (10H, m, Ar-H), 7.19 (2H, s, broad, NH), 5.28 (1H, d, $^{2}J_{HF}$ 47.7, HCF), 4.56 – 4.40 (4H, m, CH_2). ^{19}F NMR (376 MHz, chloroform-*d*) δ -197.36 (d, $^{2}J_{HF}$ 47.7). ^{13}C NMR (101 MHz, chloroform-*d*) δ 164.6 (d, $^{2}J_{CF}$ 20.8, C=O), 137.1 (s, C**4**), 129.0 (4C, s, C**5**), 128.0 (s, C**7**), 127.9 (4C, s, C**6**), 86.8 (d, $^{1}J_{CF}$ 197.2, CF), 43.7 (s, CH_2). *m/z* (EI$^-$) 299.2 (100%, $[M - H]^-$). ($[M - H]^-$, 299.1196. $C_{17}H_{16}FN_2O_2$ requires $[M - H]^-$, 299.1185). IR (neat, cm^{-1}) 3317, 3029, 2935, 1676, 1550, 1430, 1257, 1065.

Experimental Section for Chapter 3

Dimethyl 2-fluoromalonate 73

Synthesis of fluoromalonate **73** by selective direct fluorination using fluorine gas has been described previously: a) R. D. Chambers, J. Hutchinson, *J. Fluorine Chem.* **1998**, *92*, 45-52; b) A. Harsanyi, G. Sandford, *Green Chem.* **2015**, *17*, 3000-3009.

Dimethyl 2-(2-cyanoethyl)-2-fluoromalonate 246

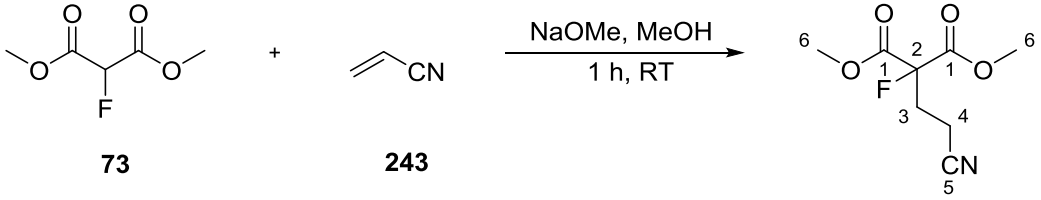

73 **243** **246** 90%

Example experimental method;

Dimethyl fluoromalonate **73** (1.50 g, 10 mmol) was added to a solution of sodium methoxide in methanol (0.046 g sodium, 2 mmol, in 40 mL methanol) before acrylonitrile **243** (1.06 g, 20 mmol) was added and the solution stirred. After 1 h the solvent was removed *in vacuo*, the residue was taken up in water (100 mL) and extracted with ethyl acetate (3 x 50 mL), washed with brine (50 mL), dried ($MgSO_4$) and concentrated *in vacuo* to yield *dimethyl 2-(2-cyanoethyl)-2-fluoromalonate* **246** (1.82 g, 90% yield) as a clear oil; ^{1}H NMR (400 MHz, chloroform-*d*) δ 3.85 (6H, s, OCH_3), 2.60 – 2.49 (4H, m, C**3**H_2, C**4**H_2). ^{19}F NMR (376 MHz, chloroform-*d*) δ -167.85 - -168.04 (m). ^{13}C NMR (101 MHz, chloroform-*d*) δ 165.4 (d, $^{2}J_{CF}$ 25.3, C=O), 117.9 (s, CN), 92.7 (d, $^{1}J_{CF}$ 201.0, CF), 53.9 (s, CH_3O), 30.2 (d, $^{2}J_{CF}$ 21.5, C**3**), 11.5 (d, $^{3}J_{CF}$ 5.5, C**4**). *m/z* (ASAP) 204.1 (100%, $[M + H]^+$), 162.1 (25%). ($[M + H]^+$, 204.0652. $C_8H_{11}FNO_4$ requires $[M + H]^+$, 204.0672). IR (neat, cm^{-1}) 2962, 2253, 1749, 1438, 1246, 1210, 1096, 1068.

DBU catalysed reaction;

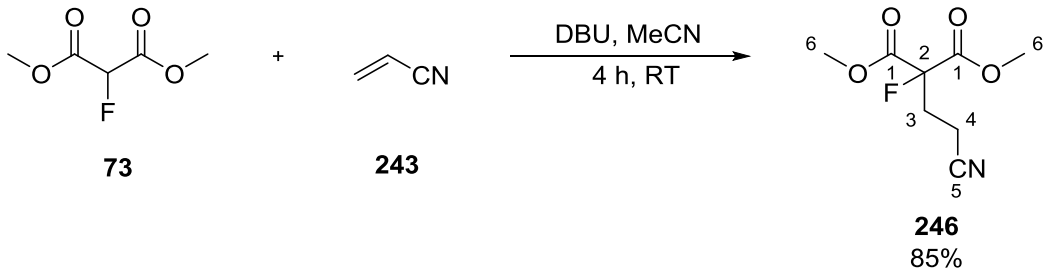

Dimethyl fluoromalonate **73** (1.50 g, 10 mmol) was added to a solution of DBU (0.30 g, 2 mmol) in acetonitrile (10 mL) before acrylonitrile **243** (0.64 g, 12 mmol) was added and the solution stirred. After 4 h the solvent was removed *in vacuo*, the residue was taken up in acidified water (15 mL water, 3 drops (0.11 g) conc. HCl) and extracted with ethyl acetate (3 x 5 mL), washed with brine (5 mL), dried ($MgSO_4$) and concentrated *in vacuo* to yield *dimethyl 2-(2-cyanoethyl)-2-fluoromalonate* **246** (1.73 g, 85% yield) as a clear oil; physical and spectroscopic data as above.

Additional experimental details:

Base screening reactions;

Base	73	243	Other	Solvent /mL	Time /h	Temp. /^{o}C	Yield* /%
K_2CO_3 2.76 g, 1.3 eq.	1.5 g, 10 mmol	0.58 g, 1.1 eq.	Aliquat 336, 0.2 g, 0.05 eq.	MeOH 40	0.5	25	(≥ 99)
NaOMe 0.05 g Na, 0.2 eq.	1.5 g, 10 mmol	1.06 g, 2 eq.	-	MeOH 40	1	25	90
NaOMe 0.46 g Na, 0.2 eq.	15 g, 100 mmol	5.8 g, 1.1 eq.	-	MeOH 150	0.5	25	94†
DBU 0.30 g, 0.2 eq.	1.5 g, 10 mmol	0.64 g, 1.2 eq.	-	MeCN 10	2	25	(≥ 99)
DBU 0.76 g, 0.25 eq.	2.64 g, 20 mmol	1.33 g, 1.25 eq.	$Cu(NO_3)_2 \cdot 2.5H_2O$ 0.47 g, 0.1 eq.	MeCN 20	17	25	(20)

DBU 1.52 g, 0.5 eq.	2.64 g, 20 mmol	1.33 g, 1.25 eq.	$Cu(NO_3)_2 \cdot 2.5H_2O$ 0.47 g, 0.1 eq.	MeCN 20	2	25	(23)
DBU 3.04 g, 1 eq.	2.64 g, 20 mmol	1.33 g, 1.25 eq.	$Cu(NO_3)_2 \cdot 2.5H_2O$ 0.47 g, 0.1 eq.	MeCN 20	1.5	25	(≥ 99)
K_3PO_4 0.13 g, 0.2 eq.	0.45 g, 3 mmol	0.19 g, 1.2 eq.	-	-	1.5	25	(≥ 99)
K_3PO_4 0.13 g, 0.2 eq.	0.45 g, 3 mmol	0.19 g, 1.2 eq.	$Cu(NO_3)_2 \cdot 2.5H_2O$ 0.07 g, 0.1 eq.	MeCN 3	1.5	25	(0)
K_3PO_4 0.64 g, 1 eq.	0.45 g, 3 mmol	0.19 g, 1.2 eq.	$Cu(NO_3)_2 \cdot 2.5H_2O$ 0.07 g, 0.1 eq.	MeCN 3	1.5	25	(≥ 99)
2-Methyl pyridine 0.06 g, 0.2 eq.	0.45 g, 3 mmol	0.19 g, 1.2 eq.	-	-	1.5	25	(0)
2-Methyl pyridine 0.06 g, 0.2 eq.	0.45 g, 3 mmol	0.19 g, 1.2 eq.	$Cu(NO_3)_2 \cdot 2.5H_2O$ 0.07 g, 0.1 eq.	MeCN 3	1.5	25	(0)

* Conversions determined by ^{19}F NMR analysis of crude reaction mixtures.

† 88% purity by ^{19}F NMR spectroscopy.

One-pot style, scaled up;

73	**F_2**	**243**	**K_3PO_4**	**$Cu(NO_3)_2 \cdot 2.5H_2O$**	**MeCN**	**Time /h**	**Temp. /°C**	**Yield /%**
21.14 g 160 mmol	6.67 g 1.1 eq.	10.53 g 1.25 eq.	41 g 1.2 eq.	3.72 g 0.1 eq.	80 mL	72	0, 25	58

Dimethyl malonate **73** (21.14 g, 160 mmol) and copper (II) nitrate hemi(pentahydrate) (3.72 g, 16 mmol) were dissolved in acetonitrile (80 mL) and the mixture was cooled to 0-5 °C and stirred at 650 rpm using an overhead stirrer. After purging the system with N_2 for 5 min, fluorine gas (20% *v/v* in N_2, 80 mL/min, 176 mmol) was introduced into the reaction mixture for 4.5 h. After purging with nitrogen for 20 min, potassium phosphate (16.98 g, 0.5 eq.) was added to the crude fluoromalonate solution. Acrylonitrile **243** (10.53 g, 1.25 eq.) was added over 30 min by syringe pump and the solution stirred. After 24 h a further portion of base (16.98 g, 0.5 eq.) was added. After a further 24 h the potassium phosphate was filtered off and washed with acetonitrile (20 mL) before 6.79 g (0.2 eq.) of fresh base was added to the filtrate and stirred. After 24 h the solution was filtered and the solvent removed *in vacuo*. The residue was taken up in water, extracted into ethyl acetate (5 x 10 mL), concentrated *in vacuo* and purified by Kugelrohr distillation to yield *dimethyl 2-(2-cyanoethyl)-2-fluoromalonate* **246** (18.96 g, 58% yield) as a clear oil; physical and spectroscopic data as above.

'Solventless', scaled up;

73	**243**	**K_3PO_4**	**MeCN***	**Time /h**	**Temp. /°C**	**Yield† /%**
4.5 g 30 mmol	1.64 g 1.03 eq.	1.28 g 0.2 eq.	4.5 mL	20	25	(≥ 99)

*To aid stirring of the solid base in solution, 1 volume of solvent was added.

†Conversion determined by ^{19}F NMR analysis of crude reaction mixture.

Temperature screen;

73	**243**	**K_3PO_4**	**MeCN**	**Time /h**	**Temp. /°C**	**Yield* /%**
4.5 g 30 mmol	1.75 g 1.1 eq.	0.64 g 0.1 eq.	4.5 mL	1.5	25	33 (1.5 h), 61 (25 h), 80 (144 h)
4.5 g 30 mmol	1.75 g 1.1 eq.	1.28 g 0.2 eq.	4.5 mL	1.5	25	36 (1.5 h), ≥ 99 (20 h)
4.5 g 30 mmol	1.75 g 1.1 eq.	1.28 g 0.2 eq.	4.5 mL	1.5	55	97 (1.5 h), ≥ 99 (3 h)
4.5 g 30 mmol	1.75 g 1.1 eq.	1.28 g 0.2 eq.	4.5 mL	1.5	85	99 (1.5 h)

* Conversions determined by ^{19}F NMR analysis of crude reaction mixtures.

Further scaled up reaction;

73	243	K_3PO_4	Time /h	Temp. /^oC	Conversion* /%
4.5 g 30 mmol	1.75 g 1.1 eq.	12.8 g 2 eq.	3.5	55	≥ 99

*Conversion measured by ^{19}F NMR spectroscopy.

Crude dimethyl fluoromalonate **73** solution (4.5 g (30 mmol) in 30 mL MeCN) was stirred with K_3PO_4 (6.4 g, 1 eq.) for 2 h before the base was filtered off and a fresh portion of base (6.4 g, 1 eq.) was added and the solution stirred at 55 ^oC. Acrylonitrile **243** (1.75 g, 1.1 eq.) was added over 30 min and the solution stirred. After 1 h ^{19}F NMR spectroscopy showed that the reaction had gone to completion.

Final one-pot style reaction;

73	F_2	243	K_3PO_4	$Cu(NO_3)_2 \cdot 2.5H_2O$	MeCN	Time /h	Temp. /^oC	Yield /%
26.40 g 200 mmol	8.36 g 1.1 eq.	12.73 g 1.2 eq.	84.90 g 2 eq.	4.65 g 0.1 eq.	100 mL	4.5, 3.25	0, 55	60

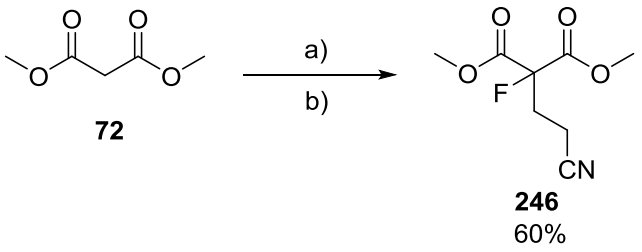

a) 20% F_2/N_2, $Cu(NO_3)_2 \cdot 2.5H_2O$, MeCN, 4.5 h, 0-5 ^oC
b) Acrylonitrile, K_3PO_4, MeCN, 3.25 h, 55 ^oC

Dimethyl malonate **73** (26.40 g, 200 mmol) and copper (II) nitrate hemi(pentahydrate) (4.65 g, 20 mmol) were dissolved in acetonitrile (100 mL) and the mixture was cooled to 0-5 °C and stirred at 650 rpm using an overhead stirrer. After purging the system with N_2 for 5 min, fluorine gas (20% *v/v* in N_2, 100 mL/min, 220 mmol) was introduced into the reaction mixture for 4 h 25 min. After purging with nitrogen for 5 min, anhydrous potassium phosphate tribasic (42.45 g, 200 mmol) was added to the crude fluoromalonate solution and stirred. After 1 h the potassium phosphate was filtered off

and rinsed with acetonitrile (2 x 20 mL) before a further portion of potassium phosphate (42.45 g, 200 mmol) was added to the solution and heated to 55 ^{o}C. Acrylonitrile **243** (12.73 g, 240 mmol) in acetonitrile (10 mL) was added over 30 min from a pressure equalised dropping funnel and the solution stirred. After a further 3.25 h the potassium phosphate was filtered off and washed with acetonitrile (3 x 20 mL) and the filtrate was concentrated *in vacuo*. Vacuum distillation (140 – 141 ^{o}C, 6 mbar) of the crude product yielded *dimethyl 2-(2-cyanoethyl)-2-fluoromalonate* **246** (24.45 g, 60%) as a clear oil; physical and spectroscopic data as above.

Dimethyl 2-(3-aminopropyl)-2-fluoromalonate hydrochloride 247

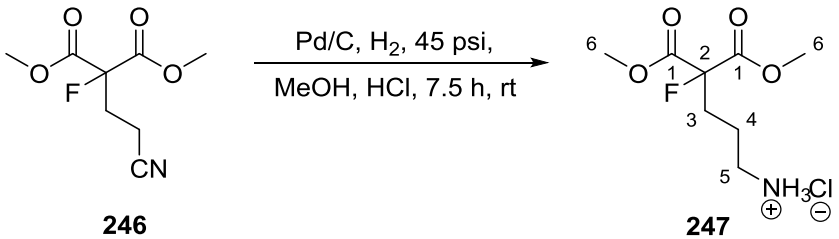

246 **247** 83%

Example experimental method;

Dimethyl 2-(2-cyanoethyl)-2-fluoromalonate **246** (10.16 g, 50 mmol), Pd/C (2.66 g of 10% Pd/C, 5 mol%) and conc. HCl (5 mL) in methanol (25 mL) were reacted in a Parr hydrogenator (H_2, 45 psi). After 7.5 h the solution was filtered through celite and the 'plug' was washed with methanol (2 x 10 mL), the filtrate was concentrated *in vacuo* in a 50 ^{o}C water bath and the solid was washed with ethyl acetate (3 x 10 mL) to yield *dimethyl 2-(3-aminopropyl)-2-fluoromalonate hydrochloride* **247** (3.60 g, 83%) as a white solid; Mp 147-148 ^{o}C. ^{1}H NMR (400 MHz, methanol-*d4*) δ 3.87 (6H, s, OCH_3), 3.08 – 2.98 (2H, m, C**5**H_2), 2.32 (2H, ddd, $^{3}J_{HF}$ 23.1, $^{3}J_{HH}$ 9.2, $^{3}J_{HH}$ 6.9, C**3**H_2), 1.89 – 1.77 (2H, m, C**4**H_2). ^{19}F NMR (376 MHz, methanol-*d4*) δ -167.20 (t, $^{3}J_{HF}$ 23.1). ^{13}C NMR (101 MHz, methanol-*d4*) δ 167.6 (d, $^{2}J_{CF}$ 25.8, C=O), 95.6 (d, $^{1}J_{CF}$ 197.4, CF), 54.1 (s, CH_3O), 40.2 (s, C**5**), 32.2 (d, $^{2}J_{CF}$ 21.6, C**3**), 22.4 (d, $^{3}J_{CF}$ 3.2, C**4**). *m/z* (ASAP) 208.1 (100%, $[M - Cl]^+$), 191.1 (14%, $[M – NH_3Cl]^+$), 176.1 (8%, $[M – CH_3, NH_3Cl]^+$). ($[M - Cl]^+$, 208.0978. $C_8H_{15}FNO_4$ requires $[M - Cl]^+$, 208.0985). IR (neat, cm^{-1}) 3016, 2942, 1749, 1581, 1437, 1249, 1033.

246	Pd/C (10%)	Conc. HCl /mL	MeOH /mL	Temp. /^{o}C	Time /h	Yield /%
6 g 29.53 mmol	1.56 g 5 mol%	4	20	25	23	57*
10.16 g 50 mmol	2.66 g 5 mol%	5	25	25	2	30
10.16 g 50 mmol	2.66 g 5 mol%	5	25	25	7.5	83

*This product was 88% pure by ^{19}F NMR spectroscopy. The other 12% is proposed to be the hydrochloride salt of the heterocycle **248**.

GSK optimised conditions;

246	Pd/C (10%)	Conc. HCl /mL	MeOH /mL	Temp. /^{o}C	Time /h	Yield /%
0.360 g 1.90 mmol	0.094 g 5 mol%	0.165	1.56	25	8	99

Dimethyl 2-(2-cyanoethyl)-2-fluoromalonate **246** (360 mg, 1.90 mmol), 10% Pd/C (94 mg, 5 mol%) and conc. HCl (165 µL) in methanol (1.56 mL) were reacted in a glass hydrogenation vessel (H_2, 4 bar). After 8 h the solution was filtered through celite (100 mg) with methanol (400 µL) and evaporated to give *dimethyl 2-(3-aminopropyl)-2-fluoromalonate hydrochloride salt* **247** (434 mg, 99%) as white crystals; physical and spectroscopic data as above.

Methyl 3-fluoro-2-oxo-3-piperidinecarboxylate 248

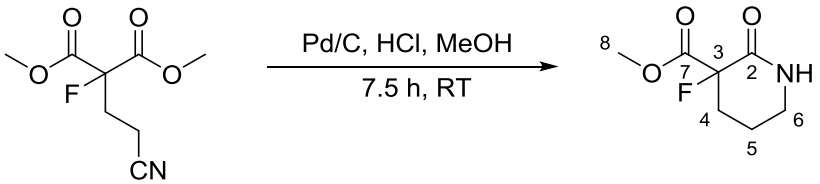

246 → **248** 63%

Experimental method from 246;

Dimethyl 2-(2-cyanoethyl)-2-fluoromalonate **246** (6 g, 29.53 mmol), Pd/C (1.56 g of 10% Pd/C, 5 mol%) and hydrochloric acid (4 mL of 37% HCl, 48 mmol) in methanol

(80 mL) were reacted in a Parr hydrogenator (H_2, 45 psi). After 7.5 h the solution was filtered through celite and concentrated *in vacuo*. The resulting solid was washed with ethanol (100 mL), dissolved in aqueous sodium bicarbonate and extracted with ethyl acetate (150 mL). The ethanol washings were concentrated *in vacuo* and the solid washed, neutralised and extracted again into ethyl acetate (100 mL). The combined organic layers were concentrated in vacuo to give a white powder which was crystallised from acetone to give *methyl 3-fluoro-2-oxo-3-piperidinecarboxylate* **248** (1.10 g, 63%) as a white, crystalline solid; Mp 115-116 ^{o}C. ^{1}H NMR (400 MHz, chloroform-*d*) δ 7.49 (1H, s, NH), 3.85 (3H, s, OCH_3), 3.45 – 3.37 (2H, m, C**6**H_2), 2.42 – 2.20 (2H, m, CH_2), 2.04 – 1.89 (2H, m, CH_2). ^{19}F NMR (376 MHz, chloroform-*d*) δ -156.07 (dd, $^{3}J_{HF}$ 28.2, $^{3}J_{HF}$ 20.0). ^{13}C NMR (101 MHz, chloroform-*d*) δ 168.7 (d, $^{2}J_{CF}$ 26.2, C**2**), 165.1 (d, $^{2}J_{CF}$ 22.4, C**7**), 90.9 (d, $^{1}J_{CF}$ 190.8, CF), 53.3 (s, CH_3O), 42.2 (s, C**6**), 31.3 (d, $^{2}J_{CF}$ 22.4, C**4**), 18.3 (d, $^{3}J_{CF}$ 2.6, C**5**). *m/z* (ASAP) 176.1 (100%, $[M + H]^+$), 162.1 (9%). ($[M + H]^+$, 176.0718. $C_7H_{11}FNO_3$ requires $[M + H]^+$, 176.0723). IR (neat, cm^{-1}) 3200, 3075, 2968, 2888, 1761, 1669, 1435, 1276, 1065.

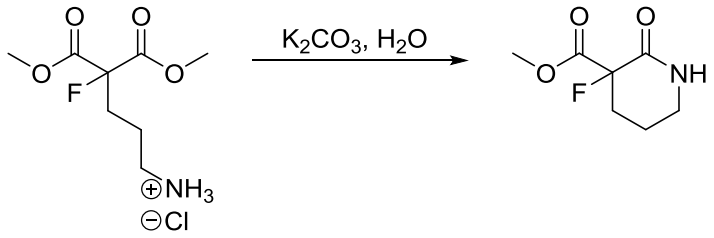

247 **248** 72%

Experimental method from 247;

Dimethyl 2-(3-aminopropyl)-2-fluoromalonate hydrochloride salt **247** (0.73 g, 3 mmol) was dissolved in water (5 mL), basified (K_2CO_3, 0.50 g, 1.2 eq.) and the solution stirred for 5 min before the solvent was removed *in vacuo* in a 50 ^{o}C water bath. The resulting solid was washed with ethyl acetate (3 x 15 mL) and the filtrate concentrated *in vacuo* to yield *methyl 3-fluoro-2-oxo-3-piperidinecarboxylate* **248** (0.38 g, 72%) as a white solid; physical and spectroscopic data as above.

No experimental sections from the GSK optimised processes or biochemistry processes performed at GSK have been included here, they are all in the appendix of this thesis (section A2.) and the supporting information of the related publication.[102]

Experimental Section for Chapter 4

Dimethyl 2-(cyanomethyl)-2-fluoromalonate 255

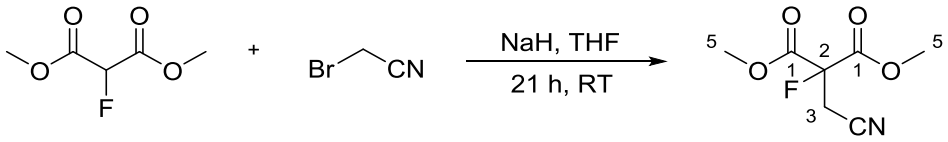

73 **253** **255** 55%

Dimethyl fluoromalonate **73** (4.50 g, 30 mmol) was added to sodium hydride (0.94 g, 39 mmol) in THF (100 mL) before bromoacetonitrile **253** (4.32 g, 36 mmol) was added and the solution stirred. After 21 h the solvent was removed under vacuum, the residue was taken up in water (100 mL), neutralised (HCl), extracted with ethyl acetate (4 x 50 mL), washed with brine (50 mL), dried ($MgSO_4$) and concentrated *in vacuo*. The yellow oil was then purified by Kugelrohr distillation (0.5 mbar, 130 ^oC) to yield *dimethyl 2-(cyanomethyl)-2-fluoromalonate* **255** (3.11 g, 55%) as a clear oil; ^1H NMR (400 MHz, chloroform-*d*) δ 3.90 (6H, s, OCH_3), 3.25 (2H, d, $^3J_{HF}$ 20.1, C**3**H_2). ^{19}F NMR (376 MHz, chloroform-*d*) δ -162.28 (s). ^{13}C NMR (101 MHz, chloroform-*d*) δ 164.1 (d, $^2J_{CF}$ 24.6, C=O), 113.5 (d, $^3J_{CF}$ 2.5, CN), 90.4 (d, $^1J_{CF}$ 208.3, CF), 54.3 (s, CH_3O), 24.2 (d, $^2J_{CF}$ 23.1, C**3**). *m/z* (ASAP) 190.1 (100%, $[M + H]^+$), 170.0 (71%), 156.0 (12%). ($[M + H]^+$, 190.0502. $C_7H_9FNO_4$ requires $[M + H]^+$, 190.0516). IR (neat, cm^{-1}) 2962, 1758, 1438, 1261, 1219, 1087, 1056.

Dimethyl 2-(2-aminoethyl)-2-fluoromalonate hydrochloride 257

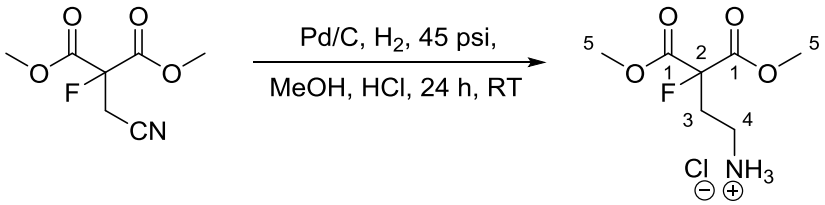

255 **257** 70%

Dimethyl 2-(cyanomethyl)-2-fluoromalonate **255** (1.89 g, 10 mmol), Pd/C (0.52 g of 10% Pd/C, 5 mol%) and HCl (1 mL) in methanol (20 mL) were reacted in a Parr hydrogenator (H_2, 45 psi). After 24 h the solution was filtered through celite, concentrated *in vacuo* and the solid was washed with ethyl acetate (250 mL) to yield

dimethyl 2-(2-aminoethyl)-2-fluoromalonate hydrochloride **257** (1.61 g, 70%) as a pale orange solid; Mp 131-132 ^{o}C. ^{1}H NMR (400 MHz, methanol-*d4*) δ 3.84 (6H, s, OCH_3), 3.10 - 3.02 (2H, m, C**4**H_2), 2.59 – 2.47 (2H, m, C**3**H_2). ^{19}F NMR (376 MHz, methanol-*d4*) δ -167.56 (t, $^{3}J_{HF}$ 21.6). ^{13}C NMR (101 MHz, methanol-*d4*) δ 165.6 (d, $^{2}J_{CF}$ 25.3, C=O), 92.9 (d, $^{1}J_{CF}$ 198.1, CF), 52.9 (s, CH_3O), 34.1 (d, $^{3}J_{CF}$ 5.0, C**4**), 31.3 (d, $^{2}J_{CF}$ 21.2, C**3**). *m/z* (ASAP) 193.9 (100%, $[M - Cl]^+$), 176.9 (42%), 132.8 (53%), 100.7 (26%). ($[M - Cl]^+$, 194.0823. $C_7H_{13}FNO_4$ requires $[M - Cl]^+$, 194.0829). IR (neat, cm^{-1}) 2947, 2891, 1765, 1749, 1433, 1235, 1165, 1136.

The GSK optimised synthesis is as follows and included here for completeness;

A solution of dimethyl 2-(cyanomethyl)-2-fluoromalonate **255** (0.446 g, 2.358 mmol) in methanol (3120 µL) was added to a glass hydrogenation vessel containing 10% palladium on carbon (0.125 g, 0.118 mmol) and 37% aq. HCl (220 µL, 2.358 mmol). The suspension was then degassed with N_2 (4 bar) three times before H_2 was charged (4 bar) and vented a further three times. The vessel was then charged with H_2 (4 bar) and the reaction mixture was stirred at 1000 rpm at 25 ^{o}C for 16 h. The slurry was then filtered through celite (50 mg), washed with methanol (0.5 mL) and the filtrate was then concentrated at RT under reduced pressure. The resultant solid was then washed with acetone (3 x 100 µL) and dried to give *dimethyl 2-(2-aminoethyl)-2-fluoromalonate hydrochloride salt* **257** (0.522 g, 96%) as white crystals; physical and spectroscopic data as above.

Methyl 3-fluoro-2-oxo-3-pyrrolidinecarboxylate 250

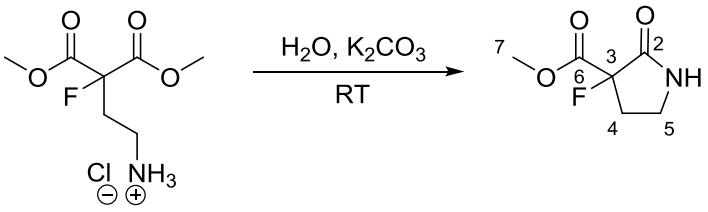

257 **250**
74%

Dimethyl 2-(2-aminoethyl)-2-fluoromalonate hydrochloride **257** (1.00 g, 4.35 mmol) was added to water (25 mL), basified to pH8 (potassium carbonate), extracted with ethyl acetate (6 x 25 mL), washed with brine (25 mL), dried ($MgSO_4$) and concentrated

in vacuo to yield *methyl 3-fluoro-2-oxo-3-pyrrolidinecarboxylate* **250** (0.52 g, 74%) as a white powder which was crystallised from acetone to form a white, crystalline solid; Mp 89-90 ^{o}C. ^{1}H NMR (400 MHz, chloroform-*d*) δ 7.96 (1H, s, NH), 3.84 (3H, s, OCH_3), 3.55 – 3.45 (2H, m, C**5**H_2), 2.80 – 2.67 (1H, m, C**4**H), 2.53 – 2.37 (1H, m, C**4**H). ^{19}F NMR (376 MHz, chloroform-*d*) δ -163.30 - -163.47 (m). ^{13}C NMR (101 MHz, chloroform-*d*) δ 169.8 (d, $^{2}J_{CF}$ 22.9, C**2**), 167.8 (d, $^{2}J_{CF}$ 28.5, C**6**), 93.4 (d, $^{1}J_{CF}$ 199.4, CF), 53.4 (s, CH_3O), 38.9 (d, $^{3}J_{CF}$ 2.7, C**5**), 32.1 (d, $^{2}J_{CF}$ 22.0, C**4**). *m/z* (ASAP) 162.1 (100%, $[M + H]^+$). ($[M + H]^+$, 162.0546. $C_6H_9FNO_3$ requires $[M + H]^+$, 162.0566). IR (neat, cm^{-1}) 3480, 3186, 3084, 1758, 1702, 1680, 1654, 1280, 1210, 1121.

Dimethyl 2-(3-cyanopropyl)-2-fluoromalonate 256

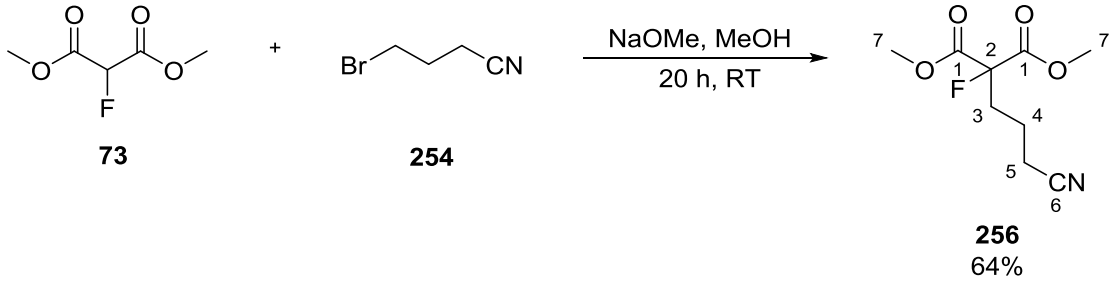

Dimethyl fluoromalonate **73** (4.95 g, 33 mmol) was added to sodium methoxide (Na (0.90 g, 39 mmol) in MeOH (40 mL)) before 4-bromobutyronitrile **254** (4.44 g, 30 mmol) was added and the solution stirred. After 20 h the solvent was removed *in vacuo*, the residue was extracted from water (10 mL) with ethyl acetate (4 x 10 mL), washed with brine (5 mL), dried ($MgSO_4$) and concentrated *in vacuo*. Kugelrohr distillation (115 ^{o}C, 0.4 mbar) of the crude oil gave *dimethyl 2-(3-cyanopropyl)-2-fluoromalonate* **256** (4.14 g, 64%) as a pale yellow oil; ^{1}H NMR (400 MHz, chloroform-*d*) δ 3.82 (6H, s, OCH_3), 2.40 (2H, t, $^{3}J_{HH}$ 7.1, C**5**H_2), 2.29 (2H, ddd, $^{3}J_{HF}$ 22.7, $^{3}J_{HH}$ 9.4, $^{3}J_{HH}$ 6.6, C**3**H_2), 1.85 – 1.68 (2H, m, C**4**H_2). ^{19}F NMR (376 MHz, chloroform-*d*) δ -166.72 (t, $^{3}J_{HF}$ 22.7). ^{13}C NMR (101 MHz, chloroform-*d*) δ 166.1 (d, $^{2}J_{CF}$ 25.5, C=O), 118.8 (s, CN), 94.2 (d, $^{1}J_{CF}$ 199.3, CF), 53.6 (s, CH_3O), 33.1 (d, $^{2}J_{CF}$ 21.4, C**3**), 19.4 (d, $^{3}J_{CF}$ 3.4, C**4**), 17.0 (s, C**5**). *m/z* (ASAP) 218.1 (100%, $[M + H]^+$), 176.1 (53%). ($[M + H]^+$, 218.0812. $C_9H_{13}FNO_4$ requires $[M + H]^+$, 218.0829). IR (neat, cm^{-1}) 2922, 2853, 1751, 1438, 1281, 1200, 1079.

Dimethyl 2-(4-aminobutyl)-2-fluoromalonate hydrochloride 258

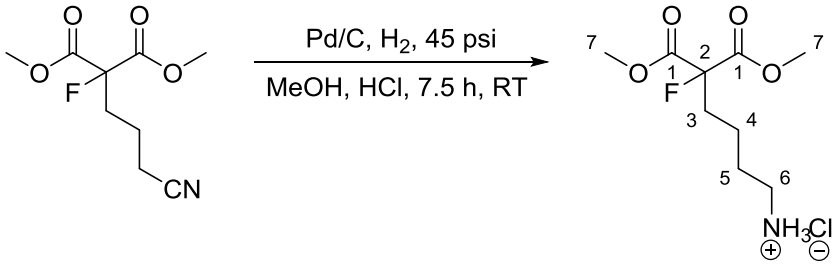

256 **258** 69%

Experimental method;

Dimethyl 2-(3-cyanopropyl)-2-fluoromalonate **256** (4.34 g, 20 mmol), Pd/C (1.06 g of 10% Pd/C, 5 mol%) and conc. HCl (2 mL) in methanol (25 mL) were reacted in a Parr hydrogenator (H_2, 45 psi). After 7.5 h the solution was filtered through celite and the 'plug' was washed with methanol (2 x 25 mL), the filtrate was concentrated *in vacuo* and the solid was washed with ethyl acetate (2 x 20 mL). Additionally, the ethyl acetate filtrate was concentrated *in vacuo* and washed with ethyl acetate (20 mL) to yield a further portion of *dimethyl 2-(4-aminobutyl)-2-fluoromalonate hydrochloride* **258** (3.54 g, 69%) as a white solid; Mp 119-120 ^{o}C. ^{1}H NMR (400 MHz, methanol-*d4*) δ 3.84 (6H, s, OCH_3), 2.96 (2H, t, $^{3}J_{HH}$ 7.4, C**6**H_2), 2.35 – 2.14 (2H, m, CH_2), 1.82 – 1.63 (2H, m, CH_2), 1.57 – 1.42 (2H, m, CH_2). ^{19}F NMR (376 MHz, methanol-*d4*) δ -167.63 (t, $^{3}J_{HF}$ 23.3). ^{13}C NMR (101 MHz, methanol-*d4*) δ 166.5 (d, $^{2}J_{CF}$ 25.9, C=O), 94.5 (d, $^{1}J_{CF}$ 197.0, CF), 52.6 (s, CH_3O), 39.1 (s, C**6**), 33.4 (d, $^{2}J_{CF}$ 21.6, C**3**), 26.8 (s, C**5**), 19.8 (d, $^{3}J_{CF}$ 3.1, C**4**). *m/z* (ASAP) 221.9 (100%, $[M - Cl]^+$). ($[M - Cl]^+$, 222.1132. $C_9H_{17}FNO_4$ requires $[M – Cl]^+$, 222.1142). IR (neat, cm^{-1}) 2960, 1746, 1439, 1281, 1243, 1153, 990.

Methyl 3-fluoro-2-oxo-3-azepanecarboxylate 251

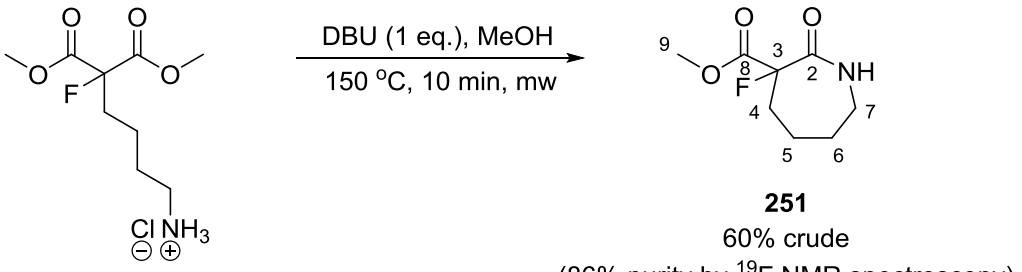

258

251
60% crude
(86% purity by ^{19}F NMR spectroscopy)

Example experimental method;

Dimethyl 2-(4-aminobutyl)-2-fluoromalonate hydrochloride **258** (0.50 g, 1.94 mmol) and DBU (0.30 g, 1.94 mmol) were dissolved in methanol (10 mL) and the solution was

heated to 150 ^{o}C in a microwave reactor. After 10 min the solvent was removed *in vacuo*, the residue was extracted from water (15 mL) with ethyl acetate (3 x 15 mL), washed with brine (15 mL), dried (Na_2SO_4) and concentrated *in vacuo* to give crude *methyl 3-fluoro-2-oxo-3-azepanecarboxylate* **251** (0.22 g, 60%, 86% purity by ^{19}F NMR spectroscopy) as an off-white solid; ^{1}H NMR (400 MHz, chloroform-*d*) δ 7.37 (1H, s, NH), 3.80 (3 H, s, CH_3), 3.45 – 3.33 (1H, m, CH_2), 3.17 – 3.04 (1H, m, CH_2), 2.27 – 2.05 (2H, m, CH_2), 1.94 – 1.70 (3H, m, CH_2), 1.62 – 1.48 (1H, m, CH_2). ^{19}F NMR (376 MHz, chloroform-*d*) δ -167.09 (t, $^{3}J_{HF}$ 23.5). *m/z* (GC-MS) 190.1 (35%, $[M + H]^+$), 158.1 (17%, $[M - OMe]^+$), 130.1 (26%, $[M - CO_2Me]^+$, 105.0 (100%), 59.0 (43%, $[CO_2Me]^+$), 43.1 (63%, $[HNC=O]^+$.

Experimental Section for Chapter 5

Ethyl 2-fluoro-3-hydroxy-butanoate 283 GC Standard

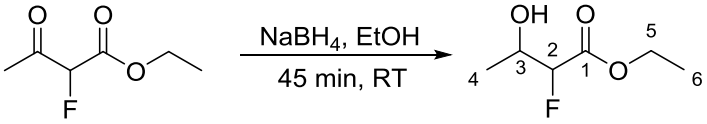

282 **283**

A solution of ethyl 2-fluoroacetoacetate **282** (0.050 g, 0.338 mmol) in ethanol (1 mL) was added slowly to sodium borohydride (0.0064 g, 0.169 mmol, 0.5 eq.) and the solution stirred. TLC analysis after 30 min showed the absence of starting material and so the reaction was quenched after a total of 45 min by the addition of sat. NH_4Cl solution (2 mL). The product was then extracted into MTBE (10 mL), washed with sodium bicarbonate solution (2 mL, saturated) and brine (2 mL), dried ($MgSO_4$) and the solvent removed *in vacuo* to give crude e*thyl 2-fluoro-3-hydroxy-butanoate* **283** (0.017 g) as a colourless oil; ^{1}H NMR (400 MHz, chloroform-*d*) δ 4.75 (0.5H, dd, $^2J_{HF}$ 49.0, $^3J_{HH}$ 3.2, HCF), 4.62 (0.5H, dd, $^2J_{HF}$ 48.3, $^3J_{HH}$ 3.2, HCF), 4.16 (1H, q, $^3J_{HH}$ 7.1, CH_2), 4.16 (1H, q, $^3J_{HH}$ 7.1, CH_2), 4.12-4.00 (m, 1H, HC**3**), 1.20 (3H, t, $^3J_{HH}$ 7.1 C**4**H_3), 1.21-1.11 (3H, m, C**6**H_3). ^{19}F NMR (376 MHz, chloroform-*d*) δ -201.96 (0.5F, dd, $^2J_{HF}$ 49.1, $^3J_{HF}$ 21.3), -206.85 (0.5F, dd, $^2J_{HF}$ 48.3, $^3J_{HF}$ 24.2).

CRED Screening of Ethyl 2-fluoroacetoacetate 282

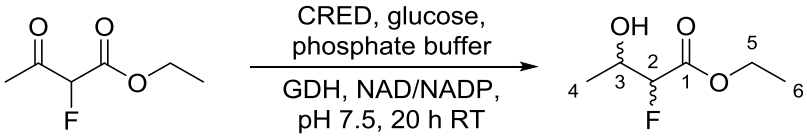

282 **283**

To each enzyme sample (~3-5 mg) in a 2 mL Eppendorf tube was added 1 mL of a 0.1M phosphate buffer solution of pH 7.5 that contained glucose (30 mg), GDH (2 mg), NAD (0.5 mg) and NADP (0.5 mg). A solution of ethyl 2-fluoroacetoacetate **282** (10 mg) in DMSO (0.1 mL) was then added, the tubes sealed and agitated at room temperature for 20 h. The products were then extracted into MTBE (1 mL) and the organic layer was dried ($MgSO_4$) and analysed by GC.

(2*S*,3*R*) 2-Fluoro-3-hydroxy-butanoate (2*S*,3*R*)-293 GC Standard*

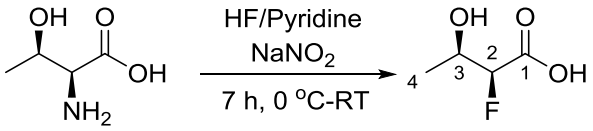

(2*S*,3*R*)-**292** (2*S*,3*R*)-**293**

*Conflicting literature debates whether this product is in fact the (2*S*,3*R*) diastereomer, see discussion for further details.

Initial reaction;

A 48:52 solution of hydrogen fluoride:pyridine was prepared by slow addition of pyridine (8 mL) to a 70:30 solution of HF/pyridine (18 mL) in a polyolefin bottle in an ice bath with stirring. The solution was stirred overnight before L-threonine (2*S*,3*R*)-**292** (1.19 g, 10 mmol) was added and the solution cooled in an ice bath. Sodium nitrite (1.04 g, 15 mmol) was added in three portions over 30 min with stirring. The solution was warmed to room temperature and stirred for 6 h. The mixture was quenched with ice water (50 mL) and extracted with diethyl ether (3 x 100 mL) and dried ($MgSO_4$) and the solvent removed *in vacuo*. ^{19}F NMR spectroscopy determined that whilst several other compounds had been extracted no *2-fluoro-3-hydroxy-butanoate* **293** was present in the crude product.

Optimised reaction;

A 48:52 solution of hydrogen fluoride:pyridine was prepared by slow addition of pyridine (8 mL) to a 70:30 solution of HF/pyridine (18 mL) in a polyolefin bottle in an ice bath with stirring. The solution was stirred overnight before L-threonine (2*S*,3*R*)-**292** (1.19 g, 10 mmol) was added and the solution cooled in an ice bath. Sodium nitrite (1.04 g, 15 mmol) was added in three portions over 30 min with stirring. The solution was warmed to room temperature and stirred for 6 h. The mixture was quenched with ice water (10 mL) and continuously extracted into DCM for 90 h. The solvent and pyridine were removed *in vacuo* at 85 ^{o}C. The crude white solid (containing a large quantity of Si-F and B-F compounds, as determined by ^{19}F NMR spectroscopy) was stirred with diethyl ether (3 x 167 mL) and filtered through two filter papers and a sinter to remove the Si-F and B-F contaminants. The solvent was removed *in vacuo* to give crude *2-fluoro-3-hydroxy-butanoate* (2*S*,3*R*)-**293** (0.113 g, 9%, 62% pure by ^{19}F NMR spectroscopy) as an off-white oil; ^{1}H NMR (400 MHz, chloroform-*d*) δ 4.83 (1H, dd,

$^{2}J_{HF}$ 48.0, $^{3}J_{HH}$ 2.8, HCF), 4.33-4.25 (m, 1H, HC**3**), 1.39 (3H, dd, $^{3}J_{HH}$ 6.6, $^{4}J_{HF}$ 1.1, CH_3). ^{19}F NMR (376 MHz, chloroform-*d*) δ -207.39 (dd, $^{2}J_{HF}$ 48.0, $^{3}J_{HF}$ 23.2).

(2*S*,3*R*) Ethyl 2-fluoro-3-hydroxy-butanoate (2*S*,3*R*)-283

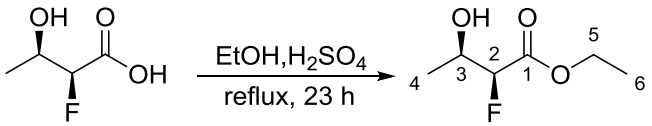

(2*S*,3*R*)-**293** (2*S*,3*R*)-**283**

* Conflicting literature debates whether this product is in fact the (2*S*,3*R*) diastereomer, see discussion for further details.

(2*S*,3*R*) 2-Fluoro-3-hydroxy-butanoate (2*S*,3*R*)-**293** (0.08 g, 0.66 mmol) was refluxed in ethanol (20 mL) with 2 drops of H_2SO_4. After 23 h the solvent was removed *in vacuo* and the residue was taken up in sat. sodium bicarbonate (10 mL), extracted into ethyl acetate (3 x 10 mL), washed with brine (5 mL), dried ($MgSO_4$ and the solvent was removed *in vacuo* to give crude (*2S,3R*) *ethyl 2-fluoro-3-hydroxy-butanoate* (2*S*,3*R*)-**283** (0.035 g, 35%, 91% pure by ^{19}F NMR spectroscopy) as a colourless oil; ^{1}H NMR (400 MHz, chloroform-*d*) δ 4.73 (1H, dd, $^{2}J_{HF}$ 48.2, $^{3}J_{HH}$ 3.3, HCF), 4.28 (2H, q, $^{3}J_{HH}$ 7.2, CH_2), 4.25-4.13 (m, 1H, HC**3**), 1.38-1.22 (6H, m, CH_3). ^{19}F NMR (376 MHz, chloroform-*d*) δ -206.65 (ddd, $^{2}J_{HF}$ 48.3, $^{3}J_{HF}$ 22.5, $^{4}J_{HF}$ 1.2).

Appendix Contents

The following information is included in the electronic appendix to this thesis:

Bibliography

[1] Martins, P.; Jesus, J.; Santos, S.; Raposo, L. R.; Roma-Rodrigues, C.; Baptista, P. V.; Fernandes, A. R. *Molecules* **2015**, 20, 16852-16891.
[2] Vitaku, E.; Smith, D. T. Njarson, J. T. *J. Med. Chem.* **2014**, 57, 10257-10274.
[3] Kirsch, P. *Modern Fluoroorganic Chemistry: Synthesis, Reactivity, Applications*, Wiley-VCH, Weinheim, **2004**.
[4] Ojima, I. (ed), *Fluorine in Medicinal Chemistry and Chemical Biology*. Wiley-Blackwell: Oxford, **2009**.
[5] O'Hagan, D. *J. Fluorine Chem.* **2010**, 131, 1071-1081.
[6] Isanbor, C.; O'Hagan, D. *J. Fluorine Chem.* **2006**, 127, 303-319.
[7] Lovering, F.; Bikker, J.; Humblet, C. *J. Med. Chem.* **2009**, 52, 6752-6756.
[8] Bobbio, C.; Gouverneur, V. *Org. Biomol. Chem.* **2006**, 4, 2065-2075.
[9] Mikami, K.; Itoh, Y.; Tamanaka, M. *Chem. Rev.* **2004**, 104 (1), 1-16.
[10] Haufe, G. *J. Fluorine Chem.* **2004**, 125, 875-894.
[11] Heidelberger, C.; Chaudhuri, N. K.; Danneberg, P.; Mooren, D.; Griesbach, L.; Duschinskey, R.; Schnitzer, R. J.; Pleven, E.; Scheiner, J. *J. Nature* **1957**, *179*, 663-666.
[12] Saravolatz, L. D.; Leggett, J. *Clin. Infect. Dis.* **2003**, 37 (9), 1210-1215.
[13] Butters, M.; Ebbs, J.; Green, S. P.; MacRae, J.; Morland, M. C.; Murtiashaw, C. W.; Pettman, A. J. *Org. Process Res. Dev.* **2001**, 5 (1), 28-36.
[14] Sever, P.S.; Dahlöf, B.; Poulter, N.R.; Wedel, H.; Beevers, G.; Caulfield, M.; Collins, R.; Kjeldsen, S. E.; Kristinsson, A.; McInnes, G. T.; Mehlsen, J.; Nieminen, M.; O'Brien, E.; Ostergren, J. *Lancet* **2003**, 361, 1149–1158.
[15] Pierce, M. E.; Parsons, R. L. Jr.; Radesca, L. A.; Lo, Y. S.; Silverman, S.; Moore, J. R.; Islam, Q.; Choudhury, A.; Fortunak, J. M. D.; Nguyen, D.; Luo, C.; Morgan, S. J.; Davis, W. P.; Confalone, P. N.; Chen, C.-Y.; Tillyer, R. D.; Frey, L.; Tan, L.; Xu, F.; Zhao, D.; Thompson, A. S.; Corley, E. G.; Grabowski, E. J. J.; Reamer, R.; Reider, P. J. *J. Org. Chem.* **1998**, 63, 8536-8543.
[16] Bondi, B. *J. Phys. Chem.* **1964**, *68* (3), 441–451.
[17] Wong, D. T.; Bymaster, F. P.; Engleman, E. A. *Life Sci.* **1995**, 57, 411-441.
[18] Swinson, J. "The Important Impact of Fluorine in Pharmaceuticals", http://www.halocarbon.com/halocarbon_media/Fluorine_final_ChemManager.pdf, accessed June 2017.
[19] Tanaka, Y.; Deluca, H. F.; Schnoes, H. K.; Ikekawa, N.; Kobayashi, Y. *Arch. Biochem. Biophys.* **1980**, 199, 473-478.
[20] Hornfeldt, C. S.; Larson, A. A. *Eur. J. Pharmacol.* **1990**, 179, 307-313.
[21] Roche, A. J. http://crab.rutgers.edu/~alroche/FCh2.pdf, accessed June 2017.
[22] Stadlbauer, W.; Laschober, R.; Lutschounig, H.; Schindler, G.; Kappe, T. *Monatsh. Chem.* **1992**, 123, 617-636.
[23] McLain, S. E.; Benmore, C. J.; Siewenie, J. E.; Urquidi, J.; Turner, J. F. C. *Angew. Chem. Int. Ed.* **2004**, 43, 1951-1955.
[24] Shipe, W. D.; Barrow, J. C.; Yang, Z.-Q.; Lindsley, C. W.; Yang, F. V.; Schlegel, K.-A. S.; Shu, Y.; Rittle, K. E.; Bock, M. G.; Hartman, G. D.; Tang, C.; Ballard, J. E.; Kuo, Y.; Adarayan, E. D.; Prueksaritanont, T.; Zrada, M. M.; Uebele, V. N.; Nuss, C. E.; Connolly, T. M.; Doran, S. M.; Fox, S. V.; Kraus, R. L.; Marino, M. J.; Graufelds, V. K.; Vargas, H. M.; Bunting, P. B.; Hasbun-Manning, M.; Evans, R. M.; Koblan K. S.; Renger, J. J. *J. Med. Chem.* **2008**, 51, 3692-3695.
[25] Okoromoba, O. E.; Han, J.; Hammond, G. B.; Xu, B. *J. Am. Chem. Soc.* **2014**, 136, 14381-14384.
[26] Cresswell, A. J.; Davies, S. G.; Roberts, P. M.; Thomson, J. E. *Chem. Rev.* **2015**, 115, 566-611.
[27] Hart, J. J.; Syvret, R. G. *J. Fluorine Chem.* **1999**, 100, 157-161.
[28] Nyffeler, P. T.; Durón, S. G.; Burkart, M. D.; Vincent, S. P.; Wong, C.-H. *Angew. Chem. Int. Ed.* **2005**, 44, 192-212.
[29] Takeuchi, Y.; Tarui, T.; Shibata, N. *Org. Lett.* **2000**, 2, 639-642.
[30] Jaroch, S.; Rehwinkel, H.; Hölscher, P.; Sülzle, D.; Burton, G.; Hillmann, M.; McDonald, F. M.; Miklautz, H. *Bioorg. Med. Chem. Lett.* **2004**, 14, 743-746.
[31] Umemoto, T.; Fukami, S.; Tomizawa, G.; Harasawa, K.; Kawada, K.; Tomita, K. *J. Am. Chem. Soc.* **1990**, 112, 8563-8575.
[32] Galante, E.; Okamura, T.; Sander, K.; Kikuchi, T.; Okada, M.; Zhang, M.-R.; Robson, M.; Badar, A.; Lythgoe, M.; Koepp, M.; Årstad, E. *J. Med. Chem.* **2014**, 57, 1023-1032.
[33] Lal, G. S.; Pez, G. P.; Pesaresi, R. J.; Prozonic, F. M.; Cheng, H. *J. Org. Chem.* **1999**, 64, 7048-7054.
[34] Umemoto, T.; Singh, R. P.; Xu, Y.; Saito, N. *J. Am. Chem. Soc.* **2010**, 132, 18199-18205.

[35] L'Heureux, A.; Beaulieu, F.; Bennett, C.; Bill, D. R.; Clayton, S.; LaFlamme, F.; Mirmehrabi, M.; Tadayon, S.; Tovell, D.; Couturier, M. *J. Org. Chem.* **2010**, 75, 3401-3411.
[36] Tang, P.; Wang, W.; Ritter, T. *J. Am. Chem. Soc.* **2011**, 133, 11482-11484.
[37] Sandford, G. *J. Fluorine Chem.* **2007**, 128, 90-104.
[38] Chambers, R. D.; Holling, D.; Sandford, G.; Batsanov, A. S.; Howard, J. A. K. *J. Fluorine Chem.* **2004**, 125, 661-671.
[39] Ma, J.-A.; Cahard, D. *J. Org. Chem.* **2003**, 68, 8726-8729.
[40] Harsanyi, A.; Sandford, G. *Org. Process Res. Dev.* **2014**, 18, 981-992.
[41] Günther, A.; Weintritt, H.; Böhm, S. US7807851, **2010**.
[42] Pattison, F. L. M.; Buchanan, R. L.; Dean, F. H. *Can. J. Chem.* **1964**, 43, 1700-1713.
[43] Ishikawa, N.; Takaoka, A.; Ibrahim, M. K. *J. Fluorine Chem.* **1984**, 25, 203-212.
[44] Chambers, R. D.; Fox, M. A.; Holling, D.; Nakano, T.; Okazoe, T.; Sandford, G. *Chem. Eng. Technol.* **2005**, 28, 344-352.
[45] Chambers, R. D.; Hutchinson, J.; Moilliet, J. S. US6300511, **2001**.
[46] Chambers, R. D.; Hutchinson, J. *J. Fluorine Chem.* **1998**, 92, 45-52.
[47] Kim, D. Y.; Kim, S. M.; Koh, K. O.; Mang, J. Y.; Lee, K. *Bull. Korean Chem. Soc.* **2003**, 24, 1425-1426.
[48] Cho, M. J.; Cho, M. G.; Huh, S. C.; Kim, S. M.; Lee, K.; Koh, K. O.; Mang, J. Y.; Kim, D. Y. *Bull. Korean Chem. Soc.* **2006**, 27, 857-862.
[49] Companyó, X.; Hejnová, M.; Kamlar, M.; Vesely, J.; Moyano, A.; R. Rios. *Tetrahedron Lett.* **2009**, 50, 5021-5024.
[50] Kang, S. H.; Kim, D. Y. *Bull. Korean Chem. Soc.* **2009**, 30, 1439-1440.
[51] Yi, W.-B.; Huang, X.; Cai, C.; Zhang, W. *Green Chem.* **2012**, 14, 3185-3189.
[52] Cheng, C.-C.; Rokita, S. E.; Burrows, C. J. *Angew. Chem. In. Ed.* **1993**, 32, 277-278.
[53] Spingler, B.; Pieve, C. D. *J. Chem. Soc. Dalton Trans.* **2005**, 1637-1643.
[54] Fisher, C. A.; Harsanyi, A.; Sandford, G.; Yufit, D. S.; Howard, J. A. K. *Chimia* **2014**, 68, 425-429.
[55] Harsanyi, A.; Sandford, G.; Yufit, D. S.; Howard, J. A. K. *Beilstein J. Org. Chem.* **2014**, 10, 1213-1219.
[56] Kawasaki, T.; Ichige, T.; Kitazume, T. *J. Org. Chem.* **1998**, 63, 7525-7528.
[57] Behenna, Stoltz, B. M.; Virgil, S. C.; White, D. E.; Yurino, T.; Liu, Y.; Duquette, D.; Eidamshaus, C.; WO2012/178129. **2012**.
[58] Behenna, D. C.; Liu, Y.; Yurino, T.; Kim, J.; White, D. E.; Virgil, S. C. *Nat. Chem.* **2012**, 4, 130–133.
[59] Norman, M. H.; Liu, L.; Lee, M.; Xi, N.; Fellows, I.; D'Angelo, N. D.; Dominguez, C.; Rex, K.; Bellon, S. F.; Kim, T.-S.; Dussault, I. *J. Med. Chem.* **2012**, 55, 1858-1867.
[60] Wang, W.; Zhao, X.; Yuan, Q.; Shi, H.; Tian, Q.; Liu, Q.; Zhou, Z.; Wang, X.; Chen, Z.; Chen, L.; Tan, H.; Fang, B.; Jiang, L.; Liu, Y.; Sun, J.; Zeng, F.; Li, T. WO2014169843 A1, **2014**.
[61] Miyashita, O.; Matsumura, K.; Kasahara, T.; Shimadzu, H.; Hashimoto, N. *Chem. Pharm. Bull.* **1982**, 30 (3), 887-898.
[62] Miyashita, O.; Matsumura, K.; Shimadzu, H.; Hashimoto, N. *Chem. Pharm. Bull.* **1981**, 29 (11), 3181-3190.
[63] Trzupek, J. D.; Lee, K. L.; Bunnage, M. E.; Han, S.; Hepworth, D.; Lovering, F. E.; Mathias, J. P.; Papaioannou, N.; Pierce, B. S.; Strohbach, J. W.; Wright, S. W.; Zapf, C. W.; Gavrin, L. K.; Lee, A.; Anderson, D. R.; Curran, K. J.; Dehnhardt, C. M.; Saiah, E.; Goldberg, J. A.; Wang, X.; Huang, H.-C.; Vargas, R.; Lowe, M. D.; Patny, A. US2015/284405 A1, **2015**.
[64] Liu, N.; Tian, Q.-P.; Yang, Q.; Yang, S.-D. *Synlett*, **2016**, 27 (18), 2621-2625.
[65] Bloxham, J.; Bradley, S. E.; Sambrook-Smith, C. P.; Smyth. D.; Keily, J.; Dawson, G. J.; Rasamison, C. M.; Bell, J. C. WO2011/117254 A1, **2011**.
[66] Atkinson, F. L.; Barker, M. D.; Douault, C.; Garton, N. S.; Liddle, J.; Patel, V. K.; Preston, A. G. S.; Wilson, D. M. US2013/0040984 A1, **2013**.
[67] Curtis, N. R.; Davies, S.; Gray, M.; Leach, S. G.; McKie, R. A.; Vernon L. E.; Walkington, A. *Org. Process Res. Dev.* **2015**, 19, 865–871.
[68] Suzuki, T.; Goto, T.; Hamashima, Y.; Sodeoka, M. *J. Org. Chem.* **2007**, 72 (1), 246-250.
[69] Shibata, N.; Suzuki, E.; Asahi, T.; Shiro, M. *J. Am. Chem. Soc*. **2001**, 123, 7001-7009.
[70] Heinrich, T.; Zenke, F.; Calderini, M.; Musil, D. US2013/296274 A1, **2013**.
[71] Hayamizu, K.; Terayama, N.; Hashizume, D.; Dodo, K.; Sodeoka, M. *Tetrahedron* **2015**, 71 (37), 6594 – 6601.
[72] Sato, M.; Kitazawa, N.; Kaneko, C. *Heterocycles* **1992**, 33 (1), 105 – 110.
[73] Wang, L.; Lin, S.; Li, B.; Wang, Y.; Yang, C.; Wu, Z.; Wei, T. CN104496737, **2015**.
[74] Pritchard, D. I.; Chhabra, S. R. WO2007/135466, **2007**.

[75] Boyd, S.; Miller, S.; Thomas, A.; Xu, R.; Lehuerou, Y.; Gunawardana, I.; Zhang, G.; Demeese, J.; McLaughlin, M.; Yanik, M.; Lupher, M. L.; Jacobson, I. C.; Thorsett, E. WO2005/019177, **2005**.
[76] Asano, Y.; Maeda, K.; Tsuruta, N.; Murase, T. WO2008/001959, **2008**.
[77] Reddy, D. S.; Shibata, N.; Nagai, J.; Nakamura, S.; Toru, T.; Kanemasa, S. *Angew. Chem. Int. Ed.* **2008**, 47 (1), 164 – 168.
[78] Huang, X.; Pham, K.; Zhang, X.; Yi, W.-B.; Hyatt, J. H.; Tran, A. P.; Jasinski, J. P.; Zhang, W. *RSC Adv.* **2015**, 5 (87), 71071 – 71075.
[79] Cosimi, E.; Saadi, J.; Wennemers, H. *Org. Lett.* **2016**, 18 (23), 6014-6017.
[80] Bischoff, A.; Raikar, S. N.; Sammeta, S. R.; Prabhu, G.; Subramanya, H.; Sundaresan, K. WO2009/117659, **2009**.
[81] Flohr, A.; Jakob-Roetne, R.; Wostl, W. US 2006/0122168 A1, **2006**.
[82] Flohr, A.; Jakob-Roetne, R.; Wostl, W. US 2007/0225273 A1, **2007**.
[83] Flohr, A.; Galley, G.; Jakob-Roetne, R.; Kitas, E. A.; Peters, J.-U.; Wostl, W. US 2005/0054633 A1, **2005**.
[84] Hong, S.; Kim, M.; Jung, M.; Ha, M. W.; Lee, M.; Park, Y.; Kim, M.-H.; Kim, T.-S.; Lee, J.; Park, H.-G. *Org. Biomol. Chem.* **2014**, 12 (9), 1510 – 1517.
[85] Kitazume, T.; Sato, T.; Lin, J. T. *Nippon Kagaku Kaishi* **1985**, 11, 2195-2198.
[86] Jadhav, G. P.; Chhabra, S. R.; Telford, G.; Hooi, D. S. W; Righetti, K.; Williams, P.; Kellam, B.; Pritchard, D. I.; Fischer, P. M. *J. Med. Chem.* **2011**, 54 (9), 3348-3359.
[87] Tsai, H.-J.; Thenappan, A.; Burton, D. J. *Phosphorus, Sulfur Silicon Relat. Elem.* **1995**, 105, 205-212.
[88] Sliskovic, D. R.; Picard, J. A.; O'Brien, P. M.; Liao, Peggy; Roark, H.; Roth, B. D.; Anderson, M. A.; Mueller, S. B.; Bocan, T. M. A.; Bousley, R. F.; Hamelehle, K. L.; Homan, R.; Reindel, J. F.; Stanfield, R. L.; Turluck, D.; Krause, B. R. *J. Med. Chem.* **1998** , 41, 682 – 690.
[89] Adolph, H. G.; Oesterling, R. E.; Sitzmann, M. E. *J. Org. Chem.* **1968**, 33, 4296-4299.
[90] Bogolyubskii, A. V.; Skrynnikova, A. A.; Il'chenko, A. Ya.; Popov, V. I.; Yagupol'skii, L. M. *Zh. Org. Khim.* **1988**, 24 (5), 1082-1087.
[91] Bogolyubskii, A. V.; Skrynnikova, A. A.; Popov, V. I.; Il'Chenko, A. Y.; Yagupolskii, L. M. *Ukr. Khim. Zh.* **1989**, 55 (4), 420-423.
[92] Portella, C.; Iznaden, M. *J. Fluorine Chem.* **1991**, 51 (1), 1-20.
[93] Svoboda, J.; Paleta, O.; Liska, F.; Dedek, V. *Collect. Czech. Chem. Commun.* **1981**, 46 (6), 1389-1396.
[94] Brooke, G. M.; Ferguson, J. A. K. J.; *J. Chem. Soc. Perkin Trans. 1* **1986**, 515 – 520.
[95] Noszticzius, Z.; McCormick, W. D.; Swinney, H. L. *J. Phys. Chem.* **1987**, 91, 5129-5134.
[96] Suzuki, K.; Watanabe, K.; Matsumoto, Y.; Kobayashi, M.; Sato, S.; Siswanta, D.; Hisamoto, H. *Anal. Chem.* **1995**, 67, 324-334.
[97] Tolomelli, A.; Cardillo, G.; Gentilucci, L.; Juris, R.; Viola, A.; Juaristi, E. *ARKIVOC* **2012**, v, 196-209.
[98] Schütte, J.; Kilgenstein, F.; Fischer, M.; Koert, U. *Eur. J. Org. Chem.* **2014**, 5302-5311.
[99] Maestro, A.; Astorga, C.; Gotor, V. *Tetrahedron Asymmetry* **1997**, 8 (18), 3153-3159.
[100] Kutney, G. W.; Still, I. W. J. *Can. J. Chem.* **1980**, 58, 1233-1238.
[101] Bailey, M. D.; Halmos, T.; Adamson, D.; Bordeleau, J.; Grand-Maître, C. *Tetrahedron Asymmetry* **1999**, 10, 3285-3295.
[102] Willis, N. J.; Fisher, C. A.; Alder, C. M.; Harsanyi, A.; Shukla, L.; Adams, J. P.; Sandford, G. *Green Chem.* **2016**, *18*, 1313-1318.
[103] https://www.imi.europa.eu/content/chem21 (accessed November 2016).
[104] http://www.gsk.com/en-gb/media/press-releases/2011/gsk-publishes-2010-corporate-responsibility-report (accessed November 2016).
[105] Phan, T. V. T.; Gallardo, C.; Mane, J. *Green Chem.* **2015**, *17* (5), 2846–2852.
[106] Curzons, A. D.; Jiménez-González, C.; Duncan, A. L.; Constable, D. J. C.; Cunningham, V. L. *Int. J. Life Cycle Assess.* **2007**, *12* (4), 272–280.
[107] Roschangar, F.; Sheldon, R. A.; Senanayake, C. H. *Green Chem.* **2015**, *17* (2), 752–768.
[108] McElroy, C. R.; Constantinou, A.; Jones, L. C.; Summerton, L.; Clark, J. H. *Green Chem.* **2015**, *17* (5), 3111–3121.
[109] Henderson, R. K.; Jiménez-González, C.; Constable, D. J. C.; Alston, S. R.; Inglis, G. G. A.; Fisher, G.; Sherwood, J.; Binks, S. P.; Curzons, A. D. *Green Chem.* **2011**, *13* (4), 854.
[110] Prat, D.; Wells, A.; Hayler, J.; Sneddon, H.; McElroy, C. R.; Abou-Shehada, S.; Dunn, P. J. *Green Chem.* **2016**, *18*, 288–296.
[111] Wagner, W. J.; Shia, G. H.; Poss, A. J. US Pat. Appl, 5403957, **1992**.
[112] Harsanyi, A.; Sandford, G. *Green Chem.* **2015**, *17*, 3000-3009.
[113] a) Bergmann, E. D.; Cohen, S.; Shani, A. *Isr. J. Chem.* **1963**, 79-85.
b) Koelsch, C. F. *J. Am. Chem. Soc.* **1943**, 65, 2458-2459.

c) Albertson, N. F.; Fillman, J. L. *J. Am. Chem. Soc.* **1949**, 71, 2818-2820.
d) Ansell, M. F.; Hey, D. H. *J. Chem. Soc.* **1950**, 1683-1686.
e) Michael, J.P.; de Koning, C. B.; van der Westhuyzen, C. W.; Fernandes, M. A. *J. Chem. Soc., Perkin Trans. 1* **2001**, 2055-2062.
f) Hong, S.; Kim, M.; Jung, M.; Ha, M. W.; Lee, M.; Park, Y.; Kim, M.; Kim, T.; Lee, J.; Park, H. *Org. Biomol. Chem.* **2014**, 12, 1510–1517.
g) Reddy, D. S.; Shibata, N.; Nagai, J.; Nakamura, S.; Toru, T.; Kanemasa, S. *Angew. Chem., Int. Ed.* **2008**, 47, 164–168.
h) Maligres, P. E.; Chartrain, M. M.; Upadhyay, V.; Cohen, D.; Reamer, R. A.; Askin, D.; Volante, R. P.; Reider, P. J. *J. Org. Chem.* **1998**, 63, 9548-9551.
i) Wilent, J.; Petersen, K. S. *J. Org. Chem.* **2014**, 79, 2303-2307.
[114] Henderson, R. K.; Hill, A. P., Redman; A. M.; Sneddon, H. F. *Green Chem.* **2015**, 17, 945-949.
[115] Banerjee, S.; Wiggins, W. J.; Geoghegan, J. L.; Anthony, C. T.; Woltering, E. A.; Masterson, D. S. *Org. Biomol. Chem.*, **2013**, 11, 6307–6319.
[116] Gutman, A. L.; Meyer, E.; Yue, X.; Abell, C. *Tetrahedron Lett.* **1992**, 33, 3943–3946.
[117] Gotor-Fernandez, V.; Busto, E.; Gotor, V. *Adv. Synth. Catal*. **2006**, 348, 797–812;
[118] van Pelt, S.; Teeuwen, R. L. M.; Janssen, M. H. A.; Sheldon, R. A.; Dunn, P. J.; Howard, R. M.; Kumar, R.; Martinez, I.; Wong, J. W. *Green Chem*. **2011**, 13, 1791–1798.
[119] Rueppel, M. L.; Rapoport, H. *J. Am. Chem. Soc.* **1972**, 94, 3877-3883.
[120] Anderson, N. A.; Campbell-Crawford, M. H. J.; Hancock, A. P.; Pritchard, J.; Redmond, J. M. WO2016/046225, **2016**.
[121] Anderson, N. A.; Campbell-Crawford, M. H. J.; Hancock, A. P.; Pritchard, J.; Redmond, J. M. WO2016/046226, **2016**.
[122] Kitazume, T; Yamazaki, T. *Top. Curr. Chem.* **1997**, 193, 91-129.
[123] Resnati, G. *Tetrahedron* **1993**, 49 (42), 9385-9445.
[124] Kalaritis, P.; Regenye, R. W.; Partridge, J. J.; Coffen, D. L. *J. Org. Chem*. **1990**, 55, 812-815.
[125] Kitazume, T.; Murata, K.; Ikeya, T. *J. Fluorine Chem.* **1986**, 31, 143-150.
[126] Kitazume, T.; Sato, T.; Kobayashi, T. *Chem. Lett*. **1984**, 1811-1814.
[127] Kitazume, T.; Sato, T.; Kobayashi, T.; Lin, J. T. *J. Org. Chem*. **1986**, 51, 1003-1006.
[128] Fukuyama, Y.; Matoishi, K.; Iwasaki, M.; Takizawa, E.; Miyazaki, M.; Ohta, H.; Hanzawa, S.; Kakidani, H.; Sugai, T. *Biosci. Biotechnol. Biochem.* **1999**, 63 (9), 1664-1666.
[129] Rokita, S. E.; Walsh, C. T. *Biochemistry* **1983**, 22, 2821-2828.
[130] Dummel, R. J.; Kun, E. *J. Biol. Chem.* **1969**, 244, 2966-2969.
[131] Borzęcka, W.; Lavandera, I.; Gotor, V. *J. Org. Chem.* **2013**, 78, 7312-7317.
[132] Matsuda, T.; Harada, T.; Nakajima, N.; Itoh, T.; Nakamura, K. *J. Org. Chem.* **2000**, 65 (1), 157–163.
[133] Nakamura, K.; Matsuda, T. *J. Org. Chem.* **1998**, 63 (24), 8957-8964.
[134] Nakamura, K.; Yamanaka, R. *Tetrahedron Asymmetry* **2002**, 13, 2529-2533.
[135] Barkakaty, B.; Takeguchi, Y.; Tsuboi, S. *Tetrahedron* **2007**, 63, 970-976.
[136] Szőri, K.; Szöllősi, G.; Bartók, M. *Adv. Synth. Catal.* **2006**, 348, 515-522.
[137] Dascier, D.; Kambourakis, S.; Hua, L.; Rozzell, J. D.; Stewart, J. D. *Org. Process Res. Dev.* **2014**, 18, 793-800.
[138] Kitazume, T.; Kobayashi, T. *Synthesis* **1987**, 2, 187-188.
[139] Kitazume, T.; Kobayashi, T. *J. Fluorine Chem.* **1986**, 31, 357-361.
[140] Moody, T. S.; Mix, S.; Brown, G.; Beecher, D. *Science of Synthesis: Biocatalysis in Organic Synthesis 2*, Thieme Publishing Group.
[141] Elkik, E.; Imbeaux-Oudotte, M. *Bull. Soc. Chim. France* **1975**, 1633-1638.
[142] Olah, G.A.; Welch, J. T.; Vankar, Y. D.; Nojima, M.; Kerekes, I.; Olah, J. A. *J. Org. Chem.* **1979**, 44, 3872-3881.
[143] Olah, G.A.; Prakash, G. K. S.; Chao, J. L. *Helv. Chim. Acta* **1981**, 64, 2528-2530.
[144] Dascier, D.; Kambourakis, S.; Hua, L.; Rozzell, J. D.; Stewart, J. D. *Org. Process Res. Dev.* **2014**, 18, 793-800, (Reference 27).
[145] O'Hagan, D. *Chem. Soc. Rev.* **2008**, 37, 308-319.
[146] Hunter, L. *Beilstein J. Org. Chem.* **2010**, 6 (38).
[147] Chen, Z.; Li, Y.; Chen, E.; Hall, D. L.; Darke, P. L.; Culberson, C.;Shafer, J.; Kuo, L. C. *J. Biol. Chem.* **1994**, 269, 26344–26348.
[148] Myers, A. G.; Barbay, J. K.; Zhong, B. *J. Am. Chem. Soc.* **2001**, 123, 7207–7219.
[149] Massa, M. A.; Spangler, D. P.; Durley, R. C.; Hickory, B. S.; Connolly, D. T.; Witherbee, B. J.; Smith, M. E.; Sikorski, J. A. *Bioorg. Med. Chem. Lett.* **2001**, 11, 1625–1628.
[150] Müller, K.; Faeh, C.; Diederich, F. *Science* **2007**, 317, 1881–1886.

[151] Böhm, H.-J.; Banner, D.; Bendels, S.; Kansy, M.; Kuhn, B.; Müller, K.; Obst-Sander, U.; Stahl, M. *ChemBioChem* **2004**, 5, 637–643.
[152] Wu, D.; Tian, A.; Sun, H. *J. Phys. Chem. A* **1998**, 102, 9901–9905.
[153] Banks, J. W. Durham University doctoral thesis (http://etheses.dur.ac.uk/3171/, accessed June 2017), **2004**.
[154] Thiehoff, C.; Rey, Y. P.; Gilmour, R. *Isr. J. Chem.* **2016**, 57, 92-100.
[155] Briggs, C. R.; Allen, M. J.; O'Hagan, D.; Tozer, D. J.; Slawin, A. M. Z.; Goeta, A. E.; Howard, J. A. K. *Org. Biomol. Chem.* **2004**, 2, 732–740.
[156] Banks, J. W.; Batsanov, A. S.; Howard, J. A. K.; O'Hagan, D.; Rzepa, H. S.; Martin-Santamaria, S. *J. Chem. Soc. Perkin Trans. 2*, **1999**, 2409-2411.
[157] Reed, A. E. *Chem. Rev.* **1988**, 88, 899-926.
[158] Briggs, C. R. S.; O'Hagan, D.; Howard, J. A. K.; Yufit, D. S. *J. Fluorine Chem.* **2003**, 119, 9-13.
[159] March, T. L.; Johnston, M. R.; Duggan, P. J.; Gardiner, J. *Chem. Biodivers.* **2012**, 9, 2410-2441.
[160] Peddie, V.; Butcher, R. J.; Robinson, W. T.; Wilce, M. C. J.; Traore, D. A. K. Abell, A. D. *Chem. Eur. J.* **2012**, 18, 6655-6662.
[161] Mathad, R. I.; Gessier, F.; Seebach, D.; Jaun, B. *Helv. Chim. Acta* **2005**, 88, 266–280.
[162] Tormena, C. F.; Amadeu, N. S.; Rittner, R.; Abraham, R. J. *J. Chem. Soc. Perkin Trans. 2* **2002**, 773–778.
[163] Tormena, C. F.; Cormanich, R. A.; Rittner, R. *Ann. Magn. Reson.* **2011**, 10, 1-27.
[164] Jones, C. R.; Baruah, P. K.; Thompson, A. L.; Scheiner, S. *J. Am. Chem. Soc.* **2012**, 134, 12064-12071.
[165] van der Veken, B. J.; Truyen, S.; Herrebout, W. A.; Watkins, G. *J. Mol. Struct.* **1993**, 293, 55–58.
[166] Abraham, R. J.; Tormena, C. F.; Rittner, R. *J. Chem. Soc. Perkin Trans. 2* **2001**, 815-820.
[167] Tormena, C. F.; Freitas, M. P.; Rittner, R.; Abraham, R. J. *Phys. Chem. Chem. Phys.* **2004**, 6, 1152-1156.
[168] Takahashi, T.; Fukuishima, A.; Tanaka, Y.; Takeuchi, Y.; Kabuto, K.; Kabuto, C. *Chem. Commun.* **2000**, 788-789.
[169] Sahnoun, R.; Fujimara, Y.; Kabuto, K.; Takeuchi, Y.; Noyori, R. *J. Org. Chem.* **2007**, 72, 7923-7929.
[170] Sahnoun, R.; Fujimara, Y.; Kabuto, K.; Takeuchi, Y.; Noyori, R. *J. Phys. Org. Chem.* **2009**, 22, 903-912.
[171] Abraham, R. J.; Jones, A. D.; Warne, M. A.; Rittner, R. Tormena, C. F. *J. Chem. Soc. Perkin Trans. 2* **1996**, 533-539.
[172] Tormena, C. F.; Rittner, R.; Abraham, R. J. *Phys. Org. Chem.* **2002**, 15, 211-217.
[173] Phan, H. V.; Durig, J. R. *THEOCHEM* **1990**, 209, 333-347.
[174] Cee, V. J.; Cramer, C. J.; Evans, D. A. *J. Am. Chem. Soc.* **2006**, 128, 2920-2930.
[175] Laato, H.; Isotalo, R. *Acta Chem. Scandinavica* **1967**, 21, 2119-2130.
[176] MChem student Joshua Walton